NUREG/CR-6152
SAND93-2519

Experiments to Investigate Direct Containment Heating Phenomena with Scaled Models of the Surry Nuclear Power Plant

Prepared by
T. K. Blanchat, M. D. Allen, M. M. Pilch, R. T. Nichols

Sandia National Laboratories
Operated by
Sandia Corporation

Prepared for
U.S. Nuclear Regulatory Commission

AVAILABILITY NOTICE

Availability of Reference Materials Cited in NRC Publications

Most documents cited in NRC publications will be available from one of the following sources:

1. The NRC Public Document Room, 2120 L Street, NW., Lower Level, Washington, DC 20555-0001

2. The Superintendent of Documents, U.S. Government Printing Office, Mail Stop SSOP, Washington, DC 20402-9328

3. The National Technical Information Service, Springfield, VA 22161

Although the listing that follows represents the majority of documents cited in NRC publications, it is not intended to be exhaustive.

Referenced documents available for inspection and copying for a fee from the NRC Public Document Room include NRC correspondence and internal NRC memoranda; NRC bulletins, circulars, information notices, inspection and investigation notices; licensee event reports; vendor reports and correspondence; Commission papers; and applicant and licensee documents and correspondence.

The following documents in the NUREG series are available for purchase from the GPO Sales Program: formal NRC staff and contractor reports, NRC-sponsored conference proceedings, international agreement reports, grant publications, and NRC booklets and brochures. Also available are regulatory guides, NRC regulations in the *Code of Federal Regulations*, and *Nuclear Regulatory Commission Issuances*.

Documents available from the National Technical Information Service include NUREG-series reports and technical reports prepared by other Federal agencies and reports prepared by the Atomic Energy Commission, forerunner agency to the Nuclear Regulatory Commission.

Documents available from public and special technical libraries include all open literature items, such as books, journal articles, and transactions. *Federal Register* notices, Federal and State legislation, and congressional reports can usually be obtained from these libraries.

Documents such as theses, dissertations, foreign reports and translations, and non-NRC conference proceedings are available for purchase from the organization sponsoring the publication cited.

Single copies of NRC draft reports are available free, to the extent of supply, upon written request to the Office of Administration, Distribution and Mail Services Section, U.S. Nuclear Regulatory Commission, Washington, DC 20555-0001.

Copies of industry codes and standards used in a substantive manner in the NRC regulatory process are maintained at the NRC Library, 7920 Norfolk Avenue, Bethesda, Maryland, for use by the public. Codes and standards are usually copyrighted and may be purchased from the originating organization or, if they are American National Standards, from the American National Standards Institute, 1430 Broadway, New York, NY 10018.

DISCLAIMER NOTICE

NUREG/CR-6152
SAND93-2519

Experiments to Investigate Direct Containment Heating Phenomena with Scaled Models of the Surry Nuclear Power Plant

Manuscript Completed: April 1994
Date Published: June 1994

Prepared by
T. K. Blanchat, M. D. Allen, M. M. Pilch, R. T. Nichols*

Sandia National Laboratories
Albuquerque, NM 87185

Prepared for
Division of Systems Research
Office of Nuclear Regulatory Research
U.S. Nuclear Regulatory Commission
Washington, DC 20555-0001
NRC FIN A1406

*Ktech Corp., 901 Pennsylvania NE, Albuquerque, NM 87110

Abstract

The Containment Technology Test Facility (CTTF) and the Surtsey Test Facility at Sandia National Laboratories are used to perform scaled experiments for the Nuclear Regulatory Commission that simulate high pressure melt ejection (HPME) accidents in a nuclear power plant (NPP). These experiments are designed to investigate the effects of direct containment heating (DCH) phenomena on the containment load. High-temperature, chemically reactive melt is ejected by high-pressure steam into a scale model of a reactor cavity. Debris is entrained by the steam blowdown into a containment model where specific phenomena, such as the effect of subcompartment structures, prototypic atmospheres, and hydrogen generation and combustion, can be studied.

Four Integral Effects Tests (IETs) have been performed with scale models of the Surry NPP to investigate DCH phenomena. These experiments were conducted for five primary purposes: (1) to measure the pressure load on the containment containing prototypic subcompartment structures, (2) to investigate the amount of hydrogen combustion due to a HPME into a prototypic steam/air/H_2 atmosphere, (3) to investigate the effect of an annular gap between the reactor pressure vessel (RPV) and the reactor support skirt, (4) to measure posttest debris distribution in a containment model, and (5) to provide data from prototypic, large-scale experiments for validation of DCH models.

The 1/6th scale Integral Effects Tests (IET-9, IET-10, and IET-11) were conducted in CTTF, which is a 1/6th scale model of the Surry reactor containment building (RCB). The 1/10th scale IET test (IET-12) was performed in the Surtsey vessel, which had been configured as a 1/10th scale Surry RCB. Scale models were constructed in each of the facilities of the Surry structures, including the RPV, reactor support skirt, control rod drive missile shield, biological shield wall, cavity, instrument tunnel, residual heat removal platform and heat exchangers, seal table room and seal table, operating deck, and crane wall. The RPV model had a hemispherical bottom head with a hole that simulated the ablated hole in the RPV that would be formed by ejection of an instrument guide tube in a severe NPP accident. A charge of thermite was used in the RPV model to simulate molten corium that would accumulate on the bottom head of an actual RPV. This chemically reactive melt was ejected by high-pressure steam from the melt generator into the scaled reactor cavity. Debris was then entrained through the incore instrument tunnel into the subcompartment structures and then into the upper dome of the containment models, where the fragmented molten debris particles encountered prototypic air/steam/hydrogen atmospheres. This report describes these experiments and gives the results.

Contents

Figures

Figures (continued)

Figures (continued)

Figures (concluded)

Tables

Executive Summary

In a light water reactor core-melt accident, an instrument guide tube penetration in the bottom head of the reactor pressure vessel (RPV) may fail while the primary system is pressurized. The blowdown of the reactor coolant system (RCS) may entrain molten core debris in the high-velocity steam blowdown gas and eject fragmented particles from the cavity into the reactor containment building (RCB). This chain of events is called a high-pressure melt ejection (HPME). As the fragmented, molten debris is dispersed into the RCB, four mechanisms may cause a rapid increase in pressure and temperature: (1) blowdown of the RCS, which would add both mass and energy to the containment atmosphere, (2) efficient debris-to-gas heat transfer, (3) exothermic metal/steam and metal/oxygen reactions, and (4) hydrogen combustion. The processes that lead to increased loads on the RCB are collectively referred to as direct containment heating (DCH). Understanding factors that enhance or mitigate DCH is necessary because the load imposed on the RCB may potentially threaten its integrity.

The Containment Technology Test Facility (CTTF) and the Surtsey Test Facility at Sandia National Laboratories are used to perform scaled experiments for the Nuclear Regulatory Commission that simulate a HPME accident in a nuclear power plant (NPP). The experiments are designed to investigate the phenomena associated with DCH. High-temperature, chemically reactive melt is ejected from a melt generator by high-pressure steam into a scale model of a reactor cavity. Debris is entrained by the steam blowdown into the containment vessel model. The effects of specific phenomena on the containment load, such as the geometry of subcompartment structures, prototypic atmospheres, and hydrogen generation and combustion, are studied.

The Surry Integral Effects Test (IET) series was conducted using 1:6 and 1:10 linear scale models of the Surry NPP structures. There were four experiments in the Surry IET test series: IET-9, IET-10, IET-11, and IET-12. The experiments used models of the Surry structures, including the bottom head of the RPV, reactor support skirt, control rod drive missile shield, biological shield wall, cavity, instrument tunnel, residual heat removal platform and heat exchangers, seal table room (STR) and seal table, operating deck, and crane wall. The 1:6 scale tests (IET-9, IET-10, and IET-11) were conducted in the CTTF. The 1:10 scale test (IET-12) was conducted in the Surtsey Test Facility. The containment vessels at these two facilities were used to simulate the upper dome of the Surry RCB.

The experiments were conducted for five primary purposes: (1) to measure the pressure load on the containment containing prototypic subcompartment structures, (2) to investigate the amount of hydrogen combustion due to a HPME into a prototypic steam/air/H_2 atmosphere, (3) to investigate the effect of an annular gap between the RPV and the reactor support skirt, (4) to measure posttest debris distribution in a containment model, and (5) to provide data from prototypic, large-scale experiments for validation of DCH models.

In the Surry IET experiments, the vessel atmosphere contained levels of steam ranging from 32 mol.% to 67 mol.%. The containment atmosphere also had preexisting hydrogen concentrations that ranged from 2 mol.% to 6 mol.%. The preexisting hydrogen represented levels produced by partial clad oxidation during the core degradation process in a NPP pump seal loss-of-coolant accident. In the IET-9, IET-10, IET-11, and IET-12 tests, the amounts of preexisting hydrogen corresponded to oxidizing 14%, 16%, 24%, and 38% of the zirconium cladding, respectively. In the IET experiments, hydrogen produced by reactions between the blowdown steam and metallic debris burned as it was ejected from the subcompartment structures and contributed significantly to the containment load. It appears that the presence of preexisting hydrogen did not have a major effect on the containment load. It is possible that the preexisting hydrogen recombined on a time scale too long to have a significant

impact on the containment load. It is also possible that the containment loads caused by the combustion of hydrogen were partially mitigated by atmosphere-structure heat transfer, since the time scales for both combustion and heat transfer are of the same order of magnitude.

A particular concern was the ejection of molten debris through the annular gap between the RPV and the reactor support skirt. This represents a direct pathway for debris to the upper dome and might have a significant impact on the containment load. The Surry RPV is insulated with reflective metal insulation and has an open annular gap between the RPV insulation and the reactor support skirt. The gap allows cooling air to circulate from the reactor cavity past the insulation to the operating deck. Two counterpart tests, a closed annular gap test (IET-10) and an open gap test with scaled reflective metal insulation on the RPV model (IET-11) were conducted. About 14% of the molten thermite was transported to the dome region in the open annular gap test, as compared to about 10% for the closed gap test. In IET-11, more hydrogen was produced (attributed to the RPV stainless steel insulation) and subsequently burned in the dome. The open gap test had the highest measured containment peak pressure, i.e., 0.43 MPa compared to the experiments with a closed gap.

The IET-12 experiment had the smallest measured containment peak pressure increase, i.e., 0.198 MPa. There was 47% dispersal of molten debris from the cavity, which was less than the 70-90% cavity dispersal measured in the 1:6 scale tests (IET-9, IET-10, and IET-11). It is believed that the absence of chromium reaction energy, in conjunction with co-ejected water in the blowdown steam, increased the retention of debris in the cavity. Consequently, only about 3% of the initial thermite mass was transported outside of the subcompartment structures and into the upper dome region. As a result, little hydrogen combustion occurred in IET-12, and thus, the measured load was comparatively small.

Acknowledgments

The authors express their gratitude to Michael Oliver and Randy Hudgens, who were the electronics and instrumentation engineers for these experiments, and to James Ross, Tim Covert, and Robert Carolan, who were the mechanical technicians. Four summer students participated in the conversion of Surtsey to the Surry geometry required for the IET-12 experiment; the authors also express their gratitude to Guillermo Negron, Jose Sotolongo, Emmanuel Williams (Science and Technology Alliance Summer Program), and Carl Essary (Youth Opportunity Trainee). The authors appreciate the technical review of this report provided by Dr. Terence Heames and Dr. David Williams.

This work was funded by the Accident Evaluation Branch of the United States Nuclear Regulatory Commission.

Acronyms

ANL	Argonne National Laboratory
ASME	American Society of Mechanical Engineers
CCD	Charge Coupled Device
CS	Cavity Side
CTTF	Containment Technology Test Facility
DCH	Direct Containment Heating
DS	Door Side
EPRI	Electrical Power Research Institute
FAI	Fauske and Associates
GE	General Electric
HPME	High Pressure Melt Ejection
IET	Integral Effects Test
IIT	Incore Instrument Tube
LOCA	Loss of Coolant Accident
LP	Liquid Propane
MAWP	Maximum Allowable Working Pressure
MOS	Metal Oxide Surface
NPP	Nuclear Power Plant
NRC	Nuclear Regulatory Commission
RCB	Reactor Containment Building
RCS	Reactor Coolant System
RHR	Residual Heat Removal
RPV	Reactor Pressure Vessel
SASM	Severe Accident Scaling Methodology
SMMD	Sieve Mass Median Diameter
SNL	Sandia National Laboratory
SS	Stainless Steel
STR	Seal Table Room
TCE	Two-Cell Equilibrium
TRG	Technical Review Group
UCSB	University of California - Santa Barbara

1.0 Introduction

In a light water reactor core melt accident, if the reactor pressure vessel (RPV) fails while the reactor coolant system (RCS) is at high pressure, the expulsion of molten core debris may pressurize the reactor containment building (RCB) beyond its failure pressure. A failure in the bottom head of the RPV, followed by melt expulsion and blowdown of the RCS, will entrain molten core debris in the high-velocity steam blowdown gas. This chain of events is called a high-pressure melt ejection (HPME). Four mechanisms may cause a rapid increase in pressure and temperature in the reactor containment: (1) blowdown of the RCS, (2) efficient debris-to-gas heat transfer, (3) exothermic metal/steam and metal/oxygen reactions, and (4) hydrogen combustion. These processes that lead to increased loads on the containment building are collectively referred to as direct containment heating (DCH).

DCH experiments have been previously conducted at Sandia National Laboratories (SNL), Argonne National Laboratory (ANL), and Fauske and Associates (FAI). These early DCH experiments were reviewed as part of a Nuclear Regulatory Commission (NRC) sponsored effort known as the Severe Accident Scaling Methodology (SASM) Program (Zuber et al. 1991). As a result of SASM recommendations, the NRC-sponsored experiment programs were redirected towards performing counterpart experiments at two different physical scales: $1/10^{th}$ linear scale at SNL and $1/40^{th}$ linear scale at ANL. These counterpart experiments included geometrically scaled simulations of the Zion nuclear power plant (NPP) structures and had the initial conditions closely tied to postulated accident scenarios. These experiments, called the Integral Effects Tests (IETs), were designed to provide integral effects data on HPME/DCH phenomena from large-scale, prototypic experiments. The primary measurements include pressures, temperatures, and gas concentrations. The technical guidance for the initial conditions of the IET experiments was provided by the Accident Evaluation Branch of the NRC and a five member Technical Review Group (TRG), who were all members of the original SASM committee. The TRG included R.E. Henry (FAI), M. Ishii (Purdue), F.J. Moody (General Electric), B.R. Sehgal (Electric Power Research Institute), and T.G. Theofanous (University of California, Santa Barbara).

The initial integral effects tests were conducted by SNL at the Surtsey Facility using 1:10 linear scale models of the Zion NPP structures; these tests are designated as IET-1, IET-1R, IET-3, IET-4, IET-5, IET-6, IET-7, IET-8A, and IET-8B [Allen et al. 1992b-g; 1993a, b]. These experiments used models of the Zion structures, including the bottom head of the RPV, biological shield wall, reactor cavity, instrument tunnel, containment basement floor, seal table room, refueling canal, steam generators, reactor coolant pumps (RCPs), and operating deck. The Surtsey vessel was used to simulate the upper dome of the Zion RCB. In three other experiments, IET-2A, 2B, and 2C, the Surtsey vessel was not used; the melt generator was attached to a nondispersive cavity [Allen et al. 1993b]. These tests were conducted specifically to determine the temperature of the melt ejected from the scaled RPV model into the reactor cavity. The experiments conducted in the Zion geometry were designed to obtain integral effects data on phenomena associated with direct containment heating. Specific effects studied in the initial SNL/ANL IET tests were the effect of: (1) physical scale, (2) basement water, (3) cavity water, (4) hydrogen production and combustion under prototypic conditions, and (5) scaled containment structures.

Condensate levels of water were present on the scaled reactor cavity floor in the majority of the Zion IET tests. Previous tests [Allen et al. 1992a] showed that small amounts of water had little effect on the containment load. In two of the IET tests (IET-8A and IET-8B), the cavity was half filled with water [Allen et al. 1993a]. Water was also present on the containment

basement floor inside the crane wall for some of these tests.

In the Zion IET experiments, the Surtsey vessel atmosphere was either inert or reactive. In IET-1 and IET-1R, the Surtsey atmosphere was inerted by purging with nitrogen (<0.1 mol.% O_2). The IET-5 experiment was "classically" inerted with carbon dioxide, which was used as a surrogate for steam. In all of the other IET experiments, the Surtsey atmosphere was reactive, i.e., about 9 mol.% O_2. In IET-5, IET-6, IET-7, IET-8A, and IET-8B, the Surtsey atmosphere also contained preexisting hydrogen. The preexisting hydrogen represented levels produced by partial clad oxidation during the core degradation process in a NPP pump seal loss-of-coolant accident (LOCA). These experiments have been documented by Allen et al. [1993b].

This report describes the experimental results of the four recent integral effects tests that have been performed by SNL under even more prototypic conditions with scale models of the Surry NPP. The experiments have been conducted at 1:6 linear scale (IET-9, IET-10, and IET-11) at the Containment Technology Test Facility (CTTF) and at 1:10 linear scale (IET-12) at the Surtsey Facility. Higher steam driving pressures were used, i.e., the debris was ejected at 12 MPa in the Surry IETs versus 6 MPa in the Zion IETs. Hydrogen combustion was examined under more prototypic atmospheric conditions, i.e. air/steam/hydrogen atmospheres likely to occur in an accident scenario.

The IET-9 experiment was the first test in the Surry IET test series to measure DCH loads in a 1:6 scale containment with scaled models of the Surry NPP. Scale models of the Surry RPV, reactor support skirt, biological shield wall, cavity, instrument tunnel, residual heat removal (RHR) platform, seal table room (STR), operating deck, and crane wall were constructed inside CTTF, which is a 1:6 scale model of the Surry reactor containment building. The IET-9 test had the highest initial steam concentration. The annular gap was partially open to provide clearance between the RPV and the support skirt for assembly of the high-pressure melt ejection system.

Additional components were modeled in the IET-10 test, which was also designed to obtain integral effects data using 1:6 scale models of the Surry NPP. Scale models of the Surry control rod drive missile shield, RHR heat exchangers, seal table, and the cutout in the operating deck for the RPV head were constructed. The annular gap between the RPV and the reactor support skirt was closed in IET-10.

The IET-11 test was the final test using 1:6 scale models of the Surry NPP. The models were identical to those used in IET-10. Scaled reflective metal insulation was placed on the RPV and partially filled the open annular gap between the RPV and the support skirt. A particular objective of the IET-11 experiment was to determine whether the RPV insulation would mitigate or enhance DCH.

The IET-12 test was designed to obtain integral effects data using 1:10 scale models of the Surry NPP. Scale models of the Surry RPV, reactor support skirt, control rod drive missile shield, biological shield wall, cavity, instrument tunnel, RHR platform and heat exchangers, seal table room and seal table, operating deck, and crane wall were constructed outside of Surtsey. The Surtsey vessel volume was reduced by constructing a floor across the vessel so that only the upper part of the vessel was used. With the false floor and structures in place, the freeboard volume in Surtsey (51 m^3) was 1:10 linear scale of the Surry plant (51,000 m^3). In IET-12, there was no annular gap between the RPV and reactor support skirt.

The initial conditions selected for IET-12 were based upon recommendations and guidance from the TRG. An agreement was reached that the IET-12 test should be conducted with: (1) the initial hole size equivalent to a diameter of 56 cm

at NPP scale, (2) melt mass scaled to 43 mtonnes in the Surry plant, (3) the atmosphere containing a minimum of one atmosphere of steam with 6% preexisting hydrogen, (4) steam driving pressure of about 12 MPa, (5) hydrogen (preexisting plus that produced during the HPME) not to exceed the amount obtained from 75% zirconium oxidation, (6) the maximum bulk gas temperature not to exceed 1000 K during the test, (7) a closed RPV annular gap, and (8) a dry containment (no water on the basement or reactor cavity floors). In addition, the TRG requested additional data on hydrogen production and combustion with an effort to focus on earlier time sampling ($\approx$3 s after the HPME initiation) with more sampling locations.

The choice for the 56 cm NPP scale equivalent exit hole was based on scaling the exit hole size (9.8 cm) from the IET-10 test. The melt composition and steam driving pressure had to be different from those used in the 1:6 scale tests to meet the constraints imposed on total hydrogen and bulk gas temperature. The steam driving pressure was reduced by about 2 MPa to decrease the total number of moles. Chromium was not used in the melt simulant. Omitting chromium from the melt and reducing the moles of steam driving gas were based on two-cell equilibrium (TCE) model [Pilch 1991] predictions to meet the target values for total hydrogen and maximum bulk gas temperature. Note that omitting chromium also meant the absence of chromium oxidation energy added to the melt during the steam reaction.

The experiments were conducted for five primary purposes: (1) to measure the pressure load on the containment containing prototypic subcompartment structures, (2) to investigate the amount of hydrogen combustion due to a HPME into a prototypic steam/air/H_2 atmosphere, (3) to investigate the effect of an annular gap between the RPV and the reactor support skirt, (4) to measure posttest debris distribution in a containment model, and (5) to provide data from prototypic, large-scale experiments for validation of DCH models.

2.0 Experiment Description

2.1 The 1:6 Scale Tests in the Containment Technology Test Facility (CTTF)

Figure 2.1 is a composite view of the CTTF vessel, the HPME delivery system, and the 1:6 scaled Surry NPP subcompartment structures used in the IET-9, IET-10, and IET-11 experiments. The HPME delivery system is inside the containment vessel. Previous integral effects tests performed in the Surtsey vessel [Allen et al. 1992b-g; Allen et al. 1993a,b] were conducted with 1:10 linear scale models of the primary structures in the Zion Nuclear Generating Station; however, the HPME system was outside of the Surtsey vessel.

Table 2.1 is a listing of the instrumentation used in the IET experiments, including the channel number, type, purpose, and location of each instrument. The circled numbers in Figures 2.2 through 2.16 correspond to the channel numbers in the data acquisition system listed in Table 2.1. Instrumentation changed slightly as the IET experiments progressed. Table 2.1 and the associated figures list the instruments used in the last few IET experiments.

The reinforced-concrete containment model was constructed by United Engineers and Constructors, Inc., to a design pressure of 46 psig in accordance with Section III, Division 1 and 2 of the American Society of Mechanical Engineers (ASME) Boiler and Pressure Vessel code. The inside diameter of the model is 6.7 m with a total height of 10.1 m. The cylinder wall is 0.247 m thick, and the dome wall is 0.178 m thick. This model has #4 (1.27 cm diameter) reinforcing bar for the primary reinforcing. The cylinder wall contains two layers of meridional, four layers of circumferential, and two layers of diagonal reinforcing steel. As these layers approach the apex of the dome, some layers are reduced in response to changes in the geometry and loading. The containment also has a steel liner on the inside surface that is 1.58 mm thick along the base and cylinder wall and 2.12 mm thick along the interior of the dome that is attached to the concrete by headed studs. Two equipment hatches, two airlocks, constrained penetrations, and several piping penetrations are also included in the containment model. All materials used in constructing the model have structural characteristics that are the same, or are as nearly the same as possible, as those of actual containment building materials. The containment had an empty volume of about 302 m^3. Construction of the model was completed in 1987 and was statically pressure tested to 1.08 MPa [Horschel 1992].

The $1/6^{th}$ scale containment model was modified for the IET tests. A 1.5-m diameter (5 ft) access penetration was constructed in the side of the containment model. The penetration was designed for 1.12 MPa with a safety factor of 4; the design calculations were performed assuming no strength from the reinforced concrete. The access penetration allows a crucible loaded with thermite to be moved into the containment. In addition, a 0.5-m rupture disk (1.14 MPa at 100°C) was installed in the containment vessel. Numerous flanges on the vessel have been modified to allow steam, noncondensible gas, water, electrical, and video service into the vessel.

The cavity and biological shield (Figure 2.2) used in the 1:6 scale IET tests were designed to withstand internal pressures of 3.4 MPa with a safety factor of 4. The RPV and support skirt are contained in the biological shield. The RPV is modeled with a melt generator consisting of a steel pressure barrier, a cast MgO crucible, a thin steel inner liner, and a crucible support (RPV side wall). The crucible support has six projections simulating the hot and cold leg loop nozzles. The melt generator/crucible has a hemispherical bottom head containing a graphite limitor plate with an exit hole to simulate the ablated hole in the RPV bottom head that would be formed by ejection of an instrument guide tube

and hole ablation in a severe NPP accident. In addition, a control rod drive missile shield (not shown in Figure 2.2) was modeled and placed over the RPV at the seal table room ceiling level in the IET-10 and IET-11 experiments.

One of the objectives of the IET-11 DCH experiment was to understand the role of the RPV insulation in mitigating debris/gas flow through the annular gap between the RPV and the reactor support skirt. The annular gap (0.02 m^2 flow area) provides a direct, open passageway from the reactor cavity sump to the operating deck and dome regions. The scaled, reflective metal insulation was manufactured by TRANSCO, Inc., who designed and manufactured the original insulation for the Surry NPP. Prototypic, stainless steel (SS) materials were used; however, there were some unavoidable compromises in geometric details, which are described in the paragraphs below.

The Surry NPP insulation consists of 123 stainless steel panels. Each panel was constructed with three layers of SS backing (24-gage inner layer, 26-gage middle layer, and 22-gage outer layer). The total width of a panel was 7.6 cm, with four SS crumpled foils (each foil was 0.005 cm thick) between each layer (for a total of eight foils). The Surry NPP insulation was estimated to weight approximately 4400 kg.

The 1:6 scaled insulation was constructed with an inner and outer layer of 28 gage SS, with two crumpled SS foils (each foil was 0.005 cm thick). The two foils approximately preserved the foil density between the backings. The panels had a thickness of 1.2 cm. This width was chosen to occlude the same fraction of the gap flow area as in the NPP. The panels were spot-welded together and the entire assembly was fitted tightly to the RPV model, completely covering the bottom and side of the model to just below the RPV nozzles. The scaled insulation weighed 29 kg. The scale factor (on a mass basis) was 5.33.

Figure 2.3 shows an isometric view of the subcompartment structures and RPV model inside th CTTF vessel. The subcompartment structures included 1:6 linear scale models of the crane wall, the biological shield wall, the cavity and incore instrument tunnel, the operating deck, the RHR platform and heat exchangers, and the seal table room and seal table. The seal table was not installed in the IET-9 experiment. The seal table was constructed from 14 gage (1.9 mm thick) steel sheet and was mounted about 6 mm above the floor opening using six steel brackets. Two levels of steel grating were used as catwalks and were mounted along the containment walls and above the structures. Figures 2.4 through 2.8 are plan views of the CTTF vessel, showing the orientation and location of the instruments at five different levels. The vessel was partitioned into two 180° halves, a cavity side (CS) and a five-foot door side (DS), with the partition line drawn between Hatch A and Hatch B for ease of debris recovery (Figures 2.5 and 2.7).

The trough (0.3 m below the basement floor) between the containment wall and the crane wall (Figures 2.1, 2.3, and 2.4), which had previously existed in the IET-9 and IET-10 experiments, was filled with concrete prior to the IET-11 experiment, reducing the freeboard volume by 4 m^3. The trough was filled to allow condensate levels of water to be placed uniformly on the basement floor. The IET-11 freeboard volume was 282 m^3. Filling the trough also reduced the vessel leak rate from $\approx$8 psi/hr to $\approx$3 psi/hr.

To obtain a prototypic steam environment in the CTTF vessel at the start of the experiments, the inside vessel wall and interior structures were heated above the saturation temperature. This was accomplished with two liquid propane (LP) straight fire-sleeve burners, each rated at 2,000,000 BTU/hr. The flames were directed toward the basement floor through two 20-cm penetrations and pipe flues mounted on the 1.5-m access door. The vessel bulk gas and structure heatup was accomplished after operating both burners for 22-36 hours. After the heatup, the vessel was purged with fresh air to remove hydrocarbon byproducts.

The containment vessel was sealed after the vessel purge was completed. The steam accumulator tank was pressurized to ≈14 MPa with superheated steam. Steam, air, and hydrogen were added to the containment model to obtain the desired atmosphere initial conditions. In IET-9, some steam condensed in the containment model. There was no condensation in the containment in IET-10. In IET-11, condensate water was added to the basement floor. Then, the background gas grab samples were taken and the mixing fans were turned off. The thermite ignition sequence commenced after the prescribed initial atmospheric conditions were reached. The iron/alumina/chromium thermite mixture was ignited remotely with a braided wire fuse placed on top of the compacted thermite. After the thermite was ignited, the pressure in the crucible rapidly increased. This pressure increase verified that the thermite reaction had started and signaled the operator to fail the burst diaphragm separating the steam accumulator tank and the molten thermite in the melt generator. This brought superheated steam into contact with the molten thermite. Upon contacting and failing a fusible brass plug at the bottom of the crucible, the molten thermite in the crucible was expelled by high-pressure steam into the cavity.

Zero time was set by the data acquisition system as the time at which the melt failed the brass plug and entered the cavity. This event was signaled by breakwires (channels 10 and 11 in Figures 2.2 and 2.3) located at the melt plug exit.

2.2 The 1:10 Scale Test in the Surtsey Test Facility

Figure 2.9 is a composite view of the Surtsey vessel, the HPME delivery system, and the 1:10 scale Surry NPP subcompartment structures used in the IET-12 experiment.

The Surtsey vessel is an ASME-approved steel pressure vessel with an internal volume of 103 m^3, which makes it slightly over-scaled (for a 1:10 linear scale) compared to most nuclear RCBs. It has a cylindrical shape with removable, dished heads attached to both ends and is 3.6 m in diameter by 10.3 m high. The Surtsey vessel has a maximum allowable working pressure of 1 MPa at 260°C, but has a burst diaphragm installed to limit the pressure in the vessel to less than 0.9 MPa. It is supported approximately 2 m off the ground by a structural steel framework with its longitudinal axis oriented vertically. A total of twenty 30.5 cm (12 inch) and 61 cm (24 inch) instrument penetration ports exist at six different levels around the perimeter of the vessel.

The Surtsey vessel was modified for the IET-12 test. A false floor was installed in the middle of Surtsey between levels 3 and 4. The false floor was constructed using steel plate welded to the vessel walls and supported with I-beams mounted vertically in the vessel. The free board volume above the false floor was 59.1 m^3. The false floor was designed for 1.03 MPa at 260°C with a safety factor of 4. Numerous flanges on the vessel have been modified to allow steam, noncondensible gas, water, electrical, and video service into the vessel.

Because of space constraints and safety regulations, the 1:10 scale Surry structures were built on a steel-reinforced concrete platform outside the Surtsey vessel. Prior to running the IET-12 test, the crucible was loaded with thermite and was bolted to the RPV support skirt. The entire assembly was then lifted into the Surtsey vessel through the open upper head using an overhead crane. After final service connections were made and instrumentation checkouts were performed, the upper head of Surtsey was lifted into place and bolted down. With the 1:10 scale Surry structures in place, the freeboard volume above the false floor was reduced to 51.0 m^3.

The cavity and biological shield used in the IET-12 test was a 1:10 scaled version of that shown in Figure 2.2, with two exceptions: (1)

the melt generator inlet pipe had a 10-cm diameter, and (2) the graphite limitor plate in the hemispherical bottom head of the RPV model had a 5.6-cm exit hole.

Figure 2.10 shows an isometric view of the subcompartment structures and RPV model inside the Surtsey vessel. The subcompartment structures included 1:10 linear scale models of the crane wall, the biological shield wall, the control rod drive mechanism missile shield, the cavity and incore instrument tunnel, the operating deck, the RHR platform and heat exchangers, and the seal table room and seal table. The seal table was constructed from 18 gage (1.2 mm thick) steel sheet and was mounted about 4 mm above the floor opening using six steel brackets. Figure 2.11 gives an overhead view of the Surtsey vessel showing the port locations above the false floor at levels 4, 5, and 6. Figures 2.12 through 2.16 are plan views of the Surtsey vessel, showing the orientation and location of the Surry structures and instruments at five different heights. Figure 2.13 shows the vessel partitioned into two 180° halves, a cavity side (CS) and a door side (DS), similar to the 1:6 scale experiments conducted in the CTTF.

To obtain a prototypic steam environment in the Surtsey vessel at the start of the IET-12 experiment, the inside vessel wall and interior structures were heated above the saturation temperature. This was accomplished with two liquid propane (LP) straight fire-sleeve burners, each rated at 2,000,000 BTU/hr. One burner directed flames above the false floor toward the structure basement floor through a 20-cm penetration at level 4. Another burner directed flames into the lower level of Surtsey below the false floor; this provided some degree of temperature regulation of the gas in the upper level after the burner at level 4 was turned off and removed. The vessel bulk gas and structure heatup was accomplished after operating both burners for about 24 hours. After the heatup, the vessel was purged with fresh air for ten minutes to remove hydrocarbon byproducts.

The Surtsey vessel was sealed after the vessel purge was completed. Steam and hydrogen were added to Surtsey to obtain the desired atmosphere initial conditions. The steam accumulator tank was pressurized to ≈ 12 MPa with superheated steam. The background gas grab samples were taken (following a two minute sample line purge) and the mixing fans were turned off. The thermite ignition sequence commenced after the prescribed initial atmospheric conditions were reached. The iron/alumina thermite mixture was ignited remotely with a braided wire fuse placed on top of the compacted thermite. After the thermite was ignited, the pressure in the crucible rapidly increased. This pressure increase verified that the thermite reaction had started and signaled the operator to fail the burst diaphragm separating the steam accumulator tank and the molten thermite in the melt generator. This brought superheated steam into contact with the molten thermite. Upon contacting and failing a fusible brass plug at the bottom of the crucible, the molten thermite in the crucible was expelled by high-pressure steam into the cavity.

2.3 Geometry and Initial Conditions: The Design Basis

The geometry and initial conditions selected for the Surry SNL/IET experiments were guided by the pump seal LOCA sequence initiated by a station blackout in the Surry NPP. The stated goal was to perform integral effects tests in geometrically scaled structures with initial conditions generally selected to be well within the expected range of full-scale plant behavior.

Table 2.2 compares some of the key geometric features in the Surry NPP, the 1:6 scale CTTF facility, and the 1:10 scale Surtsey facility. The following sections discuss the rationale and potential compromises in selecting these conditions and their expected impact on the test results.

2.3.1 Facility Geometry

A stated goal was to perform counterpart experiments at two different physical scales with geometrically scaled mockups of the Surry plant. The 1:6 and 1:10 scale counterpart experiments were conducted at SNL so that maximum advantage could be taken of already existing facilities for performing DCH experiments. Hardware constraints, however, required some compromise to the extent that the experiment facilities could match Surry. As a priority, similarity between the two test facilities was sought, even if it meant sacrificing some similarity with the full-scale plant.

The hole diameter plays a key role in determining the rate of RCS blowdown, which in turn controls the rate and magnitude of melt dispersal from the cavity. The scenario considered here is a penetration-type failure of the lower head. Such a failure could occur by the ejection of an incore instrument guide from the lower head or by melt flow into the guide tube causing the tube to rupture outside the lower head. The initial size of such a failure is ~0.025 m, but melt flow through the hole will cause it to ablate to a much larger size. A final hole size of ~0.4 m is computed with the approximate ablation model given in Pilch and Allen.[1] The calculation was carried out using the melt mass (scaled to Surry, i.e., 43 mtonnes), and composition specified in the SASM document [Zuber et al. 1991].

The ablation process could not be reliably simulated in the experiments because the initial hole size would have to be extremely small (i.e., ~2.5 mm at 1:10 scale) causing an unprototypic tendency for the melt to freeze in the hole. Consequently, it was decided to match the initial hole size in the experiment to the final hole size predicted in the reactor case. Ablation was minimized in the experiment using a graphite plate with a circular hole that was linearly scaled to the expected final hole size of NPP scale. Molten iron can dissolve graphite and thus, the final hole size reported is slightly larger than the initial hole size.

There is an annular gap around the RPV in the Surry plant that could allow some melt to be dispersed directly to the upper dome rather than into the subcompartments outside the cavity exit. The annular gap is partially filled with reflective metal insulation that is attached to the RPV. Testing with an annular gap was not feasible in the Surtsey test facility because of the difficulty of manufacturing 1:10 scale reflective metal RPV insulation. Therefore, the open annular gap tests were performed in the CTTF at 1:6 scale.

Certain details were neglected in the cavity model. In particular, the incore instrument guide tubes and their supports were not modeled. The guide tubes and their supports were simulated in the HIPS-10S experiment [Allen et al. 1990], where they were forcibly ejected from the cavity by the dispersal process. The TRG believed that neglecting these structures would have minimal impact on DCH loads.

2.3.2 Melt Mass and Composition

The corium mass and composition for the scaled Surry application are taken from the SASM effort [Zuber et al. 1991] which was based on the Surry NPP core. The experiments employ thermite as a high temperature, chemically reactive simulant for corium. Table 2.3 compares the composition of thermite and corium, and Table 2.4 compares their material properties.

The SASM scaling study addressed RPV and cavity phenomena, but it stopped short of extending the analysis to the containment building. Geometric scaling of the melt mass for the

[1] M. M. Pilch and M. D. Allen, Dec. 1990, A Scaling Methodology for Direct Containment Heating with Application to the Design and Specification of an Experiment Program for Resolving DCH Issues, SAND91-2784, to be published, Sandia National Laboratories, Albuquerque, NM.

experiment is not strictly applicable because of material property differences between corium and thermite. The amount of thermite used in the experiments was selected so that the experiments would have a similar potential for pressurization as the reactor application. The potential for pressurization is obtained by allowing airborne melt to come to thermal equilibrium with the atmosphere; a single-cell equilibrium model energy balance was used to determine this potential for the Surry IET experiments.

Simple calculations based on the actual IET initial conditions were performed to determine the amount of energy that might be added to the CTTF or Surtsey containment vessel atmosphere by the steam blowdown, exothermic steam/metal chemical reactions, debris/gas heat transfer, and hydrogen combustion. The total amount of energy was used to calculate an upper limit to the possible pressure increase in the containment vessel, $\Delta P_{equilibrium}$. The result could then be compared to the measured peak pressure increase, $\Delta P_{measured}$, to determine the total DCH efficiency, $\eta = \Delta P_{measured}/\Delta P_{equilibrium}$, in the IET experiments.

Derivation of the single-cell model has been documented by Pilch [1991]. The resulting model is given here. Thermal equilibrium between airborne debris and the Surtsey atmosphere yields a simple, bounding expression for the DCH load,

$$\frac{\Delta U}{U^\circ} = \frac{\Delta P}{P^\circ} = \frac{\sum_i \Delta E_i}{U^\circ(1 + \psi)} , \qquad (1)$$

where

ΔU = total internal energy gained by the containment atmosphere,

U° = initial internal energy of the entire containment atmosphere,

ΔP = pressure rise in the containment resulting from the DCH event,

P° = initial containment pressure,

ΔE_i = maximum energy that could be added to the containment atmosphere by the i^{th} process, where the i processes are steam blowdown, debris/gas heat transfer, debris oxidation by steam in an otherwise inert atmosphere, and hydrogen combustion, and

ψ = heat capacity ratio.

The heat capacity ratio appears because the debris still carries sensible heat that is not available for containment pressurization at thermal equilibrium between airborne debris and the atmosphere. The heat capacity ratio is defined by

$$\psi = \frac{N_d C_d}{(N^\circ + N_b) C_v} \qquad (2)$$

where

N_d = number of g·moles of debris participating in DCH,

C_d = molar heat capacity of debris,

N° = number of gas g·moles initially in the containment,

N_b = number of gas g·moles added to the containment by RCS blowdown, and

C_v = molar heat capacity of the containment atmosphere.

The g·moles of debris participating in DCH can be expressed in terms of the initial charge of thermite by

$$N_d = f_{eject}\, f_{disp} \frac{M_d^\circ}{MW_d} \qquad (3)$$

where

f_{eject} = fraction of the initial charge that is ejected from the melt generator to the cavity,

f_{disp} = fraction of the melt ejected into the cavity that is subsequently dispersed into the containment,

M_d° = initial mass charge of thermite, and

MW_d = the effective molecular weight of thermite.

The initial internal energy of the atmosphere is computed from

$$U^\circ = N^\circ C_v T^\circ \qquad (4)$$

where

T° = initial temperature of the containment atmosphere.

Equations (1), (2), and (3) show how the containment pressurization depends on the amount (moles) of molten material participating in DCH. Table 2.5 shows input parameters for the reactor application and the counterpart experiments. The melt mass selected for the experiments ensured that the potential for pressurization was preserved between the experiments and the reactor application.

Blowdown of the steam accumulator adds both mass and energy to the containment atmosphere. The maximum amount of energy that the accumulator can contribute to Surtsey vessel pressurization is given by

$$\Delta E_b = \frac{P_{acc}^\circ V_{acc}}{\gamma - 1}\left[1 - \frac{P^\circ}{P_{acc}^\circ}\right], \qquad (5)$$

where

P_{acc}° = equilibrium pressure of the accumulator/melt generator system just prior to plug failure,

V_{acc} = total free volume of the accumulator and melt generator, and

γ = ratio of specific heats.

The term preceding the brackets represents the total internal energy of the accumulator, while the bracketed term represents the fraction of this total that is convected into the containment.

Molten debris dispersed from the reactor cavity carries both latent and sensible heat that can be transferred to the atmosphere. The maximum energy source associated with debris thermal energy,

$$\Delta E_t = N_d \Delta e_t \,, \qquad (6)$$

is equal to the amount of dispersed debris, N_d, times the specific molar internal energy of the debris, Δe_t.

The energy source due to debris oxidation,

$$\Delta E_r = N_d \Delta e_r \,, \qquad (7)$$

is equal to the amount of debris participating in DCH times the specific molar oxidation energy of the debris, Δe_r, assuming all the metals react with steam.

The energy source due to hydrogen combustion is

$$\Delta E_{H_2} = N_{H_2,tot}\,\Delta e_{H_2} = (N_{H_2,pre} + \nu_{H_2} N_d)\,\Delta e_{H_2} \qquad (8)$$

where

$N_{H2,pre}$ = g·moles of preexisting hydrogen in the containment atmosphere prior to the DCH event,

ν_{H2} = the effective stoichiometric coefficient for debris oxidation, 0.740 g·moles-H_2/g·moles-debris, and

Δe_{H2} = the specific combustion energy for hydrogen, 0.242 MJ/g·mole-H_2.

The second term in the brackets, $\nu_{H2}N_d$, represents the total amount of hydrogen that can be produced from complete oxidation of the metallic constituents of the dispersed debris. There is sufficient steam in the accumulator to achieve complete oxidation of debris.

Table 2.6 shows the potential pressurization of the containment caused by the fractional contribution of RCS blowdown energy, debris thermal energy, debris oxidation energy, and hydrogen combustion energy. The potential contribution of debris oxidation is under-scaled in the experiments relative to the reactor application.

2.3.3 Initial Conditions for the IET-9 Experiment

The inside vessel wall and interior structures were heated above saturation temperature to obtain a prototypic steam environment in the CTTF vessel at the start of the IET-9 experiment. This was accomplished with two liquid propane (LP) straight fire-sleeve burners. The vessel bulk gas and structure heatup was accomplished after operating both burners for 22 hours. The vessel was purged with fresh air for one hour to remove hydrocarbon byproducts.

The containment vessel was sealed after the vessel purge was completed, and a charging process (using steam, air, and hydrogen) commenced to obtain the desired atmosphere initial conditions. It was necessary to add air because of small, preexisting leaks in the vessel inner steel liner. The vessel leak rate was about 8 psi/hour. Figure 2.17 gives the containment vessel pressure during the gas charging process prior to the HPME initiation, and compares gas temperature to saturation temperature for the 0.091 MPa steam partial pressure that existed in the containment at the HPME (0.1352 MPa x 76.24 mol.%). Figure 2.18 shows the total moles of gas (steam plus noncondensibles) in the vessel while charging, along with the total moles of noncondensibles, total moles of hydrogen, and total moles of air. Figure 2.18 also shows the total moles of steam added, the moles leaked, and the moles of steam that condensed during the charging process. Figure 2.19 gives the time-dependent noncondensible gas concentrations in the vessel during the charging process. The charging process was completed at 155 minutes and accumulator pressurization commenced. The steam accumulator tank was pressurized to ≈14 MPa with superheated steam. The following is a synopsis of the charging process in IET-9.

Time (min)	Comments
1	Saturated steam was added for a total of 155 minutes from the portable boiler at a steam rate of 0.24326 kg·mole/min. The total steam added was 37.7053 kg-mole.
30	Six bottles of air (1.7676 kg·moles) were added over a 15 min interval (0.2946 kg ·mole in a 44L air cylinder at 2015 psig).

72	Four bottles of air (1.1784 kg•moles) were added over a 15 min interval.
72	Two bottles of hydrogen (0.4982 kg•moles) were added over a 15 min interval (0.2491 kg•mole in a 44L hydrogen cylinder at 2015 psig).
86	The air and hydrogen gas bottle valves were closed.
112	A partial air bottle (0.12674 kg•moles) was added over a 1 min interval.
112	A partial hydrogen bottle (0.0623 kg•moles) was added over a 1 min interval.
113	All hydrogen and air additions stopped.
155	Steam additions stopped.
198	The background gas samples were taken, and then the thermite was ignited.

Table 2.7 lists the initial conditions of the IET-9 experiment. The initial vessel gas temperatures for IET-9, IET-10, IET-11, and IET-12 (listed in Table 2.7) were determined from a mole-average bulk gas temperature; the derivation of the equation for calculating the mole-average bulk gas temperature is given in Section 4.6.5. Due to the 5.1 hour interval between securing the LP gas burners and HPME initiation, the CTTF containment interior vessel wall had cooled to 372 K and the basement and cavity floor had cooled to 364 K. These locations were near or below the saturation temperature of 370 K. The temperatures of the interior structures was approximately 399 K and remained above saturation temperature. A water film due to condensed steam (estimated to be ≈372 kg) existed on the containment vessel wall, basement trough, and basement floor. Most of the water would have collected in the trough. The water height in the trough would have been ≈3 cm (10% of the trough volume).

2.3.4 Initial Conditions for the IET-10 Experiment

Condensation of steam occurred during the initial condition setup for IET-9; this necessitated a change in the procedure for IET-10. In IET-10, the vessel bulk gas and structure heatup was accomplished after operating both LP burners for about 36 hours. The longer heatup produced hotter structures which prevented steam from condensing. After the heatup, the vessel was purged with fresh air for thirty minutes to remove hydrocarbon byproducts. Also, the test procedure sequence was changed; only 2.6 hours was needed to reach HPME initiation after turning off the LP burners, which reduced the vessel cool down.

In IET-10, there was carbon monoxide gas (≈0.5 mol.%) in the containment model prior to the test. This is important since CO is combustible. In all DCH tests, small amounts of CO and CO_2 are produced by debris/concrete interactions. The initial CO concentration in IET-10 was due to an incomplete purge of the CTTF vessel after the 36 hour heatup. The vessel and the interior structures were heated using LP gas fire coil burners, which produced some CO and CO_2 as byproducts. The vessel purge with five volumes of fresh air normally would have removed the CO (and also reduced bulk gas temperature). The vessel purge was accomplished with the use of a 1000 scfm blower supplying fresh air into the vessel. Three high-speed mixing fans inside the vessel mixed the vessel atmosphere. The mixing fans were also used during the vessel heatup to increase the convection of heat from the hot gas to the cold structures. Near the end of the heatup the mixing fans failed. This resulted in the incomplete purge

of the vessel and a slight superheat (42 K) of the bulk gas at HPME initiation.

The containment vessel was sealed after the vessel purge was completed. The steam accumulator tank was pressurized to ≈14 MPa with superheated steam. A charging process (using steam, air, and hydrogen) was then commenced to obtain the desired atmosphere initial conditions. Figure 2.20 gives the containment vessel pressure during the gas charging process prior to the HPME initiation, and compares gas temperature to the saturation temperature of steam at a partial pressure of 0.086 MPa. Figure 2.21 shows the total moles of gas (steam plus noncondensibles) in the vessel while charging, along with the total moles of noncondensibles, total moles of hydrogen, and total moles of air. Figure 2.21 also shows the total moles of steam added, the total gas moles leaked, and the moles of steam that condensed during the charging process. The vessel leak rate was about 8 psi/hour. Figure 2.22 gives the time-dependent noncondensible gas concentrations in the vessel during the charging process. The charging process was completed at 75 minutes and the thermite ignition sequence commenced.

The following is a synopsis of the charging process in IET-10.

Time (min)	Comments
1	Saturated steam was added for a total of 35 minutes from the portable boiler at a steam rate of 0.243 kg•mole/min. The total steam add was 8.51 kg-mole.
35	The steam addition was stopped.
36	1.62 bottles of hydrogen (0.4036 kg•moles) were added over a 4-min interval.
40	The hydrogen addition was stopped.
40	Twelve bottles of air (3.5352 kg•moles) were added over a 24-min interval.
64	The air add was stopped.
74	Steam (0.24326 kg•moles) was added for one minute.
75	The steam addition was stopped.
75	The background gas samples were taken and then the thermite was ignited.

Table 2.7 lists the initial conditions of the IET-10 experiment. Due to the relatively short interval (2.6 hours) between securing the LP gas burners and HPME initiation, the CTTF containment interior vessel wall and the Surry model structures remained hot, with the containment liner at about 385 K, the crane wall at 412 K, and the basement floor at 377 K. The saturation temperature of steam was 368 K, and thus, no steam condensed on the vessel or structures.

2.3.5 Initial Conditions for the IET-11 Experiment

The initial condition setup for IET-11 was similar to that for IET-10. The vessel atmosphere and the interior structures were heated for 36 hours using LP gas fired coil burners, which produced some CO and CO_2 as byproducts. After the heatup was completed, the vessel was purged (for thirty minutes) with five volumes of fresh air. The purging process successfully removed the CO and CO_2 contaminants and reduced the bulk gas temperature. The vessel was purged by blowing fresh air into the vessel at 1000 scfm. Three high-speed mixing fans inside the vessel mixed the vessel atmosphere. The mixing fans were also used during the vessel heatup to increase the convection of heat from the hot gas to the cold structures. After the test, it was discovered that there was a small leak in one of

the pneumatic mixing fans. This resulted in an additional air source of about 0.04 kg-mole/min to the vessel when the mixing fans were operating. This extra air source increased oxygen levels to 13%, which was greater than the target value of 8%.

The containment vessel was sealed after the vessel purge was completed. The steam accumulator tank was pressurized to ≈14 MPa with superheated steam. A charging process (using steam, air, and hydrogen) was then commenced to obtain the desired atmosphere initial conditions. Figure 2.23 gives the containment vessel pressure during the gas charging process prior to the HPME initiation, and compares gas temperature to saturation temperature for the steam at a partial pressure of 0.075 MPa.

Figure 2.24 shows the total moles of gas (steam plus noncondensibles) in the vessel while charging, along with the total moles of noncondensibles, total moles of hydrogen, and total moles of air. Figure 2.24 also shows the total moles of steam added, the total gas moles leaked, and the moles of steam that condensed during the charging process. The trough in the floor between the crane wall and the vessel wall was filled with concrete to allow uniform levels of water (simulating condensate levels) on the basement floor. This reduced the vessel leak rate to about 3 psi/hour. It also reduced the vessel volume by 4 m^3.

Figure 2.24 shows the vessel pressurization with steam and hydrogen for the IET-11 experiment. Steam was added to the vessel between 25 and 45 minutes, and then hydrogen was added between 45 and 48 minutes. Bottled air was added to the vessel between 48 and 71 minutes. Condensate levels of water were added to the basement floor between 78 and 79 minutes, and the background gas grab samples were taken at 82 minutes. The leak in the mixing fan line added air to the vessel during the entire pressurization sequence until the mixing fans were turned off at 82 minutes. There was an 18 minute delay, due to a quality control check of one of the systems, before the thermite was ignited at 100 minutes. This delay resulted in the background gas grab bottles not containing representative samples of the vessel atmosphere at the HPME initiation. Basement water vaporization created additional steam in the vessel, as indicated by the increase in vessel pressure after the water addition. This additional steam source caused the noncondensible gas fraction to decrease during the 18 minute delay to $f_{NC} = 0.68$; the noncondensible fraction was still higher than the target value of 0.43. Gas mass spectroscopy analysis of the background gas samples yielded results that closely matched those predicted by the charging process calculations at 82 minutes. Therefore, the charging process calculations were used to determine the vessel background gas concentrations at the start of the HPME.

Figure 2.25 gives the time-dependent noncondensible gas concentrations in the vessel during the charging process. The charging process was completed in 72 minutes. The hot condensate water (703 kg at 373 K) was placed on the basement floor to a height of 2.4 cm. The background gas grab samples were taken at 82 minutes and the mixing fans were turned off. The thermite ignition sequence commenced 100 minutes after the start of the charging process.

The following is a synopsis of the charging process in IET-11.

Time (min)	Comments
1	Vessel pressure was at 0.1 MPa and rising due to an air leak in the mixing fan.
25.9	Saturated steam was added for a total of 19.1 minutes from the portable boiler. The total steam add was 4.64 kg-mole.
45	The steam addition was stopped.

45	Two bottles of hydrogen (0.4982 kg·moles) were added over a 4-min interval.
49	The hydrogen addition was stopped.
49	Nine bottles of air (2.6514 kg·moles) were added over a 22-min interval.
71	The air addition was stopped.
79	The basement condensate water was added.
82	The background gas samples were taken and the mixing fans were turned off.
100	The thermite was ignited.

Air leaked into the containment model from the mixing fan leak and from air designed to cool the pyrometer. The mixing fan leak added air to the containment at a rate of 0.039 kg·moles/min, between 0 and 83 minutes. The pyrometer cooling added air to the containment at a rate of 0.001 kg·moles/min, between 0 and 100 minutes.

Table 2.7 lists the initial conditions of the IET-11 experiment. Due to the relatively short interval (3.4 hours) between securing the LP gas burners and HPME initiation, the CTTF containment interior vessel wall and the Surry model structures remained hot, with the containment liner near the top of the vessel at about 394 K and the crane wall at 409 K. These locations were above the 365 K saturation temperature. No steam condensed on the vessel or structures. The containment liner near the bottom of the vessel was at 375 K and the basement floor was 364 K when the saturated water was added to the basement floor.

2.3.6 Initial Conditions for the IET-12 Experiment

In IET-12, the Surtsey vessel atmosphere and the interior structures were heated for 24 hours using LP gas fired coil burners, which produced some CO and CO_2 as byproducts. After the heatup was completed, the vessel was purged with five volumes of fresh air. The purging process successfully removed the CO and CO_2 contaminants and reduced the bulk gas temperature. The vessel was purged by blowing fresh air into the vessel at 1000 cfm. Two high-speed mixing fans inside the vessel mixed the vessel atmosphere. The mixing fans were also used during the vessel heatup to increase the convection of heat from the hot gas to the cold structures. The Surtsey vessel was sealed after the vessel purge was completed. A charging process (using steam and hydrogen) was then commenced to obtain the desired atmosphere initial conditions. Figure 2.26 gives the containment vessel pressure during the gas charging process prior to the HPME initiation, and compares gas temperature to saturation temperature for steam at a partial pressure of 0.093 MPa.

Figure 2.27 shows the total moles of gas (steam plus noncondensibles) in the vessel while charging, along with the total moles of noncondensibles, total moles of hydrogen, and total moles of air. Figure 2.27 also shows the total moles of steam added, the total gas moles leaked, and the moles of steam that condensed during the charging process. Steam (2.19 kg·moles) was added from 0 to 9 minutes. Hydrogen (0.16 kg·moles) was then added from 9 to 10 minutes, which completed the charging process. An aspirated thermocouple valve was inadvertently left open during the charging process and was closed at 14 minutes. The increased leak rate with the valve open (0.04 kg·moles/min versus 0.004 kg·moles/min) reduced the noncondensible gases inside the vessel slightly below the target values.

Figure 2.28 gives the time-dependent noncondensible gas concentrations in the vessel during the charging process. The charging process was completed in 10 minutes. The noncondensible gas fraction, f_{NC}, is an important quantity for analyzing the gas grab samples. The vessel leakage caused f_{NC} to be slightly lower than it should have been in IET-12 (0.42 versus the target value of 0.48). The vessel leakage decreased oxygen levels to 7%, which was less than the target value of 9%.

The steam accumulator tank was pressurized to ≈12 MPa with superheated steam from 18 minutes to 30 minutes. The background gas grab samples were taken at 32 minutes (following a two-minute sample line purge) and the mixing fans were turned off. Gas mass spectroscopy analysis of the background gas samples yielded results that closely matched those predicted by the charging process calculations at 32 minutes. The thermite ignition sequence commenced 33 minutes after the start of the charging process.

The following is a synopsis of the charging process in IET-12.

Time (min)	Comments
1	Saturated steam was added for a total of 9 minutes from the portable boiler. The total amount of steam added was 2.19 kg • moles.
9	The steam addition was stopped.
9	0.695 bottles of hydrogen (0.1731 kg • moles) were added over a 1-min interval.
10	The hydrogen addition was stopped.
14	The open aspirated thermocouple valve was closed.
32	The background gas samples were taken and the mixing fans were turned off.
33	The thermite was ignited.

Table 2.7 lists the initial conditions of the IET-12 experiment. Due to the relatively short interval (1.6 hours) between securing the LP gas burners and HPME initiation, the Surtsey interior vessel wall and the structures remained hot, with the containment walls at about 385 K and the crane wall at 410 K. The basement floor was 396 K. These locations were above the 370 K saturation temperature, and thus, no steam condensed on the vessel or structures.

2.4 Measurements and Instrumentation

The most significant variables measured in the Surry DCH IET experiments were (1) the increase in pressure and temperature in the CTTF and the Surtsey vessel, (2) the cavity pressure, (3) the number of g • moles of hydrogen generated by the reaction of metallic debris with steam and water, (4) the number of g • moles of hydrogen burned, (5) the debris temperature, (6) the debris particle size, and (7) the mass and location of debris recovered from the Surtsey vessel. The instrumentation and techniques used to make these measurements are described in the sections below.

2.4.1 Pressure Measurements

Four pressure transducers were used to measure the pressure in the upper dome of the CTTF vessel and in the Surtsey vessel. In the CTTF facility, two transducers, channels 19 and 22 in Figure 2.8, with ranges of 0-1.38 MPa and 0-2.07 MPa, respectively, were mounted in construction penetration CP1. Two transducers, channels 20 and 21 in Figure 2.7, each having a range of 0-1.38 MPa, were mounted in instrumentation penetration P3. The four transducers were mounted in level 6 penetrations in the

Surtsey vessel (channels 19, 20, 21, and 22 in Figures 2.10 and 2.11). These transducers were mounted in tapped holes in penetration ports in the sides of the containment vessel. The tapped holes were filled with steel turnings to protect the sensing ends from direct impact with molten debris. Two pressure transducers with a range of 0-34.5 MPa were used to measure the gas pressure in the crucible above the thermite (channels 35 and 36). Pressure transducers with a range of 0-34.5 MPa were also used to measure the gas pressure in the burst diaphragms (channels 33 and 34) and in the steam accumulator (channel 31 and 32). Two pressure transducers with a range of 0-2.07 MPa were used to measure the gas pressure in the scaled reactor cavity (channels 23 and 24). Also, only in the 1:6 scale tests, pressure transducers with a range of 0-0.69 MPa were used to measure the gas pressure in the basement, RHR platform, and in the seal table room (channels 29, 25, and 27 in Figures 2.3, 2.5, 2.6, and 2.7). All of the transducers were metal diaphragm strain gauge-type pressure transducers (Precise Sensor, Inc., Monrovia, CA). The specified accuracy from the manufacturer for the pressure transducers is less than $\pm$ 0.50 percent at full-scale output. These instruments are routinely recalibrated at SNL against instruments traceable to the National Institute of Standards and Technology, and accuracies are always within the manufacturer's specifications. The frequency response is 22 kHz (16 μs rise time) for the 0-0.69 MPa range pressure transducers. The data acquisition system recorded data from the pressure transducers at a rate of 1400 data points per second per channel from thermite ignition to about 120 seconds following the HPME.

2.4.2 Temperature Measurements

The gas temperatures near the walls of the CTTF and Surtsey containment vessels were measured with two aspirated thermocouple assemblies. An aspirated thermocouple assembly consisted of three bare type-K thermocouples (0.127-mm wire) mounted in an anodized aluminum tube. Each tube was opened with a solenoid-operated valve that was actuated remotely by a signal from the breakwire under the melt plug immediately after the HPME transient. In the CTTF vessel, one assembly was installed through instrumentation port P3 (channels 13, 14, and 15 in Figure 2.7). The other thermocouple assembly was installed in construction penetration CP1 (channels 69, 70, and 71 in Figure 2.8). In the Surtsey vessel, one assembly was installed through a level 6 port (channels 13, 14, and 15 in Figures 2.10 and 2.11). The other thermocouple assembly was installed in a vessel upper head penetration (channels 69, 70, and 71 in Figures 2.10 and 2.11). Calculations by SNL have shown that the worst-case temperature underprediction by the thermocouple assemblies would be 13 percent at the beginning of the HPME event when the gas temperatures are low, and 6 percent at equilibrium when the gas temperatures have peaked.[2]

Three thermocouple arrays (channels 52 through 68 in Figures 2.3, 2.8, 2.9, 2.10, and 2.16) were installed in each vessel to measure bulk gas temperature above the operating deck. An array consisted of six type-K thermocouples vertically suspended from the dome to the operating deck. The thermocouples were equally spaced (1.22 m apart in CTTF and 0.61 m in Surtsey) on each array. All type-K thermocouples were made of 0.254-mm wire with a 1.6-mm sheath. The temperature range was 273 K to 1523 K. The maximum error using the manufacturer's calibration is $\pm$ 9.4 K at 1523 K with a 0.3-s time constant. The thermocouples had the sheath removed at the tip, exposing the junction to ensure a fast time response.

Four type-K thermocouples (channels 41, 42, 43, and 44 in Figures 2.3, 2.5, 2.10, and 2.12) were installed inside the basement about 7 cm below

[2]T. K. Blanchat, May 1992, "Aspirated Thermocouple Calculations," Letter Report to the U.S. Nuclear Regulatory Commission, Sandia National Laboratories, Albuquerque, NM.

the operating deck. Four type-K thermocouples (channels 45, 46, 47, and 48 in Figures 2.3, 2.6, 2.10, and 2.15) were installed in the annulus formed by the containment wall and the crane wall, midway between the basement ceiling and the top of the cranewall. These thermocouples measured the temperature of the gas as it flowed through the basement and behind the crane wall.

In the 1:6 scale tests, seven high-temperature tungsten-rhenium type-C thermocouples (channels 1 through 7 in Figures 2.3 and 2.5-2.7), comprised of 0.38-mm-diameter wire with a 1.6-mm-diameter stainless steel sheath, were installed. They were located at the RHR platform ceiling above and behind the cofferdam, at the RHR platform left and right side windows, below the seal table room ledge directly in front of the RHR platform, at the exit hole in the seal table room ceiling, on the seal table room back wall, and at the cofferdam exit. These thermocouples measured the temperature of the debris/gas as it exited the cavity and entered the subcompartment structures. The temperature range for the thermocouples was 273 K to 2593 K. The maximum error using the manufacturer's calibration is $\pm$ 25.9 K with a 0.9-s time constant. The type-C thermocouples were not used in the IET-12 experiment.

The temperature of the driving gas in the steam accumulator tank was measured using two type-K thermocouples (channels 75 and 76) that extended through the accumulator shell and were secured in place using pressure-tight fittings. Measurements from these thermocouples were important because the measured temperature and pressure in the accumulator tank were used to calculate the number of g $\cdot$ moles of steam driving gas. The temperature of the steam accumulator shell was measured using three type-K thermocouples (channels 72, 73, and 74) that were placed in the top and bottom hemispheres and in the vertical cylindrical wall. These thermocouples monitored and were used to control the electric heaters on the accumulator shell, which heated the accumulator steel to the desired steam temperature prior to the addition of saturated steam from the boiler.

An optical pyrometer (channel 37 in Figures 2.3 and 2.6) was used to measure the temperature of the debris as it exited the cavity in the 1:6 scale tests. The pyrometer (type 11x30, Ircon Inc., Niles, IL) was located in the basement and was focused just above the cavity cofferdam exit. A debris emissivity of 0.9 was assumed when converting the results in mV from the optical pyrometers to temperature in K. A debris emissivity near the blackbody value was assumed because the debris appeared black when inspected posttest. The calculated debris temperature is not very sensitive to the assumed debris emissivity. For example, at approximately 2000 K a 13 percent change in the assumed emissivity resulted in only a 1.9 percent change in the calculated debris temperature.

The optical pyrometer had a response time of 1.5 ms to 95 percent of its full range. A high-range controller was installed on the 11 x 30 pyrometer. The high-range controller could measure temperatures between 1873 K and 2773 K with a specified accuracy of 1 percent of the full-scale temperature. In a transient event such as a HPME experiment, the accuracy of the pyrometer measurement was expected to be no better than $\pm$25 K. The pyrometer was factory calibrated and is routinely recalibrated by the Sandia Radiant Heat Facility.

Data points from the thermocouples and the pyrometers were recorded by the data acquisition system at a rate of 10 per second prior to thermite ignition. Then, just prior to thermite ignition, the data acquisition system was switched to the fast data acquisition mode, in which data points were recorded at a rate of 1400 per second.

2.4.3 Gas Composition

In the IET-9 and IET-10 tests, twelve pre-evacuated 500-cm^3 gas grab sample bottles

were used to collect samples from the vessel (labeled G1, G2, and G3 in Figures 2.3 and 2.7) at several locations and times. Four gas grab sample bottles were located at instrumentation penetration P3 (G1), four bottles were located at equipment hatch B (G2), and four bottles were located at construction penetration CP1 (G3). The G1 and G2 sample lines extended through the crane wall. All bottles were opened remotely for 10 s. Three background samples were opened about 1 minute prior to ignition of the thermite. Three gas grab sample bottles were opened at 15 seconds after melt ejection. Three gas grab sample bottles were opened at 2 minutes after melt ejection. Three gas grab sample bottles were opened at 15 minutes after melt ejection.

In the IET-11 experiment, sixteen pre-evacuated 500-cm^3 gas grab sample bottles were used to collect samples from the vessel (labeled G1, G2, G3, and G4 in Figures 2.3 and 2.6-2.8) at several locations and times. Four gas grab sample bottles were located at instrumentation penetration P3 (G1), four bottles were located at equipment hatch B (G2), four bottles were located at construction penetration CP1 (G3), and four bottles were located near the vessel hydrogen charging connection (Figure 2.6). The G1 and G2 sample lines extended through the crane wall. The G3 sample line was extended from penetration CP1 to the top of the dome, and the line was purged for 15 s prior to taking a gas grab sample due to its long length. The G4 sample bottles sampled the vessel/cranewall annulus about midway between the basement floor and the top of the cranewall. All bottles were opened remotely for 10 s. Due to a delay in the ignition sequence, the four background samples were opened about 18 minutes prior to ignition of the thermite. Four gas grab sample bottles were opened at 15 seconds after melt ejection. Four gas grab sample bottles were opened at 2 minutes after melt ejection. Four gas grab sample bottles were opened at 15 minutes after melt ejection.

In the IET-12 experiment, twenty pre-evacuated 500-cm^3 gas grab sample bottles were used to collect samples from the vessel at several locations and times. The vessel was roughly divided into four vertical regions (dome, high, low, and operating deck/basement) and three 120° azimuthal regions, each centered on a thermocouple array. Gas grab sample suction lines were attached to the thermocouple arrays at the following locations: (1) three sampling lines in the dome region near thermocouples 56, 62, and 68, (2) three sampling lines high in the vessel near thermocouples 54, 60, and 66, (3) three sampling lines low in the vessel near thermocouples 52, 58, and 64, and (4) three sampling lines in or near subcompartment structures, i.e., one just above the operating deck, one in the basement, and one in the vessel/ cranewall annulus midway between the basement floor and the top of the cranewall. Gas grab samples were taken at each location 3 s after the HPME. In addition, four background samples were taken, one at each vertical position. Also, four long-term posttest samples were taken, two at 5 min and two at 15 min after the melt ejection. The four posttest samples used a common point located near thermocouple 60 on the C thermocouple array.

The IET-12 gas grab bottles and isolation valves were located in heated, insulated boxes that were maintained at 425 K. All sample lines were heated and insulated to prevent condensation of steam while taking the sample. This was necessary to allow determination of the noncondensible fraction of the gas sample. All sample lines were purged prior to filling the gas grab bottles to ensure representative samples. Five out of the twenty gas grab sample bottles failed to fill or only partially filled and were discarded. It was suspected that the high ambient heat caused the failures, even though high-temperature seals and valves were used (the maximum temperature rating for the high-temperature seals was near 425 K). The sample bottle locations for

the bottles that operated (G1 - G15) are shown in Figure 2.9.

All of the Surry DCH tests gas samples were analyzed using gas mass spectroscopy by Battelle Pacific Northwest Laboratories in Richland, WA. Tests were performed at SNL to measure the fill times of the 500-cm^3 gas grab sample bottles at three different initial pressures (atmospheric, 0.26 MPa, and 0.43 MPa). An evacuated bottle at $\approx$295 K was separated from a pressure source by a remotely operated solenoid valve. A pressure transducer was installed downstream of the valve and pressure source, and the fill time was recorded by the data acquisition system. The data indicate that all bottles were filled in less than 2 s, regardless of the upstream pressure.

2.4.4 Posttest Debris Recovery

In IET-9 and IET-10, the total debris mass dispersed into the CTTF containment vessel and the debris mass in specific locations were determined by a very careful posttest debris recovery procedure. The following measurements were made: (1) the mass of the molten debris in the cavity and in the incore instrument tunnel; (2) the mass recovered from horizontal and vertical surfaces on the cavity side of the basement (the vessel was split into two halves by a line drawn between equipment hatch A and equipment hatch B, yielding a 'cavity' side and a five foot 'door' side); (3) the mass recovered from horizontal and vertical surfaces on the 'door' side of the basement; (4) the mass recovered from the trough floor 'T' region (in front of the cavity and extending to an edge marked by the STR ledge); (5) the mass recovered from the trough floor on the cavity side (excluding the trough 'T' region); (6) the mass recovered from the trough floor on the 'door' side; (7) the mass recovered from the annulus formed by the containment vessel wall and the crane wall in the 'T' region in front of the RHR platform (from trough floor to ledge); (8) the mass recovered from the annulus on the cavity side (excluding the trough 'T' region); (9) the mass recovered from the annulus on the 'door' side; (10) the mass recovered from the operating deck horizontal and vertical surfaces on the 'door' side; (11) the mass recovered from the operating deck horizontal and vertical surfaces on the 'cavity' side and including the STR ceiling; (12) the mass recovered from all RHR platform surfaces; (13) the mass recovered from all seal table room and STR ledge surfaces; (14) the mass recovered from the upper level grating and containment wall surfaces to the top of the dome; (15) in the annular gap between the RPV vessel model and the biological shield accessed from the operating deck; and (16) the mass recovered from the melt generator/crucible.

In IET-11, the basement trough was filled in with concrete; therefore, the three trough areas mentioned above were incorporated into the appropriate basement location.

The IET-12 posttest debris recovery procedure was very similar to IET-11. The following measurements were made: (1) the mass of the molten debris in the cavity and in the incore instrument tunnel; (2) the mass recovered from horizontal and vertical surfaces on the cavity side of the basement (the vessel was split into two halves by a line drawn through the biological shield normal to the incore instrument tunnel (similar to the split used in the 1:6 scale IET tests that were performed in the CTTF), yielding a 'cavity' side and a 'door' side); (3) the mass recovered from horizontal and vertical surfaces on the door side of the basement; (4) the mass recovered from the annulus formed by the Surtsey vessel wall and the cranewall on the cavity side; (5) the mass recovered from the annulus on the door side; (6) the mass recovered from the operating deck horizontal and vertical surfaces on the door side; (7) the mass recovered from the operating deck horizontal and vertical surfaces on the cavity side and including the STR ceiling; (8) the mass recovered from all RHR platform surfaces; (9) the mass recovered from all seal table room and STR ledge surfaces; (10) the mass recovered from the wall surfaces to the

top of the dome; (11) in the annular gap between the RPV vessel model and the reactor support skirt; and (12) the mass recovered from the melt generator/crucible.

A posttest sieve analysis of the debris that was recovered outside of the subcompartment structures was performed for each test. A standard set of 35 sieves was used (U. S. series 9.5 mm to 38 μm).

2.4.5 Debris Velocity

Breakwires were placed across the cofferdam opening, seal table room floor opening, and at the opening in the ceiling of the seal table room (channels 18, 12, and 17 in Figures 2.3 and 2.6-2.9). When the debris front severed the breakwire, a timing signal was recorded by the data acquisition system. The breakwire was intended to give timing information on entry of debris out of the cavity, and into and out of the seal table room. The breakwire failure time, in conjunction with measured distances, allowed the measurement of debris velocity.

2.4.6 Cameras

In the 1:6 scale tests, a high resolution 1/2" change-coupled device (CCD) color camera was used. The camera was mounted inside the construction penetration CP2, viewing the DCH event through a tempered glass window. In addition to the digital camera, two camcorders were used. One camcorder was mounted outside the CTTF containment vessel in front of equipment hatch A and the other camcorder was set up outside in front of equipment hatch B to give overall views of the CTTF vessel during the DCH test.

The high resolution 1/2" CCD color camera was also used in IET-12 and was mounted inside the dome penetration, viewing the DCH event through a tempered glass window. Three video camcorders were used in IET-12. One camcorder viewed the DCH event through a tempered glass window mounted on a level 6 port, with a view that looked across the RPV model and toward the seal table room ceiling exits. One camcorder was mounted outside the Surtsey vessel on the north side and the other camcorder was set up outside on the south side to give overall views of the Surtsey vessel during the DCH test.

Table 2.1 Surry IET instrumentation location and purpose

Channel	Instrument	Location	Purpose
1	Thermocouple Type C	RHR room ceiling	Measure debris/gas temperature
2	Thermocouple Type C	RHR room right window exit	Measure debris/gas temperature
3	Thermocouple Type C	RHR room left window exit	Measure debris/gas temperature
4	Thermocouple Type C	Below seal table room ledge	Measure debris/gas temperature
5	Thermocouple Type C	Seal table room ceiling exit	Measure debris/gas temperature
6	Thermocouple Type C	Seal table room back wall	Measure debris/gas temperature
7	Thermocouple Type C	Cofferdam exit	Measure debris/gas temperature
8	Thermocouple Type C	Annular gap	Measure gas temperature
10	Breakwire	Crucible melt plug	Signal initiation of HPME
11	Breakwire	Crucible melt plug	Signal initiation of HPME
12	Breakwire	Seal table room floor	Measure debris velocity
13	Aspirated thermocouple*	P3	Measure gas temperature
14	Aspirated thermocouple	P3	Measure gas temperature
15	Aspirated thermocouple	P3	Measure gas temperature
16	Ignitor	Crucible	Thermite ignition
17	Breakwire	Seal table room ceiling	Measure debris velocity
18	Breakwire	Cofferdam exit	Measure debris velocity
19	Pressure transducer	Vessel construction penetration	Measure gas pressure
20	Pressure transducer	Vessel P3 penetration	Measure gas pressure
21	Pressure transducer	Vessel P3 penetration	Measure gas pressure
22	Pressure transducer	Vessel construction penetration	Measure gas pressure

Table 2.1 Surry IET instrumentation location and purpose (continued)

Channel	Instrument	Location	Purpose
23, 24	Pressure transducer	Cavity	Measure gas pressure
25, 26	Pressure transducer	RHR room	Measure gas pressure
27, 28	Pressure transducer	Seal table room	Measure gas pressure
29, 30	Pressure transducer	Basement	Measure gas pressure
31, 32	Pressure transducer	Accumulator	Measure steam pressure
33, 34	Pressure transducer	Burst diaphragm	Measure gas pressure
35, 36	Pressure transducer	Crucible	Measure gas pressure
37	11x30 optical pyrometer	Cofferdam	Measure debris temperature
38	Thermocouple	Vessel wall	Measure structure temperature
40	Thermocouple	Accumulator	Heater Controller
41	Thermocouple	Basement	Measure gas temperature
42	Thermocouple	Basement	Measure gas temperature
43	Thermocouple	Basement	Measure gas temperature
44	Thermocouple	Basement	Measure gas temperature
45	Thermocouple	Crane wall	Measure gas temperature
46	Thermocouple	Crane wall	Measure gas temperature
47	Thermocouple	Crane wall	Measure gas temperature
48	Thermocouple	Crane wall	Measure gas temperature
49	Thermocouple	Crucible	Measure temperature
50	Thermocouple	Cavity	Measure temperature
51	Thermocouple array - A1	Bottom	Measure gas temperature
52	Thermocouple array - A2		Measure gas temperature
53	Thermocouple array - A3		Measure gas temperature
54	Thermocouple array - A4		Measure gas temperature
55	Thermocouple array - A5		Measure gas temperature
56	Thermocouple array - A6	Top	Measure gas temperature

Table 2.1 Surry IET instrumentation location and purpose (continued)

Channel	Instrument	Location	Purpose
57	Thermocouple array - B1	Bottom	Measure gas temperature
58	Thermocouple array - B2		Measure gas temperature
59	Thermocouple array - B3		Measure gas temperature
60	Thermocouple array - B4		Measure gas temperature
61	Thermocouple array - B5		Measure gas temperature
62	Thermocouple array - B6	Top	Measure gas temperature
63	Thermocouple array - C1	Bottom	Measure gas temperature
64	Thermocouple array - C2		Measure gas temperature
65	Thermocouple array - C3		Measure gas temperature
66	Thermocouple array - C4		Measure gas temperature
67	Thermocouple array - C5		Measure gas temperature
68	Thermocouple array - C6	Top	Measure gas temperature
69	Aspirated thermocouple	Construction penetration	Measure gas temperature
70	Aspirated thermocouple	Construction penetration	Measure gas temperature
71	Aspirated thermocouple	Construction penetration	Measure gas temperature
72	Thermocouple	Accumulator skin - top	Measure outside surface temperature
73	Thermocouple	Accumulator skin - middle	Measure outside surface temperature
74	Thermocouple	Accumulator skin - bottom	Measure outside surface temperature
75	Thermocouple	Accumulator gas - 2 in. from top	Measure steam temperature
76	Thermocouple	Accumulator gas - 4 in from bottom	Measure steam temperature
77	Thermocouple	Vessel wall liner - top	Measure structure temperature
78	Thermocouple	Vessel wall liner - bottom	Measure structure temperature

Table 2.1 Surry IET instrumentation location and purpose (concluded)

Channel	Instrument	Location	Purpose
79	Thermocouple	Crane wall - in concrete	Measure structure temperature
80	Thermocouple	Vessel floor - in concrete	Measure structure temperature
G1-G15	Gas grab sample	Various	Measure gas composition prior to and after HPME

* All thermocouples were type K unless noted as type C

Table 2.2 Geometric comparisons for the Surry IET counterpart experiments

Geometric Parameters	Surry	CTTF	Surtsey
Scale	1:1	1:5.75	1:10
Reactor Coolant System			
RCS Volume (m^3)	237.5	1.25	0.25
Melt Mass (kg)		158	30
Melt Volume (m^3)		0.0381	0.0075
RPV I.D. (m)	3.9878	0.7658	0.3969
Crucible Volume (m^3)		0.1945	0.0312
Melt/Crucible Volume Ratio		0.1573	0.1859
RPV Length (shell and bottom head) (m)	10.0604	1.8823	1.0824
RPV O.D. (m)	4.3942	0.9652	0.5461
RPV Nozzle Diameter (m)	1.3462	0.2540	0.1524
Support Skirt I.D. (m)	4.7244	1.0109	0.5730
Hole Diameter (m)	0.4000	0.0700	0.0400
RPV Insulation Mass (kg)	~4400	29	N/A
Annular Gap (m)	0.1651	0.0229	N/A
Annular Gap Flow Area (without nozzles, without insulation) (m^2)	2.3648	0.0709	N/A
Annular Gap Flow Area (with nozzles, without insulation) (m^2)	1.0313	0.0360	N/A
Annular Gap Flow Area (with nozzles, with insulation) (m^2)	0.5765	0.0174	N/A
Insulation Thickness (m)	0.0762	0.0121	N/A
Insulation Area (m^2)	1.0702	0.0371	N/A
Fraction of Gap Blocked by Nozzles	0.5638	0.4922	N/A
Fraction of Gap Blocked by Nozzles & Insulation	0.7562	0.7546	N/A

Table 2.2 Geometric comparisons for the Surry IET counterpart experiments (continued)

Geometric Parameters	Surry	CTTF	Surtsey
Scale	1:1	1:5.75	1:10
Cavity / Incore Instrument Tunnel			
Cavity and IIT Floor Area (m^2)	58.1167	2.1146	0.7053
Cavity and IIT Height (m)	4.1392	0.7144	0.4032
Cavity and IIT Volume (m^3)	240.5566	1.5107	0.2844
Support Skirt Archway Exit Flow Area (m^2)	7.2474	0.2229	0.0718
IIT Length (m)	7.3152	1.1589	0.6652
IIT Width (m)	3.048	0.5302	0.3048
IIT Height (m)	4.1392	0.7144	0.4032
IIT Volume (m^3)	92.2903	0.4390	0.0817
IIT Flow Area (m^2)	12.6163	0.3788	0.1229
IIT Cofferdam Exit Flow Area (m^2)	5.5742	0.1756	0.0581
IIT Vent Duct Exit Flow Area (m^2)	0.8361	0.0253	0.0084
Melt Plug Exit to Cavity Floor (m)	4.5446	0.7800	0.4404
Melt Plug Centerline to Cofferdam Centerline (m)	9.4488	1.6711	0.9609
Cavity Floor to Cofferdam Exit (m)	6.8834	1.2930	0.7356
Debris Flight Path (Exit hole to top of cofferdam) (m)	20.8768	3.7441	2.1369
Subcompartment/Containment			
Biological Shield Volume (without RPV) (m^3)	515.78	3.9701	0.7593
Biological Shield Volume (below RPV) (m^3)	160.4900	1.1633	0.2196
RHR Platform Floor Area (m^2)	87.02	2.6324	0.8702
RHR Platform Height (m)	8.839	1.5372	0.8839
RHR Platform Volume (m^3)	769.16	4.0465	0.7692
RHR Platform Side Windows Total Area (m^2)	38.45	1.1551	0.3845
RHR Platform Front Wall Opening Area (m^2)	80.39	2.3736	0.8039

Table 2.2 Geometric comparisons for the Surry IET counterpart experiments (concluded)

Geometric Parameters	Surry	CTTF	Surtsey
Scale	1:1	1:5.75	1:10
Seal Table Room Floor Area (m^2)	44.91	1.3583	0.4491
Seal Table Room Height (m)	8.077	1.4046	0.8077
Seal Table Room Volume (m^3)	362.74	1.9079	0.3627
Seal Table Room Penetration Areas (m^2) :			
Instrument Tubes (floor)	1.56	0.0471	0.0156
Left RHR HX (floor)	0.87	0.0264	0.0087
Right RHR HX (floor)	0.87	0.0264	0.0087
Instrument Tubes (front wall)	0.20	0.0061	0.0020
Personnel Doorway (front wall)	0.83	0.0144	0.0083
Left RHR HX (ceiling)	12.14	0.3672	0.1214
Right RHR HX (ceiling)	0.87	0.0264	0.0087
Basement Height (m)	7.950	1.2292	0.7318
Basement Floor Area (to cranewall, with cavity and biological shield removed) (m^2)	651.56	22.2903	7.3629
Cavity / Biological Shield Outer Floor Area (m^2)	107.6	3.8408	1.2877
Basement Volume (m^3)	5179.9	27.3992	5.3882
Containment Length (m)	55.8038	9.6774	4.6258
Containment Diameter (m)	38.4048	6.7056	3.6576
Containment Freeboard Volume (m^3)	51000.0	282.0	51.0
Containment Aspect Ratio (L/D)	1.4530	1.4432	1.2647

Table 2.3 Melt composition

Constituent	Mass fraction		Mole fraction		Volume fraction	
	Corium	Thermite	Corium	Thermite	Corium	Thermite
UO_2	0.527	0.000	0.230	0.000	0.420	0.000
ZrO_2	0.098	0.000	0.094	0.000	0.149	0.000
Zr	0.139	0.000	0.180	0.000	0.173	0.000
Fe	0.142	0.505 (0.566) [1]	0.299	0.592 (0.685)	0.158	0.322 (0.348)
Cr	0.035	0.108 (0.000)	0.079	0.136 (0.000)	0.042	0.074 (0.000)
Ni	0.020	0.000	0.040	0.000	0.020	0.000
Al_2O_3	0.000	0.374 (0.419)	0.000	0.241 (0.279)	0.000	0.574 (0.620)
Al	0.000	0.013 (0.015)	0.000	0.032 (0.037)	0.000	0.029 (0.032)
CRM*	0.039	0.000	0.078	0.000	0.038	0.000

[1] The parenthetical values are for the chromium-free thermite used in IET-12.

* Control rod materials.

Table 2.4 Material properties of the melt

Property	Corium	Thermite w/ chromium	Thermite w/o chromium
C_p (J/mole/K)	70.4	74.7	79.4
C_p (J/kg/K)	597	1139	1172
K (W/m/K)	13.9	20.7	20.9
ρ (kg/m^3)	7241	4146	3993
ρ (mole/m^3)	6.14×10^4	6.32×10^4	5.90×10^4
μ (Pa s)	7.78×10^{-3}	6.44×10^{-3}	7.12×10^{-3}
σ (N/m)	0.904	0.926	0.869
MW_{eff} (kg/mole)	0.1179	0.0656	0.0677

Table 2.5 Equilibrium models for estimating containment pressurization

Modeling parameter	Surry NPP scale	IET-9, -10, -11 1:6 scale	IET-12 1:10 scale
N_d (g • mole)	3.87×10^5	2408	443
C_d (J/g • mole K)	70.4	74.7	79.4
N^0 (g • mole)	3.13×10^6	1.75×10^4	3.13×10^3
N_b (g • mole)	5.72×10^5	3102	640
C_v (J/g • mole K)	28.6	28.6	28.6
U^0 (J)	3.31×10^{10}	1.85×10^8	3.31×10^7
ΔE_b (J)	9.24×10^9	5.01×10^7	1.03×10^7
Δe_t (J/g • mole)	1.55×10^5	1.64×10^5	1.75×10^5
Δe_r (J/g • mole)	1.25×10^5	4.19×10^4	1.62×10^4
Δe_{H2} (J/g • mole)	2.42×10^5	2.42×10^5	2.42×10^5
ν_{H2} (g • mole-H_2/g • mole-debris)	0.778	0.843	0.741
ψ	0.252	0.299	0.320
$\Delta P/P^0$ 1-cell	5.1	4.8	4.4

Table 2.6 Fractional contribution to containment pressurization

Contributor	Surry NPP scale	IET-9, -10, -11 1:6 scale	IET-12 1:10 scale
Blowdown	0.044	0.044	0.053
Thermal	0.226	0.339	0.392
Combustion	0.449	0.531	0.519
Oxidation	0.281	0.086	0.036

Table 2.7 Initial conditions for the IET experiments

		IET-9	IET-10	IET-11	IET-12
Test Date		01/29/93	03/19/93	05/02/93	08/12/93
Thermite composition (kg) iron oxide chromium aluminum Mass of the initial thermite charge (kg)			107.52 17.08 33.40 158.00		22.89 0.00 7.11 30.00
Mass of the RPV SS insulation (kg)		0	0	29	0
Gas pressure at plug failure (MPa)		12.9	12.1	13.2	11.2
Gas temperature at plug failure (K)		787	713	693	696
Moles of driving gas (g • moles)		3005	3275	3705	604
Initial hole diameter (cm)		7.0	7.0	7.0	5.6
Final hole diameter (cm)		7.4	9.8	7.6	5.6
Initial annular gap area (m^2)		0	0	0.0174	0
Final annular gap area (m^2)		0.012	0	0.0360	0
Seal Table Model		No	Yes	Yes	Yes
Water on basement floor (kg)		372	0	703	0
Initial vessel absolute pressure (MPa)		0.1351	0.1791	0.2209	0.1635
Initial vessel gas temperature (K)		392	410	399	408
Initial vessel gas moles (g • moles)		11870	15027	18802	2461
Initial gas composition in the containment vessel (mol. %)	Steam	67.24	48.20	32.25	57.98
	N_2	24.01	38.47	50.98	28.45
	O_2	6.14	10.17	13.66	7.28
	H_2	2.20	1.98	2.39	5.66
	CO	0.00	0.51	0.00	0.03
	CO_2	0.13	0.21	0.02	0.26
	Other	0.28	0.46	0.70	0.34
Freeboard volume inside subcompartment structures (m^3)			83.1	79.1	12.8
Freeboard volume in upper dome (m^3)			202.9	202.9	38.2
Total freeboard volume (m^3)			286.0	282.0	51.0

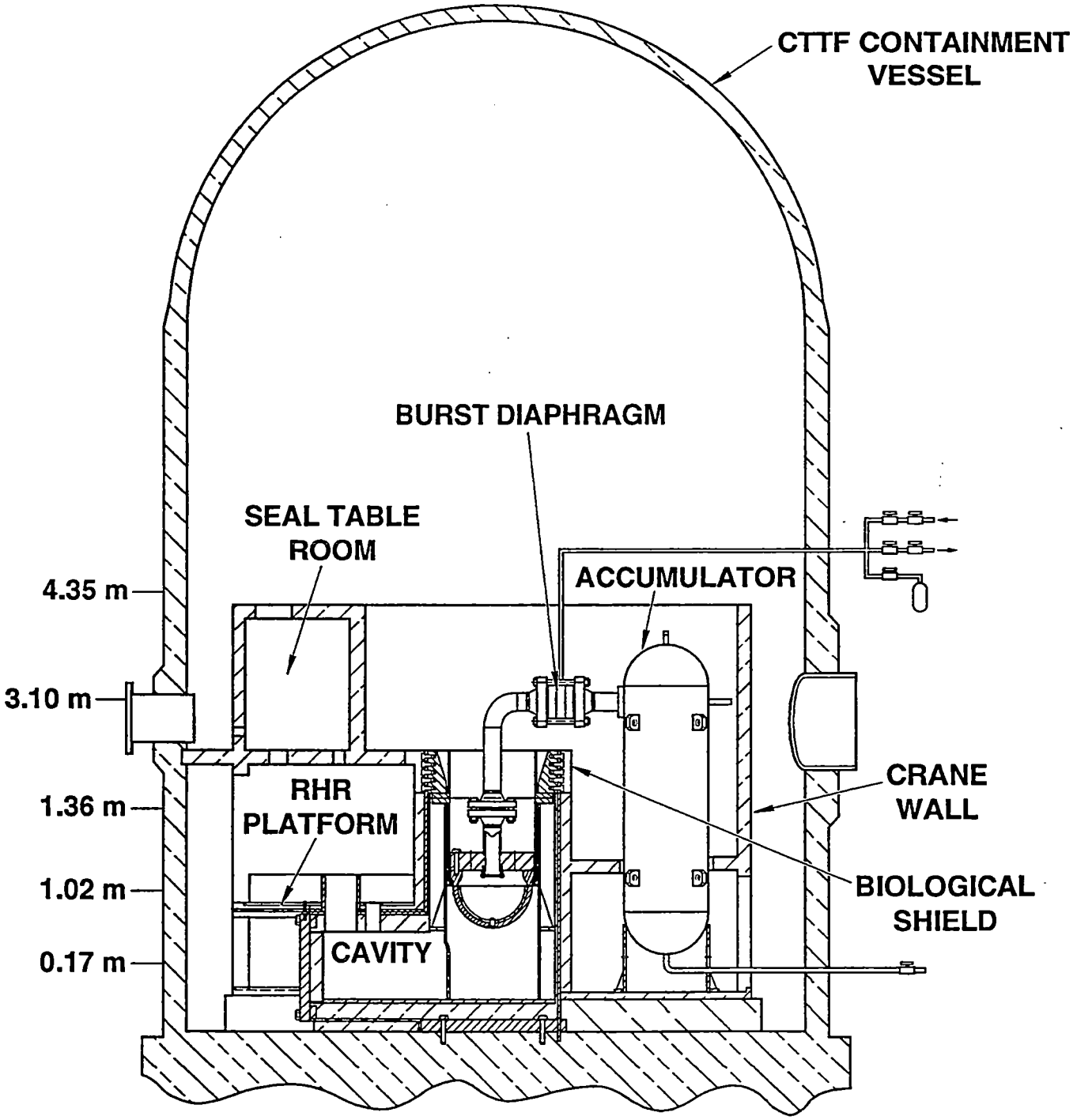

Figure 2.1. **CTTF vessel, high-pressure melt ejection system, and subcompartment structures used in the 1:6 scale IET experiments (facility dimensions are listed in Table 2.2)**

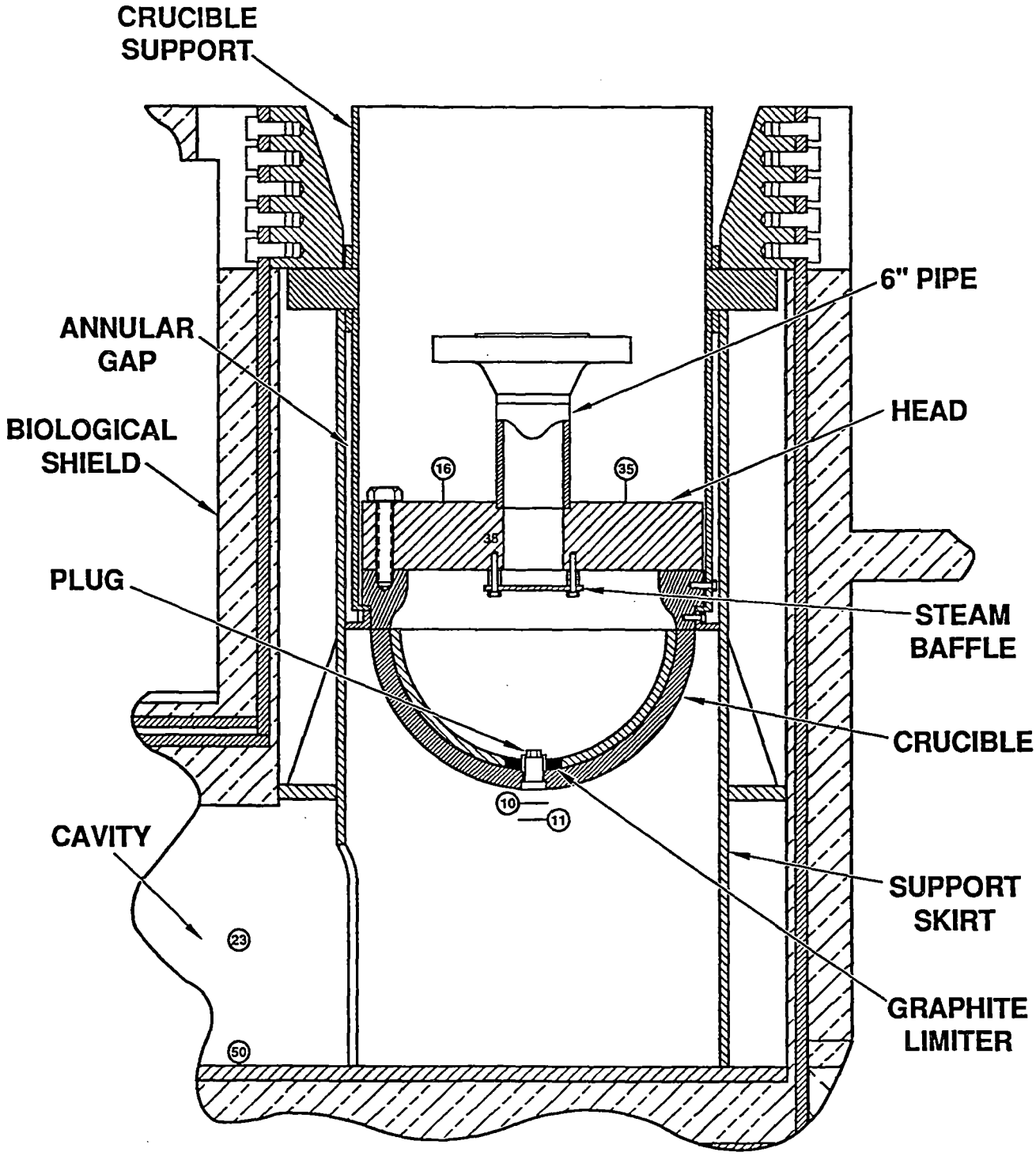

Figure 2.2. RPV model (with melt generator) and cavity used in the 1:6 scale IET experiments

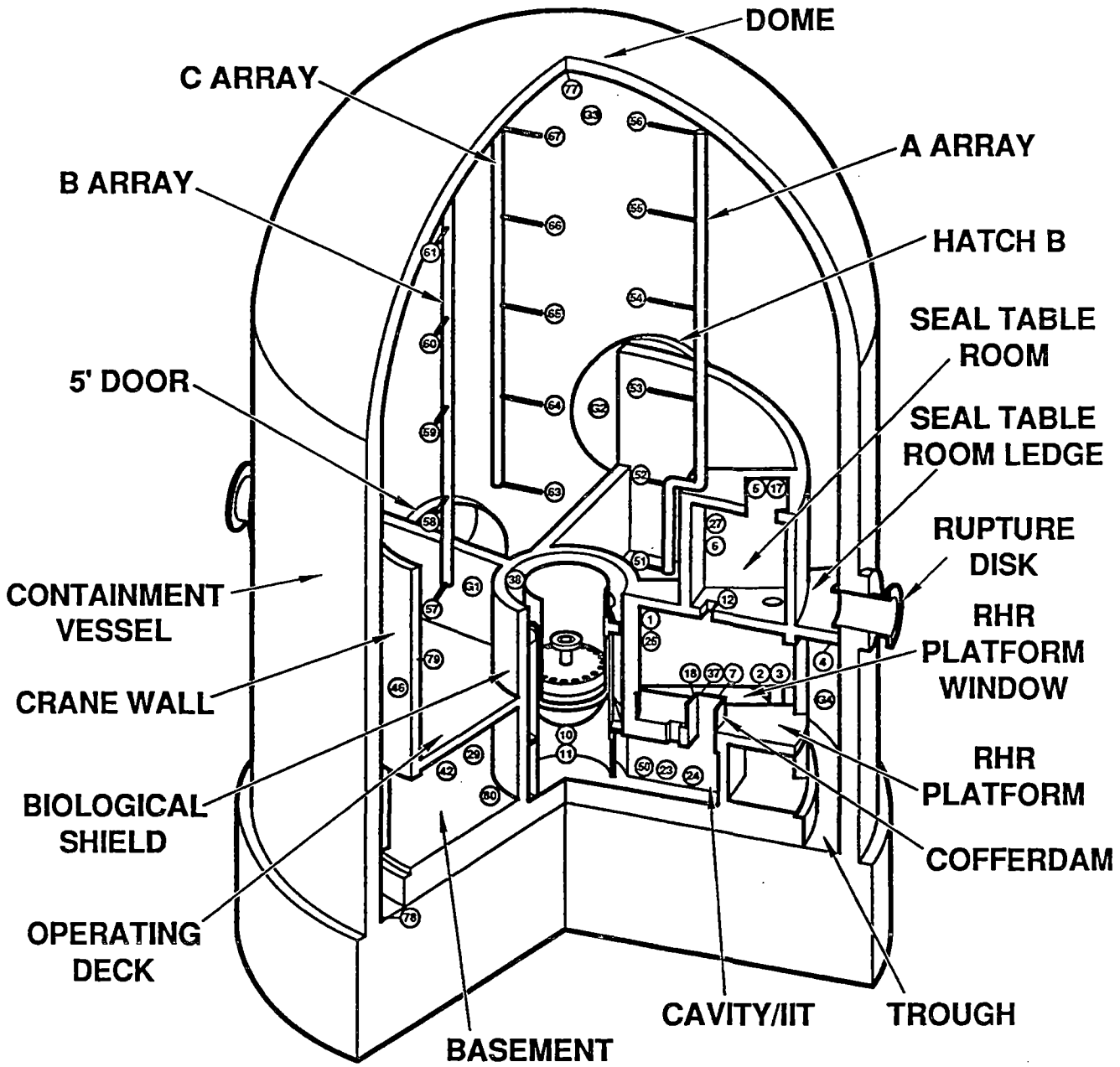

Figure 2.3. Isometric view of the subcompartment structures and RPV model inside the CTTF vessel

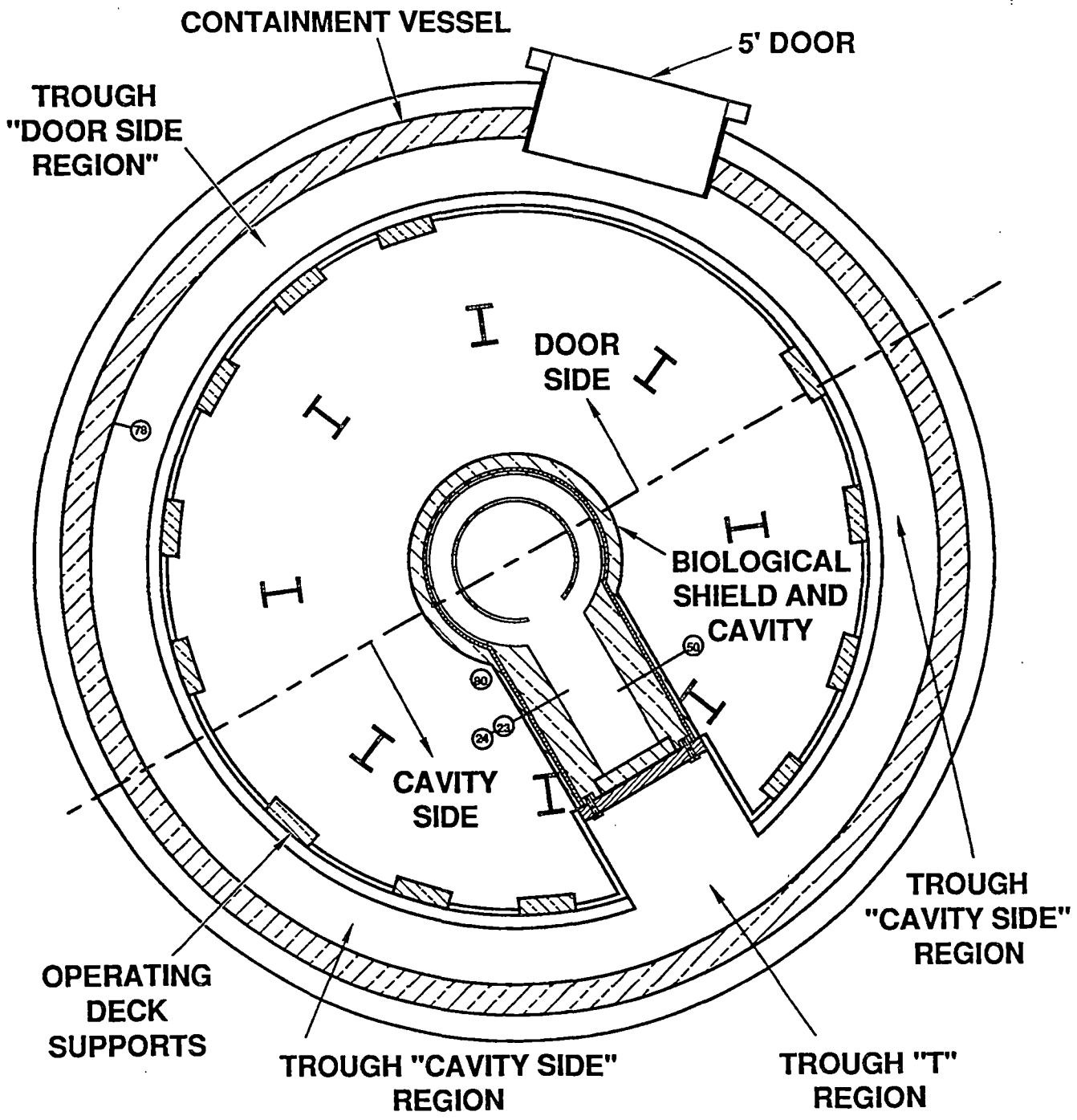

Figure 2.4. Basement floor plan view of structures inside the CTTF vessel

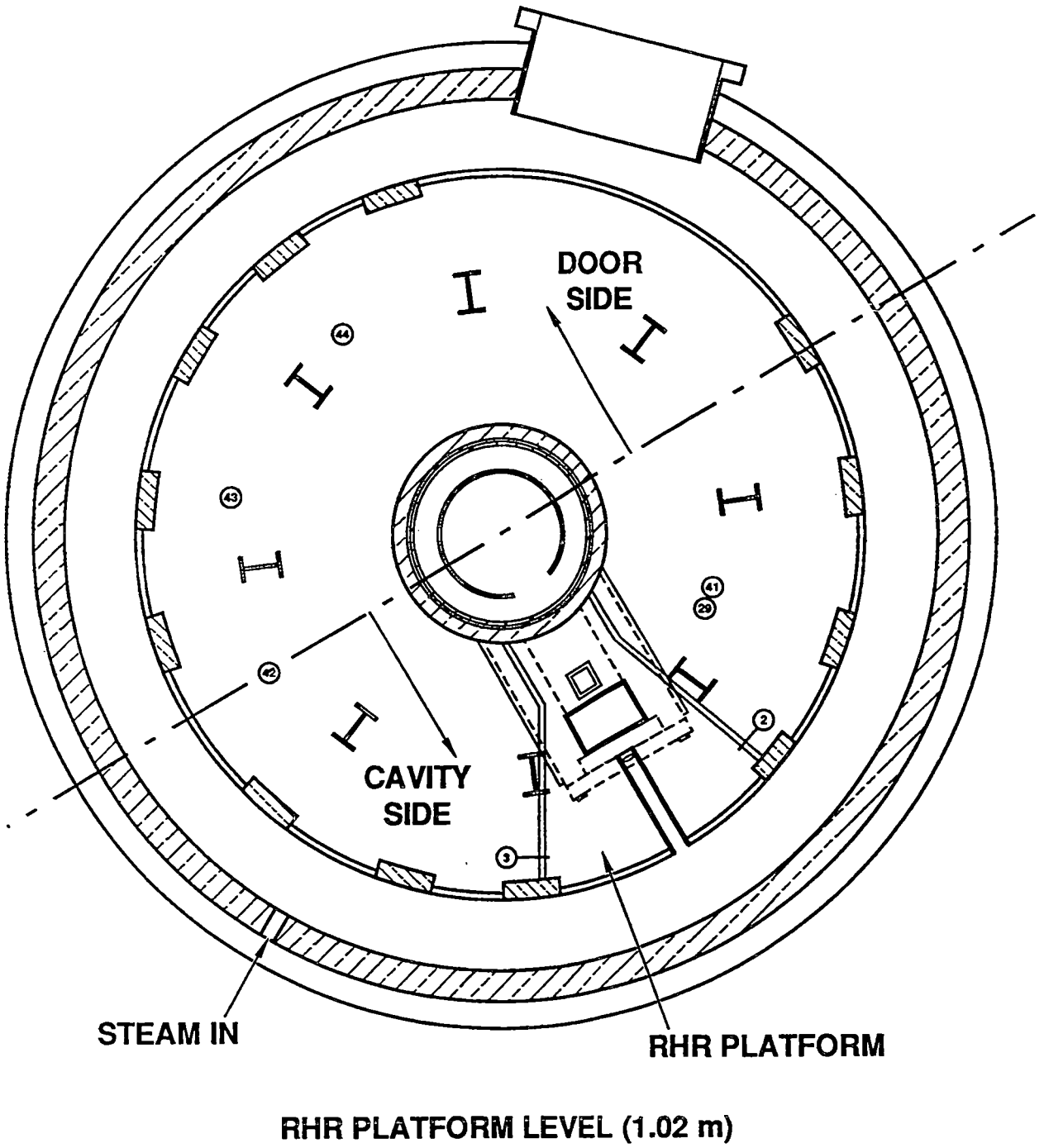

Figure 2.5. RHR platform plan view of structures inside the CTTF vessel

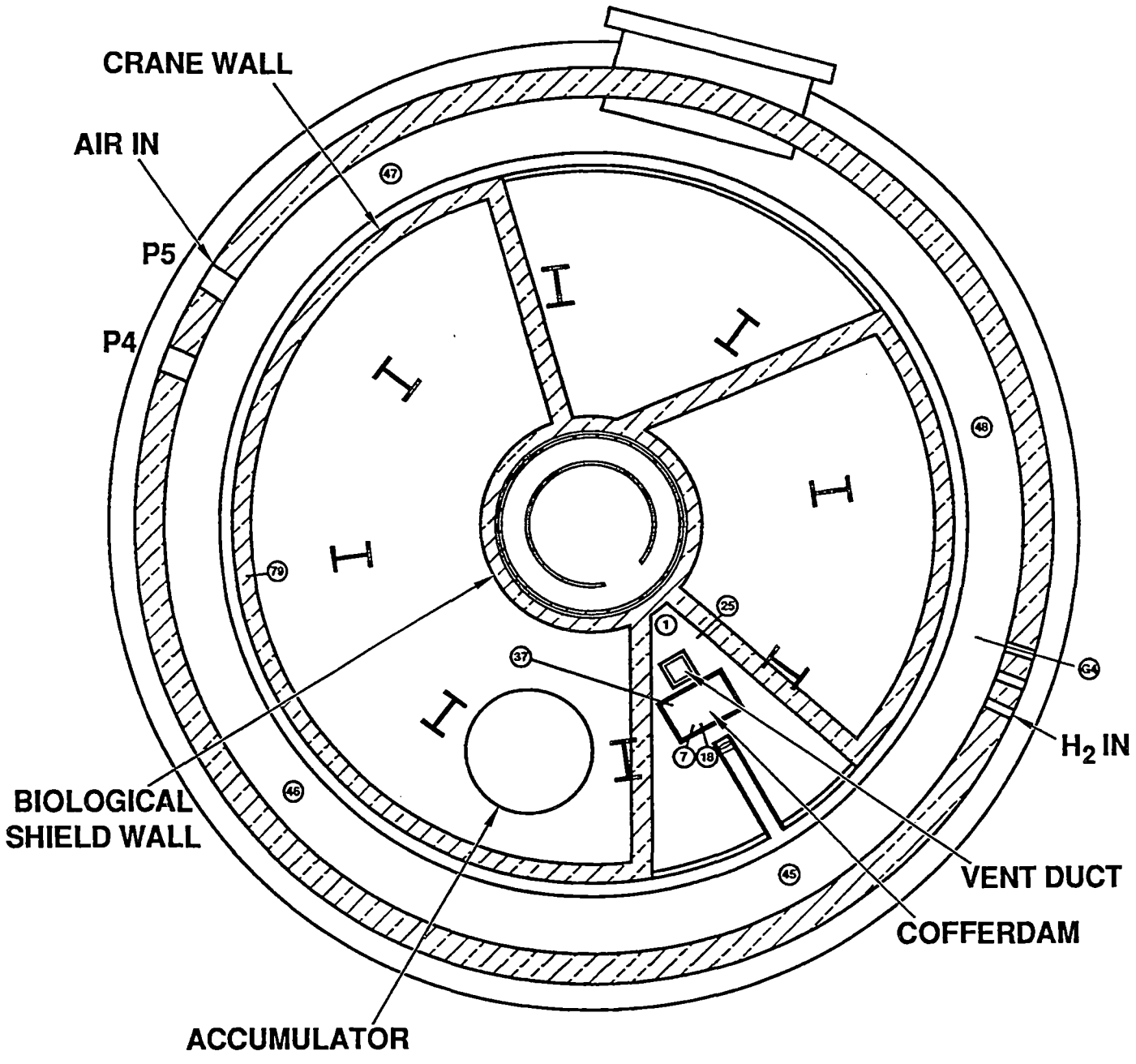

Figure 2.6. Operating deck plan view of structures inside the CTTF vessel

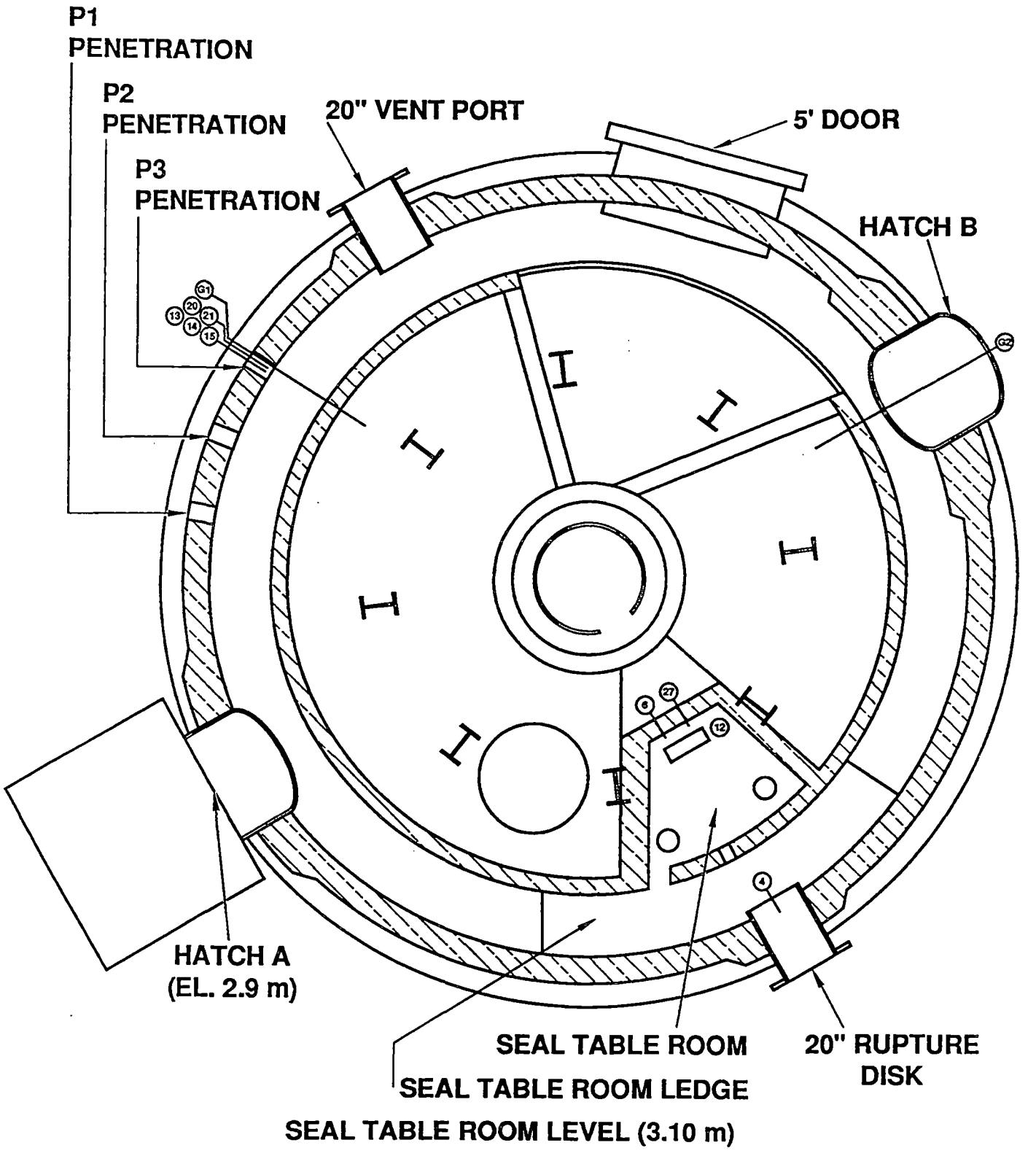

Figure 2.7. Seal table room plan view of structures inside the CTTF vessel

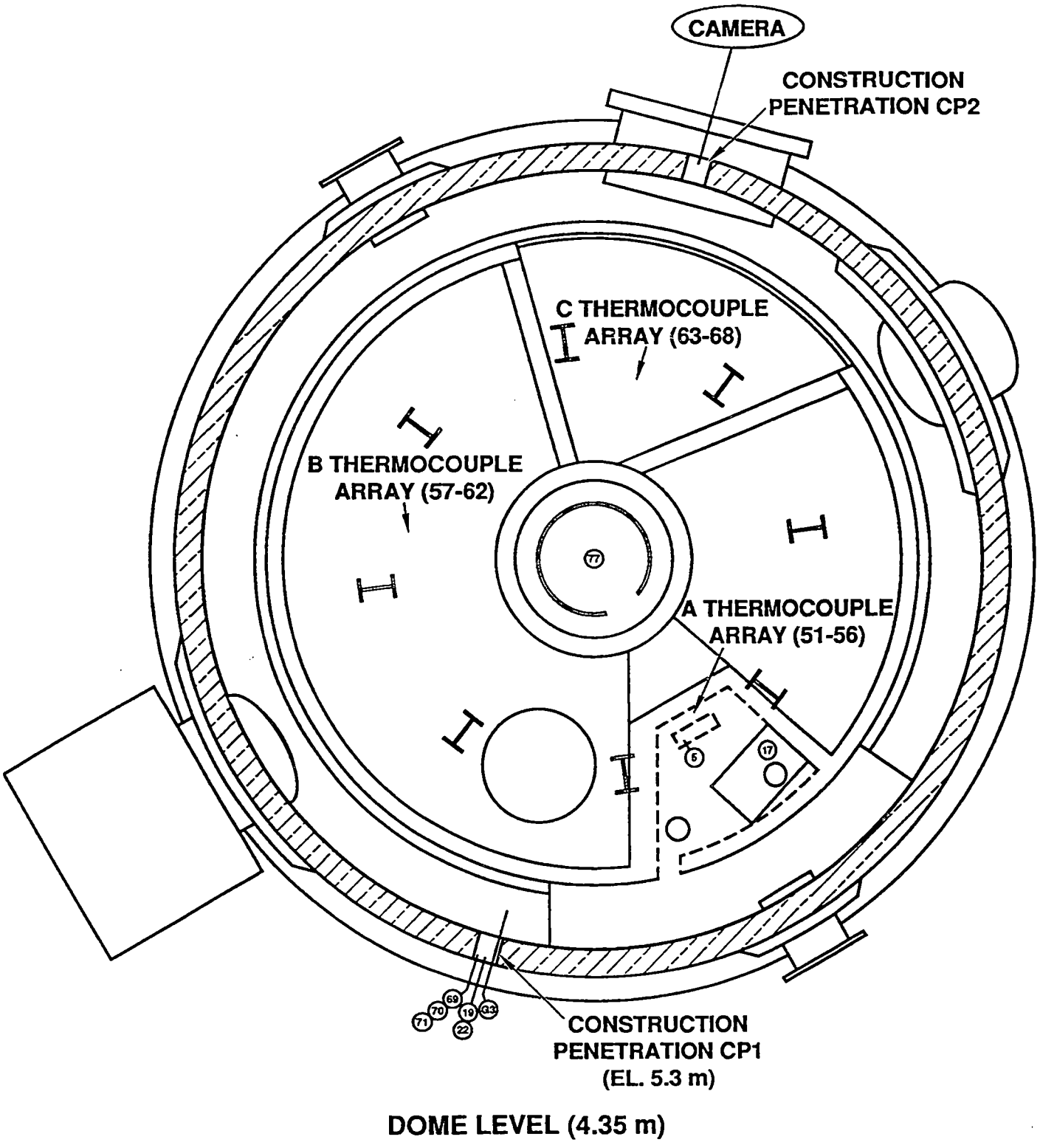

Figure 2.8. Dome level plan view of structures inside the CTTF vessel

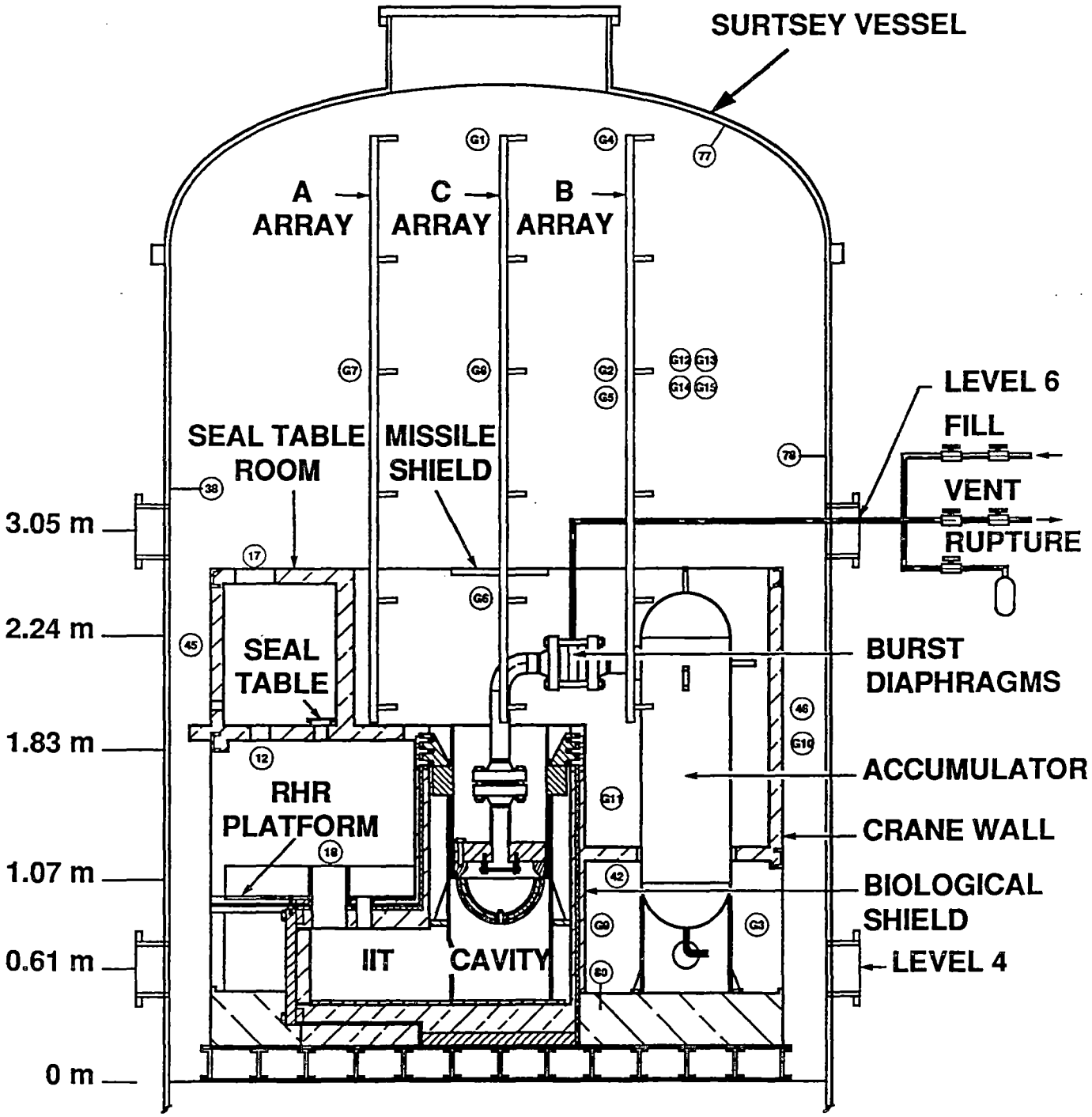

Figure 2.9. Surtsey vessel, high-pressure melt ejection system, and subcompartment structures used in the 1:10 scale IET experiment

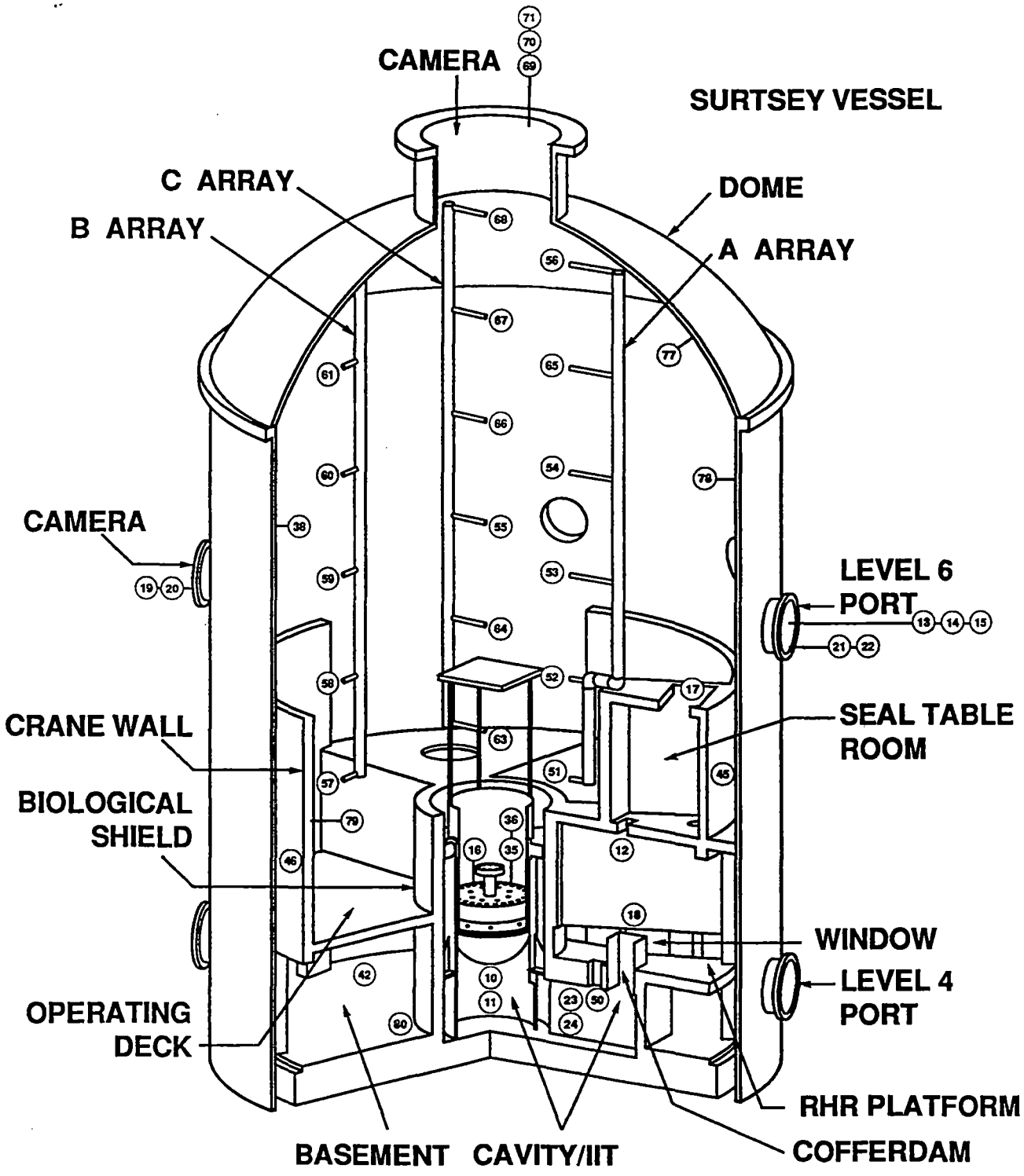

Figure 2.10. Isometric view of the subcompartment structures and RPV model inside the Surtsey vessel

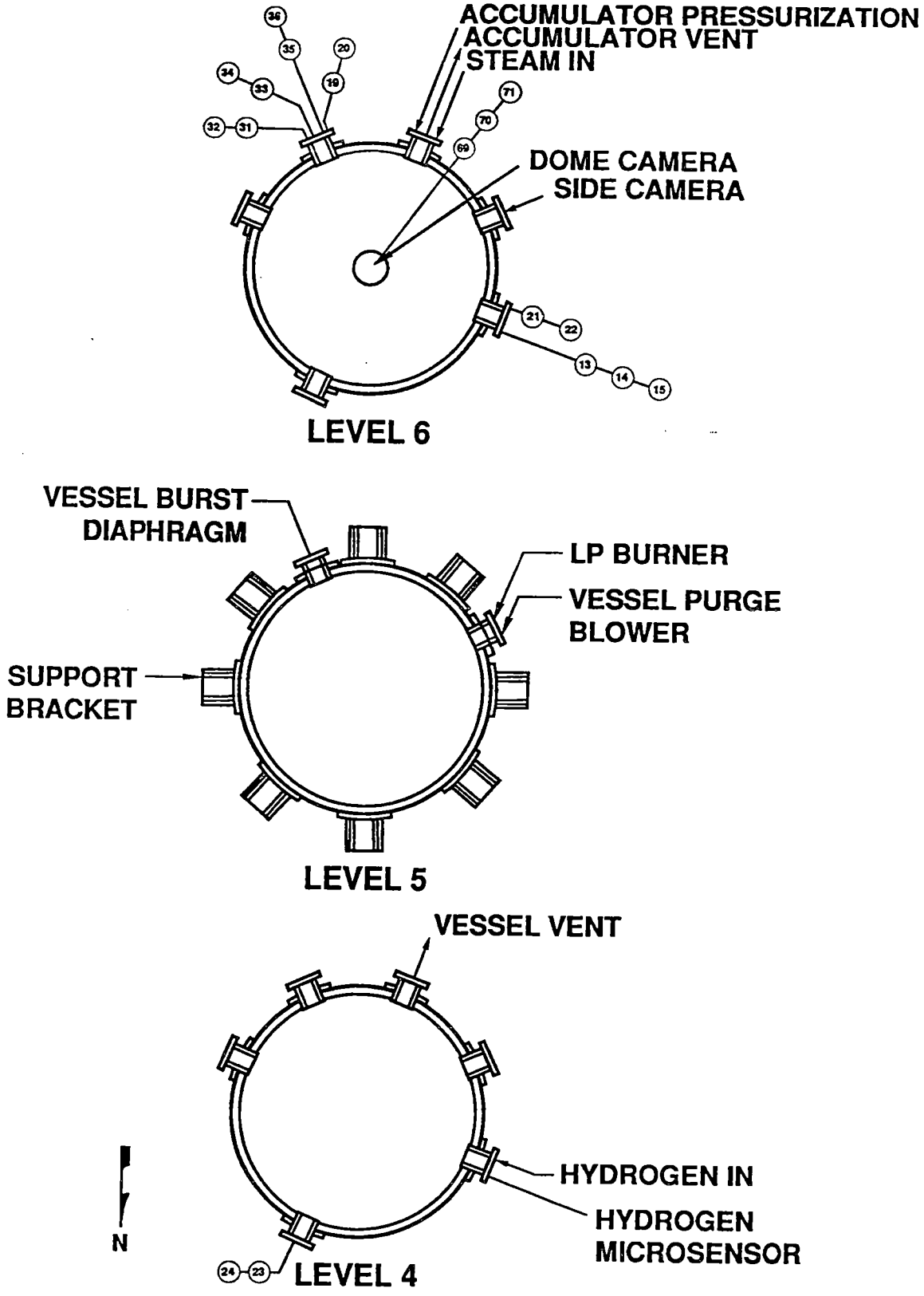

Figure 2.11. Top view of the Surtsey vessel showing instrumentation ports

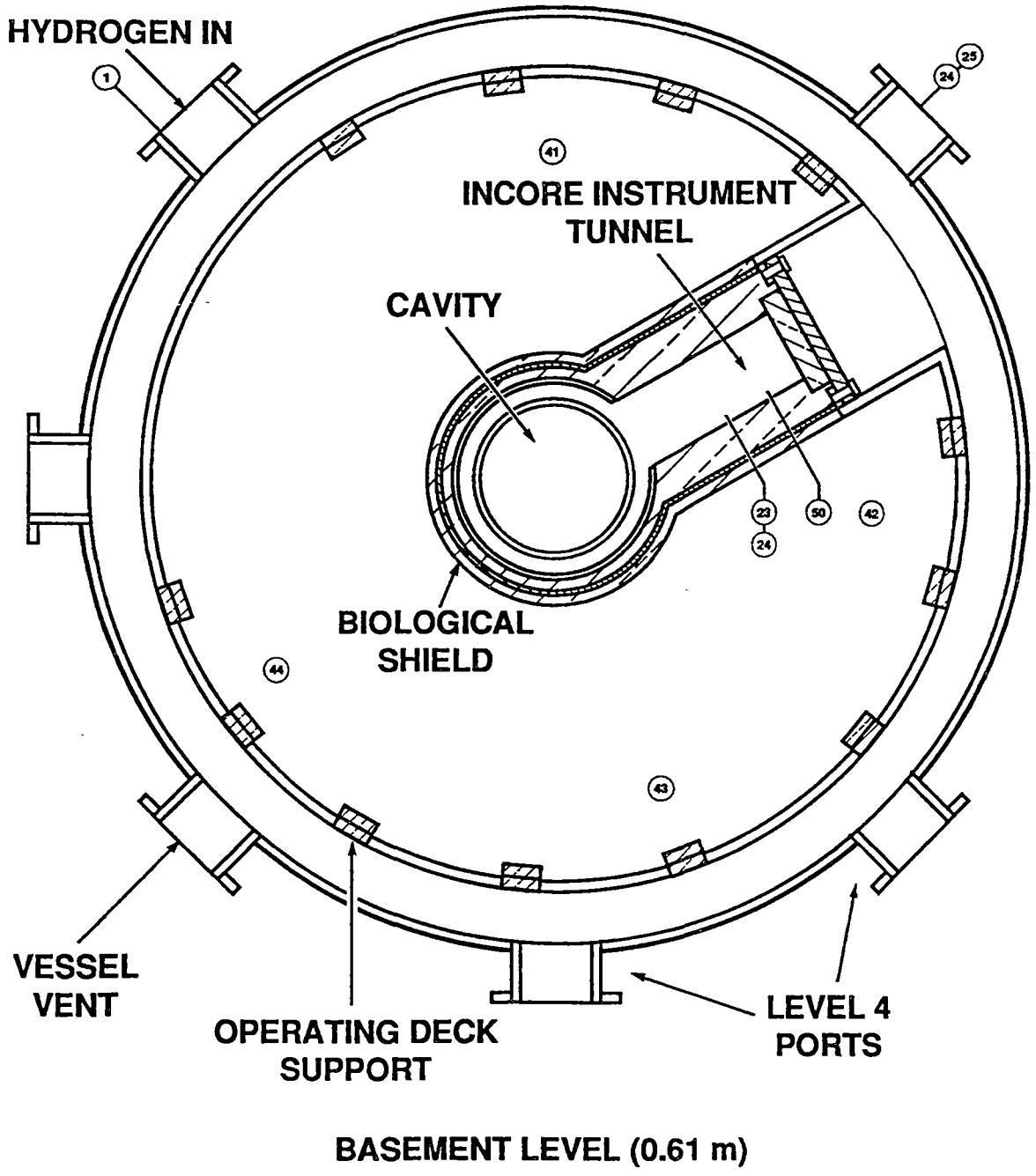

Figure 2.12. Basement floor plan view of structures inside the Surtsey vessel

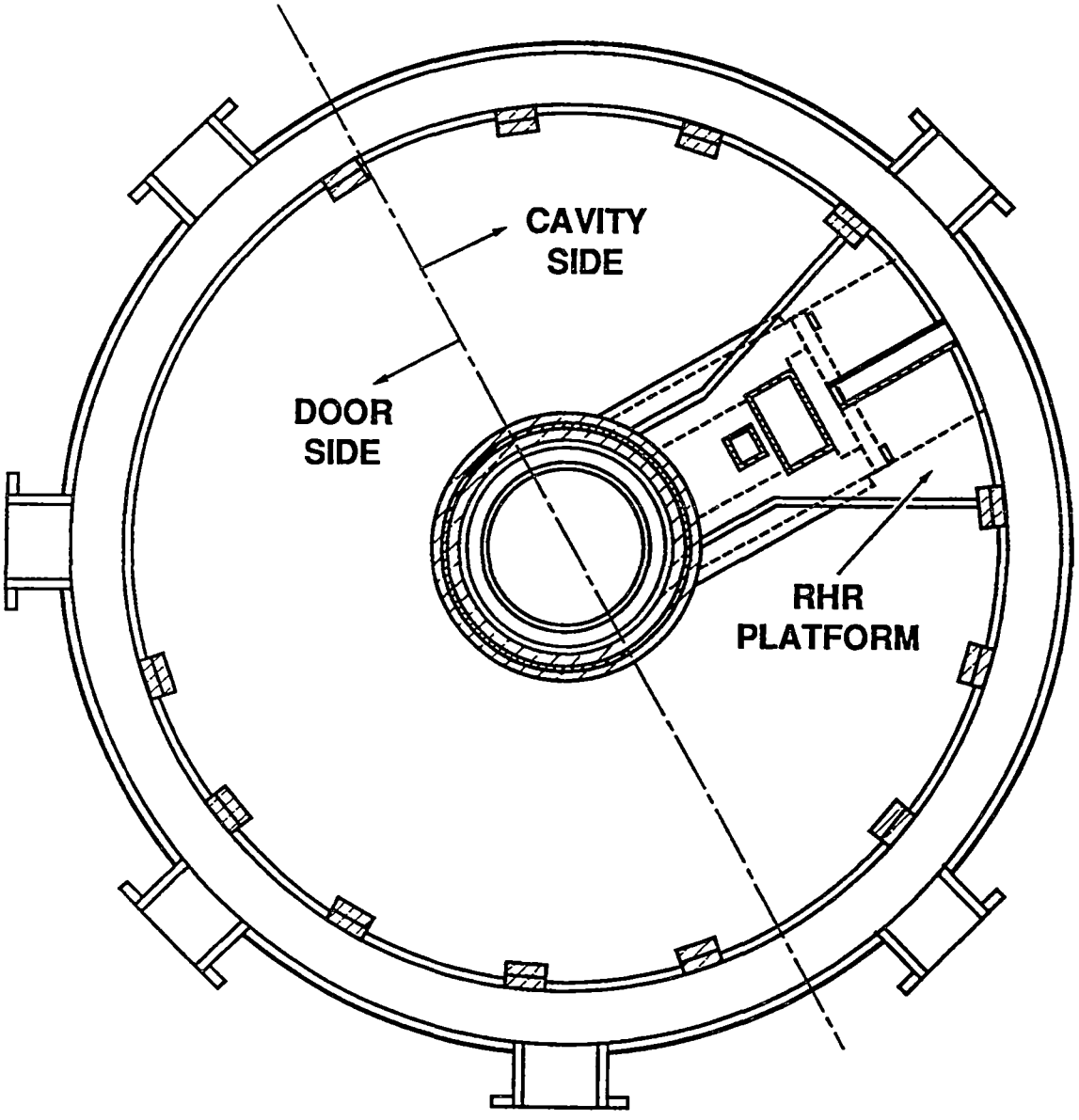

Figure 2.13. RHR platform plan view of structures inside the Surtsey vessel

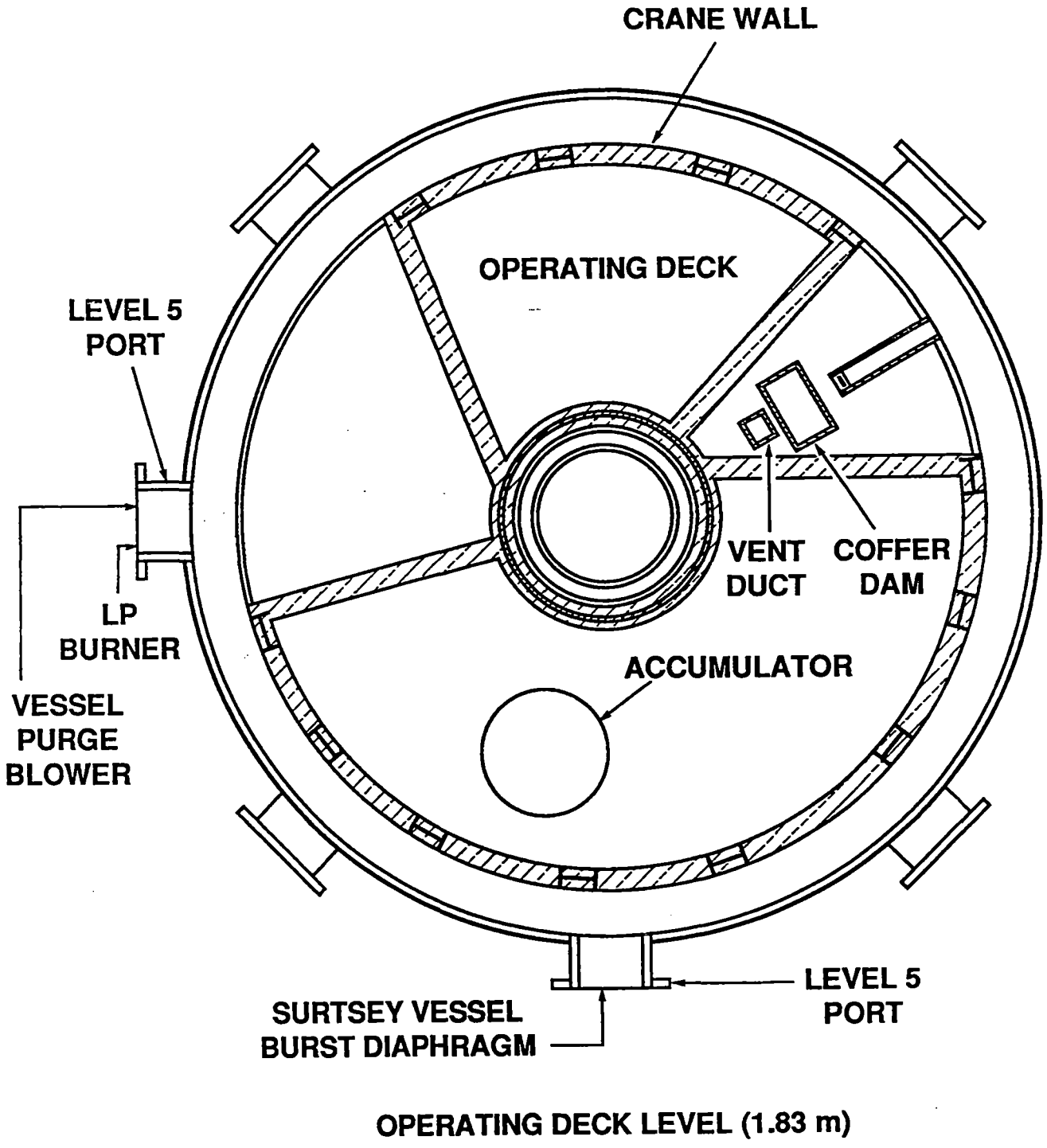

Figure 2.14. Operating deck plan view of structures inside the Surtsey vessel

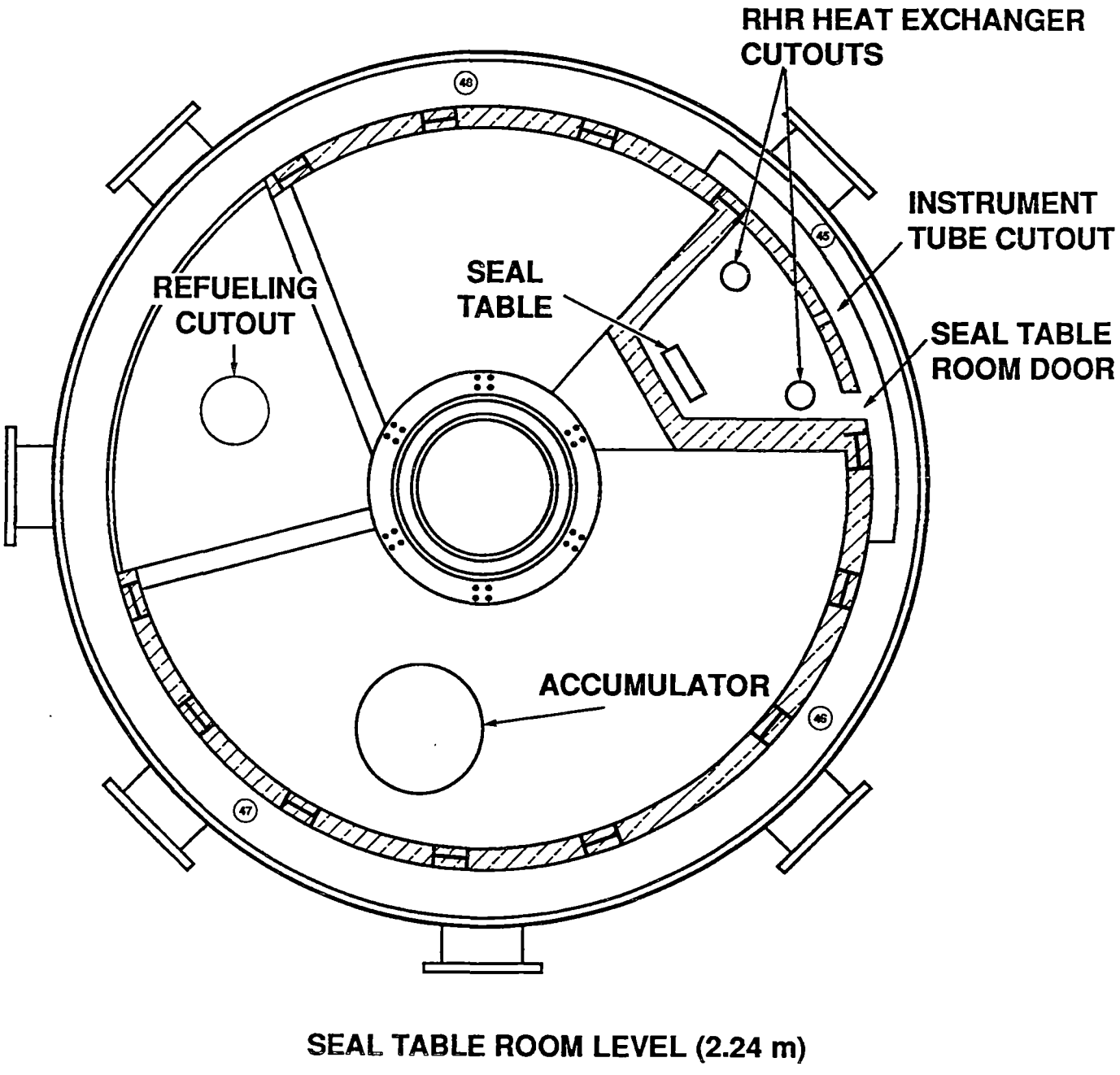

Figure 2.15. Seal table room plan view of structures inside the Surtsey vessel

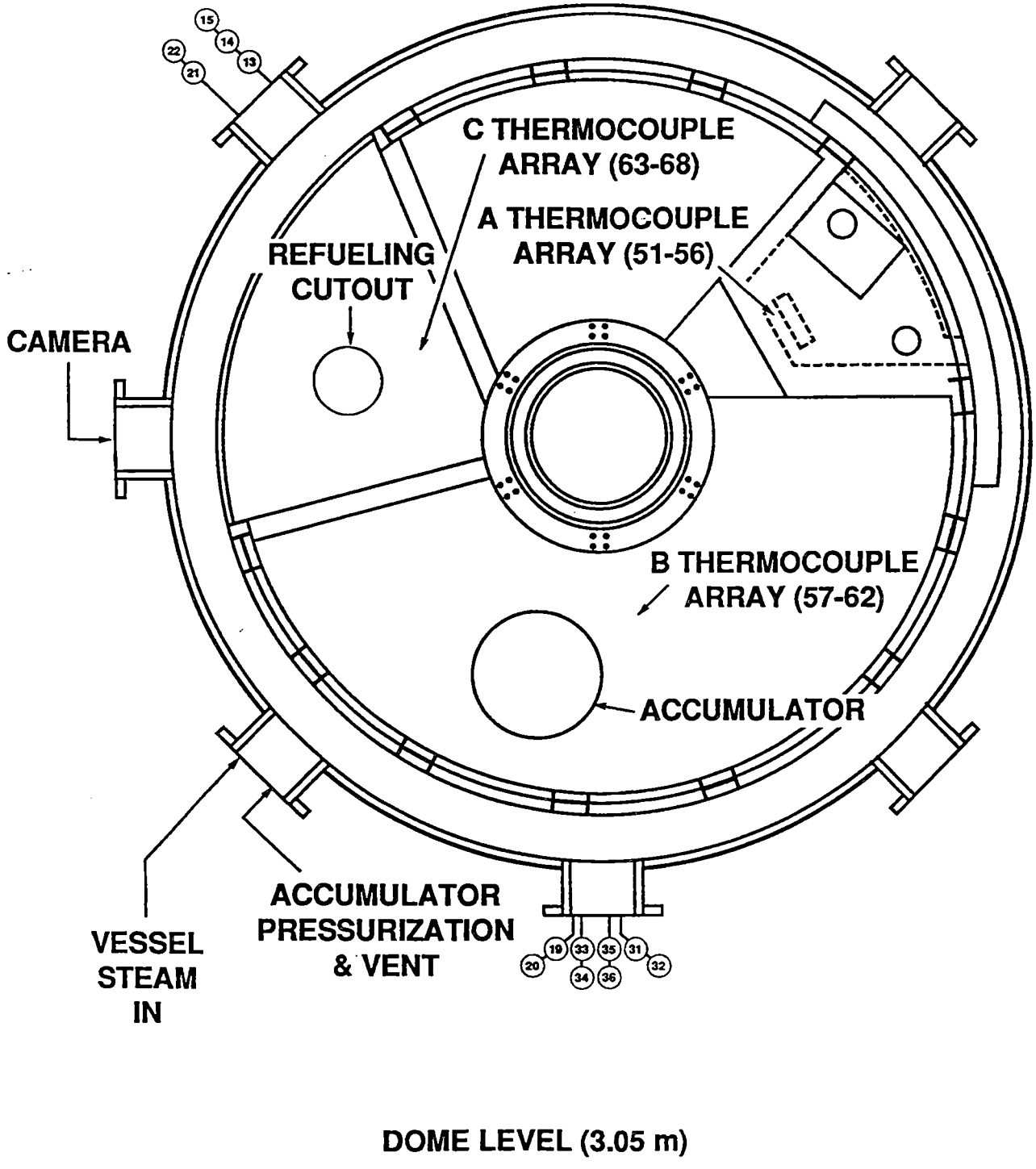

Figure 2.16. Dome level plan view of structures inside the Surtsey vessel

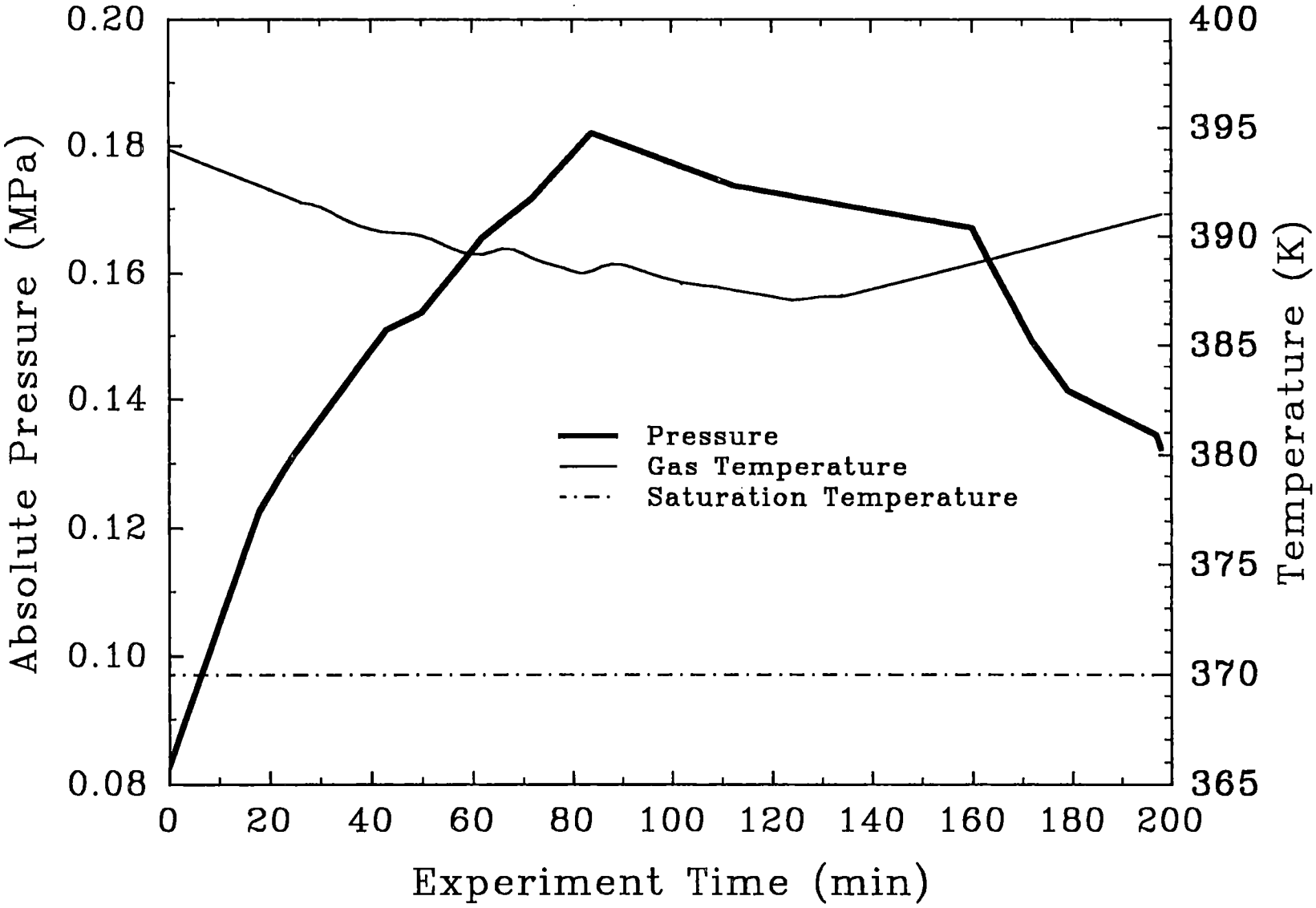

Figure 2.17 Containment vessel pressurization during the IET−9 initial condition setup.

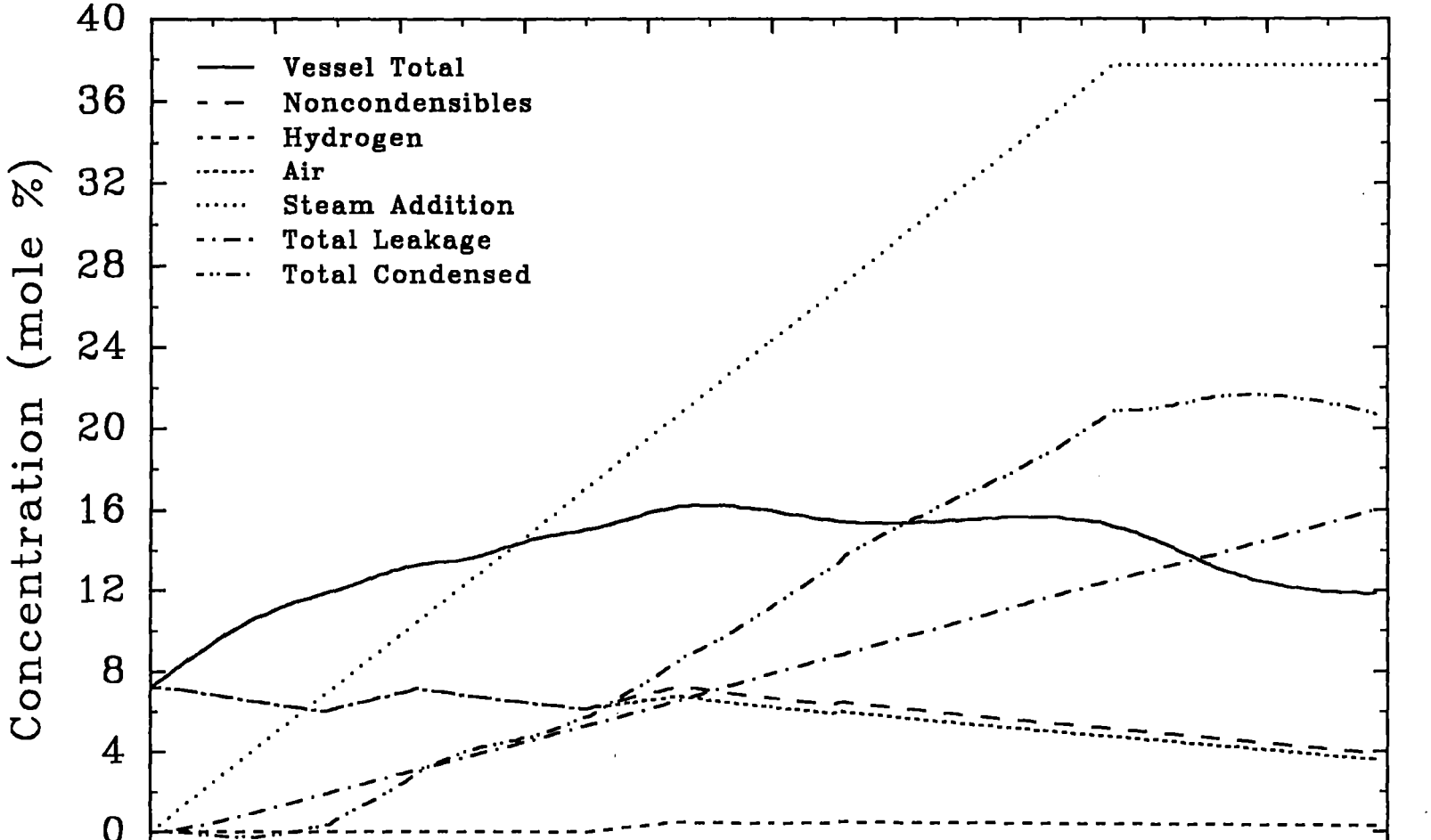

Figure 2.18 Containment vessel gas moles during the IET–9 initial condition setup.

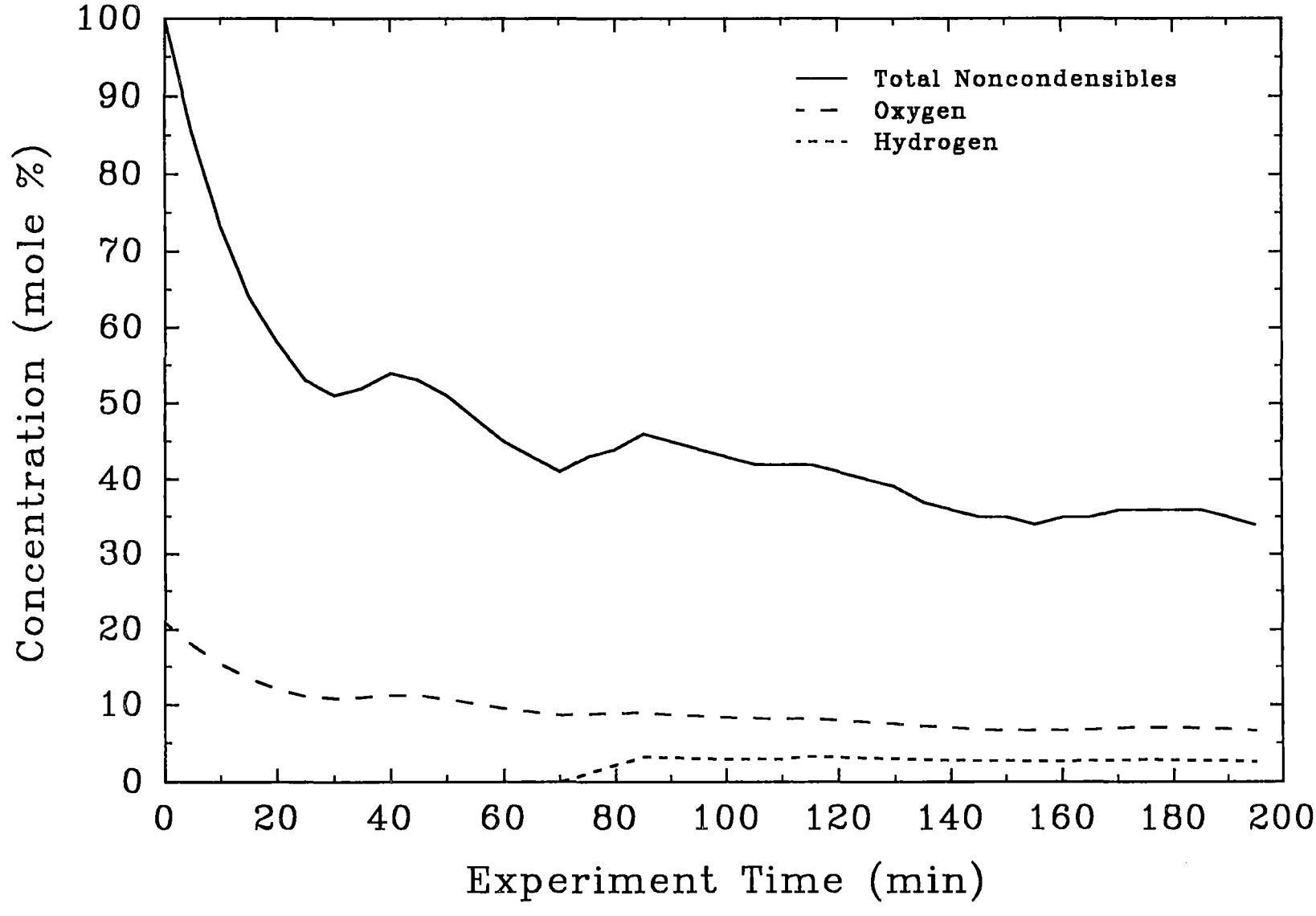

Figure 2.19 Containment vessel gas concentrations during the IET−9 initial condition setup.

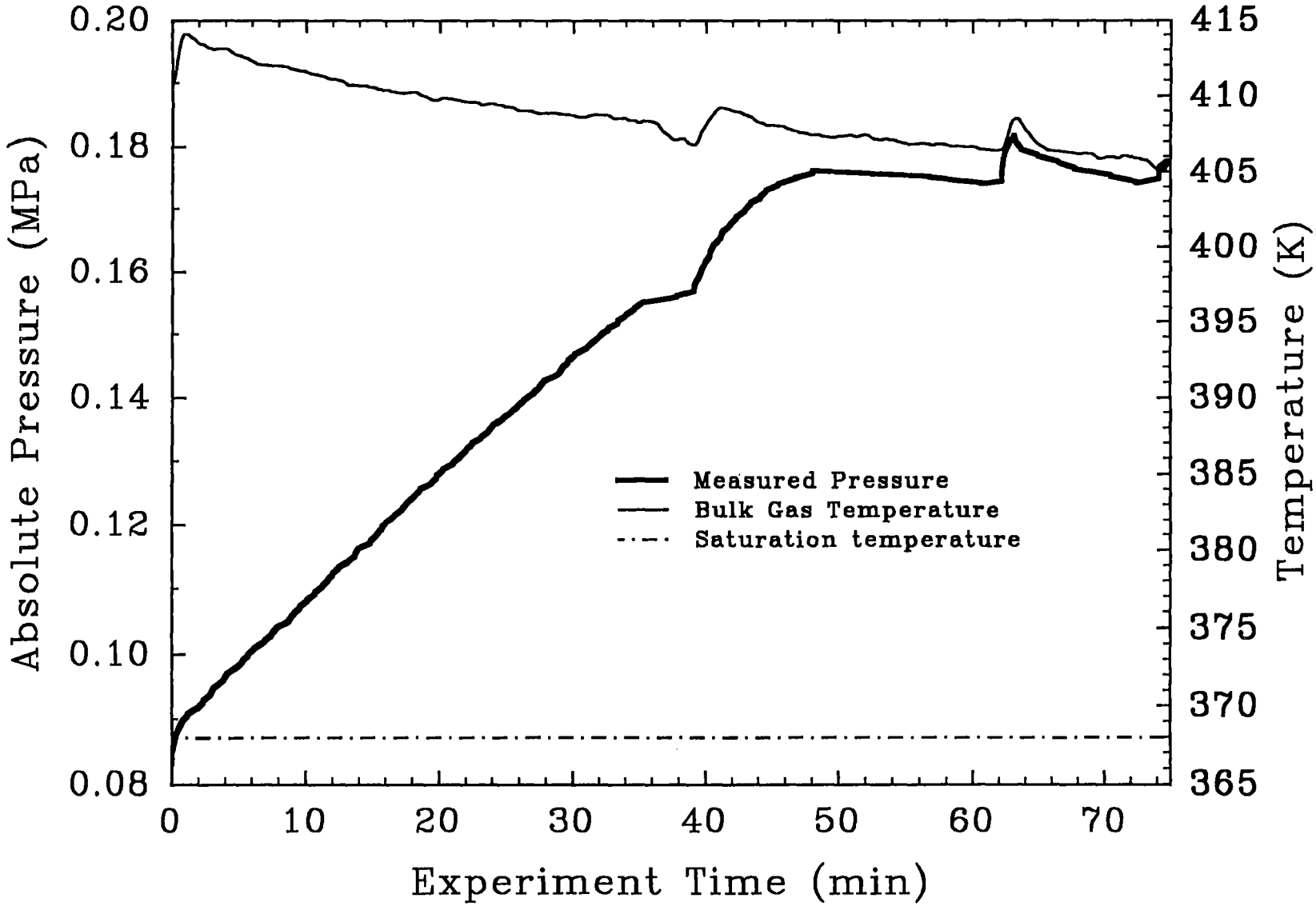

Figure 2.20 Containment vessel pressurization during the IET−10 experiment initial condition setup.

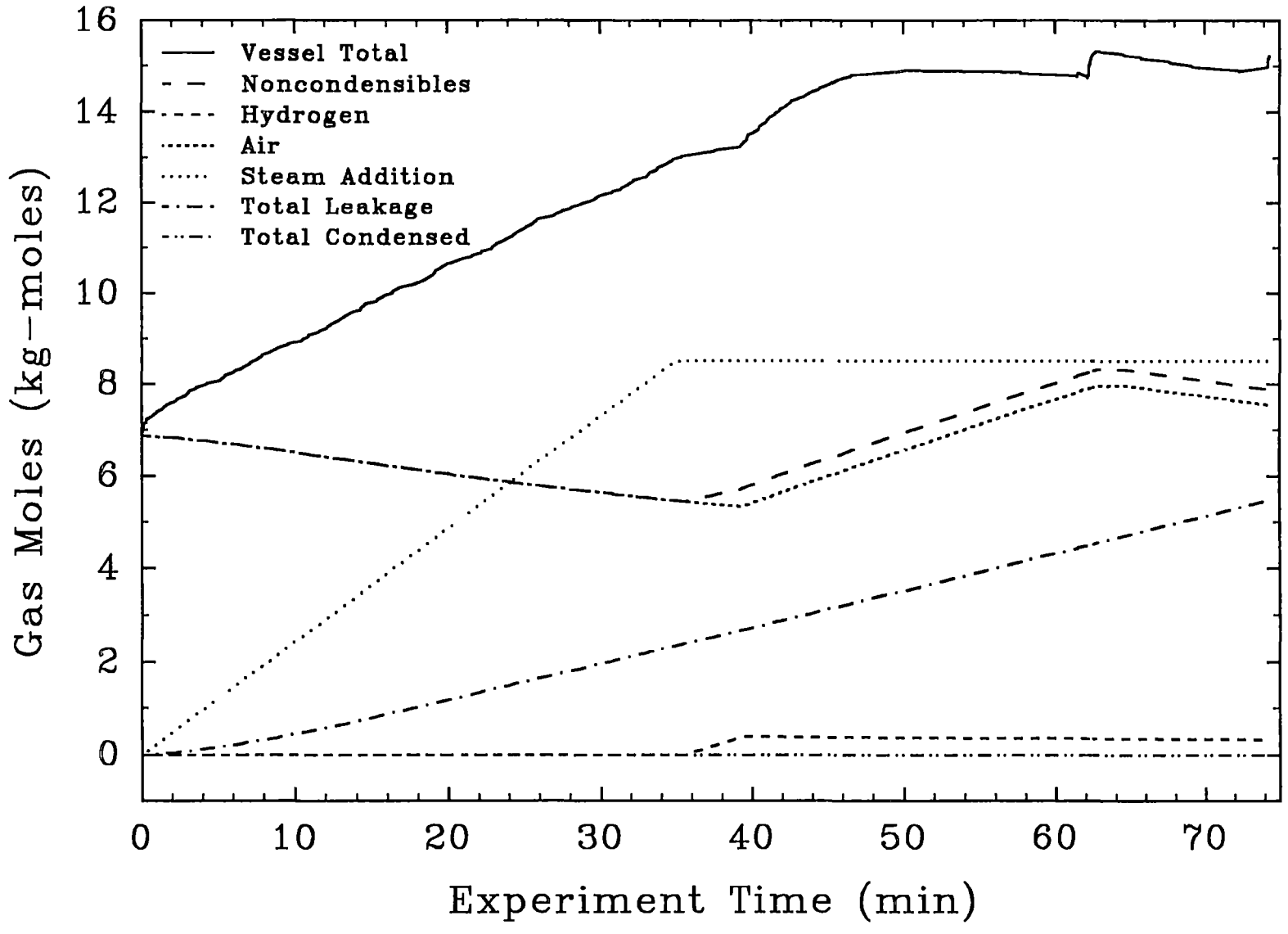

Figure 2.21 Containment vessel gas moles during the IET-10 initial condition setup.

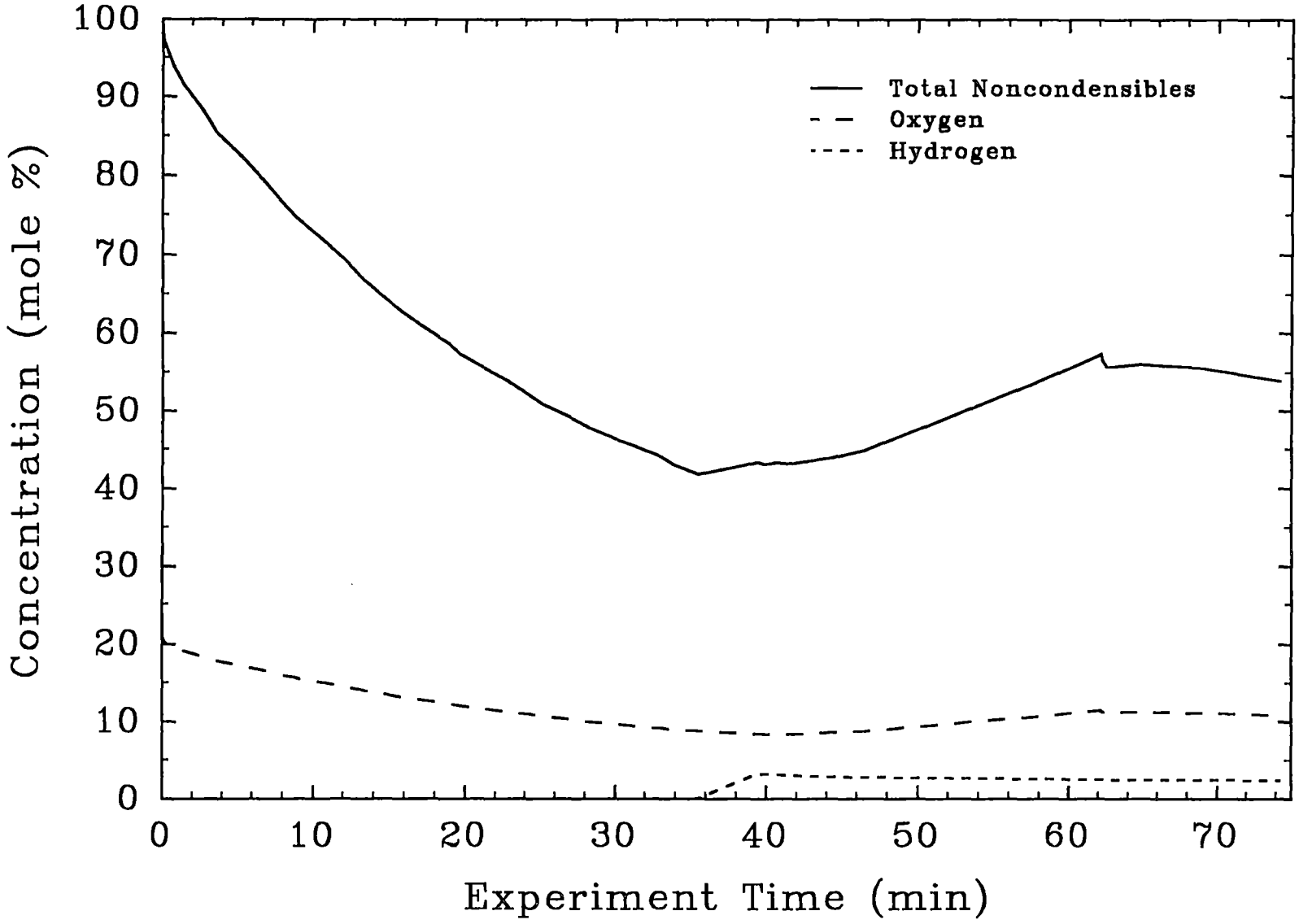

Figure 2.22 Containment vessel gas concentrations during the IET–10 initial condition setup.

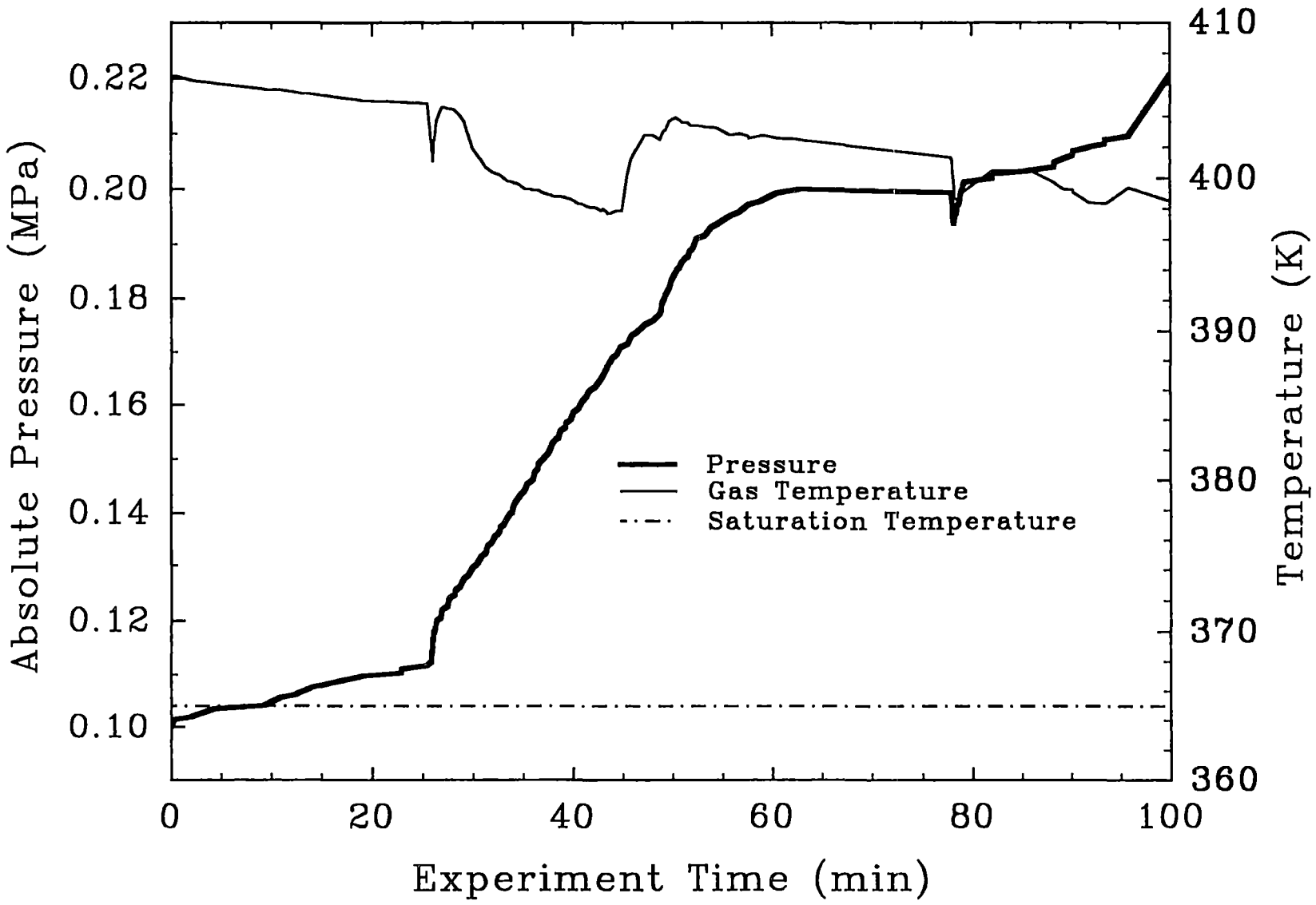

Figure 2.23 Containment vessel pressurization during the IET−11 initial condition setup.

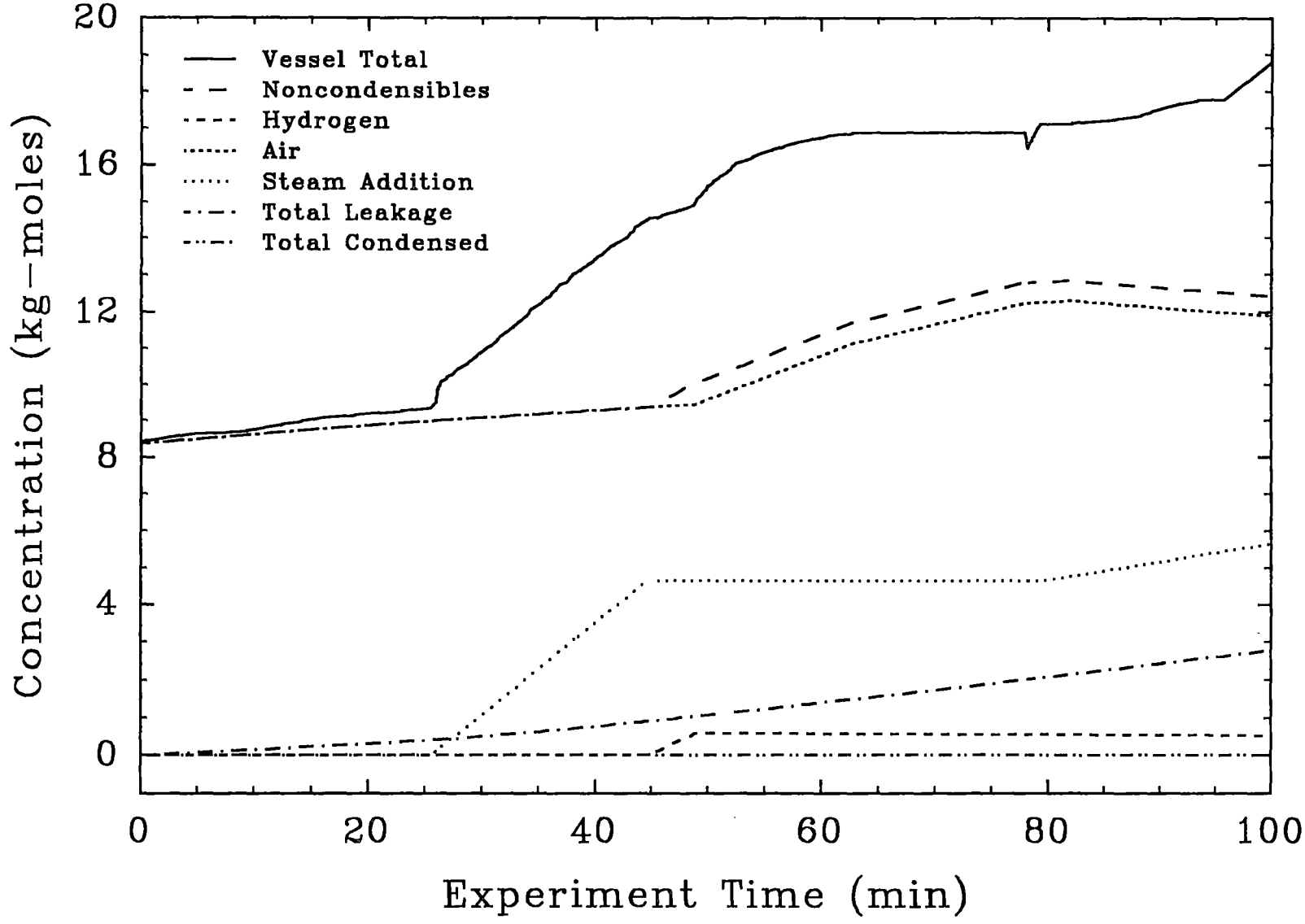

Figure 2.24 Containment vessel gas moles during the IET-11 initial condition setup.

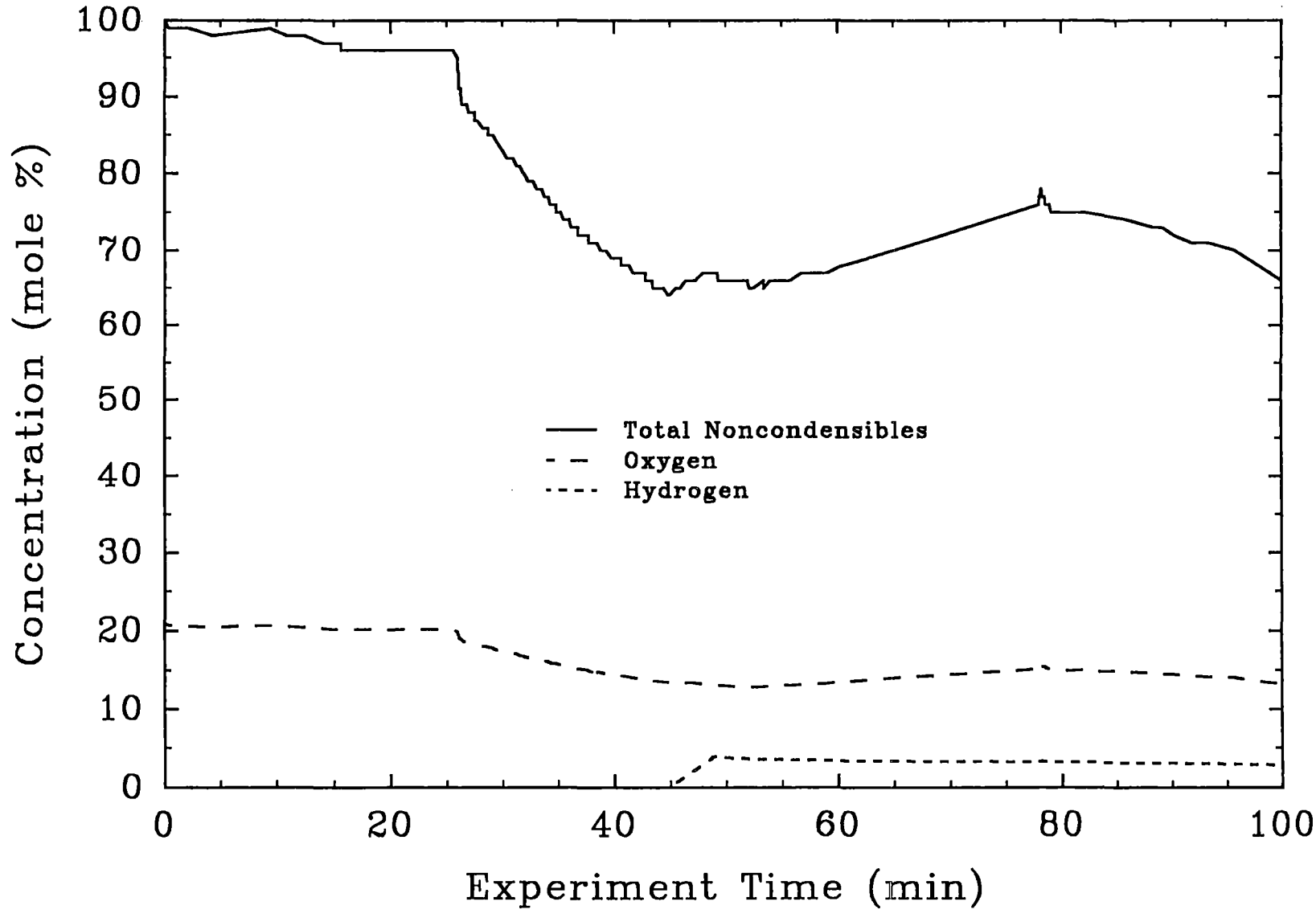

Figure 2.25 Containment vessel gas concentrations during the IET−11 initial condition setup.

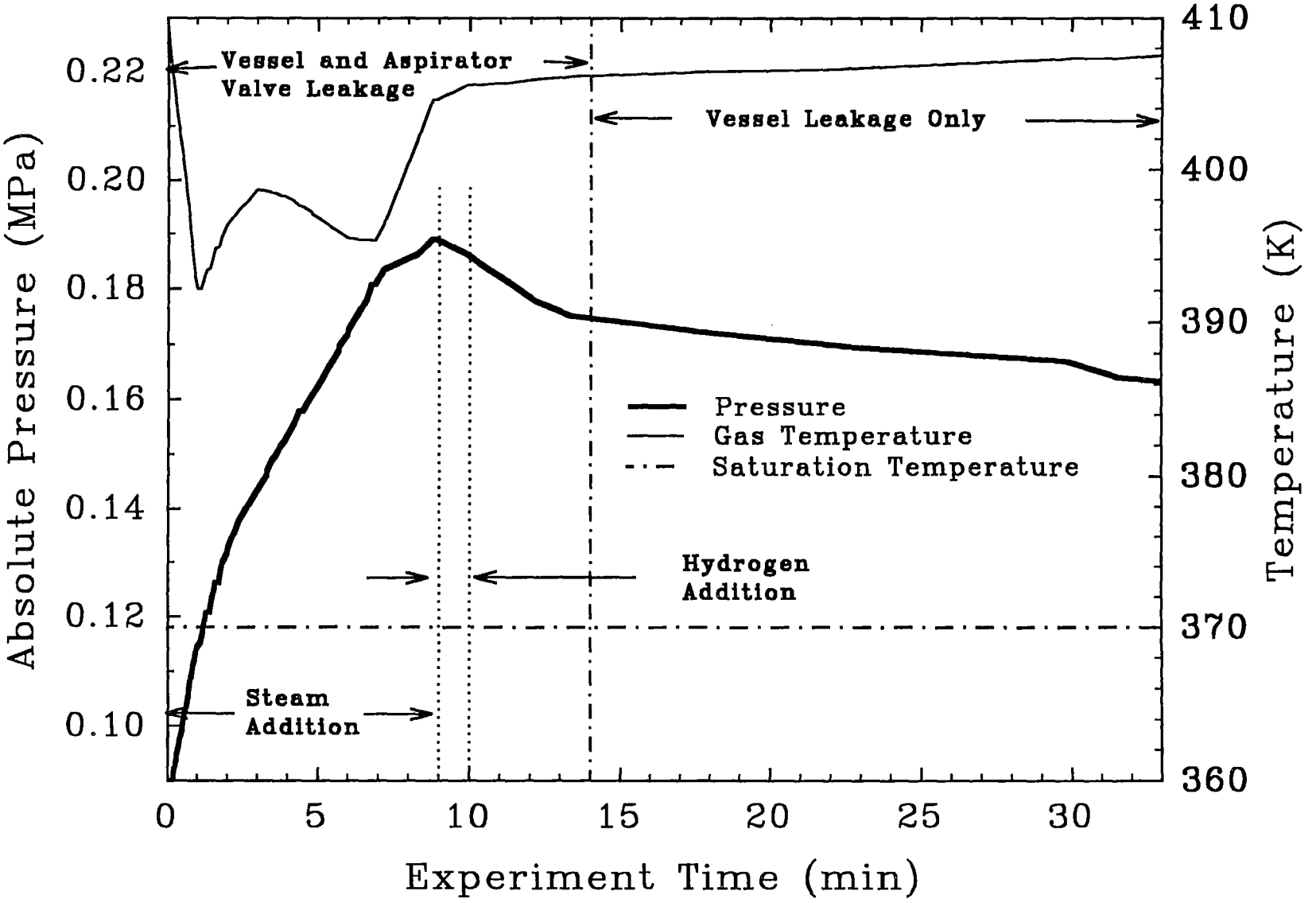

Figure 2.26 Surtsey vessel pressurization during the IET−12 initial condition setup.

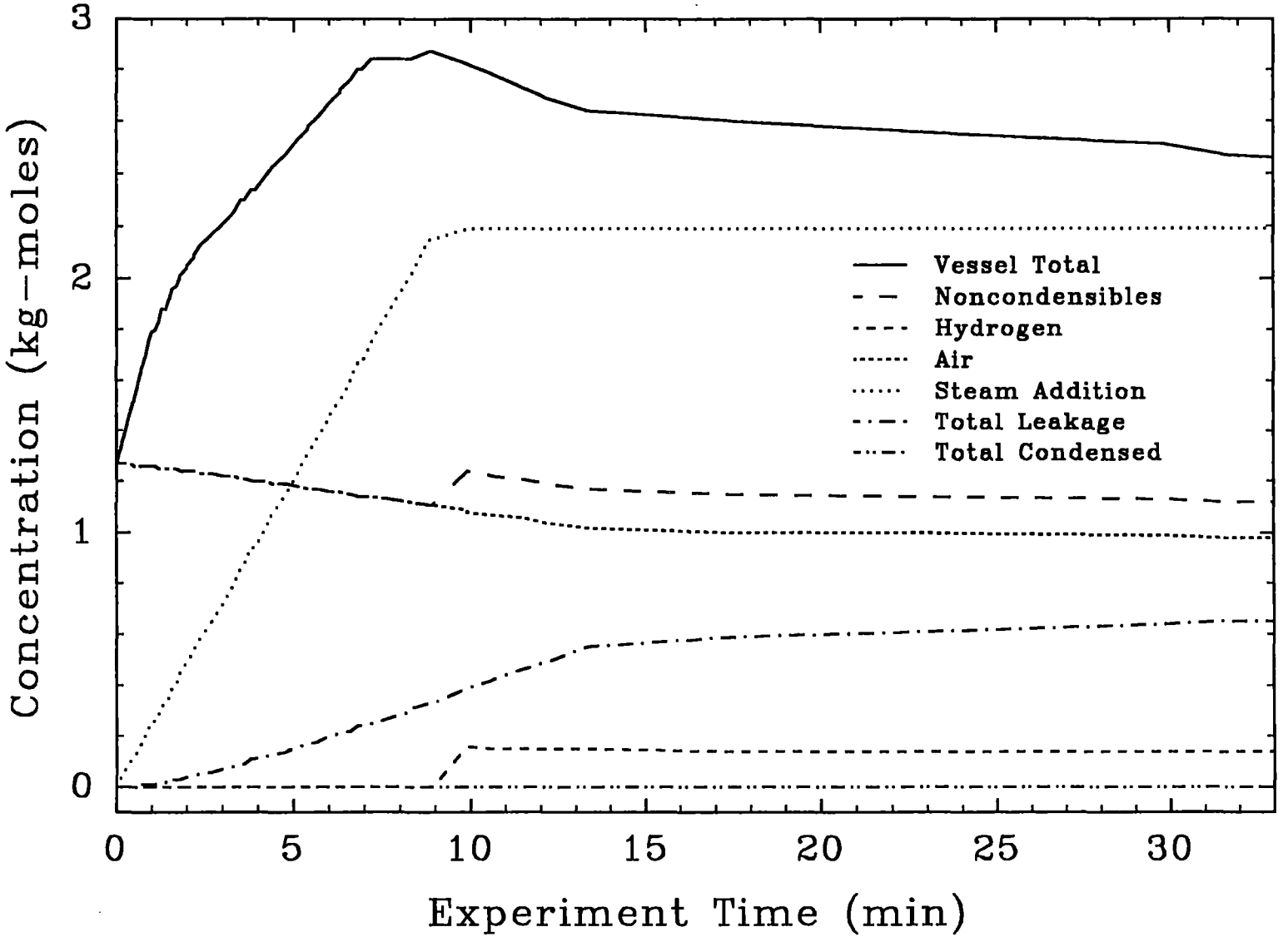

Figure 2.27 Surtsey vessel gas moles during the IET-12 initial condition setup.

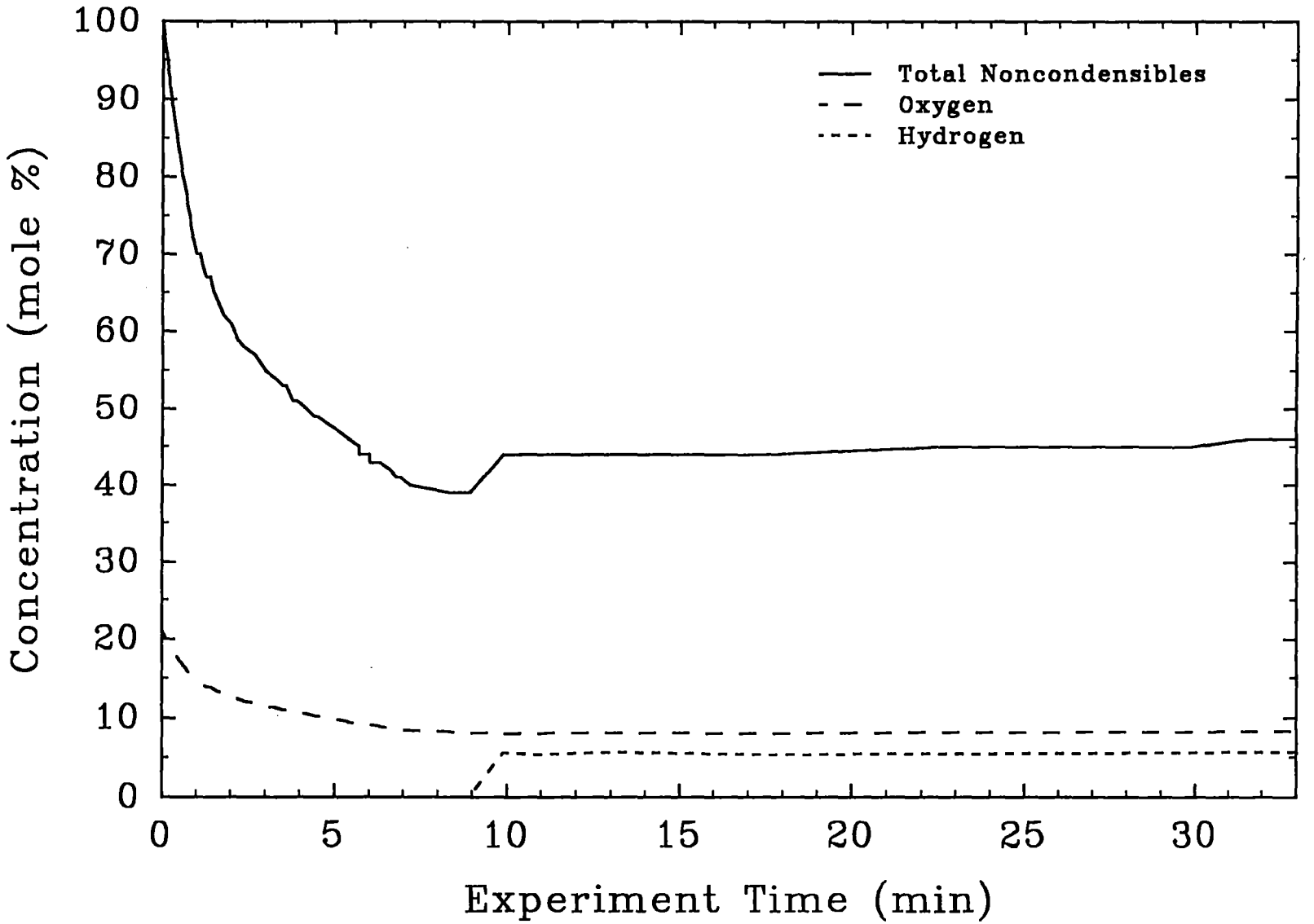

Figure 2.28 Surtsey vessel gas concentrations during the IET−12 initial condition setup.

3.0 Hydrogen Flammability

An important issue in HPME sequences is the contribution of hydrogen combustion to the peak containment pressure. Hydrogen that is produced by steam/metal reactions in the cavity and subcompartments, along with any preexisting hydrogen in the containment atmosphere, may recombine with oxygen in the subcompartments or upper dome. Hydrogen combustion will release energy to the atmosphere and could significantly increase the loads on the containment building. The extent of hydrogen combustion in a HPME event can be estimated using a hydrogen/air/steam flammability chart, such as the one presented in Figure 3.1 [Kumar 1985].

Figure 3.1 indicates that the initial atmospheric conditions in the IET experiments are on or just below the edge of the envelope of flammable concentrations. This implies that global combustion of the hydrogen in the containment atmosphere will not occur. However, it is possible that the atmospheric conditions in the subcompartments and in the upper dome during the HPME event would change sufficiently to permit hydrogen combustion. For example, higher gas temperatures expand the flammable envelope, decrease the minimum flammable concentration of hydrogen, and therefore, increase the possibility that global combustion of hydrogen will occur. This is illustrated in Figure 3.1 by showing the flammability limit at 473 K. Although global hydrogen combustion was unlikely under the conditions in these experiments, hydrogen apparently burned as a jet as it exited the subcompartments and entered the upper dome atmosphere. Blowdown steam reacted with metallic debris in the cavity/IIT region to form hydrogen, and thus, the blowdown gas entering the upper dome region was a mixture of steam and hydrogen. During the peak of the debris entrainment the blowdown gas was probably primarily hydrogen, and near the end of the blowdown, the gas was probably primarily steam. A line has been drawn in Figure 3.1 from a 100% hydrogen concentration to a 100% steam concentration. This line represents all possible concentrations of gases leaving the cavity/IIT region during the HPME after the initial sweep out of the ambient atmosphere.

Lines have been drawn in Figure 3.1 from the ambient conditions in the Surry DCH experiments to the point corresponding to the peak hydrogen levels in the cavity predicted by CONTAIN. These lines represent all possible gas concentrations and indicate that the gas concentrations in the plume pass through the flammable region. The lines clearly indicate the potential for combustion of the steam/hydrogen/air jet as it entered the upper dome.

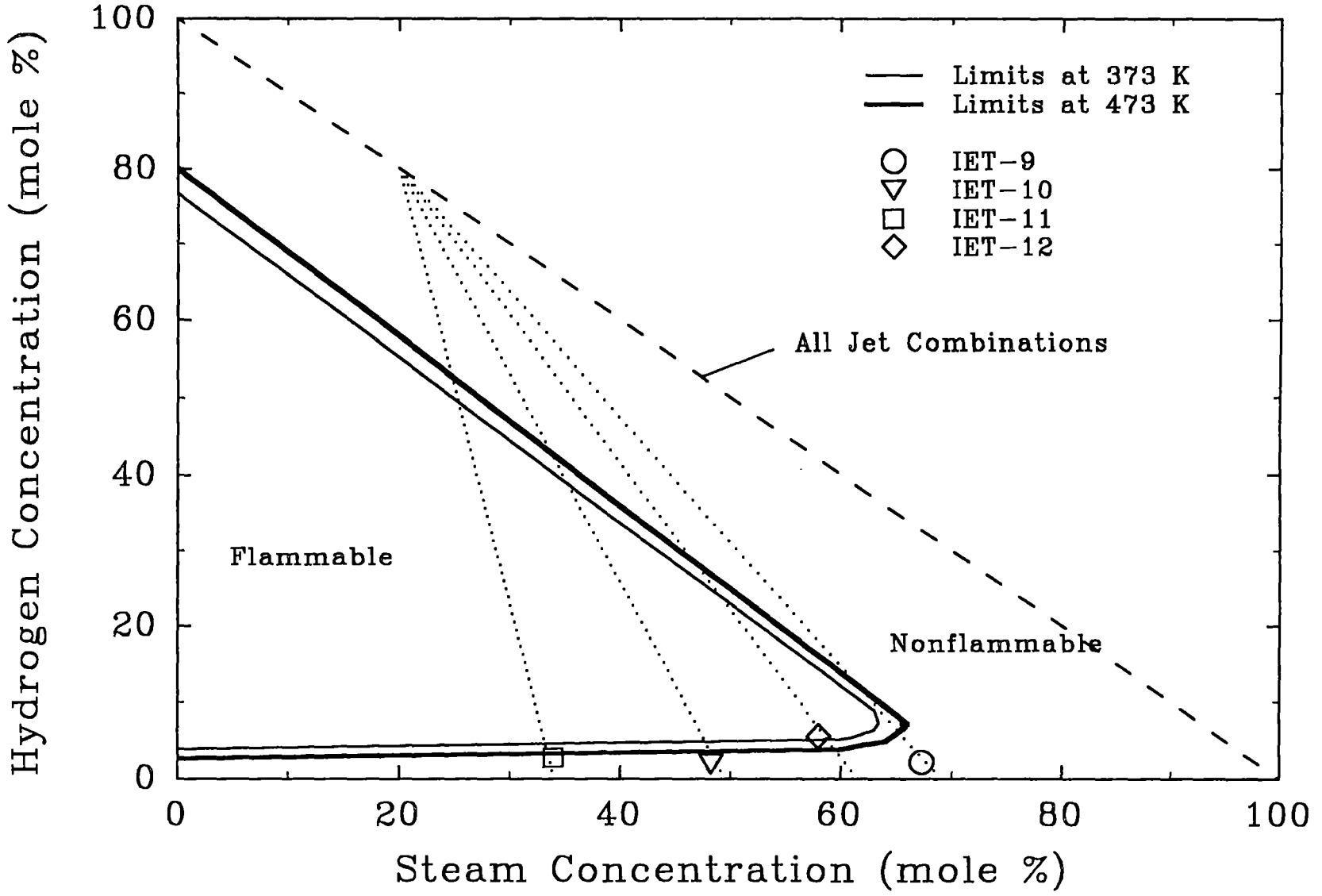

Figure 3.1 Upward propagation limit for hydrogen/air/steam mixtures.

4.0 Experimental Results

Some general pretest and posttest observations from the four Surry DCH tests are described in the following paragraphs. The specific experimental results are then presented in the following sections.

In the IET-9 test, a seal ring (Figure 2.2) was used to plug the large annular gap (0.036 m^2) that existed between the RPV and the reactor support skirt. A small gap (0.012 m^2) existed between the edge of the seal ring and the support skirt to provide clearance for assembly at the high-pressure melt ejection system. The CCD camera viewing the interior of the containment vessel showed a small grey cloud of aerosols being ejected through the partially opened annular gap at melt plug failure. Molten debris was then ejected from the annular gap and from the seal table room ceiling openings. This was followed by an orange fireball in the vessel that completely filled the view, possibly indicating that a hydrogen burn occurred at these locations. Seconds later, molten debris rained down in front of the camera port before aerosols obscured the view. The camera port is located on the opposite side of the vessel from the seal table room. It appeared that the molten debris that was ejected from the STR ceiling openings struck the liner on the cavity side of the containment, glanced off and followed the dome around and downward in front of the camera, and fell on the basement floor in front of the five-foot door.

Posttest examination of the CTTF containment vessel several days later revealed that the trough at the vessel perimeter contained about 2-4 cm of water mixed with large amounts of debris. The interior structures and basement and operating deck floors were dry. This supports the conclusion that water was condensing on the interior containment vessel wall and floor as steam was added to get the initial atmosphere conditions in the IET-9 test. A small amount of water was drained from the trough about one hour prior to the test. No water was found on the cavity floor at that time. The structures sustained no damage during the experiment. The seal table was not modeled in the IET-9 test.

In IET-10, the crucible pressure transducer line attached to the crucible head was hit and severed by melt immediately after burst diaphragm failure. The crucible pressure measurement indicated that this occurred at about -1 s. This opened a 1/2-inch diameter hole through which steam and debris exited. Debris (about 0.8 kg) from this hole impacted and froze on the underside of the control rod drive missile shield. The failure of this fitting caused an increase in vessel pressure of $\approx$0.015 MPa prior to the HPME initiation. This is 4.6% of the total pressure change. The average bulk gas temperature in the vessel increased $\approx$10 K during this 1 s interval. This is 2.2% of the total temperature change. The failure of this fitting 1 s prior to melt plug failure had inconsequential effects on the outcome of the IET-10 experiment.

The seal ring used to plug the large annular gap (0.036 m^2) that existed between the RPV and the reactor support skirt was redesigned after IET-9; a completely closed annular gap was maintained in IET-10. The CCD camera viewing the interior of the containment vessel showed a small grey jet of steam and/or aerosols being ejected through the pressure fitting on the crucible head after burst diaphragm rupture. This was followed by a fireball that overexposed the CCD camera and completely 'whited out' the view, possibly indicating that a hydrogen burn occurred. Seconds later, molten debris (that was probably ejected from the STR) rained down in front of the camera port before aerosols obscured the view.

Posttest examination of the CTTF containment vessel several days later revealed that the trough at the vessel perimeter contained no water. The interior structures, basement, and operating deck floors were also dry. The structures sustained no damage during the IET-10 experiment.

The seal table apparently remained intact for most of the cavity debris entrainment interval. A long, thin slot was ablated through the side of the seal table away from the crucible. A few of the mounting brackets had pulled loose from one end of the seal table, and the seal table was found partially bent upward and away from the seal table room floor opening.

Posttest examination of the crucible exit hole revealed that a portion of the graphite disk was missing. Sometime during the HPME, the disk must have broken and some parts were ejected along with the melt. As a consequence, the hole was larger in IET-10 than in IET-9. In IET-9, the ablated hole size was 7.44 cm. In IET-10, the ablated hole size was 9.84 cm. Note that the original graphite disk had a outer diameter of 13.3 cm and an inner diameter of 7.0 cm.

In the IET-11 experiment, the annular gap seal ring was not used and scaled reflective metal insulation was placed on the RPV model. The CCD camera viewing the interior of the containment vessel showed molten debris ejection from the annular gap. This was followed by a fireball in the vessel after the HPME that overexposed the CCD camera and completely 'whited out' the view.

Posttest examination of the CTTF containment vessel several days later revealed that the structures sustained no damage during the experiment. Large quantities of debris were seen on the horizontal surfaces of the operating deck, as compared to IET-10. Most of the scaled reflective metal insulation was completely removed from the bottom of the scale model of the RPV. A few pieces that did remain in the annular gap were caught below the nozzles and were heavily encrusted with debris. Small pieces of insulation were found on the operating deck and on the metal grating in the upper dome region, with the largest piece about 10 cm long. Some of the molten debris exiting the annular gap impacted on the underside of the missile shield and some impacted and stuck on the bottom of the I-beams that support the upper deck gratings. The top of the missile shield had more debris on it than was found in IET-10, which indicated that large quantities of debris were ejected into the dome region and subsequently 'rained' down.

The seal table remained anchored to the seal table room floor. A long, thin slot was ablated through the side of the seal table away from the crucible. Posttest examination of the crucible exit hole revealed that the graphite disk was intact. In IET-11, the final hole size was 7.60 cm.

There was an attempt to add condensate levels of water to the cavity and containment basement floor. Posttest investigation showed that the tube that supplied water to the cavity had plugged. The cavity pressure traces verified that no water was in the cavity during the HPME.

During the IET-12 experiment, the CCD camera viewing the interior of the vessel showed a small amount of molten debris ejection from the RHR platform. A burning gas jet was also seen exiting from the top of the crucible and striking the underside of the missile shield. However, the video of the experiment gave the general impression that little hydrogen burned during the test, especially when compared to the 1:6 scale tests in the CTTF.

Posttest examination of the Surtsey vessel several days later revealed that the structures sustained no damage during the experiment. Little debris was seen on the horizontal surfaces of the operating deck. The annular gap remained sealed throughout the test. The top of the missile shield had no debris on it. This indicated that very small quantities of debris were ejected into the dome region. The seal table remained anchored to the seal table room floor and was not ablated by molten debris. Posttest examination of the crucible exit hole revealed that the graphite disk was intact and had not ablated. In IET-12, the initial and final hole size were the same, 5.6 cm.

The crucible pressure transducer line attached to the crucible head failed due to interactions with molten debris. The crucible pressure measurement indicated that this occurred immediately before melt plug failure. This opened a 1.3-cm diameter hole through which steam and/or burning gas exited, as indicated on the video. No debris appeared to have exited through this pathway because none was found on the underside of the control rod drive missile shield (as was the case in the IET-10 experiment), probably because the crucible was pressurized for only ≈0.1 s prior to melt plug failure. Since the area ratio between the crucible exit hole and the pressure transducer hole was ≈20:1, the failure of this fitting at melt plug failure had inconsequential effects on the outcome of the IET-12 experiment.

4.1 Blowdown History

Figures 4.1 through 4.4 are the blowdown histories for the IET-9, IET-10, IET-11, and IET-12 tests, respectively. The blowdown histories are essentially the 'signature' curves for the experiments; the accumulator, burst diaphragm, and crucible pressure traces indicate whether the tests went as planned. The blowdown history figures give the thermite ignition time, the steam driving pressure at t = 0 s, the steam blowdown time, and the time that steam was in contact with the molten thermite prior to melt plug failure.

In the 1:6 scale IET experiments, the accumulator tank and the 15-cm-diameter pipe up to the burst diaphragm (volume = 1.282 m^3) was pressurized with superheated steam to ≈14 MPa, and the burst diaphragm was concurrently pressurized to about 6 MPa. The crucible pressure started at about 0.1 MPa. The thermite was ignited at about t ≈ -7 s.

In the 1:10 scale IET experiment, the accumulator tank and the 10-cm-diameter pipe up to the burst diaphragm (volume = 0.238 m^3) was pressurized with superheated steam to ≈12 MPa, and the burst diaphragm was concurrently pressurized to about 5 MPa. The crucible pressure started at about 0.1 MPa. The thermite was ignited at about t ≈ -2 s; the time to melt plug failure was shorter than in the 1:6 scale tests.

After thermite ignition, crucible pressure started to rise, and at a pressure of ≈1.5 MPa, the burst diaphragm separating the steam accumulator tank and the molten thermite was failed remotely by the operator. This equilibrated the accumulator, burst diaphragm, and crucible pressures and brought steam into contact with the molten thermite a few seconds before the HPME in IET-9, IET-10, and IET-11; however, the steam was in contact for only 0.05 s in IET-12.

In all of the IET experiments, the number of g•moles of steam driving gas was calculated prior to burst diaphragm failure using accumulator steam pressure, temperature, and volume. Figure 4.5 shows the measured steam temperature for all of the IET tests.

In IET-9, the steam pressure was 13.93 MPa and the steam temperature was 796 K at t = -8 s. The steam driving gas was calculated to be 3005 g•moles. The horizontal dotted line across Figure 4.1 shows that the steam driving gas pressure at the initiation of the HPME (t = 0 s) was 12.94 MPa. The crucible pressure transducer tap became plugged with melt at about 1 s.

In IET-10, the steam pressure was 13.46 MPa and the steam temperature was 713 K at t = -2 s. This gives an uncorrected amount of 3457 g•moles of steam driving gas. This value should be reduced because of the steam that was lost when the crucible fitting failed. An estimate of the amount of steam that was lost was obtained by utilizing the pressure reduction in the accumulator after the burst diaphragm failed and before the melt plug failed. A ratio of the pressure drop during this 1 s interval indicated that 5.25% of the initial steam moles ((12.75-12.08) / 12.75) was lost, or that 181.6 g•moles

of steam leaked out of the crucible head (0.0525 x 3457) prior to failure. Therefore, 3275 g•moles of steam is the estimated amount of blowdown steam in the IET-10 experiment. The horizontal dotted line across Figure 4.2 shows that the steam driving gas pressure at the initiation of the HPME was 12.08 MPa.

In IET-11, the steam pressure was 14.03 MPa and the steam temperature was 709 K at t = -4 s. This gives 3705 g•moles of steam driving gas from the accumulator blowdown in the IET-11 experiment. The horizontal dotted line across Figure 4.3 shows that the steam driving gas pressure at the initiation of the HPME was 13.2 MPa.

In IET-12, the steam pressure was 12.33 MPa and the steam temperature was 696 K at t = -2 s. This gives 604 g•moles of steam driving gas from the accumulator blowdown in the IET-12 experiment. The horizontal dotted line across Figure 4.4 shows that the steam driving gas pressure at the initiation of the HPME was 11.2 MPa. The crucible pressure transducer measured vessel pressure upon failure of the transducer pressure line.

There was a small amount of saturated water that was co-ejected with the blowdown steam during the IET-12 test. A general description of the accumulator hardware and the accumulator charging process is necessary to understand how water was co-ejected with the blowdown steam. The accumulator is composed of a vertical cylindrical shell (136 cm long with a 40 cm I.D.) with hemispherical heads capping the ends. Five electrical band heaters are arranged equidistant along the cylindrical shell. Two gas-space thermocouples are mounted 10 cm inside the shell near the ends. Three thermocouples are mounted in the accumulator steel; one is in the center of the shell and two are in the heads about 45° from the vertical. The accumulator bottom head is welded to a support skirt that is bolted to the basement floor. The accumulator is insulated from the top head to the basement floor. The accumulator is pressurized with steam through a penetration in the bottom head. There is about 12 m of unheated, insulated steel tubing (2-cm I.D.) that connects the boiler to the accumulator. The boiler can provide up to 13.8 MPa of saturated steam at a rate of 263 kg/hr.

Figure 4.6 gives the temperature and pressure of the steam and the temperature of the accumulator from the start of the accumulator pressurization to 24 minutes after the blowdown. The accumulator steam pressurization valve was opened six times (-36 min, -18 min, -17 min, -9 min, -7 min, and -1 min). Each time the valve opened, about 1.5 kg of saturated water could have been added if all of the steam in the charging line had condensed. This water collected in the bottom head and boiled off. This cooled the bottom head as shown by the temperature decrease measured by thermocouple channel 74. The addition of steam at t = -7 min caused a reduction in the bottom head temperature to ≈585 K, which is below the 600 K saturation temperature for the accumulator pressure of 12.33 MPa. The bottom head temperature partially recovered, but did not rise above saturation temperature. This implied some amount of water boiling in the bottom head.

Further evidence of water in the bottom head is also shown on Figure 4.6. The bottom head temperature dropped to and remained at saturation for 18 minutes after the blowdown. The bottom head temperature rose to 600 K after the water boiled off. If it is assumed that the entire bottom head contributed heat, about 3 kg of saturated water boiled off posttest.

The data from the 1:6 scale tests conducted in the Containment Technology Test Facility (IET-9, IET-10, and IET-11) was examined and no evidence of behavior similar to that shown in Figure 4.6 was found. The steam accumulator tank and delivery system were unique to IET-12, and thus, the observations on the effects of co-ejected water from the accumulator are unique to IET-12.

The expanded accumulator pressure curves for all of the IET experiments (Figure 4.7) are given to allow calculation of the blowdown time constant (τ_b). These curves, along with the cavity pressure curves presented in Section 4.2.2, can be used to determine the steam-to-debris coherence ratio used in the two-cell equilibrium model [Pilch 1991] to calculate the containment load.

The pressure, temperature, and number of moles of steam driving gas for each experiment are listed in Table 2.7.

4.2 Pressure Measurements

Pressure transducers were used in IET-9, IET-10, and IET-11, to measure the pressure increase in the CTTF containment vessel, in the cavity, in the basement region below the operating deck, in the RHR platform, and in the seal table room. Pressure transducers were used in IET-12 to measure the pressure increase in the Surtsey vessel and in the cavity. The following sections describe the results of the pressure measurements.

4.2.1 Vessel Pressure

Figures 4.8, 4.9, 4.10, and 4.11 show the absolute pressure in the containment vessel versus time for the IET-9, IET-10, IET-11, and IET-12 experiments, respectively. Each figure shows a horizontal dotted line to indicate the initial pressure in the containment vessel prior to the HPME transient. Each figure also shows a horizontal dotted line at the peak pressure caused by the HPME. The pressures measured at two levels on opposite sides of the containment vessels with four different pressure transducers were virtually identical.

In the IET-9 experiment, the initial absolute pressure was 0.134 MPa, as listed in the table of initial conditions (Table 2.7). The peak pressure increase in the IET-9 experiment was 0.283 MPa, and the peak pressure was reached at $\approx$3.0 s after the beginning of the HPME transient.

In the IET-10 experiment, the initial absolute pressure was 0.179 MPa. The peak pressure increase in the IET-10 experiment was 0.326 MPa, and the peak pressure was reached at $\approx$2.5 s after the beginning of the HPME transient.

In the IET-11 experiment, the initial absolute pressure was 0.22 MPa. The peak pressure increase in the IET-11 experiment was 0.430 MPa, and the peak pressure was reached at $\approx$2.8 s after the beginning of the HPME transient.

In the IET-12 experiment, the initial absolute pressure was 0.163 MPa. The peak pressure increase in the IET-12 experiment was 0.198 MPa, and the peak pressure was reached at $\approx$1.4 s after the beginning of the HPME transient.

4.2.2 Cavity Pressure

The timing of debris ejection from the cavity into the subcompartment structures is important when analyzing a HPME/DCH event and is best understood by comparing the cavity pressure with the Surtsey vessel pressure. Figures 4.12, 4.14, 4.16, and 4.18 give the cavity pressures measured in the IET experiments plotted against time, where t = 0 is the beginning of the HPME. These cavity pressure curves, along with the steam blowdown curves (Figure 4.7), are used to estimate the coherence ratio.

Previous DCH tests [Allen et al. 1992a-g; 1993a,b] have characterized cavity pressure curves and have determined that three distinct peaks in the cavity pressure can be produced. The small first peak was caused by efficient gas heating as molten brass, steel, and thermite entered the cavity. The second peak was due to thermite/water interactions if water was present in the cavity. The water could produce two

distinctly different types of interactions: energetic interactions, which are often referred to as steam explosions, or rapid vaporization of cavity water. Those peaks caused by steam explosions had a short duration and a large magnitude compared to those which resulted from simple vaporization of cavity water. The third broad peak in all the tests was the result of debris entrainment from the cavity by the steam blowdown. The debris entrainment occurred between ≈0.3 s and ≈1.0 s for all of the 1:6 scale IET tests. In the 1:10 scale test (IET-12), the debris entrainment interval occurred between ≈0.0 s and ≈0.9 s, which is an indication that there was immediate blowthrough in IET-12.

Figure 4.12 is a plot comparing the cavity pressure measured in the IET-9 experiment to the vessel pressure. The broad peak, which appears between ≈0.0 and ≈0.3 s, was probably due to vaporization of cavity water caused by thermite/water interactions. The CTTF vessel liner and cavity were at saturation temperature; some of the steam in the atmosphere condensed in the cavity. The debris entrainment time constant (τ_c) can be calculated using Figure 4.12. Debris entrainment by the steam blowdown occurred between t ≈0.3 s and t ≈1.0 s.

Figure 4.13 gives the cofferdam exit pyrometer signal versus time in the IET-9 experiment. The voltage signal from the pyrometer was too small to allow conversion to a debris temperature measurement. However, the signal clearly verifies the debris entrainment interval given on the cavity pressure plot. The pyrometer was mounted in the basement underneath the operating deck. The pyrometer was located about 2 m from the cofferdam exit, and viewed the exit through the RHR platform right side wall 'window'. Cooling water is supplied to the instrument and a small purge gas flowed across the window to prevent condensation from obscuring the view. Either condensation formed on the window or enough aerosols were trapped in the RHR platform area to partially obscure the pyrometer view. In all of the tests, the pyrometer signal was too small to allow conversion of the signal to temperatures.

Figure 4.14 is a plot comparing the cavity pressures measured in the IET-10 experiment to the vessel pressure. This figure shows a relatively small peak in the cavity pressure just after the HPME due to efficient gas heating caused by the molten brass, steel, and thermite entering the cavity. The lack of a broad peak appearing between ≈0.0 and ≈0.3 s indicated that there was no water in the cavity. Debris entrainment by the steam blowdown occurred between t ≈0.3 s and ≈1.0 s. Figure 4.15 gives the cofferdam exit pyrometer signal versus time in the IET-10 experiment.

Figure 4.16 is a plot comparing the cavity pressures measured in the IET-11 experiment to the vessel pressure. Again, a relatively small peak occurred in the cavity pressure just after the HPME began due to efficient gas heating. There was no water in the cavity. Debris entrainment by the steam blowdown occurred between t ≈0.4 s and ≈1.0 s. Figure 4.17 gives the cofferdam exit pyrometer signal versus time, which verifies the debris entrainment interval in the IET-11 experiment.

Figure 4.18 is a plot comparing the cavity pressure measured in the IET-12 experiment to the vessel pressure. Cavity pressurization was immediate and continuous. However, the early cavity pressurization between ≈0.0 and ≈0.3 s in IET-12 was not believed to have been caused by water in the cavity since there was no external water source and the cavity temperature was too high (T_{cavity} = 397 K compared to T_{sat} = 370 K) to have allowed condensation to form. The early cavity pressure is believed to be caused by immediate (t = 0 s) steam blowthrough. The principle cause for the immediate steam blowthrough was the large (scaled) exit hole. Debris entrainment by the steam blowdown occurred between t ≈0.0 s and ≈0.9 s. The

pyrometer was not used in the IET-12 experiment.

4.2.3 Pressure Measured Inside the Subcompartment Structures

The subcompartment structures in the Surry containment can be defined as the basement area under the operating deck, the RHR platform, and the seal table room. Figures 4.19, 4.20, and 4.21 show the absolute pressure measured inside the basement, RHR platform, and seal table room compared to the pressure measured in the containment vessel plotted against time in the IET-9, IET-10, and IET-11 experiments, respectively. Little or no differential pressure existed between the subcompartment structures and the vessel. (The RHR platform pressure transducer failed to record a signal in IET-9.) No differential pressures were anticipated since the basement and RHR platform are open to the upper dome by the cranewall annulus, and because the seal table room has a much larger opening in the ceiling than in the floor.

Pressures were not measured inside the basement, RHR platform, and seal table room in the IET-12 experiment since little or no differential pressure was measured between the subcompartment structures and the vessel in the IET-9, IET-10, or the IET-11 tests.

4.3 Debris Velocity Measured with Breakwires

In IET-9, a breakwire was placed across the seal table opening in the seal table room floor to measure the timing of debris entering the seal table room. This opening is directly above the cofferdam exit. In IET-10, IET-11, and IET-12, two additional breakwires were mounted; a breakwire was installed at the cofferdam exit, and a breakwire was also installed at the large opening in the seal table room ceiling.

In the 1:6 scale tests, the cofferdam exit breakwire is 3.75 m from the crucible melt plug. The seal table room floor breakwire is 1.54 m from the cofferdam exit, and the seal table room ceiling breakwire is 1.41 m from the seal table room floor. In the 1:10 scale test, the cofferdam exit breakwire is 2.14 m from the crucible melt plug. The seal table room floor breakwire is 0.88 m from the cofferdam exit, and the seal table room ceiling breakwire is 0.81 m from the seal table room floor.

In IET-9, the breakwire across the seal table opening failed at 0.08 s; this was due to thermite/water vaporization during the initial cavity pressurization period and prior to the debris entrainment interval (Figure 4.12).

Figure 4.22 shows the breakwire signals for the IET-10 experiment. The cofferdam exit breakwire failed at 0.029 s. The seal table room floor breakwire failed at 0.225 s. The seal table room ceiling breakwire failed at 0.594 s. This yields debris/gas velocities; 132 m/s in the cavity, 7.9 m/s through the RHR platform, and 3.8 m/s through the seal table room. Also, an average debris/gas velocity through the subcompartment structures of 11.2 m/s was calculated. The average debris/gas velocity was calculated by dividing the distance between the melt plug and the seal table room ceiling breakwire by the time at which that breakwire failed.

Figure 4.23 shows the breakwire signals for the IET-11 experiment. The cofferdam exit breakwire failed at 0.063 s. The seal table room floor breakwire failed at 0.037 s. The cofferdam exit and seal table room floor breakwires probably were failed by the initial cavity pressure pulse at about 0.04 s (Figure 4.16). The seal table room ceiling breakwire failed at 0.621 s, they may have been failed by the initial momentum of the debris ejected into the cavity. An average debris/gas velocity through the subcompartment structures of 10.8 m/s was calculated.

Figure 4.24 shows the breakwire signals for the IET-12 experiment. The cofferdam exit breakwire failed at 0.03 s. The seal table room floor

breakwire failed at 0.04 s. The cofferdam exit and seal table room floor breakwires failed near the initial cavity pressure pulse at about 0.04 s (Figure 4.18). The seal table room ceiling breakwire failed at 0.56 s during the debris entrainment interval when the cavity pressure was at a maximum. An average debris/gas velocity through the subcompartment structures of 6.8 m/s was calculated.

4.4 Video Results and Interpretation

In IET-9, IET-10, and IET-11, the video camera viewed the HPME through a tempered-glass window installed inside construction penetration CP2 which was directly above the five foot door. The CP2 penetration was located high in the vessel at the dome-to-cylinder transition line; this location along with a wide-angle lens allowed an almost completely unrestricted view of the structures above the operating deck.

In the IET-9 experiment, the first frame of the CCD camera, at the beginning of HPME, showed a gray aerosol cloud exiting from the annular gap between the RPV and the support skirt at the top of the biological shield. There was a 0.5 cm clearance between the seal ring and the support skirt. Between 0.03 s and 0.16 s, six jets (divided by the six RPV nozzles) of hot burning gases and aerosols violently exited the annular gap into the upper dome. These burning gas jets and aerosols impinged on the grating and structures in the upper dome region. The velocity of these jets exiting the annular gap were $\approx$100 m/s. Burning gases were also seen exiting the holes at the seal table room ceiling. At 0.16 to 0.20 s, individual luminous molten debris particles started to rise from the annular gap. By 0.25 s, much larger amounts of debris flowed out of the annular gap, which caused the CCD camera to become overexposed. The camera view became completely white. At 2.2 s the camera view returned and molten debris particles were seen moving downward directly in front of the camera. Dark grey and black clouds were seen swirling upward. At 3.5 s no more molten debris particles were seen moving downward, and the view went completely black by 5 s.

The bright orange burning gas jet seen in the upper dome of the containment indicated that a hydrogen burn did occur. Individual luminous molten debris particles were ejected from the subcompartment structures and were observed moving toward the upper dome. Hydrogen formed by steam/metal reactions in the HPME was intimately mixed with molten particles, which act as ignition sources for hydrogen combustion. Hydrogen entrained in the debris plume appeared to burn in the upper dome of the vessel.

In IET-10, the CCD camera showed what appears to be burning gas jets (orange color) exiting the crucible head through the pressure transducer fitting when the burst diaphragms were intentionally ruptured at t = -1.2 s. This jet turned to whitish gray steam at t = -0.5 s. At t = -0.1 s, the jet had turned a brownish color. At melt plug failure (t = 0 s), the view immediately became overexposed and remained overexposed until t = 3.3 s, when molten debris particles were seen falling downward. Debris stopped falling downward by t = 5 s, but the background still glowed an orange color until about t = 6.5 s. Before the view went completely black at t = 7 s, aerosols were seen swirling from right to left across the camera view.

In the IET-11 experiment, the first frame of the CCD camera, at the beginning of the HPME, showed a hot or burning gas jet exiting from a small section of the annular gap from the side nearest the instrument tunnel. The flow area out of the annular gap formed by the metal reflective RPV insulation and the reactor support skirt was 0.02 m^2. The burning gas jet grew, and filled about half of the annular gap by 0.08 s. At 0.12 s, the exit hole at the seal table room ceiling was illuminated from within by burning gas jets or molten debris. By 0.13 s, molten debris and

burning jets were seen exiting the entire circumference of the annular gap, reaching to the height of the missile shield. In IET-9, the debris was sharply divided by the six nozzles; this was not seen in the IET-11 video. The entire operating deck was illuminated at 0.15 s by burning gas jets exiting from the annular gap. Burning gas jets or molten debris exiting the annular gap had reached the monorail hoist near the top of the dome by 0.38 s. The entire view of the vessel became overexposed, and remained overexposed until about 2.7 s; however, molten debris was seen impacting the camera window between 1.3 and 1.5 s. When the camera view returned, molten debris particles were seen moving downward between 2.7 and 3.7 s, in a background that glowed an intense orange color. The intense orange background color was probably due to hydrogen burning and/or molten debris radiation. Note that a very hot, aerosol-laden gas can glow without hydrogen combustion, and it may not be correct to equate the presence of a glow with ongoing combustion in all cases. The orange color slowly faded to black, and the view of brownish black aerosols inside the containment vessel disappeared by 6 s. This indicated that the background illumination was not sufficient to see the aerosols.

In the IET-12 experiment, the CCD camera looked down inside the Surtsey vessel through a tempered glass window mounted inside the 0.3-m diameter Surtsey top head penetration. The wide-angle lens allowed a view of the operating deck, RPV model (covered by the missile shield), accumulator, seal table room ceiling openings and the annulus formed by the Surtsey vessel wall and the cranewall. The first frame of the CCD camera, at the beginning of the HPME, showed an orange glow underneath the missile shield, probably due to hot or burning gas jets exiting from the broken pressure transducer line at the crucible head. The orange glow was much more intense at 0.03 s, especially on the side near the seal table room, which corresponded to the side of the crucible head where the penetration was located. At 0.05 s, the basement floor on the cavity side was illuminated by molten debris exiting from the RHR platform. At 0.15 s, a small amount of what appears to be molten debris moved from underneath the missile shield horizontally across the vessel and struck the containment wall above the seal table room. An orange glow filled the vessel on the seal table room side at 0.5 s; it was unclear if this was due to burning gas jets or molten debris. A few molten particles were seen moving across and up the vessel, from the seal table room side to the 'door' side of the vessel near the removable operating deck section. The view was completely black by 1.5 s.

A camcorder viewed the inside of the Surtsey vessel at a level 6 penetration, which had a tempered glass viewing window. The side view looked underneath the missile shield and directly across the RPV model. The seal table room ceiling openings were also seen on the opposite side of the vessel. The side view showed a burning gas jet rising and striking the underside of the missile shield at 0.02 s. The camera became overexposed and 'whited out' at 0.05 s. The view returned at 0.42 s, and brown-black aerosols were seen. An orangish glow appeared at the bottom of the view, was brightest at 0.58 s, and faded away by 0.75 s. Molten debris was seen rising directly in front of the camera at 0.83 s, probably exiting from the RHR platform and following the annulus formed by the vessel wall and the cranewall. Molten debris was seen heading toward the camera and rising upward between 1.05 and 1.66 s, probably due to debris exiting the seal table room through its ceiling and door openings and ricocheting off the Surtsey wall. The side camera view started to fade at 2 s and was completely black by 3 s.

4.5 Debris Temperature Measurements

Figures 4.25, 4.26, and 4.27 give the temperature measurements from the type-C thermocouples installed in or near debris exit paths in the 1:6 scale experiments. The type-C

thermocouples were installed to measure debris and debris/gas mixture temperatures in the CTTF containment vessel, and are clustered around the RHR platform region. An average debris/gas mixture for the RHR platform region is also presented.

Figure 4.25 shows that in IET-9 the only type-C thermocouple directly impacted by hot melt was the thermocouple installed above the cofferdam and attached to the RHR platform ceiling. This thermocouple reached a peak temperature of 2160 K at 0.52 s. This was immediately after the start of the cavity debris ejection interval. Most of the type-C thermocouples peaked at temperatures of 1200-1500 K, probably recording hot gas heated by debris.

Figure 4.26 gives the temperature measurements from the type-C thermocouples in the IET-10 experiment. The peak temperatures of the type-C thermocouples ranged from temperatures of 1200 to 1800 K. The cofferdam exit thermocouple reached 1692 K at 0.6 s. The RHR platform right side opening peaked to 1850 K at 0.5 s and the thermocouple under seal table room front ledge peaked to 1619 K at 0.8 s. The seal table room ceiling showed 1833 K at 0.6 s and the seal table room back wall showed 1210 K at 0.9 s.

Figure 4.27 gives the type-C thermocouple temperature measurements in the IET-11 experiment. The peak temperatures of the type-C thermocouples ranged from temperatures of 1200 to 2200 K. The cofferdam exit thermocouple reached 2593 K and over-ranged at 0.36 s, due to direct hits by molten debris. The RHR platform right side opening peaked to 2130 K at 0.6 s and the thermocouple under seal table room front ledge peaked to 1290 K at 0.8 s. The seal table room ceiling showed 1130 K at 1.1 s and the seal table room back wall showed 1550 K at 1.3 s. The RHR ceiling thermocouple above and behind the cofferdam peaked to 1190 K at 0.8 s.

The type-C thermocouples were not installed in the IET-12 experiment.

4.6 Gas Temperature Measurements

Type-K thermocouples were used to measure the temperature of the gas in the basement, in the annulus between the vessel wall and the cranewall, near the vessel wall (with aspirated type-K thermocouple assemblies), and in the bulk of the containment above the operating deck with three vertical arrays. The following sections describe the results of the temperature measurements. Mole-averaging of the temperature measurements was used to allow interpretation and comparison of the temperature increase to the pressure increase.

4.6.1 Basement Gas Temperature

Figures 4.28 through 4.31 show the gas temperature measured by the four type-K thermocouples located in the basement about 7 cm below the operating deck. An average basement gas temperature is also shown.

Figure 4.28 shows that in IET-9, the highest reading thermocouple (channel 41) was mounted near a RHR platform side window and measured 1295 K at 0.92 s. The average of the three thermocouples in the basement (channel 42 failed) determined a mean peak basement gas temperature of 861 K at 2.4 s.

Figure 4.29 shows that in IET-10, the highest reading thermocouple was also channel 41 and measured 1458 K at 0.95 s. The average of the three thermocouples in the basement (channel 42 failed) determined a mean peak basement gas temperature of 1073 K at 3.6 s.

Figure 4.30 shows the basement gas temperatures in IET-11. Again, the highest reading thermocouple was channel 41 and measured 1290 K at 0.94 s. The average of the three thermocouples (channel 42 failed) in the basement indicated a mean peak basement gas temperature of 950 K at 2.4 s.

Figure 4.31 shows the IET-12 basement gas temperatures. The highest reading thermocouple (channel 42) was mounted near a RHR platform side opening and measured 1400 K at 0.6 s. The average of the four thermocouples in the basement indicated a mean peak basement gas temperature of 970 K at 0.9 s.

4.6.2 Cranewall Annulus Gas Temperature

Figures 4.32 through 4.35 show the gas temperatures measured by the four type-K thermocouples located in the annulus formed by the containment vessel wall and the cranewall, midway between the basement ceiling and the top of the cranewall.

Figure 4.32 shows the cranewall annulus gas temperatures for IET-9. The highest reading thermocouple was channel 48, which measured 1000 K at 1.5 s. The average of the four thermocouples yielded a mean peak temperature of 900 K at 1.8 s. Thermocouple channel 48 data was not included in the temperature average after 9 s as it appeared to have been affected by hot debris.

Figure 4.33 shows the cranewall annulus gas temperatures for IET-10. The highest reading thermocouple was channel 48, which measured 1157 K at 0.6 s. The average of the four thermocouples yielded a mean peak temperature of 1029 K at 2.2 s.

Figure 4.34 shows the cranewall annulus gas temperatures for IET-11. The highest reading thermocouple was channel 46, which measured 1230 K at 2.3 s. The average of the four thermocouples yielded a mean peak temperature of 910 K at 2.6 s.

Figure 4.35 shows the cranewall annulus gas temperatures for IET-12. The highest reading thermocouple was channel 45, which measured 1250 K at 0.6 s. The average of the four thermocouples yielded a mean peak temperature of 905 K at 0.9 s.

4.6.3 Gas Temperature with Aspirated Thermocouples

Figures 4.36 through 4.39 shows the gas temperatures measured with the aspirated thermocouples at penetration CP1 and P3 in the CTTF vessel, and at dome and side penetrations in the Surtsey vessel. The aspirated thermocouples show lower temperatures than those given from the bulk gas array thermocouples, probably because they are sampling relatively cooler gas which is near the containment vessel walls.

Figure 4.36 shows the aspirated thermocouple temperatures for IET-9. The aspirated thermocouple located at instrumentation penetration P3 peaked to 1095 K at about 1 s. The thermocouples at the P3 penetration were found posttest pulled loose from their mounting in the aspirator tube. This probably occurred at about 10 s as indicated by the drop in the temperature measurement.

Figure 4.37 shows the aspirated thermocouple temperatures for IET-10. The aspirated thermocouple located at instrumentation penetration P3 peaked to 1473 K at 1.3 s. The thermocouples at the P3 penetration were found posttest pulled loose from their mounting in the aspirator tube. This probably occurred at about 1.5 s as indicated by the drop in the temperature measurement.

Figure 4.38 shows the aspirated thermocouple temperatures for IET-11. The aspirated thermocouple located at instrumentation penetration P3 peaked to 1220 K at 1.3 s.

Figure 4.39 shows the aspirated thermocouple temperatures for IET-12. The aspirated thermocouple located at a level 6 penetration peaked to 750 K at 0.6 s. This thermocouple sampled gas at the top of the cranewall annulus and was close to the RHR platform exit. The aspirated thermocouple measuring dome gas temperature reached 575 K at 2.3 s.

4.6.4 Bulk Gas Temperature

Bulk gas temperatures from the operating deck to the dome of the containment vessels were measured with three vertical arrays; each array consisted of six equally-spaced type-K thermocouples. Figures 4.40 through 4.51 show the gas temperatures measured with each array for each Surry IET experiment. Typically, the bottom thermocouple measured a lower temperature than the top thermocouple. Also, it appeared that the vessel becomes stratified in temperature. The average bulk temperature for each array is also shown.

Gas temperatures from the three CTTF vessel thermocouple arrays used in IET-9 are shown in Figures 4.40, 4.41, and 4.42. The vessel bulk gas temperature (obtained by averaging the eighteen thermocouples from the three arrays) peaked to 922 K at 4.5 s.

Gas temperatures from the three CTTF vessel thermocouple arrays used in IET-10 are shown in Figures 4.43, 4.44, and 4.45. The vessel bulk gas temperature (obtained by averaging the eighteen thermocouples from the three arrays) peaked to 869 K at 6.4 s.

Gas temperatures from the three CTTF vessel thermocouple arrays used in IET-11 are shown in Figures 4.46, 4.47, and 4.48. The vessel bulk gas temperature (obtained by averaging the eighteen thermocouples from the three arrays) peaked to 1150 K at 1.8 s. Note the average bulk gas temperature in the hemispherical upper dome region (obtained by averaging the six thermocouples in this area, channels 55, 56, 61, 62, 67, and 68) yielded very high gas temperatures, with the upper dome bulk gas temperature reaching 1480 K at 1.9 s.

Gas temperatures from the three Surtsey vessel thermocouple arrays used in IET-12 are shown in Figures 4.49, 4.50, and 4.51. The vessel bulk gas temperature (obtained by averaging the eighteen thermocouples from the three arrays) peaked to 560 K at 3.1 s. The Surtsey vessel was stratified $\approx$ 10 s after the melt ejection.

4.6.5 Mole-Average and Interpretation of Gas Temperatures

A mole-average bulk gas temperature can be derived from

$$<T>_{average} = \frac{\sum N_i T_i}{\sum N_i} = \frac{\sum \frac{P V_i}{R T_i} T_i}{\sum \frac{P V_i}{R T_i}} \quad (9)$$

This simplifies to

$$<T>_{average} = \frac{V_{Tot}}{\sum \frac{V_i}{T_i}} = \frac{1}{\sum \frac{f_i}{T_i}} \quad (10)$$

where

f_i = subcompartment or dome volume fraction

N_i = subcompartment or dome gas moles

P = vessel pressure

R = universal gas constant

T_i = subcompartment or dome average gas temperature

V_{Tot} = freeboard gas volume

V_i = subcompartment or dome gas volume.

Table 4.1 gives the subcompartment volumes and volume fractions used with equation (10) for the Surry IET tests. For example, in the IET-12 experiment, the following volumes were used: (1) dome - 38.15 m^3, (2) basement - 5.39 m^3,

(3) cranewall annulus - 6.05 m^3, (4) RHR platform - 0.77 m^3, (5) seal table room - 0.36 m^3, and (6) cavity/incore instrument tunnel (IIT) - 0.28 m^3. The RHR platform, seal table room, and cavity/IIT volumes (1.42 m^3) were added to the basement volume for the calculation since there was no average temperature data for these regions. (In the 1:6 scale tests, the RHR platform, seal table room, and cavity/IIT volumes used the average temperature calculated with the type-C thermocouples located in and around the RHR platform region.)

Figures 4.52, 4.53, 4.54, and 4.55 compare the calculated mole-average gas temperatures in IET-9, IET-10, IET-11, and IET-12, respectively, to the average temperatures of the bulk gas in: (1) the dome region, (2) the basement region, (3) the cranewall annulus region, and (4) for the 1:6 scale tests, the RHR platform region.

Figure 4.56 compares the mole-average gas temperatures for all of the Surry DCH tests. The peak mole-average gas temperature was 889 K at 4.0 s in IET-9, 879 K at 4.9 s in IET-10, 1062 K at 2.5 s in IET-11, and 598 K at 2.3 s in IET-12. The mole-average gas temperature was used (along with vessel pressure and volume) to calculate the time-dependent gas moles in the containment vessel which is a necessary quantity in the calculation of the gas composition.

Figures 4.57 through 4.60 compares the relative magnitude of the containment vessel pressure increase to the relative magnitude of the mole-averaged gas temperature increase. The relative magnitude is calculated by dividing the measured value by the initial value at t = 0 s. The relative magnitude increase in pressure and temperature should be similar assuming an ideal gas. These figures appear to indicate that vessel pressure is higher than expected, given the temperatures seen in the experiment. However, a portion of the vessel pressure increase is due to the addition of steam moles during the accumulator blowdown. The relative magnitude curve was adjusted by a blowdown factor; the factor ranged from 1 at beginning of the HPME to $\approx$0.8 (initial vessel moles/initial vessel moles plus accumulator steam moles) at the end of the blowdown, with the rate of the decrease in the blowdown factor proportional to the rate of decrease in accumulator pressure during the blowdown. This gave better agreement with the temperature magnitude.

In IET-12, Figure 4.60 shows that the adjusted pressure curve has a magnitude higher than the temperature magnitude. If there was saturated water in the steam blowdown gas, the additional steam moles produced by cooling or quenching molten debris would allow a further reduction in the corrected pressure curve. Only 200 g · moles of saturated water in the blowdown steam would cause the adjusted pressure curve and the average temperature curve to overlay each other.

4.7 Vessel and Structure Temperature Measurements

Figures 4,61, 4.62, 4.63 and 4.64 give structure temperature histories in IET-9, IET-10, IET-11, and IET-12 for the thermocouples attached to the steel liner at the top and at the bottom of the CTTF containment vessel inside wall and to the steel wall and dome in the Surtsey vessel. Also, the temperature measurements in the cavity and from thermocouples imbedded in the cranewall and in the basement floor are also shown and compared to saturation temperature. The basement temperature does not change during the DCH time frame because it is a large heat sink, with much thermal mass. However, the containment vessel wall does heat up initially, until conduction to the environment removed enough heat to stop the temperature increase.

In IET-9, condensation certainly was possible on the vessel liner and basement floor since these locations were at or below saturation temperature. In IET-9, the cranewall thermocouple was hit by molten debris at about 3 s and was destroyed.

In IET-10, the containment wall and structures were well above saturation temperature. The cavity appears to be near saturation temperature, however, the cavity pressure curve showed that no water condensed in the cavity prior to the HPME.

In IET-11, the structure temperature history shows the effect of adding 702 kg of hot water (373 K) directly to the basement floor immediately prior to the HPME. The basement and vessel liner near the floor are at saturation temperature. The vessel liner near the dome and the concrete cranewall remain above saturation temperature. It is unclear why the cavity temperature is at saturation prior to the HPME and also why it remained low during the HPME.

In IET-12, no condensate water was added, and no water condensed prior to the HPME, since the vessel wall and structures were well above saturation temperature.

4.8 Gas Composition Measurements

The gas grab samples were taken from an atmosphere containing a mixture of steam and noncondensible gases. If the sample lines, valves, and bottles were heated above saturation temperature, the sample bottles contained a mixture of steam and noncondensible gases when they were filled. If the sample bottles were cold, it was determined experimentally that they would pressurize to vessel pressure with only noncondensible gas. Gas mass spectroscopy was performed on gases from sample bottles at room temperature. Since the steam in the bottle condensed prior to analysis, the measurements are only of noncondensible gases; thus, the mole percent of the individual gas species determined for each bottle must be adjusted by a noncondensible gas fraction (f_{NC}).

The pretest or background noncondensible gas fraction could be calculated based on the gas and steam additions to the Surtsey vessel during the charging process. Leakage processes (based on measured pressure-dependent containment vessel leak rates) are accounted for in the time-dependent calculation

$$N_{NC}(i+1) = N_{NC}(i) + N_{H_2,add}(i) + N_{Air,add}(i) - N_{Leaked}(i)\frac{N_{NC}(i)}{N_{Total}(i)} \quad (11)$$

where

$N_{NC}(i+1)$ = noncondensible gas moles (new time step)

$N_{NC}(i)$ = noncondensible gas moles (old time step)

$N_{H2,add}$ = hydrogen gas moles added in time step

$N_{Air,add}$ = air gas moles added in time step

N_{Leaked} = total gas leakage

N_{Total} = total vessel moles (gas and steam).

The posttest noncondensible fraction can be calculated using two methods. The first method utilizes a steam fraction:

$$f_{NC} = 1 - f_{steam} = 1 - \frac{\text{vessel steam moles}}{\text{vessel total moles}} \quad (12)$$

The moles of steam in the vessel when the 15 s gas sample bottles are closed (t = 25 s) is estimated to be the initial vessel steam moles plus the steam moles added by the accumulator

blowdown. The moles of steam at 2 min and at 15 min are estimated to be the moles at 3 s plus any additional moles of steam produced by hot debris vaporizing water on the basement floor (there was no basement water in IET-10 or IET-12). Particles of molten debris (5 mm) can cool/quench in ≈3 s, and 5 cm particles can cool in ≈300 s, with about 59 g·moles of steam produced for each kilogram of molten debris in water.

Another method used to calculate the posttest noncondensible gas fraction is based upon the ratio of noncondensibles gas moles in the vessel to the total vessel moles. The posttest noncondensible mole (N_{NC}) mass balance is

$$N_{NC} = N^{0}_{NC} + N_{H_2,\ produced} - N_{H_2,\ burned} - N_{O_2,\ burned} - N_{O_2,\ oxidized} \quad (13)$$

where

N^{o}_{NC} = initial noncondensible moles (= f^{o}_{NC} N^{o}, the background noncondensible gas fraction times the total initial vessel moles)

$N_{H2,\ produced}$ = hydrogen moles produced from steam oxidation of molten debris

$N_{H2,\ burned}$ = hydrogen moles removed by combustion

$N_{O2,\ burned}$ = oxygen moles removed by combustion

$N_{O2,\ oxidized}$ = oxygen moles removed by direct oxidation of metallic debris.

The posttest total vessel mole (N_{Total}) mass balance is

$$N_{Total} = N^{0}_{Steam,\ preexisting} + N_{Steam,\ produced} + N_{Steam,\ blowdown} + N_{Steam,\ vaporization} - N_{Steam,\ reacted} + N_{NC} \quad (14)$$

where

$N^{o}_{Steam,\ preexisting}$ = initial steam moles in the vessel

$N_{Steam,\ produced}$ = steam moles produced from combustion of hydrogen and oxygen

$N_{Steam,\ blowdown}$ = steam moles added from accumulator blowdown

$N_{Steam,\ vaporization}$ = steam moles produced from vaporization of condensate water by molten debris

$N_{Steam,\ reacted}$ = steam moles reduced by oxidation of molten debris.

The time-dependent number of moles of a gas species (N_i) in the containment are calculated by multiplying the gas bottle species concentration (X_i) measurement by the noncondensible gas fraction and the measured number of total gas moles (from the ideal gas law) in the containment.

$$N_i = X_i\ f_{NC}\ N_{Total}\ . \quad (15)$$

The calculated change of oxygen (ΔN_{O2}) and hydrogen (ΔN_{H2}) gas moles are used to calculate the parameters in the posttest noncondensible mole mass balance.

$$N_{H_2,\,produced} - N_{H_2,\,burned} = N_{H_2}^{f} - N_{H_2}^{0} = \Delta N_{H_2} \quad (16)$$

$$-(N_{O_2,\,burned} + N_{O_2,\,oxidized}) = N_{O_2}^{f} - N_{O_2}^{0} = \Delta N_{O_2} \quad (17)$$

The stoichiometric combustion of hydrogen and oxygen will produce two moles of steam for each mole of oxygen that is burned (or produce one mole of steam for each mole of hydrogen that is burned)

$$N_{Steam,\,burned} = 2N_{O_2,\,burned} = N_{H_2,\,burned} . \quad (18)$$

The steam moles removed by the molten debris is equal to the number of hydrogen moles produced during the debris oxidation reaction

$$\begin{aligned} N_{Steam,\,reacted} &= N_{H_2,\,produced} \\ &= \Delta N_{H_2} + N_{H_2,\,burned} \\ &= \Delta N_{H_2} + N_{Steam,\,produced} \end{aligned} \quad (19)$$

The derived time-dependent posttest noncondensible fraction equation is:

$$\begin{aligned} f_{NC} &= \frac{N_{NC}}{N_{total}} \\ &= \frac{f_{NC}^{\circ} N^{\circ} + \Delta N_{H_2} + \Delta N_{O_2}}{N^{\circ} + \Delta N_{O_2} + N_{Steam,\,blow} + N_{Steam,\,vapor}} . \end{aligned} \quad (20)$$

Note that the above equation must be solved iteratively since the noncondensible fraction is used to determine the change in hydrogen and oxygen gas moles.

If the bottles were heated and contained a mixture of steam and noncondensible gases, the noncondensible gas fraction (f_{NC}) for each individual bottle could be computed from temperature and pressure measurements. The f_{NC} in the vessel at each sample point would then be measured if it is assumed that the bottle contained the same proportionate mixture.

The equation that allows a measured noncondensible fraction is:

$$f_{NC} = \frac{P_c}{P_h} \frac{T_h}{T_c} \quad (21)$$

where

$P_{h,c}$ = bottle pressure (hot or cold)

$T_{h,c}$ = bottle temperature (hot or cold).

Twelve unheated gas grab samples were taken from the CTTF vessel in the IET-9 experiment. The gas concentrations measured in the gas grab samples are listed in Table 4.2. Background samples from the containment vessel were taken just prior to ignition.

Twelve unheated gas grab samples were taken from the CTTF vessel in the IET-10 experiment. The gas concentrations measured in the gas grab samples are listed in Table 4.3. Background samples from the containment vessel were taken just prior to ignition.

Sixteen gas grab samples were taken from the CTTF vessel in the IET-11 experiment. Insulated gas sample lines and bottles were heated with heat tape in an attempt to measure the bottle noncondensible fraction, however, a control circuitry problem caused the bottle temperatures to range from 323-363 K, which is below the desired temperature of 423 K. The noncondensible gas fraction in the bottle could not be measured. The gas concentrations measured in the gas grab samples are listed in Table 4.4. Background samples from the containment vessel were taken 18 minutes prior to ignition. The results from the background gas grab sample match well with that calculated from the charging process at t = -18 min. However,

since the vessel atmosphere concentrations changed in the 18 minutes prior to thermite ignition, the charging process calculations were used to determine vessel background gas levels at HPME initiation. The background noncondensible fraction for IET-11 was 0.678.

Twenty heated gas grab samples were taken from the Surtsey vessel in the IET-12 experiment. The sample bottles were placed inside insulated containers whose inside temperature was maintained at 423 K using hot air. Sample lines were also heated similarly. This resulted in uniform heating of gas sample lines and bottles with no cold spots where steam could condense. However, five bottles failed to fill satisfactorily, probably due to exceeding temperature limits on the valve seals (the high-temperature valve seals were operated at their upper limit). Again, all gas grab samples were taken through sampling lines and bottles that were maintained at 423 K. The gas pressure and the bottle temperature were measured posttest and then the bottles were placed in a cold-water bath (306 K). Table 4.5 shows the noncondensible fraction for each bottle calculated using Equation 20. The measured noncondensible fraction for each bottle was used to adjust the gas species concentrations obtained from the gas grab sample analyses. The gas concentrations measured in the fifteen successful gas grab samples are listed in Table 4.5. Background samples from the Surtsey vessel were taken less than 1 minute prior to ignition. The results from the background gas grab samples match well with those calculated from the charging process.

The posttest oxygen and hydrogen concentrations in mol. % are compared in Figures 4.65 and 4.66 for all of the Surry IET experiments.

Analysis of the gas samples taken from the three sample points in IET-9 at the same time in the CTTF vessel showed large deviations at 15 s and at 2 m.

Analysis of the gas samples taken from the three sample points at the same time in the CTTF vessel showed large deviations at short times and excellent agreement at 15 min for the IET-10 experiment.

Analysis of the gas samples taken from the four sample points in IET-11 at 15 seconds showed large deviations; the gas samples from the four sample points at 2 min and 15 min after the HPME in the CTTF vessel are in good agreement.

Analysis of the IET-12 gas samples taken from the eight sample points in the Surtsey vessel 3 seconds after the HPME showed large deviations. These measurements indicate that the gas was not well mixed at t = 3 s. The results of the gas samples taken from the four sample points at the 5 minute and the 15 minute times in the Surtsey vessel are in excellent agreement for the IET-12 experiment. These measurements indicate the gas was well-mixed by t = 5 min. The IET-12 test shows oxygen levels essentially remained unchanged, whereas hydrogen levels increased by a factor of 2.

The 3 s mean gas concentrations in IET-12 were calculated differently than the mean values for the background samples and the 5 and 15 minute samples (which used simple averaging) because of the large deviations. The total number of moles of a gas species ($N_{i,\,Tot}$) at 8 s in the Surtsey vessel was calculated using a mole-averaging method

$$N_{i,Tot} = \sum X_i \frac{P\ V_i}{R_u\ T_i} \qquad (22)$$

where

X_i = measured gas species concentration

V_i = subcompartment or dome gas volume

T_i = subcompartment or dome gas temperature

P = vessel pressure

R_u = universal gas constant.

The time of 8 s was selected since the bottles were opened at t = 3 s and sampled the atmosphere until t = 8 s. The following containment gas volumes were used in association with the eight gas grab sample bottles listed in Table 4.5: 9.54 m^3 for bottles #4, #6, and #11; 3.18 m^3 for bottles #5, #7, and #8; 6.80 m^3 for bottle #9; and 6.05 m^3 for bottle #10. Gas species concentrations at 8 s were found by dividing gas moles at 8 s by total vessel moles at 8 s, which was calculated to be 3322 g·moles using the ideal gas law with the mole-average temperature from Equation (10).

Figure 4.67 compares the signal obtained with a hydrogen microsensor to the calculated pretest hydrogen amounts and the measured background and posttest hydrogen values in the Surtsey vessel. The hydrogen microsensor was mounted external to the Surtsey vessel at the same level 4 penetration as the hydrogen charging connection. The Sandia Robust, Wide-Range hydrogen microsensor (currently in development at SNL) has a PdNi MOS device and a PdNi resistor; both devices absorb hydrogen which causes a resistance change, indirectly measuring the hydrogen concentration. At about t = -24 min on Figure 4.67, hydrogen was added to the Surtsey vessel for about one minute; the spike in the sensor signal showed a high local concentration during the addition. The mixing fans mixed the hydrogen gas with the atmosphere, and the signal showed levels consistent with the pretest calculation and also with the measured gas grab sample background value. The sensor signal matched reasonably well with the 3 s and the 5 min posttest gas measurements. However, after 5 minutes the sensor lost temperature regulation which caused the signal to rise unexpectedly.

Oxygen concentrations measured at the same location decreased between the short-term samples and the long-term samples. There are three possible explanations for the observed oxygen depletion: (1) there could have been long-term production of hydrogen by steam/metal reactions, and subsequent oxygen depletion by reaction with hydrogen; (2) there could have been some oxygen depletion due to direct reaction with iron; or (3) nonuniform gas concentrations in the containment atmosphere might make it appear as if oxygen was consumed between early and late times. Item number 3 requires some additional explanation. For example, in IET-11, there were four sampling locations: one at the top of the dome, two low in the dome but above the operating deck, and one in the annulus between the vessel wall and the cranewall. Analyses of the gas grab samples indicate that the containment atmosphere was not well mixed at t = 15 s, but was well mixed at t = 15 min. The concentrations of oxygen and hydrogen were depleted high in the upper dome compared to lower in the containment atmosphere. If the lower three gas sampling ports were located where the localized oxygen concentrations were higher than the average, then long-term mixing would make the oxygen concentrations appear to decrease, whereas the total number of moles of oxygen in the containment remained unchanged.

The hydrogen combustion for the short-term samples (3 s or 15 s) was based on assuming all oxygen depletion is due to reaction with hydrogen and is calculated using the stoichiometric chemical reaction for the formation of water. Metal oxidation reactions can account for some of the small decrease in measured vessel oxygen concentration, with ≈9.5 g·moles of oxygen consumed for each kilogram of debris transported outside subcompartment structures. Figure 4.68 shows the Surtsey vessel oxygen concentration being decreased by metal oxidation reactions in the DCH-3 experiment [Allen et al. 1991a]. In that experiment, 80 kg of iron oxide/alumina melt was driven by nitrogen into an air atmosphere. There was no steam, water, or subcompartment

structures. Very little oxygen was reduced by 3 s, and by 5 minutes, the reaction had reached steady-state. Therefore, a hierarchy of metal oxidation reactions and combustion reactions were utilized for the Surry IET long-term hydrogen combustion results (2 min, 5 min, and 15 min). For the 2 min results, half of the total potential for metal oxidation reduction was assumed to have depleted the oxygen between 15 s and 2 min, the remaining depletion was assumed to be due to hydrogen combustion. For the 15 min results (and also the 5 min results in IET-12), all of the total potential for metal oxidation reduction depleted the oxygen between 15 s and 2 min and the remaining depletion was assumed to be due to hydrogen combustion.

The measured amounts of hydrogen gas burned, produced, and the net difference between production and combustion of hydrogen are compared in Figures 4.69, 4.70, and 4.71, respectively, for all of the Surry IET tests. The figures show a combination of hydrogen and carbon monoxide gas for the IET-10 experiment. Tables 4.6 through 4.9 list the amounts of preexisting hydrogen in the vessel, and for the posttest sample times, the amount produced by steam/metal reactions in the HPME, the amount burned, and the amount measured posttest for all of the IET experiments. These tables also list the vessel mole-average gas temperature, pressure, total gas moles (including steam), and the noncondensible gas fraction at the various sample times. In addition, a hydrogen gas burned fraction (moles burned/moles preexisting + moles produced) is also listed, along with steam moles from various sources (vessel, accumulator, and vaporization of basement water by molten debris) that can be used to calculate the noncondensible gas fraction based on the steam fraction method.

It was discovered that when metal oxidation reactions were utilized, they could easily account for all of the oxygen consumed long-term; therefore, Figure 4.69 showed constant combustion amounts after the initial (15 s) sample times. Combustion amounts appear to be correlated with the vessel atmosphere, as indicated by the flammability chart, Figure 3.1. The more reactive the atmosphere (high oxygen levels and low steam concentrations), the greater the combustion. In IET-12, very little hydrogen burned; this was probably due to the lack of chromium in the melt and/or the presence of water in the blowdown steam. This is discussed in more detail in the debris recovery section.

The measured amount of hydrogen burned at 15 s does not appear to be consistent with the peak vessel pressure measured at $\approx$3 s. If all the hydrogen had burned on the DCH time scale ($\approx$3 s), an adiabatic calculation suggests that pressures much higher than those measured would have resulted. It is possible that heat transfer to structures is so dominant that the process cannot be considered adiabatic. It is also possible that the molten debris particles and hot gases are not mixed uniformly with the containment atmosphere at short times ($\approx$ 3 s). Only the hydrogen mixed with hot gases can burn. In IET-11, the hydrogen burned at 3 s would include the hydrogen produced in the HPME and some of the preexisting hydrogen drawn into the plume and near the upper dome. Note the extreme depletion of measured oxygen and hydrogen in the upper dome (G3) sample at 15 s (Table 4.4). Hydrogen in the remainder of the containment would continue to burn between 3 s and 15 s as hot gases mixed throughout the containment. Therefore, not all of the measured amount of hydrogen burned at t = 15 s would have contributed to the peak pressure measured at t = 3 s.

Production amounts are calculated by subtracting the pretest hydrogen amount from the sum of the posttest amount and the amount of hydrogen gas that burned, calculated from oxygen depletion measurements. In the calculation for IET-10 it is important to consider CO in addition to the hydrogen (CO was preexisting in the containment vessel because of the incomplete purge). Since

CO burns with a stoichiometric reaction similar to that for H_2 (i.e. a 2:1 ratio with oxygen),

($2CO + O_2 \rightarrow 2CO_2$, heat of formation: -94.0 kcal/mole)
($2H_2 + O_2 \rightarrow 2H_2O$, heat of formation: -57.8 kcal/mole)

the oxygen depletion calculations give the number of moles of combustible gases (i.e. H_2 and CO) that burned in IET-10. The number of moles of H_2/CO produced can then be calculated by subtracting the pretest hydrogen and carbon monoxide amounts from the sum of the posttest amounts and the amount of combustible gases that burned, calculated from oxygen depletion measurements.

The need to estimate the *posttest* noncondensible fraction in the preceding analysis introduces uncertainty in the calculated amounts of hydrogen. The nitrogen-ratio method described below does not require an estimate of the posttest noncondensible fraction. It does, however, require the *pretest* noncondensible fraction. The data and assumptions required for the nitrogen-ratio method are listed below:

1. The initial noncondensible fraction, f^0_{NC}, must be known.
2. The total pretest moles of gas, N^0_{total}, including steam and noncondensible gases, must be known.
3. The measured ratios of the pretest and posttest noncondensible gases must be known.
4. It must be assumed that nitrogen is neither produced nor consumed by chemical reactions.
5. It must be assumed that leakage between the time for which the pretest numbers apply and the time of the posttest samples does not change the ratios of the noncondensible gases.

Let X^0_i be the initial (pretest) mole fraction (from Tables 4.2-4.5) of species i at time t = 0 in the containment vessel and let N^0_{total} be the initial number of steam and noncondensible gas moles in the vessel (from Tables 4.6-4.9). The initial number of gas moles for all species is

$$N_i^0 = X_i^0 \, N_{total}^0 \, . \qquad (23)$$

Let X^t_i be the mole fraction (from Tables 4.2-4.5) of species i at time t. For the various posttest times, the number of moles of nitrogen is assumed to be unchanged, and the numbers of moles of the other gases are therefore given by

$$N_i^t = N_{N_2}^0 \frac{X_i^t}{X_{N_2}^t} \, . \qquad (24)$$

It is not necessary to know the posttest noncondensible fraction; only the ratio of the posttest gas species mole fractions is needed. Furthermore, provided all noncondensible gases leak in the same proportion, a correction for posttest leakage is not needed.

Given the pretest moles of O_2 and H_2 from the noncondensible fraction method and posttest moles of O_2 and H_2 from the nitrogen-ratio method, the moles H_2 burned and the moles H_2 produced can be computed from

$$N_{H_2,\,produced}^t = N_{H_2}^t - N_{H_2}^0 + N_{H_2,\,burned}^t \qquad (25)$$

$$N_{H_2,\,burned}^t = 2 \, (N_{O_2}^0 - N_{O_2}^t) \, . \qquad (26)$$

Tables 4.6-4.9 also give the results for the amounts of hydrogen produced and burned based on the nitrogen-ratio method. The nitrogen-ratio hydrogen combustion results assume metal/steam reactions only; none of the oxygen decrease was due to direct metal/oxygen reaction. There is probably little direct metal/oxygen reaction, even in the dome, that occurs during the DCH pressurization time scale. The steam/oxygen

ratios are large and hydrogen generated by the steam reaction very likely reacts with oxygen in the immediate vicinity of the hot debris particle, reducing still further the oxygen concentration at the drop surface. In terms of total energy release it makes no difference that direct metal/oxygen reaction initially deposits more energy in the debris and less in the gas because, for the small particles that react efficiently, heat transfer is also efficient.

A comparison of the results based on the nitrogen-ratio method and the results based on the estimated posttest noncondensible gas fraction (which utilizes a small correction for direct metal/oxygen reaction) shows that the results are similar for IET-9, IET-10, and IET-12. For IET-11, the amount of hydrogen produced and burned using the nitrogen-ratio method are smaller than the previous method. The discrepancy may be due to an overestimate of the steam moles produced from vaporization of condensate water by molten debris on the basement floor. This would yield a smaller posttest noncondensible gas fraction estimate (Equation 19). In IET-9, it is believed that most (if not all) of the water (372 kg) in the basement was in the annular trough. The majority of basement floor debris was found in the trough (directly in front of the RHR platform). There was sufficient water in the trough to cool all of the debris found in the trough. The initial water level in the trough was 3.5 cm, and it was estimated that the 43 kg of debris found in the trough vaporized 12.3% of the trough water and produced 2542 g·moles of steam. A similar estimate was performed for IET-11. Condensate levels of water (703 kg) were added to the basement floor; though in IET-11 the trough had been filled with concrete. It was estimated that the 43 kg of debris found on the basement floor vaporized 6.5% of the trough water and produced 2547 g·moles of steam. If the floor was a level surface, the water level would have been 2.4 cm. However, the floor in front of the RHR platform was slightly higher than the rest of the containment floor, and the debris may not have vaporized the total potential. Therefore, Table 4.8 gives a range of posttest noncondensible fractions and hydrogen amounts for IET-11 based on no vaporization of basement floor water and on the maximum potential vaporization. Table 4.6 also gives a range at posttest noncondensible fractions and hydrogen amounts for IET-9 based on no vaporization of basement water, and on the maximum potential vaporization. The range is smaller for IET-9 (0.25-0.21) due to the smaller initial noncondensible fraction, as compared to IET-11 (0.53-0.47).

Figure 4.70 compares the production of combustible gases for the Surry DCH experiments. Production amounts appear to correlate well with levels of blowdown steam moles; larger amounts of steam moles produced more hydrogen. Also, prototypic reactor structures in the melt path, such as the RPV metal insulation installed in IET-11 and instrument guide tubes, might provide additional sources of hydrogen production.

In IET-11, the RPV metal insulation appeared to be a source for hydrogen production. The metal content of thermite is predominately Fe and Cr with trace quantities of Al. At thermitic temperatures, the oxide states are expected to be FeO, Cr_2O_3, and Al_2O_3. There is sufficient steam in the accumulator to oxidize all of the metal in the 158 kg thermite charge; this has the potential to produce 2027 g·moles of hydrogen. Similarly, there is sufficient excess steam to completely oxidize all of the 29 kg of reflective metal insulation; this has the potential to produce an additional 550 g·moles of hydrogen. The total amount of hydrogen that could be produced if all of the metal is oxidized is 2577 g·moles. However, this amount of hydrogen is not expected for three reasons: (1) thermodynamic limitations preclude complete conversion of Fe, (2) incomplete ejection from the melt generator and incomplete dispersal from the cavity, and (3) noncoherence of the melt and steam during the dispersal and blowdown processes. Thermodynamic limitations to the Fe reaction in the

158 kg charge reduces the potential to produce hydrogen from 2027 g·moles to 1629 g·moles. To this, we might reasonably add a minimum of 150 g·moles of hydrogen from reactions with Cr in the insulation to a maximum of 550 g·moles of hydrogen (complete oxidation of the insulation). Thus, thermodynamic limitations alone reduce the potential for hydrogen production to a range of 1779 - 2179 g·moles. Interestingly, the experiment value of 1876 g·moles in IET-11, which was determined from gas measurements at 15 s, compares favorably with the lower range for hydrogen production potential.

The potential to produce hydrogen may be further reduced because of the noncoherence of the dispersal and blowdown processes, i.e., some of the steam may never have a chance to interact with the dispersed material. Considering only the dispersed melt, the TCE model [Allen et al. 1993b] predicts that 1097 g·moles of hydrogen could be produced. These calculations account for the thermodynamic limitations considered above. In addition, 150 g·moles of hydrogen may be produced by reactions with Cr in the insulation. Thus, the TCE model predicts that a bound on the amount of hydrogen produced by the HPME in IET-11 is 1247 g·moles. The amount of hydrogen calculated from gas grab samples that were drawn from the containment atmosphere between t = 15 s and 25 s ranges from 1550 g·moles to 1876 g·moles. It is possible that the disparity between the amount of hydrogen calculated by the TCE model (1247 g·moles) and the amount measured at a later time (1550-1876 g·moles) is the result of metal oxidation as metallic debris continues to oxidize with steam in the containment atmosphere and with water on the containment basement floor.

It is useful to apply the same reasoning to the IET-12 experiment. The metal content of chromium-free thermite is predominately Fe with trace quantities of Al. At thermitic temperatures, the oxide states are expected to be FeO and Al_2O_3. There was sufficient steam in the accumulator to oxidize all of the metal in the 30 kg thermite charge; this has the potential to produce 327 g·moles of hydrogen. However, thermodynamic limitations to the Fe reaction in the 30 kg charge reduces the potential to produce hydrogen from 327 g·moles to 236 g·moles. As in IET-11, the potential to produce hydrogen may be further reduced because of the noncoherence of the dispersal and blowdown processes. The TCE model predicts that a bound on the amount of hydrogen produced by the HPME in IET-12 is 127 g·moles. The experiment produced between 203 g·moles and 227 g·moles, which was determined from gas measurements at 15 min. Again, the disparity between the amount of hydrogen calculated by the TCE model (127 g·moles) and the amount measured at a later time (203-227 g·moles) may be due to long-term metal oxidation.

Figure 4.71 shows the net difference between hydrogen production and combustion. For comparison purposes only, it will be assumed that a hydrogen combustion hierarchy exists; hydrogen that was produced burned first, then preexisting hydrogen burned. (Actually, there is no way to determine which 'hydrogen' burned.) The small positive value at 15 s in IET-9 indicated that while most of the produced hydrogen burned, none of the preexisting hydrogen burned. In IET-10, all of the produced hydrogen burned and 117-167 g·moles of the preexisting hydrogen burned. In IET-11, all of the produced and 332-347 g·moles of the preexisting hydrogen had burned by 15 s, yielding a 94-96% burn fraction. The large positive value in IET-12 at 3 s (and also at 5 and 15 min) indicates that little hydrogen had burned. Possible causes for the lack of combustion in IET-12 are discussed in the following section.

4.9 Debris Recovery Summary

Debris in the containment vessel was recovered from ten basic locations: (1) all surfaces inside the basement, (2) in the vertical annulus between the vessel wall and the crane wall, (3) on the

trough floor at the bottom of the annulus between the vessel wall and the crane wall (only in IET-9 and IET-10), (4) all surfaces on the RHR platform, (5) all surfaces in the seal table room and including the seal table room ledge, (6) on the operating deck, (7) on the vessel wall, dome surface, and structures above the operating deck, (8) from the cavity and incore instrument tunnel, (9) in the annular gap between the reactor support skirt and the RPV model, and (10) from the crucible.

Table 4.10 gives the debris recovery summary which lists the locations and amounts of all debris recovered in the Surry DCH experiments. Table 4.10 also totals the amounts of debris collected in five general areas (basement, trough, vessel/cranewall annulus, seal table room, and operating deck). Three regions collected most of this debris: the RHR platform, the basement (including the trough), and the vessel wall directly in front of the RHR platform. Most of the debris in the basement and trough was collected on the cavity side of the vessel. The majority of the debris found in the RHR platform and in the seal table room existed as a thin film covering concrete surfaces. The debris found on the operating deck, upper level walls and surfaces, and dome surface were included in the amount of debris recovered outside structures. In IET-9, the removable operating deck section that covered the basement floor in front of the five foot door was not installed; therefore, the basement floor below the open deck was included because it is believed that the majority of the debris found in this area fell from above. In IET-11, the trough regions that had been filled with concrete were included in the appropriate basement regions.

There was a concern that the molten debris exiting the front of the RHR platform would impact on and possibly damage the CTTF vessel steel liner. Insulation board (Maronite) was placed on the liner in IET-9. Posttest inspection revealed little damage to the board; however, a large amount of debris (33 kg) was found frozen on the board. The board was removed in IET-10. Posttest examination of IET-10 revealed no damage to the liner; the debris impacted the liner, froze out and then sloughed off into the trough region. This increased the amount of debris recovered from the trough cavity 'T' region, and decreased the amount recovered from the vessel/cranewall annulus directly in front of the RHR platform.

The IET-11 debris recovery procedure indicated that the crucible had lost 35 kg, an unrealistic amount. An investigation determined that the scale used to measure the pretest weight of the IET-11 crucible had not functioned properly. Comparative visual inspection between the similar posttest IET-9 crucible determined that the mass loss was slight, thus the mass of debris recovered from the crucible was assumed to be zero.

Table 4.11 gives the mass balance for the Surry DCH experiments. The total molten mass available for dispersal into the vessel was 26% to 37% greater than the initial thermite charge due to the melting of the inner wall of the crucible, vaporization of the fusible brass plug, ablation of concrete in the cavity and structures, contaminants (breakwires, thermocouples, and RPV insulation), and oxidation of metallic debris.

Table 4.11 also gives transport fractions based on the mass balance. The definitions for computing the transport fractions from the mass balance are also shown. The transport fractions depend on the mass recovered from the locations specified (Table 4.10). The mass transported to the upper dome, $M_{d,dome}$, is computed from

$$M_{d,dome} = f_{eject}\, f_{disp}\, f_{dome}\, M_d^{\circ} \quad . \qquad (27)$$

For example, this method predicts that 28.95 kg of thermite were transported to the upper dome in IET-9; this is less than the 37.0 kg of material that were actually recovered in the upper dome

(see Table 4.11, mass recovered from outside structures). The difference represents contaminants and oxygen uptake. The transport fractions are computed based on the assumption that the bulk of contaminants and oxygen uptake occurred in the cavity, and that the initial thermite and additional masses are equally distributed. This introduces an element of subjectivity into the definition of transport fractions; however, the adopted procedure is recommended because it more closely represents the fraction of thermite dispersed to each location.

Two sets of transport fractions were calculated for IET-11: (1) a material transport fraction to account for the mass of material recovered in the upper dome, and (2) a thermite transport fraction to account for the energy of the material transported to the upper dome, since the processes which melted and ablated the RPV insulation reduced the total energy content of the debris. The difference between the transport fractions is due to subtracting the initial mass of the RPV stainless steel insulation (29 kg) from the mass of material recovered outside structures. The thermite transport fraction calculation assumed all of the insulation went to the dome. Note that this assumption ends up making f_{dome} (for thermite) less than that in IET-9. Initially, this may not seem reasonable, since the gap around the vessel was larger in IET-11. However, the seal table installed in IET-11 appeared to have blocked a significant debris path (as compared to IET-9 which had no seal table). Table 4.11 gives both sets of transport fractions. This method predicts that 39.9 kg of *material* were transported to the upper dome in IET-11; this is less than the 54.6 kg of material that were actually recovered in the upper dome. The difference represents contaminants and oxygen uptake transported to the dome. However, adjusting for the RPV insulation, the method predicts that 21.6 kg of *thermite* were transported to the upper dome in IET-11. The thermite transport fractions were used in the single-cell equilibrium model energy balance (Section 4.10).

Figure 4.72 compares the transport fractions for thermite transported to the dome. The annular gap provides a significant open pathway for material transport to the dome region. The IET-9 experiment had a partially open annular gap (0.012 m^2) and no seal table (seal table floor opening area = 0.047 m^2); the thermite transport fraction to the dome was 18.3%. The IET-10 experiment had a closed annular gap and a seal table model, which was found posttest partially ablated and lifted off of three of its six floor supports; the thermite transport fraction was 9.6%. The IET-11 experiment had an open annular gap (0.036 m^2 without the RPV insulation and 0.017 m^2 with the RPV insulation) and the seal table was found partially ablated but securely fastened to all six floor mounts; the thermite transport fraction was 13.7%.

Surprisingly, 53% of the total debris recovered (39.6 kg) remained in the cavity in IET-12. As a result of the low cavity dispersal, only 3% of the debris was dispersed into the upper dome. Three items contributed significantly to the small outside subcompartment transport fraction (0.074) and the dome transport fraction (0.034) listed in Table 4.11. The annular gap remained sealed; this removed a potentially significant pathway for material transport to the dome region. The seal table was found securely fastened to all six floor mounts; no ablation of the seal table by molten debris was discovered. However, the most significant item that contributed to reduce debris transport was the small cavity dispersal fraction. There was 47% dispersal of molten debris from the cavity, which was less than the 73-88% dispersal seen in the 1:6 scale tests (IET-9, IET-10, and IET-11). Figure 4.73 compares the transport fractions for the thermite dispersed from the cavity.

It is believed that co-ejected water and/or removal of the chromium from the melt caused low dispersal from the cavity. It is known that $\approx$1.2-1.6 kg of saturated water can cool/quench 1 kg of molten debris to ambient temperatures; it can also be calculated that $\approx$0.19 kg of saturated

water can cool 1 kg of the chromium-free melt from 2659 K to 2300 K (the liquidus temperature of the alumina in the melt). Comparing the retention of debris in the cavity (f_{disp} - f_{eject}) between the 1:6 scale tests and IET-12, it is evident that IET-12 had a much larger retention fraction (0.51) than the 1:6 scale tests (average retention fraction of 0.19). This implies that there was an extra 9.6 kg of melt retained in the IET-12 cavity (30 kg times (0.51-0.19)) compared to the 1:6 scale tests. It would require only about 1.8 kg (102 g·moles) of saturated water co-ejected with the blowdown steam to reduce the temperature of 9.6 kg of melt to the liquidus temperature. Note that this amount of entrained saturated water matched well with the amount necessary to match the pressure and temperature magnitude curves shown in Figure 4.60.

The absence of chromium reaction energy needed to keep the melt hot may have affected debris dispersal. It may also have produced a cooler steam/hydrogen jet which, along with the low debris dispersal, may have contributed to the lack of hydrogen combustion. To evaluate this possibility more quantitatively, a heat-mass transfer analogy to estimate the amount of heat transfer that will occur in parallel with the oxidation of iron can be used [Williams 1992]. It is estimated that about 9.2 - 16.1 MJ of thermal energy would be removed from the iron in the process of generating about 115 - 200 g·moles of hydrogen. The energy required to cool the iron from 2650 K to liquid just above its freezing point (1800 K) is about 0.64 MJ/kg; to go from 2650 K to the solid at 1750 K requires about 0.93 MJ/kg. Assuming 30 kg of reacted thermite is 56.6% by weight iron (i.e., about 17 kg Fe), the removal of 10.9-15.7 MJ would largely quench the reaction. This range closely brackets the energy loss estimated to occur during the production of the 115 - 200 g·moles of hydrogen measured in the IET-12 experiment.

The preceding analysis neglects possible heat transfer from the alumina to the iron, which might well keep the latter molten. However, the energy losses from the alumina are likely to be large enough to bring about the onset of its solidification, possibly reducing dispersal as previously suggested in conjunction with co-ejected water. In either event, the estimated energy losses appear to be sufficient to have significant effects upon debris behavior.

The melt would have included about 3.63 kg of Cr if the same composition was used as in previous tests. Reacting the Cr with the steam would have released about 14.5 MJ of energy; this is the calculated energy loss during the generation of $\approx$180 g·moles of hydrogen. The presence of chromium could have kept the melt temperature well above the freezing point of any of its constituents. This could have allowed the production of more hydrogen, a hotter steam/hydrogen jet, and more efficient debris dispersal.

Figure 4.74 compares the posttest sieve analysis of the debris recovered from outside the subcompartment structures in the Surry DCH experiment. The particle size analysis discounted all debris with sizes $>$9.4 mm and $<$0.038 mm. The particle size distribution was near lognormal. The vertical line at the 50th percentile crosses the sieve mass median diameter (SMMD) for each of the IETs.

Figure 4.75 compares the SMMD for debris recovered from outside the subcompartment structures in the Surry DCH experiment. The SMMD correlates proportionally with amount of debris transported outside subcompartments. The greater the amount of debris transported outside of the subcompartment structures, the larger the SMMD. Figure 4.75 also lists the amount of debris transported outside of the subcompartment structures for each experiment.

4.10 Energy Balance

Table 4.12 summarizes the energy balance for the Surry DCH experiments. The energy balance was calculated using the single-cell equilibrium model (Section 2.3.2). The dominant energy processes were hydrogen combustion and debris/gas heat transfer, usually in that order.

The thermal (latent and sensible heats) and chemical energy (debris oxidation) are computed for the dispersed thermite mass only. The single-cell DCH efficiency for the 1:6 scale DCH experiments ranged from 44-46%. For IET-12, the DCH efficiency was 34.5%.

Table 4.1 Subcompartment volumes and volume fractions for the Surry IET tests

Subcompartment	IET-9, IET-10		IET-11		IET-12	
	Volume (m^3)	Fraction	Volume (m^3)	Fraction	Volume (m^3)	Fraction
Dome	202.90	0.709	202.90	0.720	38.15	0.748
Cranewall	48.23	0.169	44.23	0.157	6.05	0.119
Basement	27.40	0.096	27.40	0.097	5.39	0.106
RHR Platform	4.05	0.014	4.05	0.014	0.77	0.015
Seal Table Room	1.91	0.007	1.91	0.007	0.36	0.007
Cavity/IIT	1.51	0.005	1.51	0.005	0.28	0.005
Total	286.00	1.000	282.00	1.000	51.00	1.000

Table 4.2 Gas concentrations measured in the IET-9 experiment

Location	Label	Start time → duration	f_{NC}	Species (mol.%)				
				N_2	O_2	H_2	CO	CO_2
1 (P3)	G1-B	-2 m → 10 s		23.97	6.16	2.21	0.00	0.12
	G1-15s	15 s → 10 s		18.48	3.36	2.28	0.05	0.27
	G1-2m	2 m → 10 s		15.90	1.61	2.56	0.16	0.41
	G1-15m	15 m → 10 s		15.86	1.65	2.56	0.15	0.40
2 (Hatch B)	G2-B	-2 m → 10 s		-	-	-	-	-
	G2-15s	15 s → 10 s		17.95	2.47	3.36	0.22	0.39
	G2-2m	2 m → 10 s		16.05	2.78	1.50	0.23	0.25
	G2-15m	15 m → 10 s		15.90	1.53	2.60	0.15	0.41
3 (CP)	G3-B	-2 m → 10 s		24.05	6.12	2.20	0.00	0.13
	G3-15s	15 s → 10 s		21.01	1.73	1.19	0.01	0.48
	G3-2m	2 m → 10 s		16.07	1.65	2.42	0.10	0.41
	G3-15m	15 m → 10 s		15.90	1.90	2.30	0.10	0.39
Background Mean[¶]			0.33	24.01	6.14	2.20	0.00	0.13
Background Standard Deviation[¶]				±0.06	±0.03	±0.01	±0.00	±0.01
Posttest Mean (15 s)			0.25	19.15	2.52	2.27	0.09	0.38
Posttest Standard Deviation				±1.63	±0.82	±1.08	±0.11	±0.11
Posttest Mean (2 m)			0.21	16.01	2.01	2.16	0.16	0.36
Posttest Standard Deviation				±0.09	±0.66	±0.58	±0.06	±0.09
Posttest Mean (15 m)			0.21	15.89	1.69	2.49	0.13	0.40
Posttest Standard Deviation				±0.02	±0.19	±0.16	±0.03	±0.01

Notes:

[¶] Background mean and standard deviations were computed for the two samples taken before the HPME at locations 1 and 3 in the containment vessel.

Table 4.3 Gas concentrations measured in the IET-10 experiment

Location	Label	Start time → duration	f_{NC}	Species (mol.%)				
				N_2	O_2	H_2	CO	CO_2
1 (P3)	G1-B	-2 m →10 s		38.49	10.05	1.95	0.60	0.25
	G1-15s	15 s → 10 s		31.77	5.50	0.78	0.31	0.58
	G1-2m	2 m → 10 s		32.37	4.80	0.99	0.34	0.79
	G1-15m	15 m → 10 s		32.04	4.43	1.14	0.33	1.14
2 (Hatch B)	G2-B	-2 m →10 s		38.23	10.26	2.03	0.65	0.18
	G2-15s	15 s → 10 s		32.05	5.35	0.63	0.29	0.63
	G2-2m	2 m → 10 s		31.65	6.03	0.69	0.35	0.54
	G2-15m	15 m → 10 s		32.07	4.39	1.15	0.32	0.85
3 (CP)	G3-B	-2 m →10 s		38.69	10.20	1.96	0.27	0.21
	G3-15s	15 s → 10 s		32.17	4.05	1.60	0.12	0.98
	G3-2m	2 m → 10 s		32.85	4.44	1.08	0.03	0.88
	G3-15m	15 m → 10 s		32.38	4.39	1.13	0.00	0.86
Background Mean[¶]			0.52	38.47	10.17	1.98	0.51	0.21
Background Standard Deviation[¶]				±0.23	±0.11	±0.04	±0.21	±0.04
Posttest Mean (15 s)[§]			0.39	31.99	4.97	1.00	0.24	0.73
Posttest Standard Deviation[§]				±0.21	±0.80	±0.52	±0.11	±0.22
Posttest Mean (2 m)[§]			0.40	32.29	5.09	0.92	0.24	0.74
Posttest Standard Deviation[§]				±0.60	±0.83	±0.21	±0.18	±0.18
Posttest Mean (15 m) [§]			0.39	32.16	4.40	1.14	0.21	0.95
Posttest Standard Deviation[§]				±0.19	±0.02	±0.01	±0.18	±0.17

Notes:

[¶] Background mean and standard deviations were computed for the three samples taken before the HPME at locations 1, 2, and 3 in the containment vessel.

[§] Posttest mean and standard deviations were computed for the three samples taken after the HPME at locations 1, 2, and 3 in the containment vessel.

Table 4.4 Gas concentrations measured in the IET-11 experiment

Location	Label	Start time → duration	f_{NC}	Species (mol.%)				
				N_2	O_2	H_2	CO	CO_2
1 (P3)	G1-B	-18 m → 10 s		58.49	15.50	1.97	0.00	0.17
	G1-15s	15 s → 10 s		43.04	8.05	0.68	0.00	0.45
	G1-2m	2 m → 10 s		39.42	6.34	0.48	0.00	0.55
	G1-15m	15 m → 10 s		38.95	6.51	0.63	0.00	0.53
2 (Hatch B)	G2-B	-18 m → 10 s		57.23	15.28	3.50	0.00	0.10
	G2-15s	15 s → 10 s		42.66	9.00	0.18	0.00	0.37
	G2-2m	2 m → 10 s		-	-	-	-	-
	G2-15m	15 m → 10 s		39.04	6.53	0.51	0.00	0.53
3 (Dome)	G3-B	-18 m → 10 s		58.09	15.62	2.32	0.00	0.09
	G3-15s	15 s → 10 s		46.52	4.82	0.00	0.00	0.83
	G3-2m	2 m → 10 s		39.05	6.50	0.69	0.00	0.55
	G3-15m	15 m → 10 s		37.83	6.93	0.34	0.00	1.52
4 (RHR Annulus)	G4-B	-18 m → 10 s		58.28	15.53	2.19	0.00	0.12
	G4-15s	15 s → 10 s		42.65	7.82	1.26	0.00	0.50
	G4-2m	2 m → 10 s		38.52	7.01	0.90	0.00	0.46
	G4-15m	15 m → 10 s		38.36	7.38	0.47	0.00	0.39
Background Mean (t = -18 m) Background Standard Deviation			0.77	58.02 ±0.55	15.48 ±0.14	2.50 ±0.68	0.00 ±0.00	0.12 ±0.04
Background Mean[¶] (t = -18 m)			0.77	57.78	15.48	2.68	0.00	0.22
Background Mean[¶] (t = 0 s)			0.68	50.98	13.66	2.39	0.00	0.20
Posttest Mean (15 s) Posttest Standard Deviation			0.53	43.71 ±1.88	7.42 ±1.81	0.53 ±0.57	0.00 ±0.00	0.54 ±0.20
Posttest Mean (2 m)[§] Posttest Standard Deviation[§]			0.47	39.00 ±0.45	6.62 ±0.35	0.69 ±0.21	0.00 ±0.00	0.52 ±0.05
Posttest Mean (15 m) Posttest Standard Deviation			0.47	38.55 ±0.56	6.84 ±0.41	0.49 ±0.12	0.00 ±0.00	0.74 ±0.52

Notes:

[¶] Background mean determined from vessel charging process.

[§] Posttest 2 min mean and standard deviations were computed for the three samples taken after the HPME at locations 1, 3, and 4 in the containment vessel.

Table 4.5 Gas concentrations measured in the IET-12 experiment

Number & Location	Start time → duration	f_{NC}	Species (mol.%)				
			N_2	O_2	H_2	CO	CO_2
#1 - Leg C - Dome	-30 s → 5 s	0.43	28.82	7.38	5.76	0.10	0.27
#2 - Leg B - High	-30 s → 5 s	0.42	28.33	7.19	5.64	0.00	0.27
#3 - Basement	-30 s → 5 s	0.42	28.18	7.29	5.58	0.00	0.25
#4 - Leg B - Dome	3 s → 5 s	0.59	41.11	9.59	6.47	0.31	0.79
#5 - Leg B - High	3 s → 5 s	0.64	44.75	11.20	6.66	0.40	0.39
#6 - Leg C - Low	3 s → 5 s	0.45	33.54	8.22	2.28	0.00	0.45
#7 - Leg A - High	3 s → 5 s	0.39	24.32	5.51	8.21	0.36	0.40
#8 - Leg C - High	3 s → 5 s	0.51	34.87	8.55	6.17	0.24	0.34
#9 - Basement	3 s → 5 s	0.35	17.31	3.08	13.29	0.77	0.54
#10 - Cranewall	3 s → 5 s	0.27	11.41	1.52	12.86	0.82	0.56
#11 - Ops Deck	3 s → 5 s	0.39	24.04	5.48	8.61	0.34	0.37
#12 - Leg B - High	5 min → 5 s	0.39	22.94	4.90	9.96	0.55	0.52
#13 - Leg B - High	5 min → 5 s	0.40	23.51	5.10	10.21	0.56	0.47
#14 - Leg B - High	15 min → 5 s	0.40	23.40	4.87	10.30	0.53	0.51
#15 - Leg B - High	15 min → 5 s	0.39	22.50	4.90	9.81	0.54	0.47
Background Mean (measured)		0.42 ±0.01	28.45 ±0.33	7.28 ±0.09	5.66 ±0.09	0.03 ±0.06	0.26 ± 0.01
Background Mean[¶]		0.46	31.07	8.32	5.70	0.00	0.12
Posttest Mean (3 s)[§]		0.44	29.03	6.66	7.63	0.37	0.51
Posttest Standard Deviation[§]		±0.12	±11.60	±3.32	±3.66	±0.27	± 0.15
Posttest Mean (5 m)		0.40	23.22	5.00	10.08	0.56	0.50
Posttest Standard Deviation		±0.01	±0.41	±0.14	±0.18	±0.01	± 0.04
Posttest Mean (15 m)		0.39	22.98	4.89	10.05	0.54	0.49
Posttest Standard Deviation		±0.01	±0.60	±0.03	±0.35	±0.01	± 0.03

Notes:

[¶] Background mean determined from vessel charging process.

[§] Posttest 3 s mean and standard deviations were computed using a vessel mole-averaging technique.

Table 4.6 Gas sample data analysis for the IET-9 experiment

	0 s	15 s	2 min	15 min
Vessel pressure (MPa)	0.1351	0.2644	0.2037	0.1663
Vessel gas temperature (K)	392	643	453	381
Vessel gas moles (g • moles)	11870	14145	15468	15015
Initial steam moles (g • moles)	7981			
Accumulator moles (g • moles)	3005			
Debris vaporization steam moles (g • moles)	2542			
Vessel steam moles (g • moles)[¶]	7981	10986	13528	13528
f_{NC}[•] (f_{NC} by steam method)[§]	0.33 (0.33)	0.25 (0.22)	0.25-0.21[M] (0.13)	0.25-0.21[M] (0.10)
O_2 concentration (mole %)	6.14	2.52	2.44-2.01	2.06-1.69
H_2 concentration (mole %)	2.20	2.27	2.63-2.16	3.03-2.49
Moles of O_2 (g • moles)	729	356	378-311	304-254
Moles of H_2 (g • moles)	262	321	407-334	455-374
Moles of H_2 produced (g • moles)	0 0	806 (786)[£]	847-820 (865)	941-859 (1037)
Moles of H_2 burned (g • moles)	0 0	747 (710)	702-747 (741)	747-747 (852)
Fraction Burned	0	0.70 (0.68)	0.63-0.69 (0.66)	0.62-0.67 (0.66)

[¶] steam moles (0 s) = initial moles
steam moles (15 s) = initial moles + accumulator moles
steam moles (2 min) = initial moles + accumulator moles + vaporization moles
steam moles (15 min) = initial moles + accumulator moles + vaporization moles

[•] $f_{NC} = (f_{NC}^{\circ} N^{\circ} + \Delta N_{H2} + \Delta N_{O2}) / (N^{\circ} + \Delta N_{O2} + N_{blow} + N_{vapor})$

[§] f_{NC} = (1 - steam moles / vessel gas moles)

[£] The hydrogen amounts shown in parenthesis were based on the nitrogen-ratio analysis method.

[M] The 2 min. and the 15 min. gas analyses are based on a f_{NC} calculation with and without basement floor water vaporization.

Table 4.7 Gas sample data analysis for the IET-10 experiment

	0 s	15 s	2 min	15 min
Vessel pressure (MPa)	0.1791	0.3267	0.2502	0.2107
Vessel gas temperature (K)	410	672	471	420
Vessel gas moles (g • moles)	15027	16770	18273	17257
Initial steam moles (g • moles)	7243			
Accumulator moles (g • moles)	3275			
Debris vaporization steam moles (g • moles)	0			
Vessel steam moles (g • moles)[¶]	7243	10518	10518	10518
f_{NC}* (f_{NC} by steam method)[§]	0.52 (0.52)	0.39 (0.37)	0.40 (0.42)	0.39 (0.39)
O_2 concentration (mole %)	10.17	4.97	5.09	4.40
H_2 concentration (mole %)	1.98	1.00	0.92	1.14
CO concentration (mole %)	0.51	0.24	0.24	0.21
Moles of O_2 (g • moles)	1528	834	932	760
Moles of H_2 (g • moles)	298	168	168	196
Moles of CO (g • moles)	77	40	44	38
Moles of H_2/CO produced (g • moles)	0 0	1222 (1143)[£]	1030 (1103)	1248 (1382)
Moles of H_2/CO burned (g • moles)	0 0	1389 (1260)	1192 (1235)	1389 (1475)
Fraction Burned	0	0.87 (0.83)	0.85 (0.84)	0.86 (0.84)

[¶] steam moles (0 s) = initial moles
steam moles (15 s) = initial moles + accumulator moles
steam moles (2 min) = initial moles + accumulator moles + vaporization moles
steam moles (15 min) = initial moles + accumulator moles + vaporization moles

* $f_{NC} = (f_{NC}^{\circ} N^{\circ} + \Delta N_{H2} + \Delta N_{O2}) / (N^{\circ} + \Delta N_{O2} + N_{blow} + N_{vapor})$

[§] f_{NC} = (1 - vessel steam moles / vessel total moles)

[£] The hydrogen amounts shown in parenthesis were based on the nitrogen-ratio analysis method.

Table 4.8 Gas sample data analysis for the IET-11 experiment

	0 s	15 s	2 min	15 min
Vessel pressure (MPa)	0.2209	0.4197	0.3175	0.2683
Vessel gas temperature (K)	399	725	496	432
Vessel gas moles (g • moles)	18802	19635	21712	21066
Initial steam moles (g • moles)	6064			
Accumulator moles (g • moles)	3705			
Debris vaporization steam moles (g • moles)	2547			
Vessel steam moles (g • moles) [¶]	6064	9769	12316	12316
f_{NC}[•] (f_{NC} by steam method)[§]	0.68 (0.68)	0.53 (0.50)	0.53-0.47[M] (0.55-0.43)	0.53-0.47[M] (0.53-0.42)
O_2 concentration (mole %)	13.66	7.42	7.48-6.62	7.72-6.84
H_2 concentration (mole %)	2.39	0.53	0.78-0.69	0.55-0.49
Moles of O_2 (g • moles)	2568	1457	1623-1437	1627-1441
Moles of H_2 (g • moles)	450	104	168-150	115-102
Moles of H_2 produced (g • moles)	0 0	1876 (1550)[£]	1609-1923 (1606)	1548-1875 (1405)
Moles of H_2 burned (g • moles)	0 0	2223 (1882)	1890-2223 (1885)	1882-2223 (1734)
Fraction Burned	0	0.96 (0.94)	0.92-0.94 (0.92)	0.94-0.96 (0.93)

[¶] steam moles (0 s) = initial moles
steam moles (15 s) = initial moles + accumulator moles
steam moles (2 min) = initial moles + accumulator moles + vaporization moles
steam moles (15 min) = initial moles + accumulator moles + vaporization moles

• $f_{NC} = (f_{NC}^{\circ} N^{\circ} + \Delta N_{H2} + \Delta N_{O2}) / (N^{\circ} + \Delta N_{O2} + N_{blow} + N_{vapor})$

[§] f_{NC} = (1 - vessel steam moles / vessel total moles)

[£] The hydrogen amounts shown in parenthesis were based on the nitrogen-ratio analysis method.

[M] The 2 min. and the 15 min. gas analyses are based on a f_{NC} calculation with and without basement floor water vaporization.

Table 4.9 Gas sample data analysis for the IET-12 experiment

	0 s	3 s	5 min	15 min
Vessel pressure (MPa)	0.1635	0.3076	0.2275	0.2227
Vessel gas temperature (K)	408	568	423	414
Vessel gas moles (g • moles)	2461	3322	3299	3301
Initial steam moles (g • moles)	1427			
Accumulator moles (g • moles)	604			
Debris vaporization steam moles (g • moles)	0			
Vessel steam moles (g • moles) [¶]	1427	2031	2031	2031
f_{NC} - gas bottle measurement (f_{NC} by calculation)[•] (f_{NC} by steam method)[§]	0.42 (0.42) (0.42)	0.44 (0.37) (0.39)	0.40 (0.40) (0.38)	0.39 (0.40) (0.38)
O_2 concentration (mole %)	7.28	6.66	5.00	4.89
H_2 concentration (mole %)	5.66	7.63	10.08	10.05
Moles of O_2 (g • moles)	179	221	165	161
Moles of H_2 (g • moles)	139	253	333	332
Moles of H_2 produced (g • moles)	0 0	114 (82)[£]	197 (221)	203 (227)
Moles of H_2 burned (g • moles)	0 0	0 (37)	4 (57)	11 (60)
Fraction Burned	0	0.00 (0.17)	0.01 (0.16)	0.03 (0.16)

[¶] steam moles (0 s) = initial moles
steam moles (3 s) = initial moles + accumulator moles
steam moles (5 min) = initial moles + accumulator moles + vaporization moles
steam moles (15 min) = initial moles + accumulator moles + vaporization moles

[•] $f_{NC} = (f_{NC}^{\circ} N^{\circ} + \Delta N_{H2} + \Delta N_{O2}) / (N^{\circ} + \Delta N_{O2} + N_{blow} + N_{vapor})$

[§] f_{NC} = (1 - vessel steam moles / vessel total moles), initial vessel steam calculated using the f_{NC} from gas bottle measurements

[£] The hydrogen amounts shown in parenthesis were based on the nitrogen-ratio analyses method.

[M] The 2 min. and the 15 min. gas analyses are based on a f_{NC} calculation with and without basement floor water vaporization.

Table 4.10 Debris recovery summary for the Surry DCH experiments

	IET-9		IET-10		IET-11		IET-12	
Location	Mass (kg)	Total (kg)	Mass (kg)	Total (kg)	Mass (kg)	Total (kg)	Mass (kg)	Total (kg)
Basement (CS) ¶	7.915	10.475	3.200	14.590	39.150	43.175	3.693	5.180
Basement (DS) § *	2.560		11.390		4.025		1.487	
Trough (Cavity 'T')	19.675	43.085	33.825	59.845	N/A	N/A	N/A	N/A
Trough (CS)	9.490		13.195		N/A		N/A	
Trough (DS)	13.92		12.825		N/A		N/A	
Vessel/Crane Wall Annulus (RHR platform from trough to ledge)	32.060	33.325	0.715	1.775	N/A	1.0985	N/A	3.372
Vessel/Crane Wall Annulus (CS)	0.430		0.350		0.6230		3.109	
Vessel/Crane Wall Annulus (DS)	0.835		0.710		0.4756		0.263	
RHR Platform		26.915		34.215		35.840		5.309
Seal Table Room	0.970	12.270	25.415	26.680	12.460	17.345	2.642	2.689
Seal Table Room (Ledge)	2.560		1.265		4.885		0.047	
Operating Deck (CS) *	14.175	27.790	10.845	18.320	22.690	37.470	0.764	1.038
Operating Deck (DS) *	13.615		7.475		14.780		0.274	
Upper Level * (Between level 3 grating and dome)		6.600		2.460		12.520		0.344
Annular Gap		15.675		0.000		22.810		0.000
Cavity		22.995		58.280		38.180		20.970
Crucible		2.270		-6.810		-35.00		0.687
Monorail (Topside) *		NC		0.0875		1.2991		N/A
Missile Shield (underside)		NC	0.825	0.9338	3.195	5.889	0.000	0.000
Missile Shield (topside) *		NC	0.1088		2.694		0.000	
Accumulator (topside) *		NC		NC		0.6232		N/C
Total Recovered (without crucible)		199.1		217.2		216.3		39.589

¶ CS - Vessel split between equipment hatch A and equipment hatch B on cavity side.
§ DS - Vessel split between equipment hatch A and equipment hatch B on five foot door side.
* Denotes debris/aerosols that participated outside subcompartment structures (Basement (DS) used only in IET-9).
NC - not collected separately for the test.
N/A - not applicable for the test.

Table 4.11 Mass balance for the Surry DCH experiments

Mass Balance (kg)	IET-9	IET-10	IET-11	IET-12
Initial Thermite Charge, M_d° (a)	158.000	158.000	158.000	30.000
Crucible (b)	2.270	-6.810	-35.000	0.687
Cavity (c)	22.995	58.280	38.180	20.970
Inside Structures (d) (d = f - e - c)	139.185	137.930	123.464	17.237
Outside Structures (e)	36.950	20.976	54.606	1.382
Total Recovered (f) *	199.130	217.186	216.250	39.589
Recovery Fraction $f_{recovery} = f/a$	1.260	1.375	1.369	1.320
Thermite Transport Fractions				
Ejected into Cavity, $f_{eject} = 1 - b/a$ (only if < 1)	0.986	1.000	1.000	0.977
Dispersed from Cavity, ¶ $f_{disp} = (d + e')/(c + d + e')$	0.885	0.732	0.796 (0.823)	0.470
Transported Outside Subcompartment, $f_{dome} = e'/(d + e')$	0.210	0.132	0.172 (0.307)	0.074
Transported to Dome, $f_{trans} = f_{eject} * f_{disp} * f_{dome}$	0.183	0.096	0.137 (0.253)	0.034
Thermite Transported to Dome, $M_d = M_d^\circ * f_{trans}$	28.95	15.27	21.63 (39.90)	1.019

* The molten mass available for dispersal into the vessel was 26% to 37% greater than the initial iron oxide/alumina/chromium thermite charge due to melting of the inner wall of the crucible, vaporization of the fusible brass plug, ablation of concrete in the cavity, contaminants (breakwires, thermocouples, and RPV insulation), and oxidation of metallic debris by steam.

¶ The thermite transport fraction was determined by reducing the amount of material recovered outside the subcompartment by the mass of the RPV insulation ($e' = e - 29$), due to the RPV reflective metal insulation representing such a large contaminant. The numbers in parentheses indicate the total material transport fraction.

Table 4.12 Energy balance for the Surry DCH experiments

Modeling parameter	Description	IET-9 1:6 scale	IET-10 1:6 scale	IET-11 1:6 scale	IET-12 1:10 scale
N_d (g • mole)	Debris participating in DCH	2102	1763	1993	203
C_d (J/g • mole K)	Debris heat capacity	74.7	74.7	74.7	79.4
P^o (MPa)	Atmosphere pressure	0.1351	0.1791	0.2209	0.1635
N^0 (g • mole)	Containment gas	11870	15027	18802	2461
C_v (J/g • mole K)	Atmosphere heat capacity	29.66	28.06	25.37	28.88
ψ	Heat capacity ratio	0.373	0.269	0.268	0.184
U^0 (MJ)	Atmosphere internal energy	130	163	179	29
N_b (g • mole)	RCS blowdown gas	3005	3275	3705	574
ΔE_b (MJ)	Blowdown energy	50	47	51	9
ΔE_t (MJ)	Thermal energy	346	290	315	38
ΔE_r (MJ)	Chemical energy	88	74	80	3
ΔE_{H2} (MJ)	Hydrogen combustion energy	341	448	522	70
$\Delta P_{measured}$ (MPa)	Measured peak pressure increase	0.283	0.326	0.430	0.198
$\Delta P_{1\text{-cell}}$ (MPa)	Predicted peak pressure increase	0.624	0.743	0.941	0.574
η	DCH efficiency	0.453	0.439	0.457	0.345

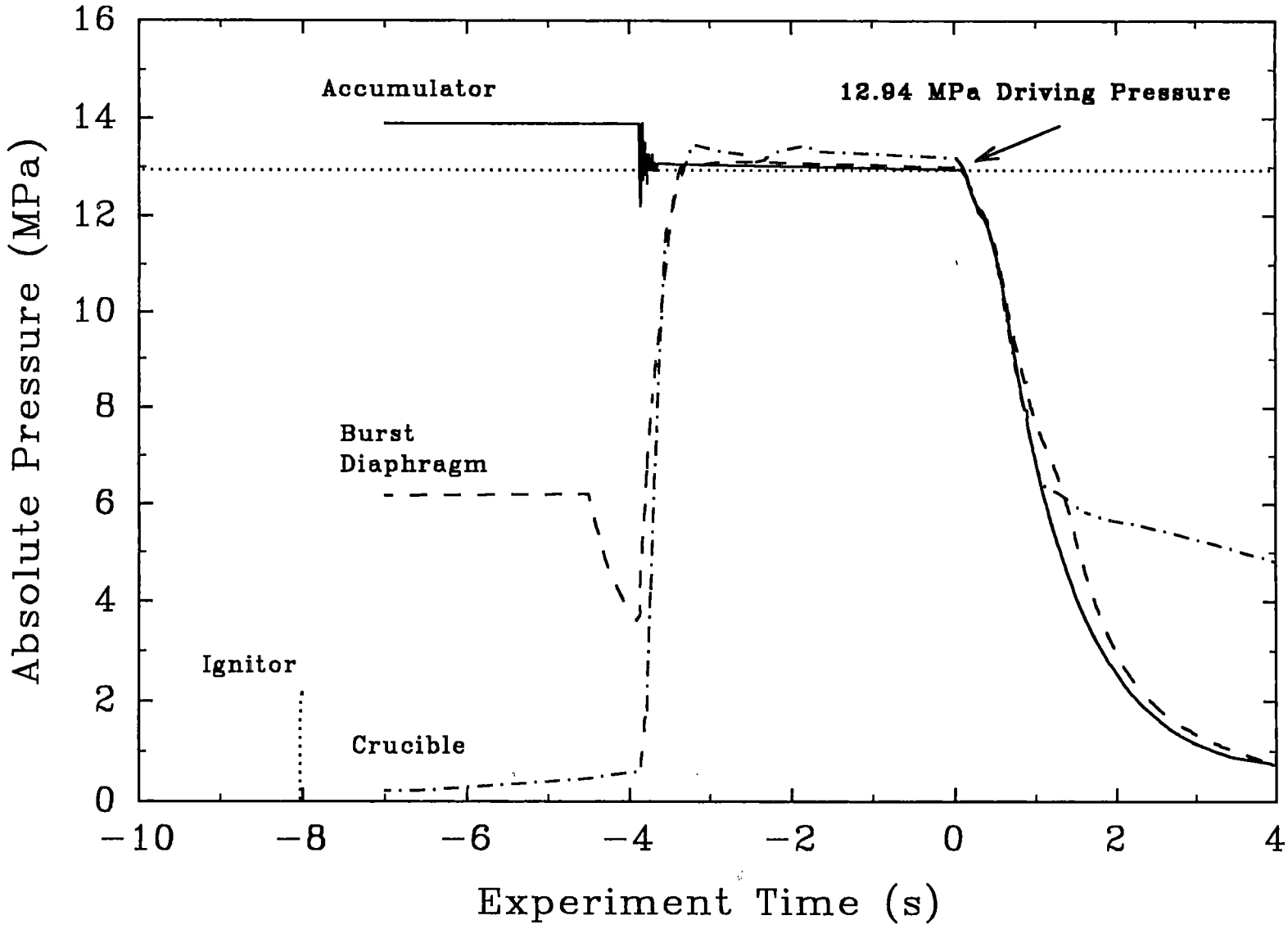

Figure 4.1 Blowdown history of the IET−9 experiment.

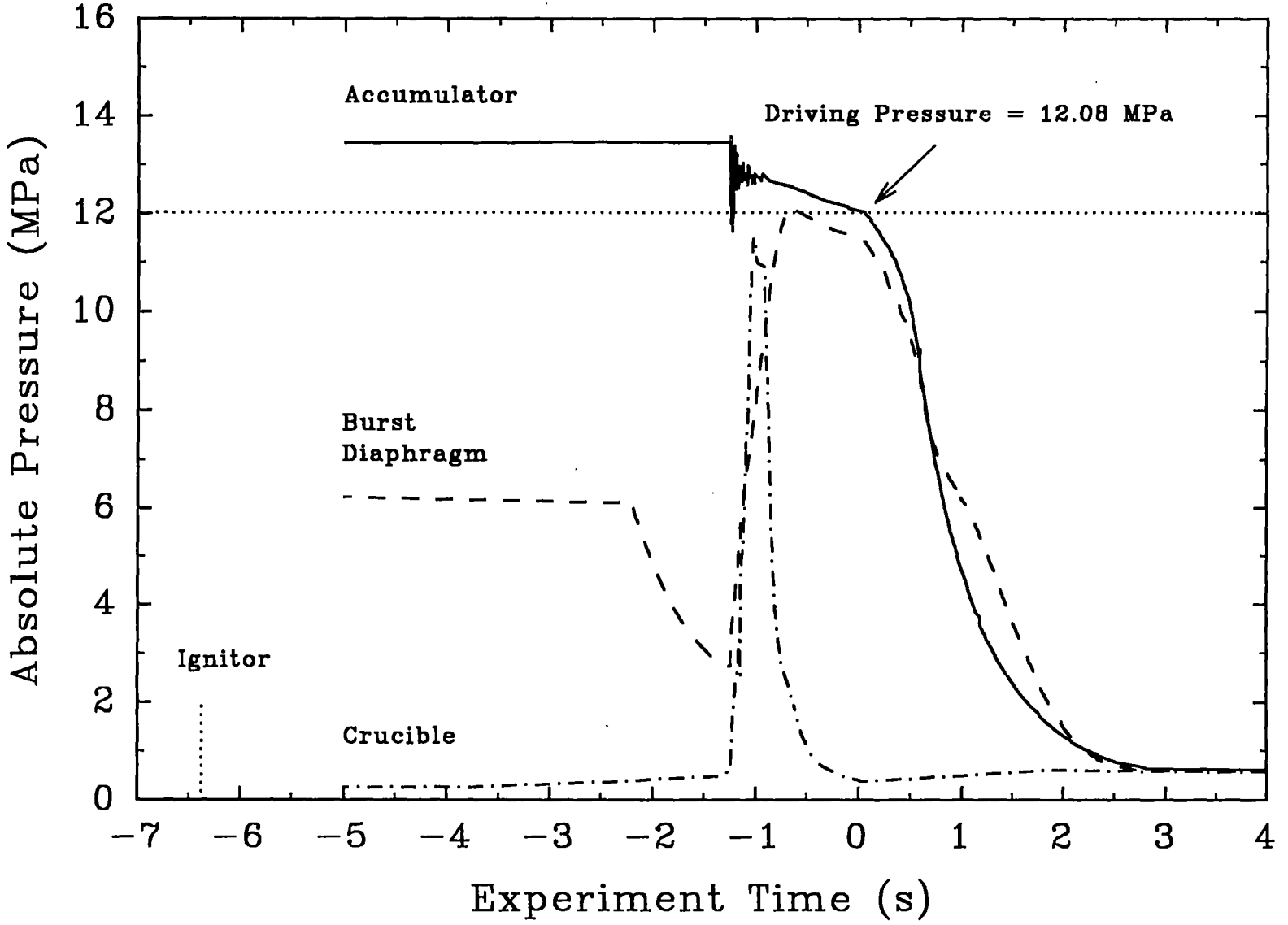

Figure 4.2 Blowdown history of the IET−10 experiment.

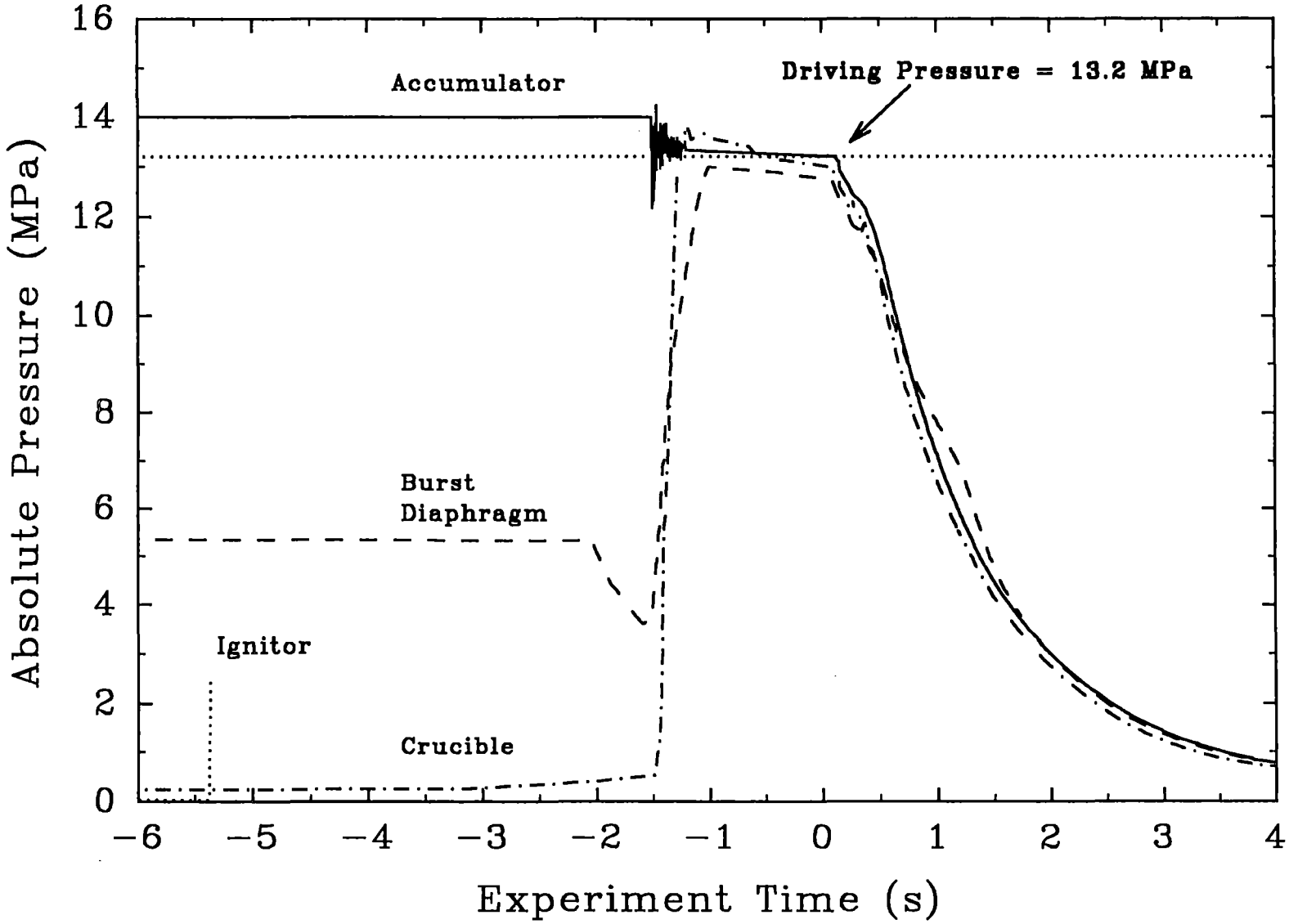

Figure 4.3 Blowdown history of the IET−11 experiment.

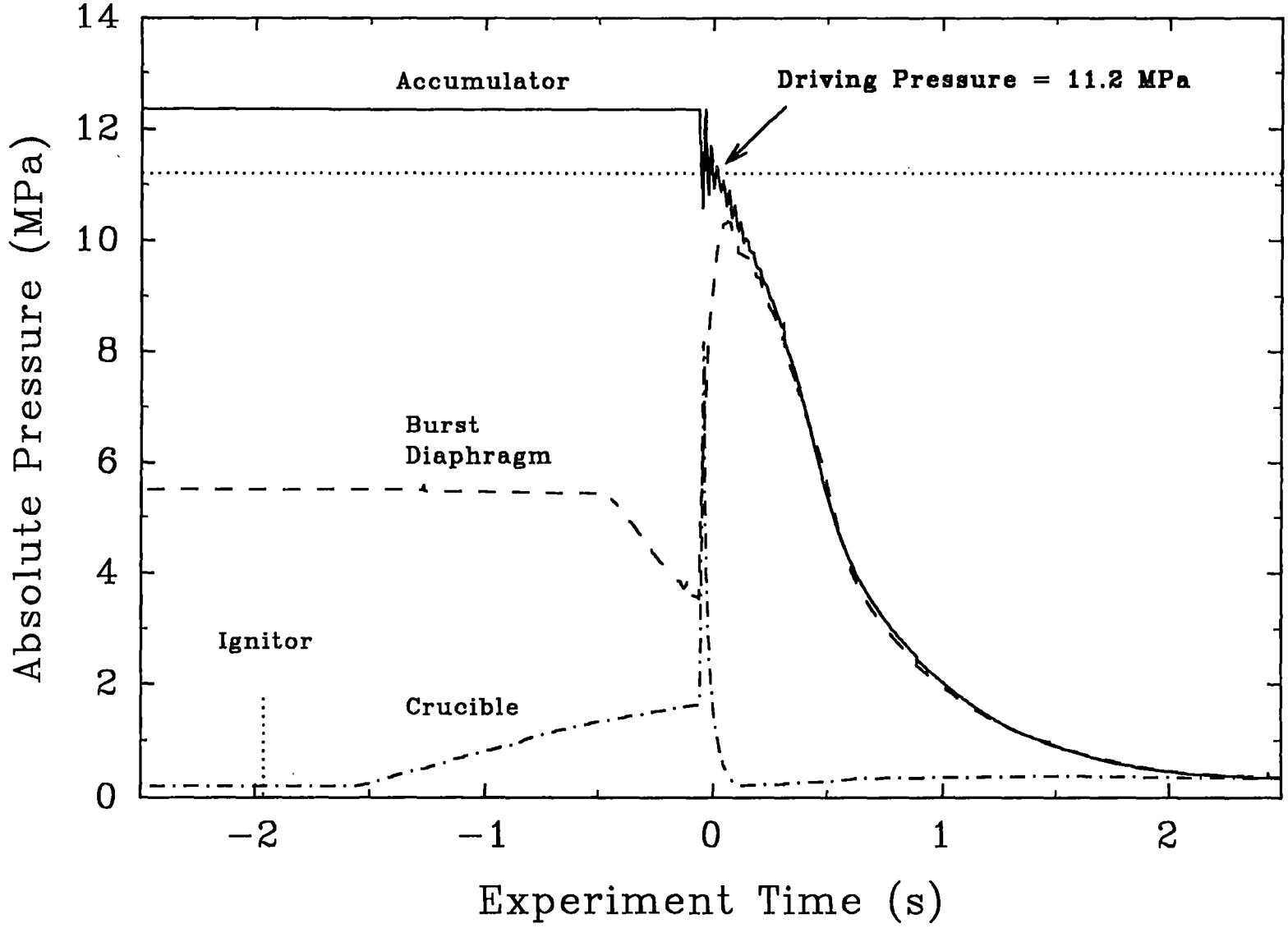

Figure 4.4 Blowdown history of the IET−12 experiment.

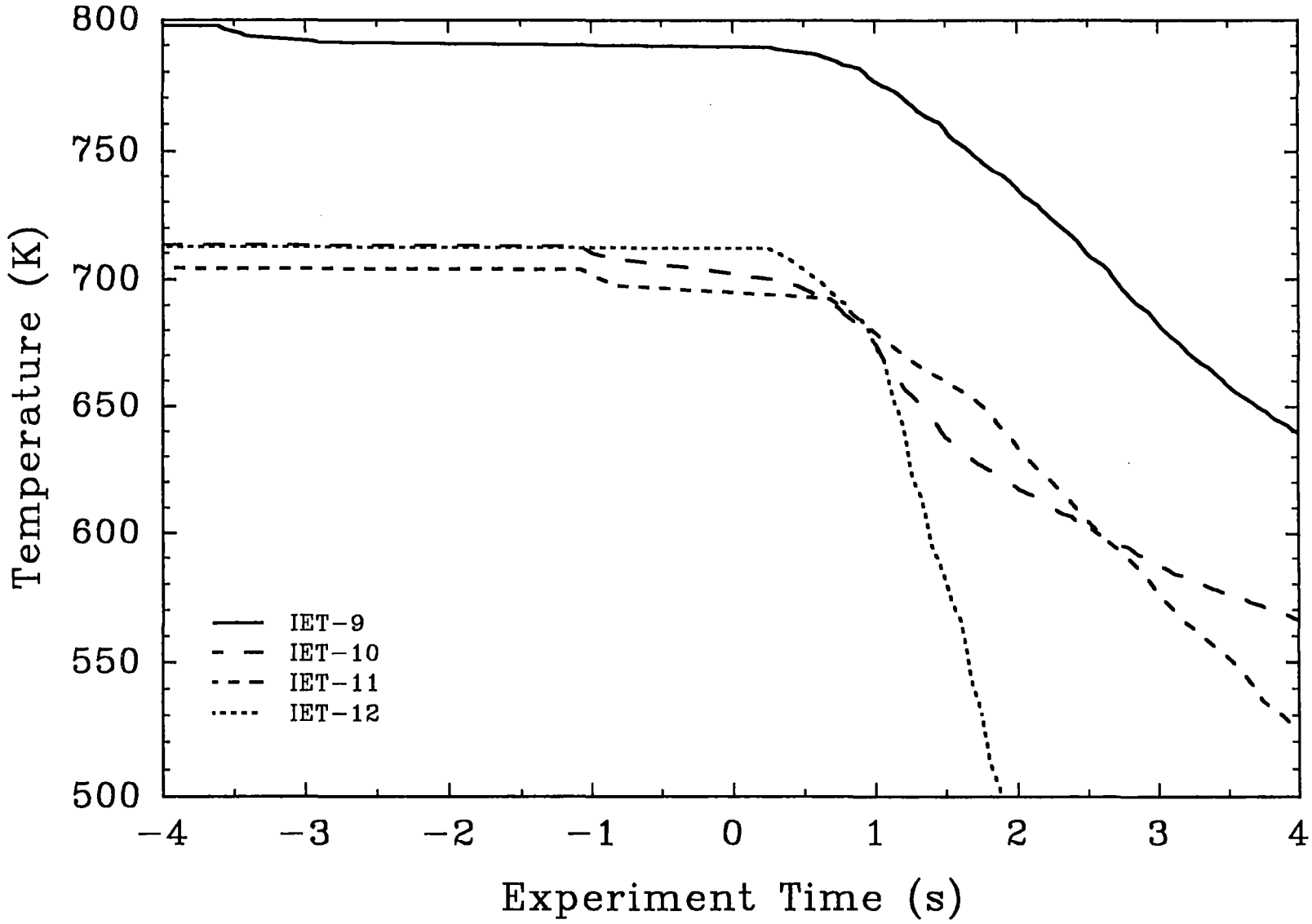

Figure 4.5 Steam blowdown temperatures measured in the steam accumulator for the Surry IET experiments.

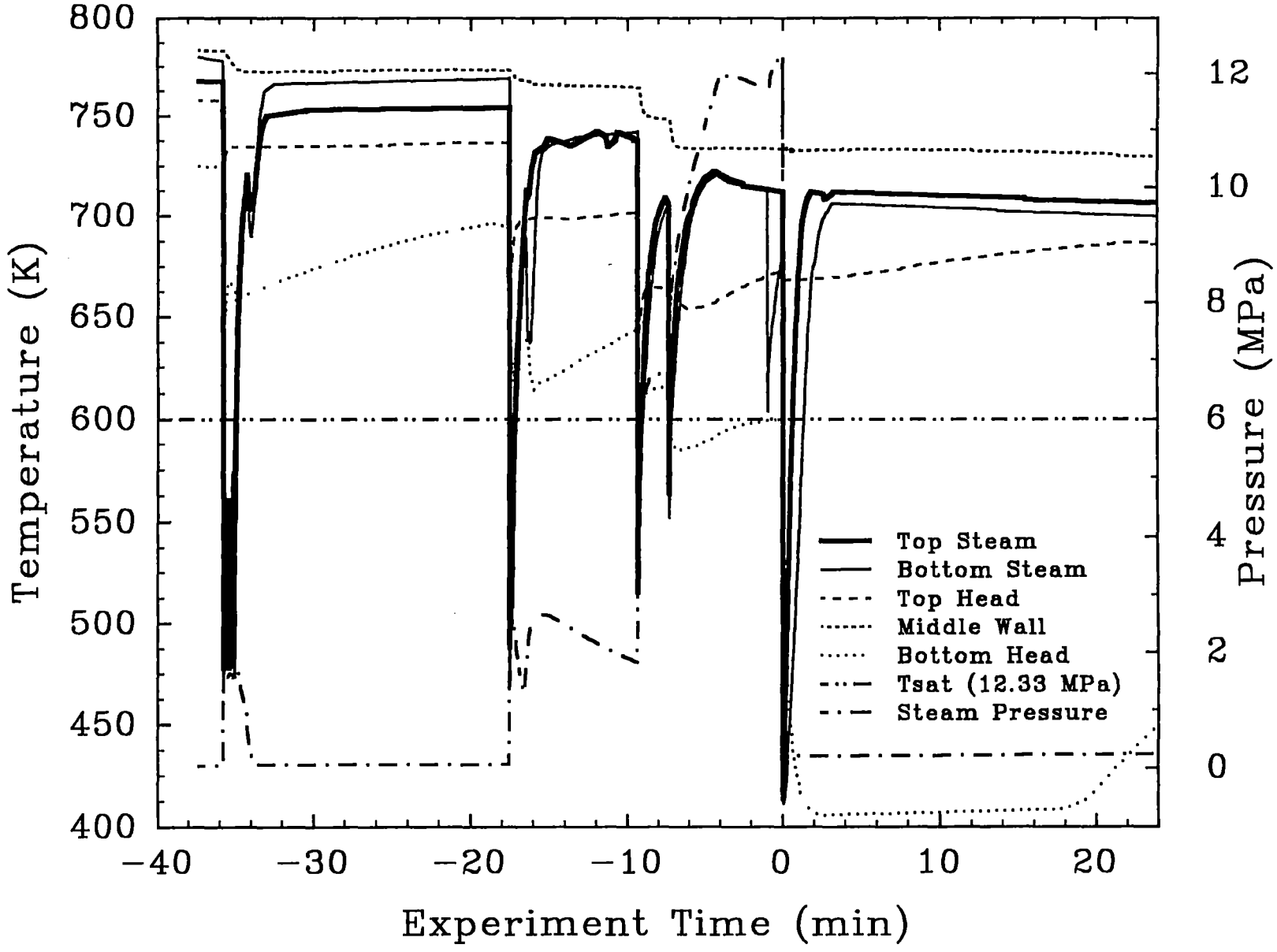

Figure 4.6 Accumulator temperature and pressure history in the IET−12 experiment.

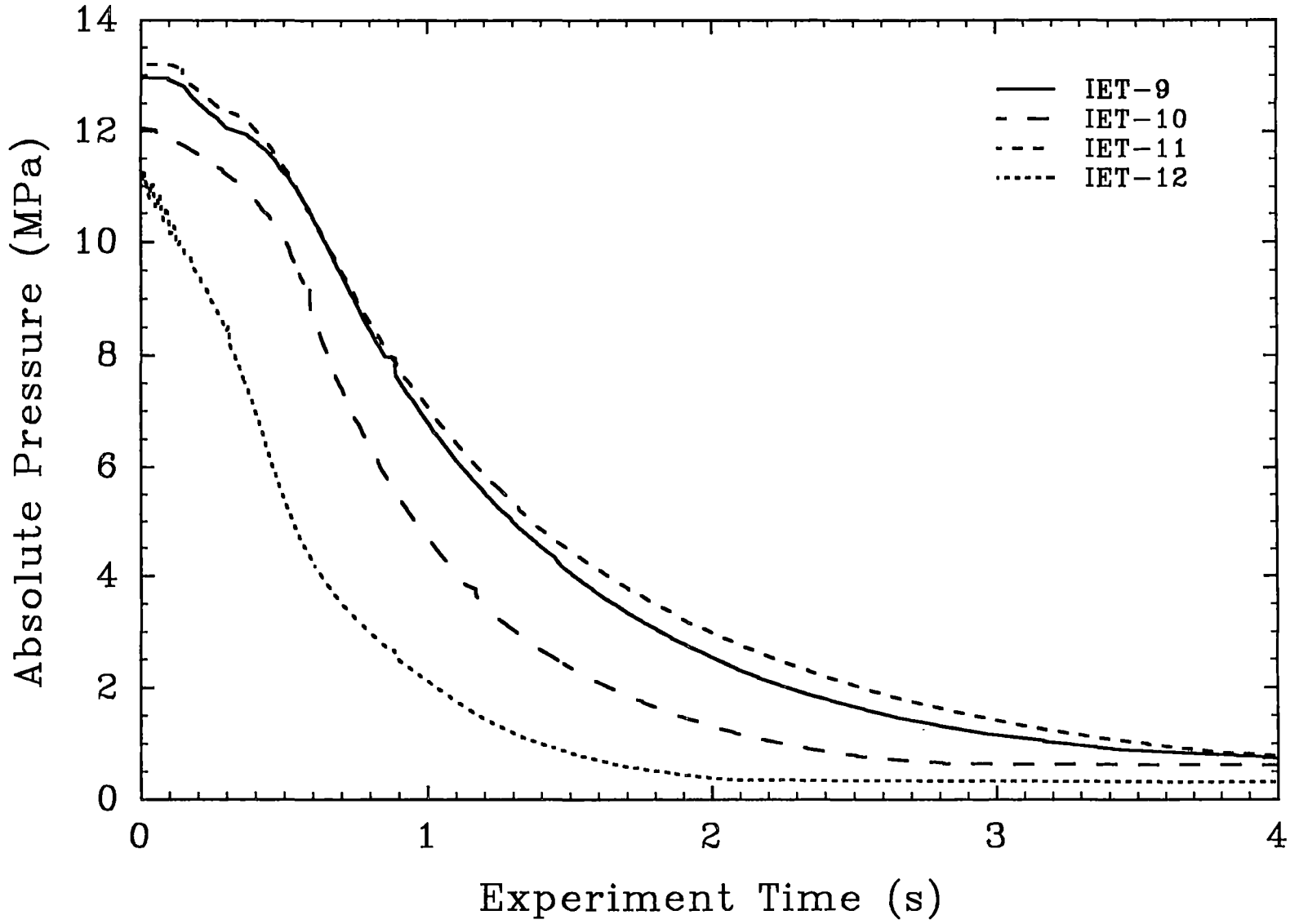

Figure 4.7 Accumulator pressure history for the Surry DCH experiments.

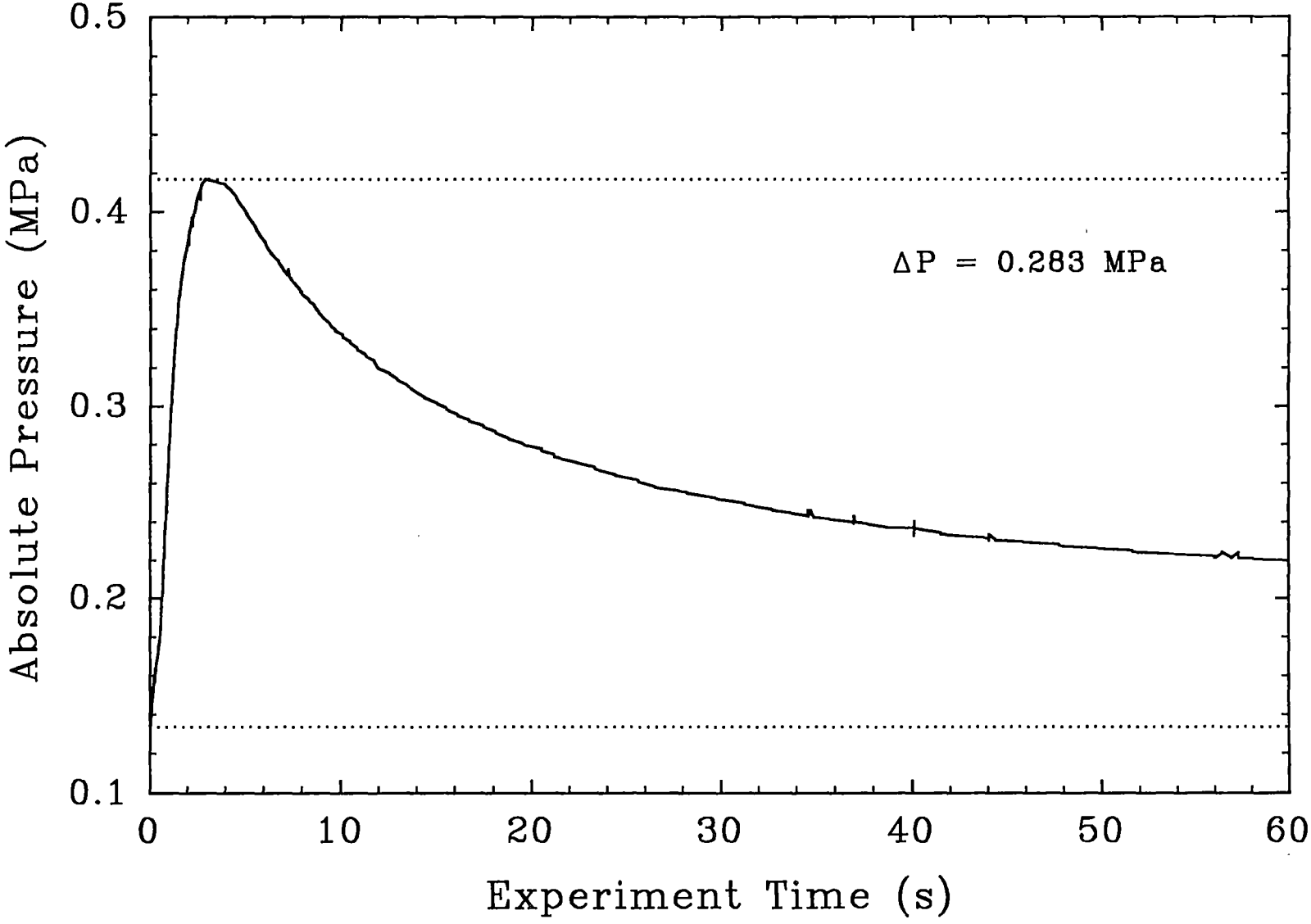

Figure 4.8 CTTF vessel pressure versus time in the IET−9 experiment.

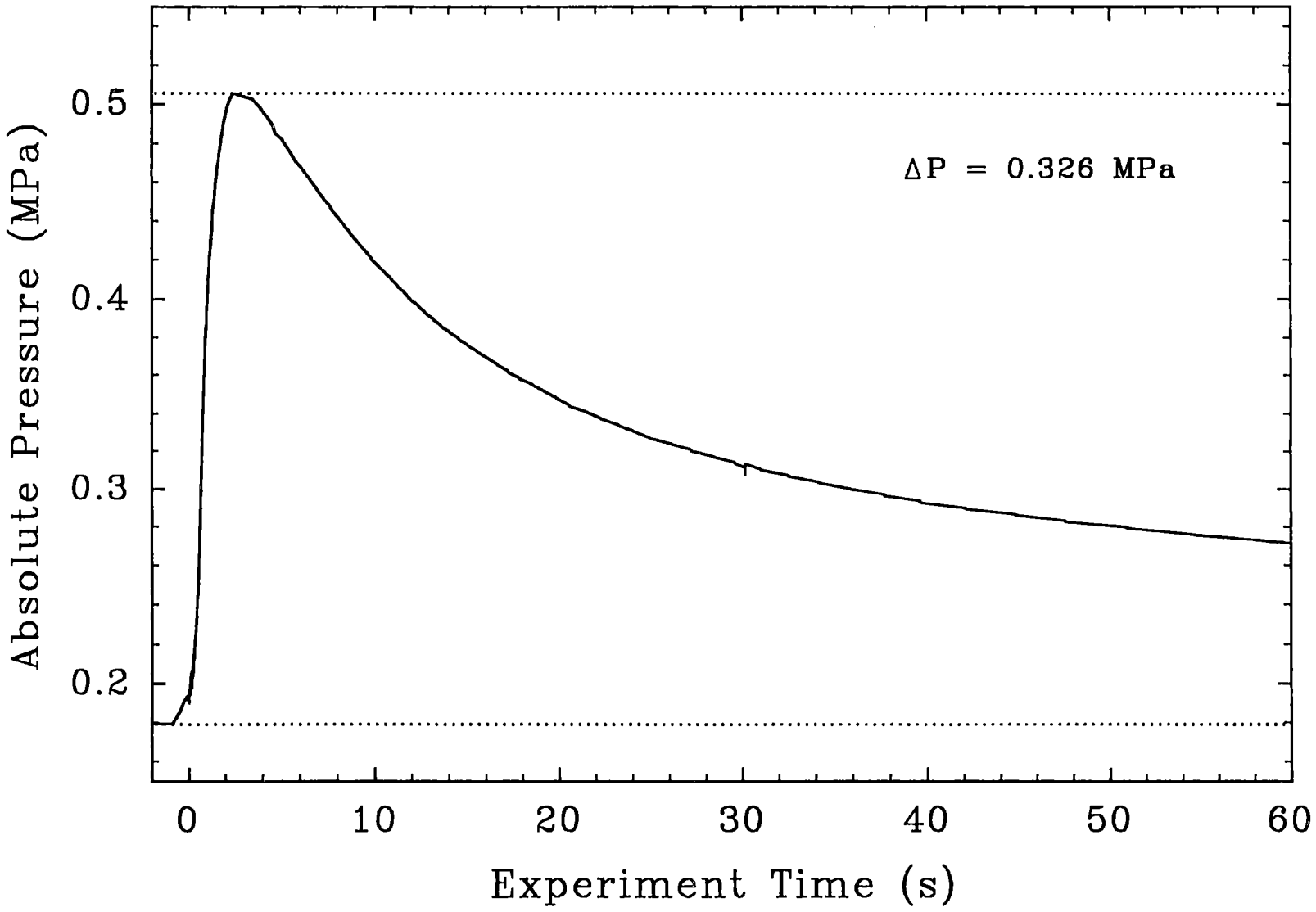

Figure 4.9 CTTF vessel pressure versus time in the IET-10 experiment.

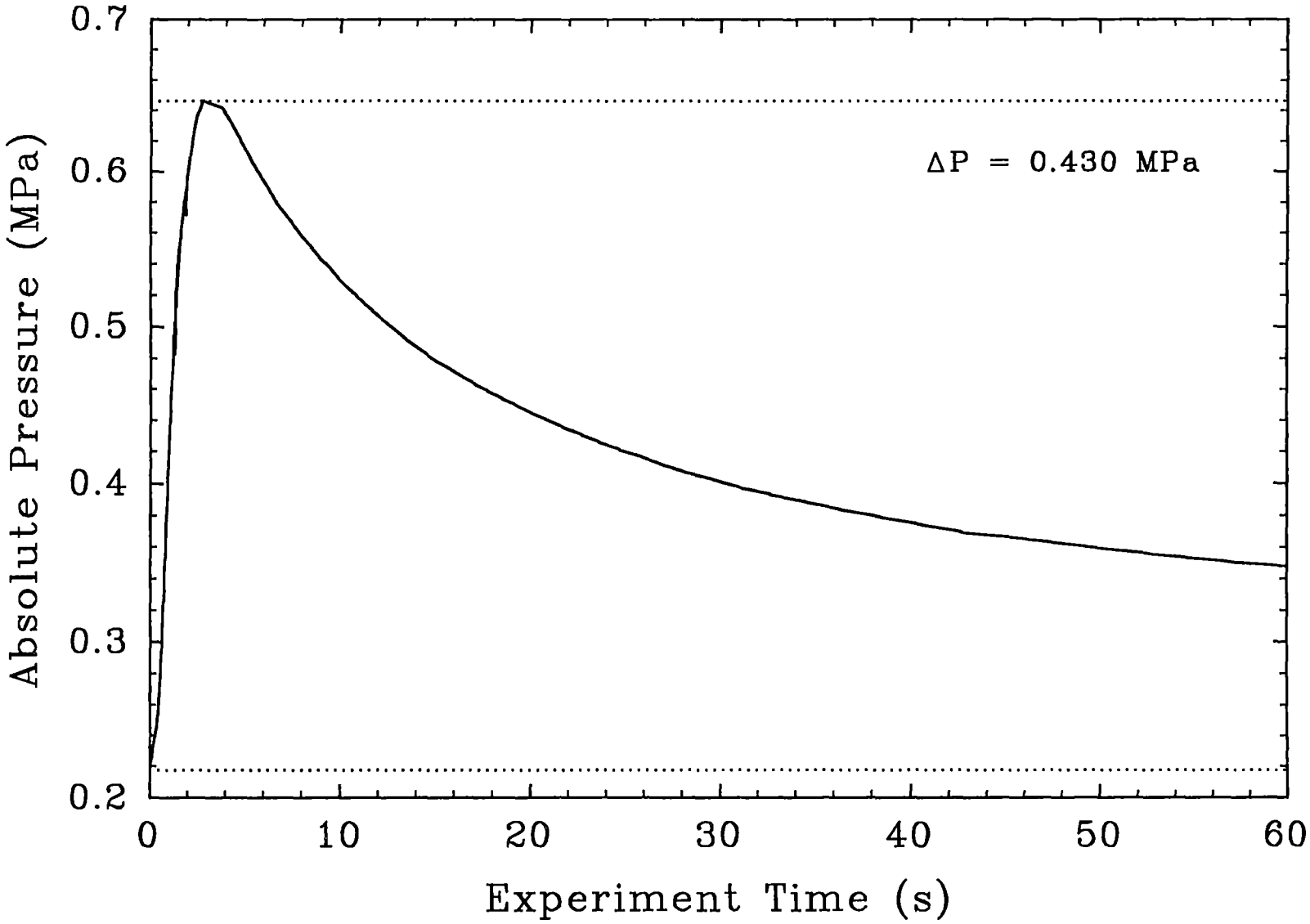

Figure 4.10 CTTF vessel pressure versus time in the IET−11 experiment.

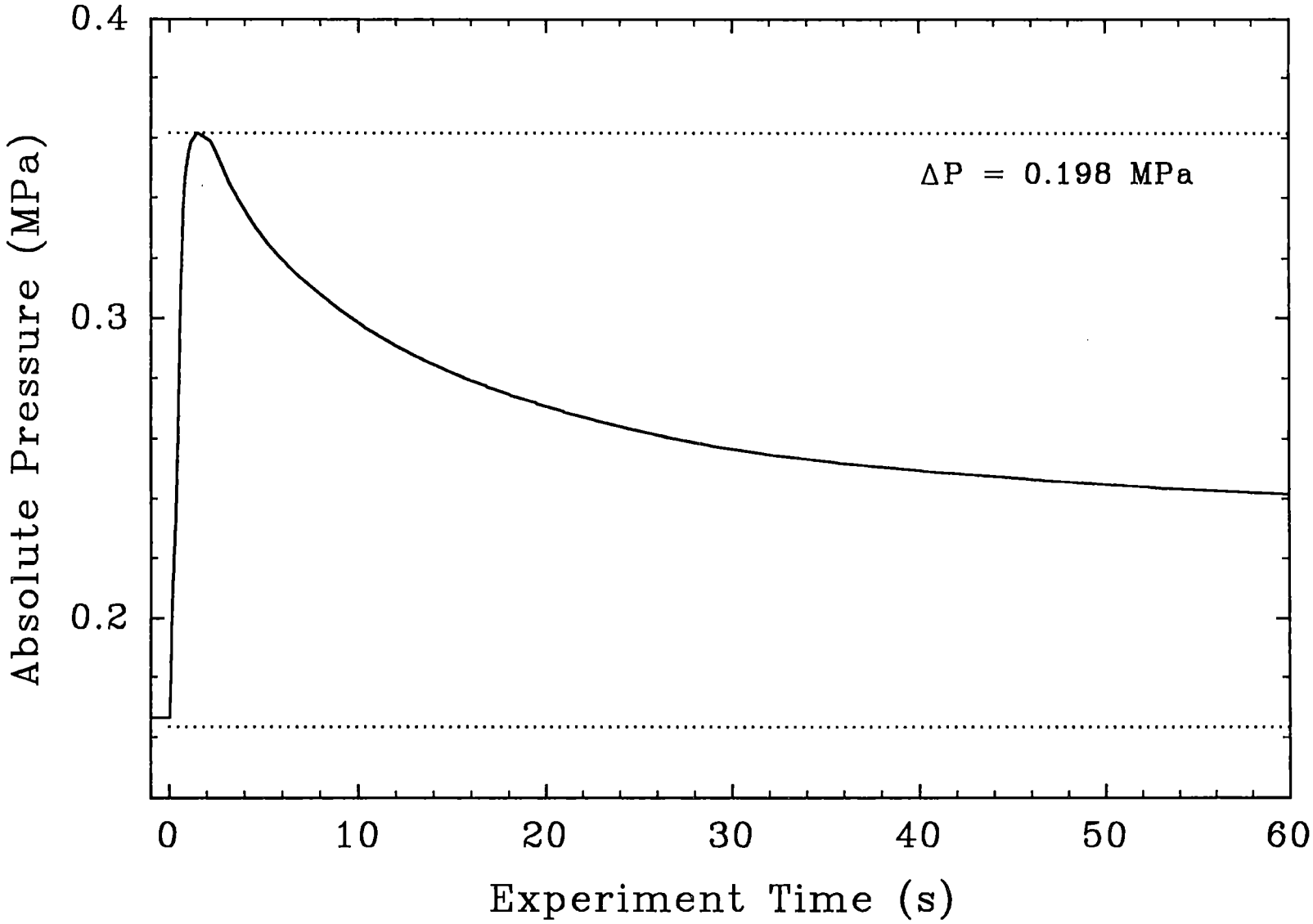

Figure 4.11 Surtsey vessel pressure versus time in the IET−12 experiment.

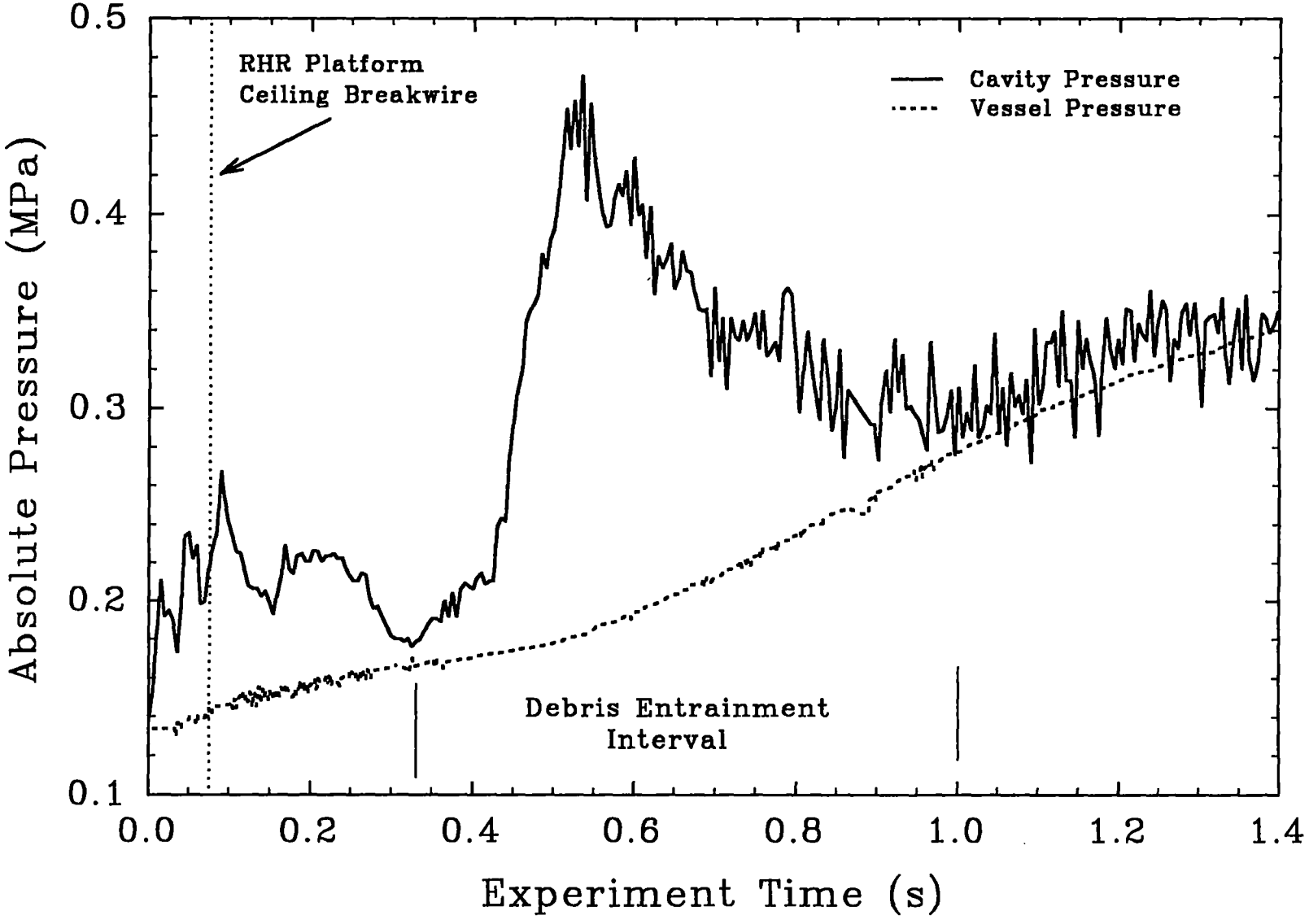

Figure 4.12 Cavity pressure and CTTF vessel pressure versus time in the IET−9 experiment.

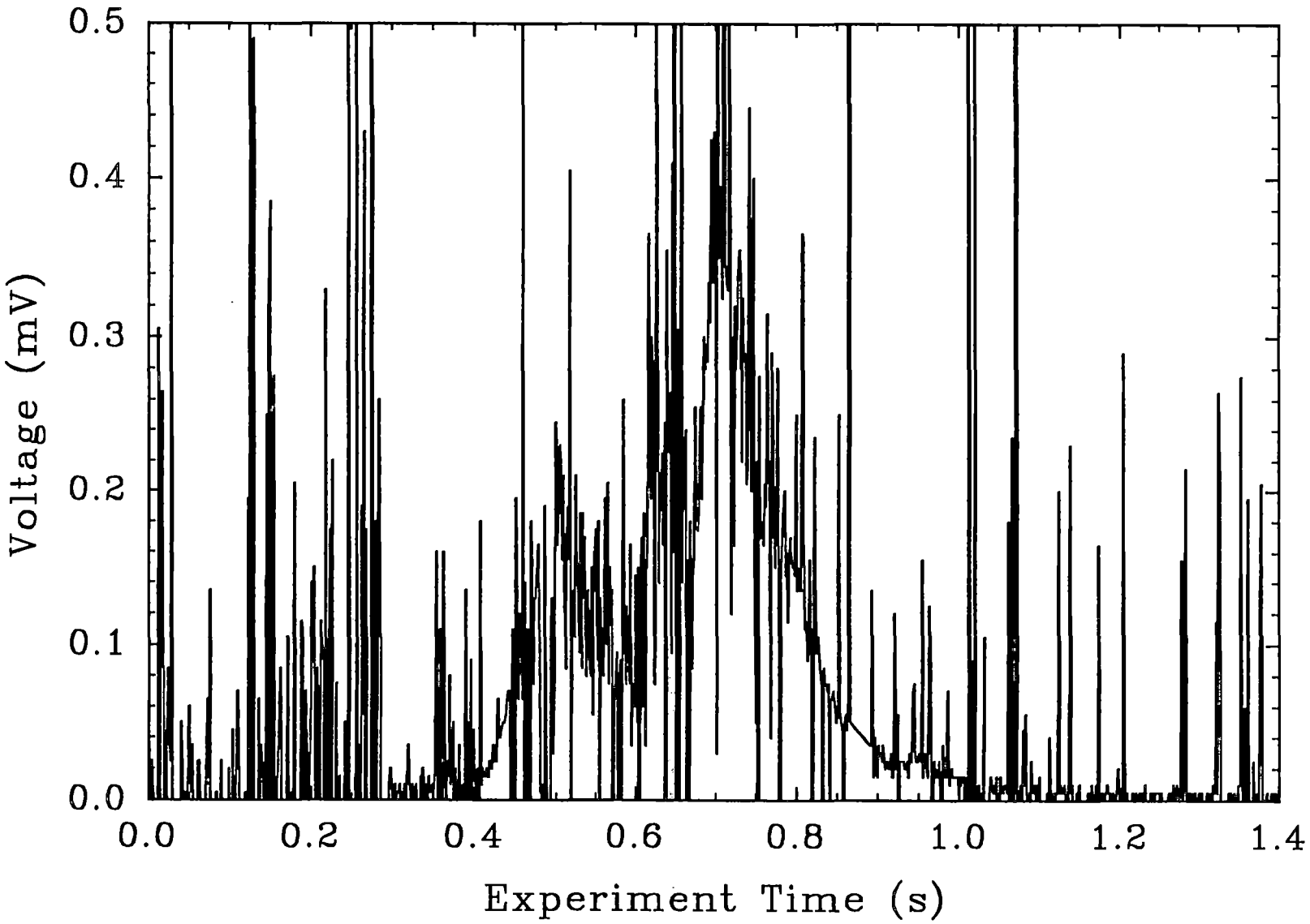

Figure 4.13 Cavity debris ejection verified by the pyrometer signal in the IET−9 experiment.

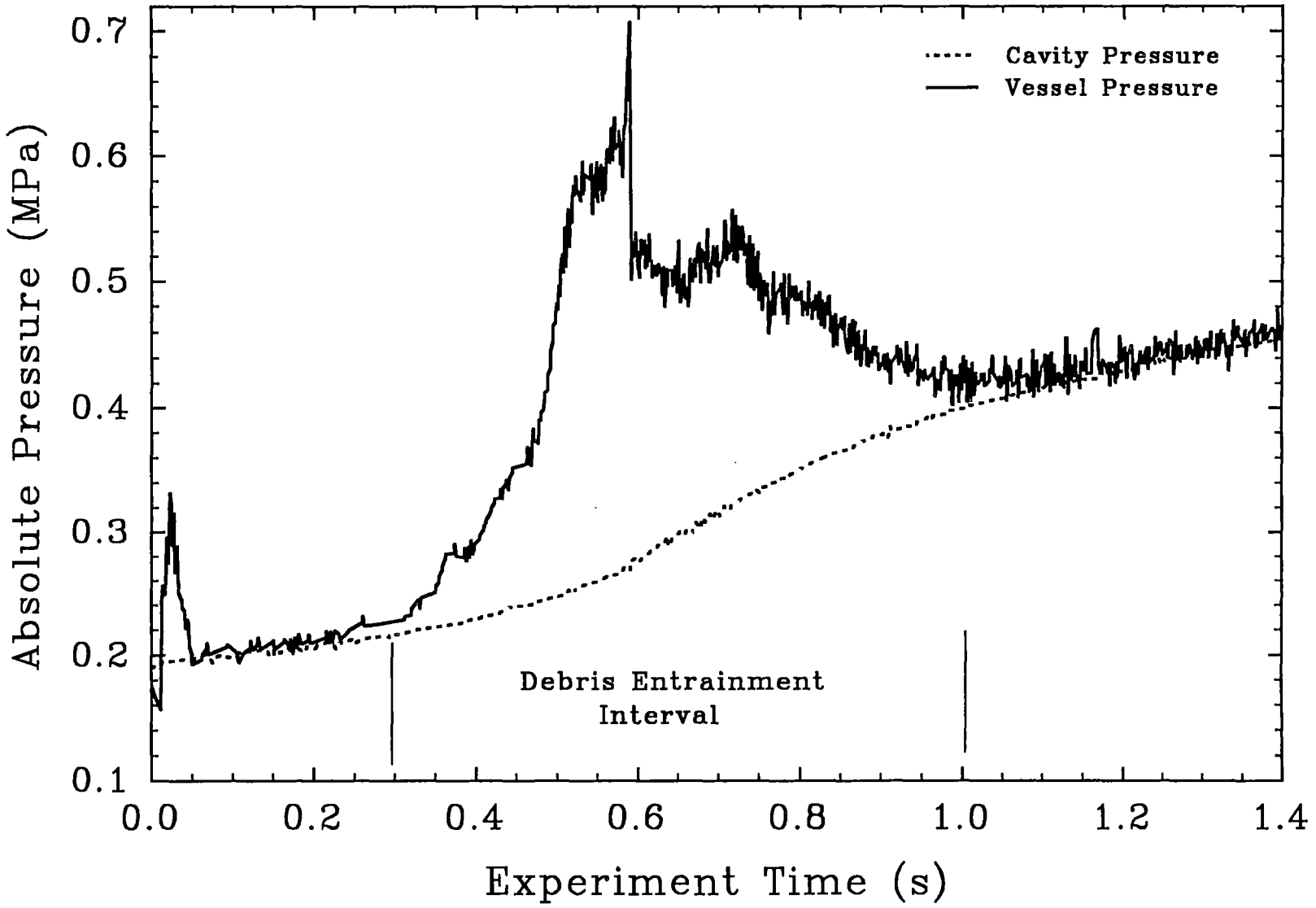

Figure 4.14 Cavity pressure and CTTF vessel pressure versus time in the IET−10 experiment.

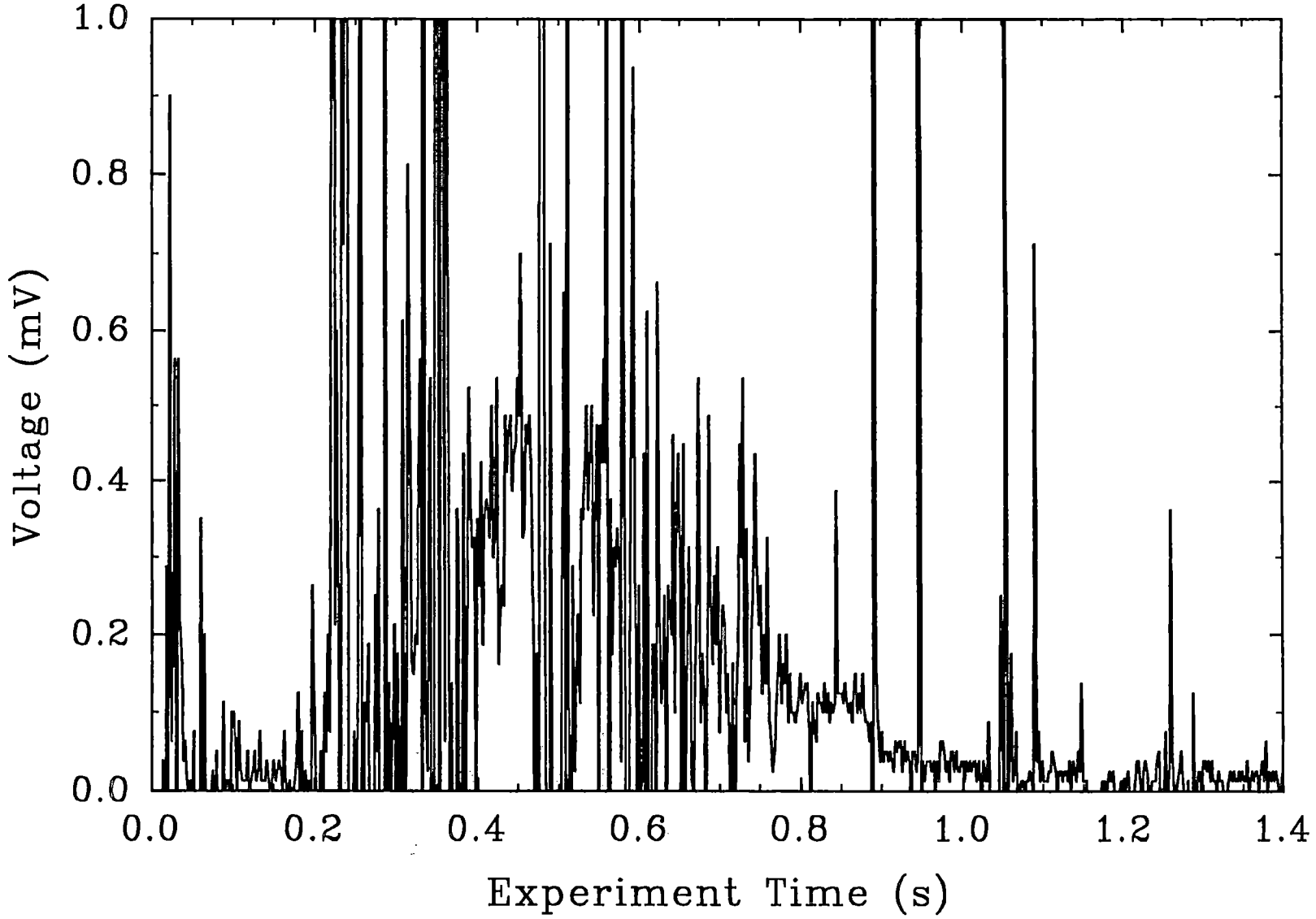

Figure 4.15 Cavity debris ejection verified by the pyrometer signal in the IET−10 experiment.

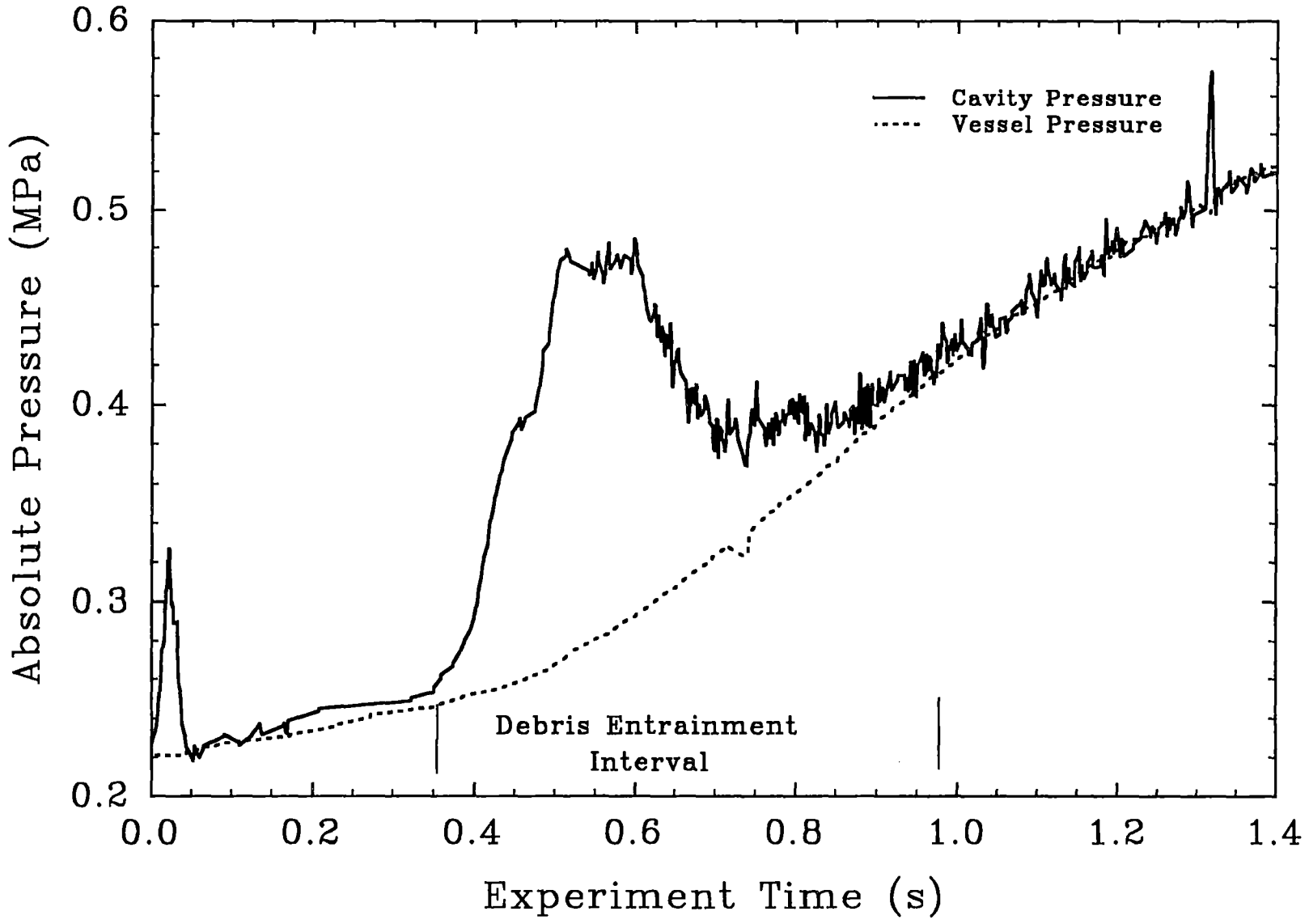

Figure 4.16 Cavity pressure and CTTF vessel pressure versus time in the IET−11 experiment.

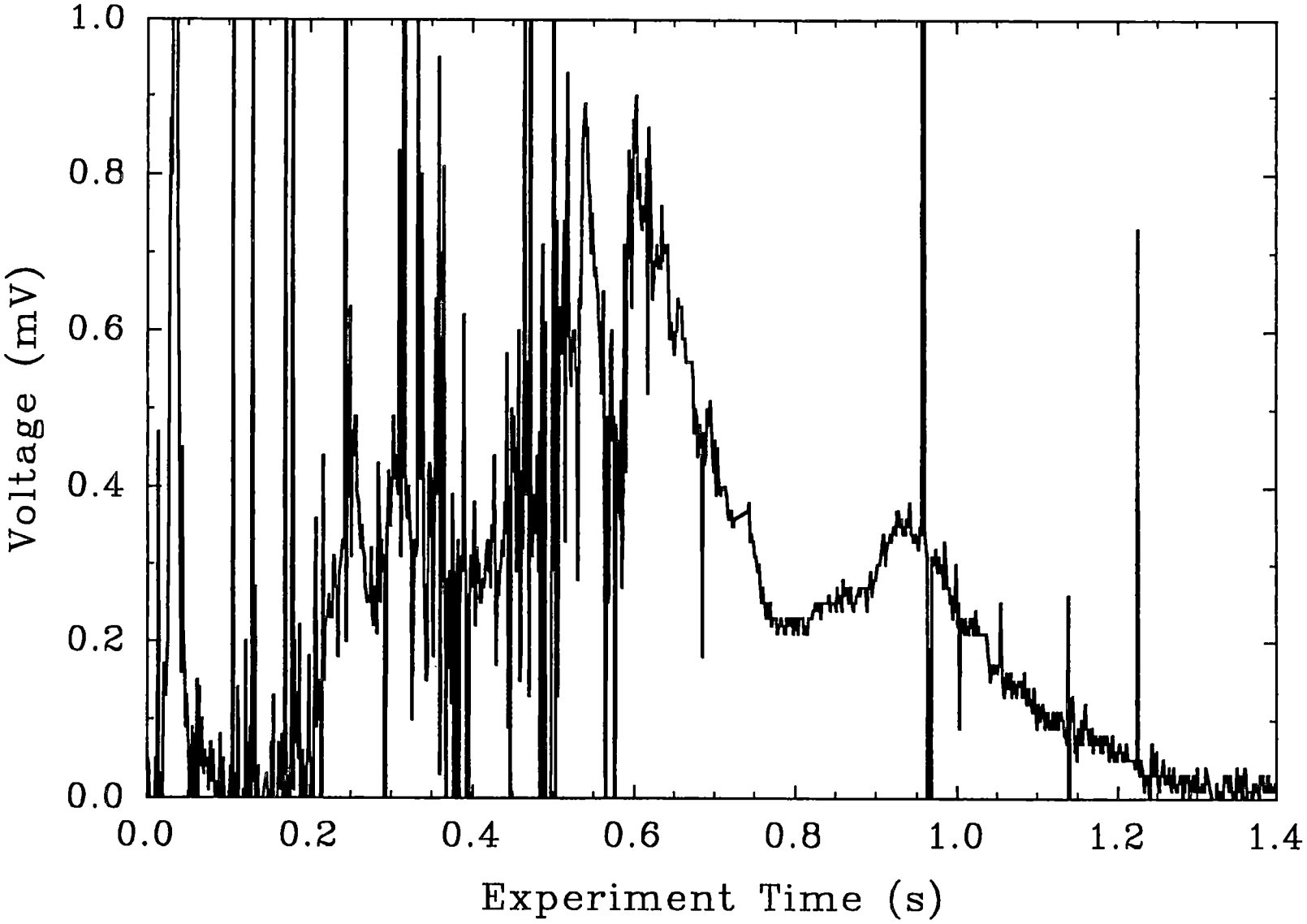

Figure 4.17 Cavity debris ejection verified by the pyrometer signal in the IET−11 experiment.

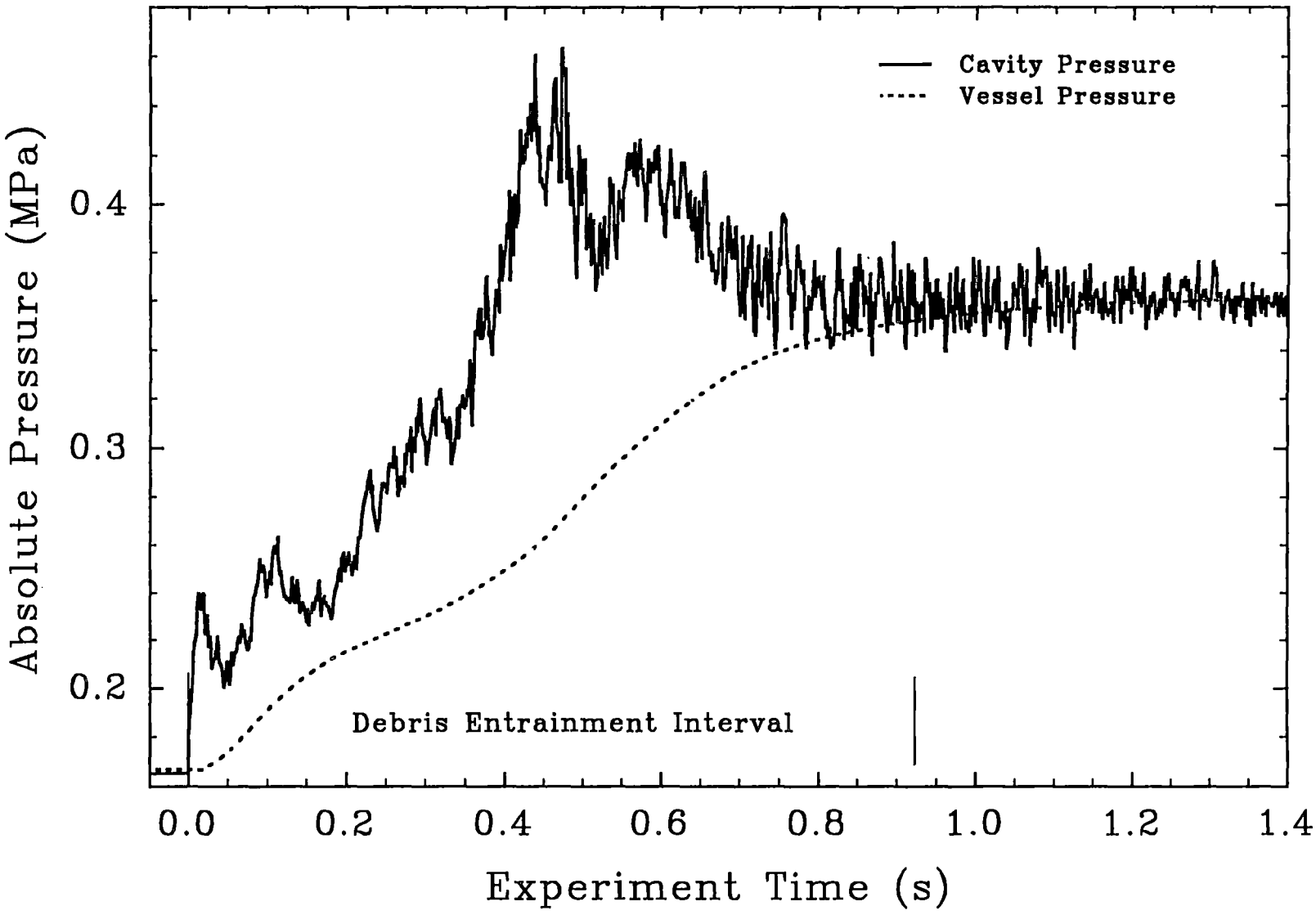

Figure 4.18 Cavity pressure and Surtsey vessel pressure versus time in the IET−12 experiment.

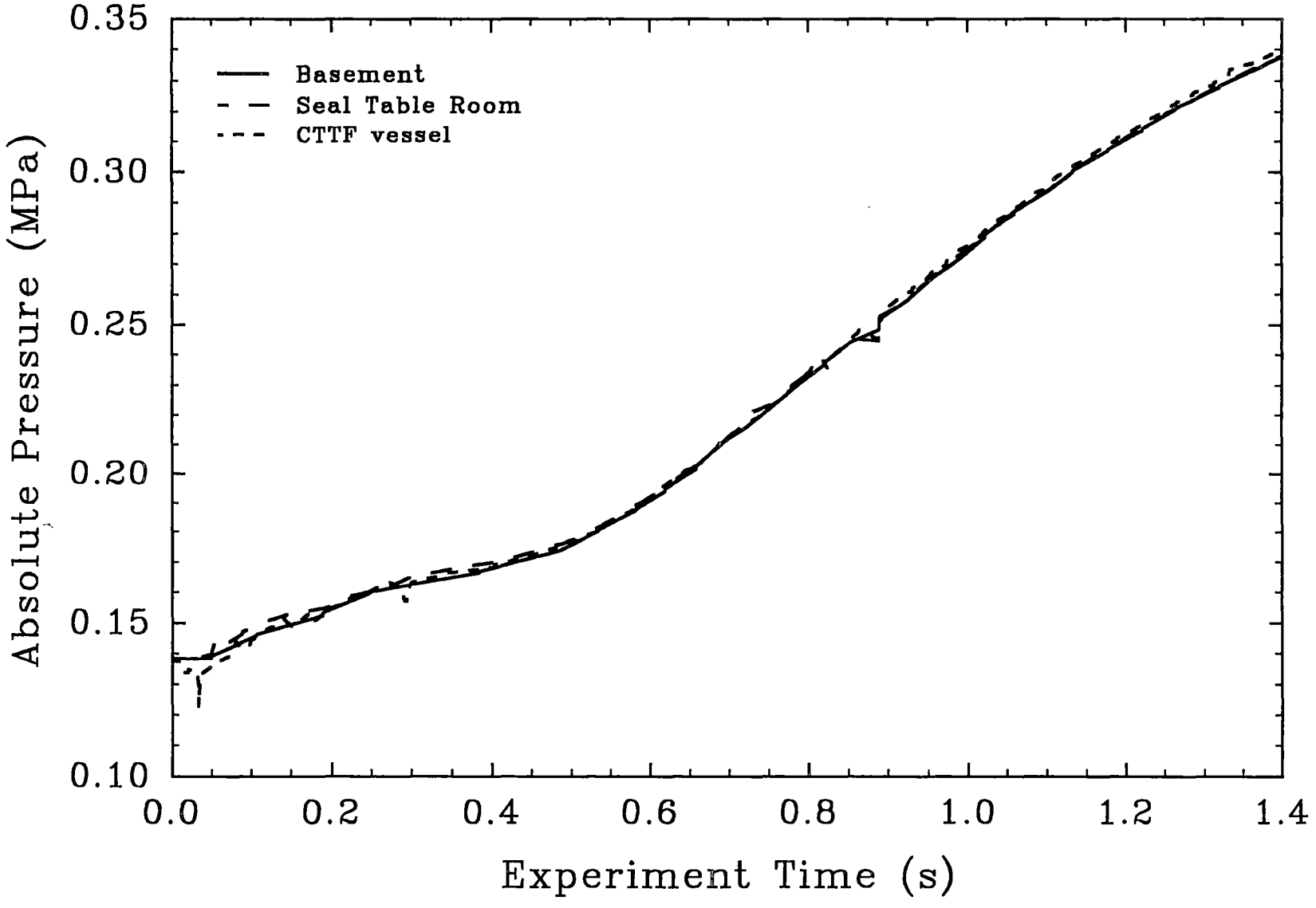

Figure 4.19 CTTF vessel, basement, and seal table room pressure comparisons in the the IET−9 experiment.

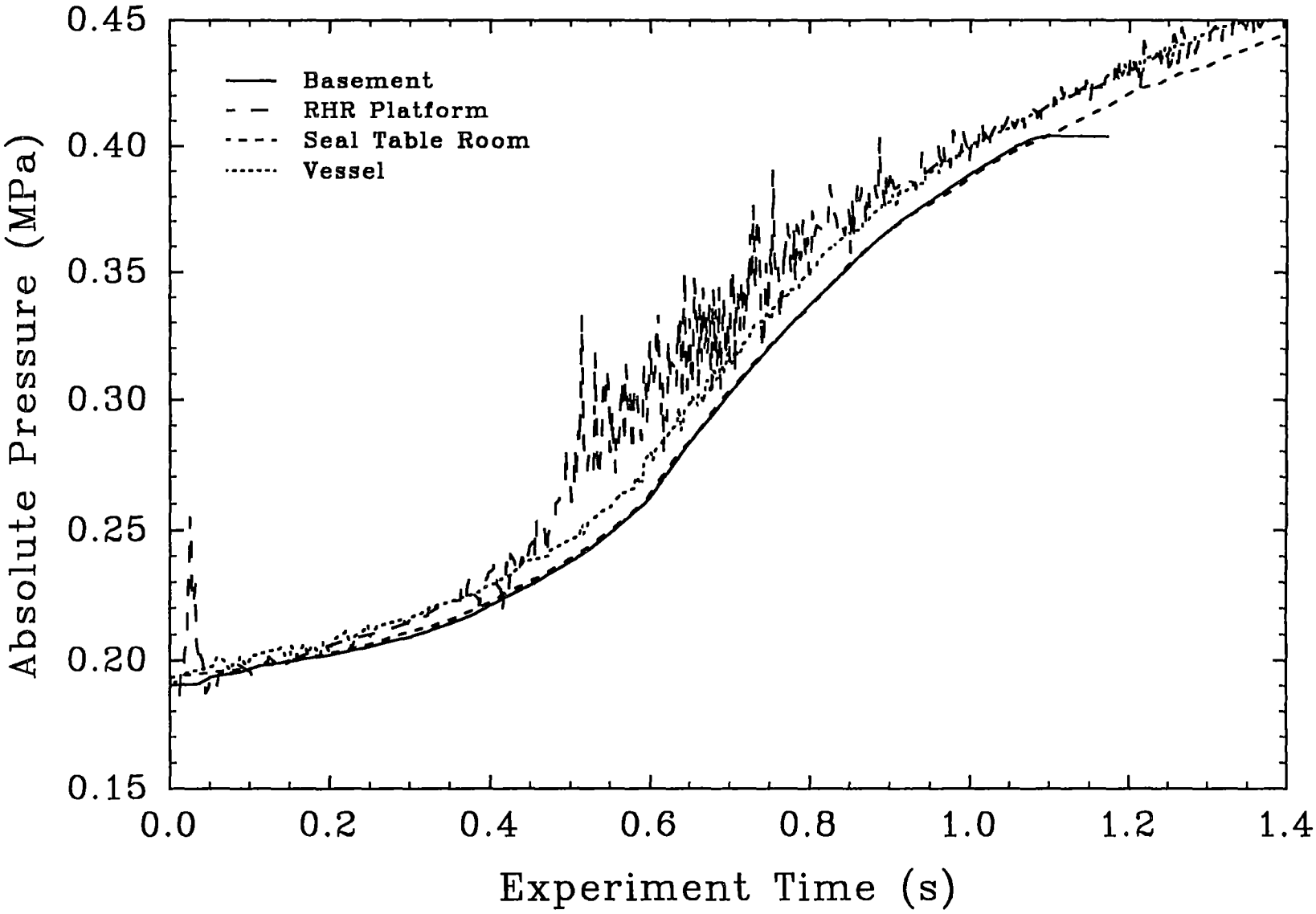

Figure 4.20 CTTF vessel, basement, RHR platform, and seal table room pressure comparisons in the IET−10 experiment.

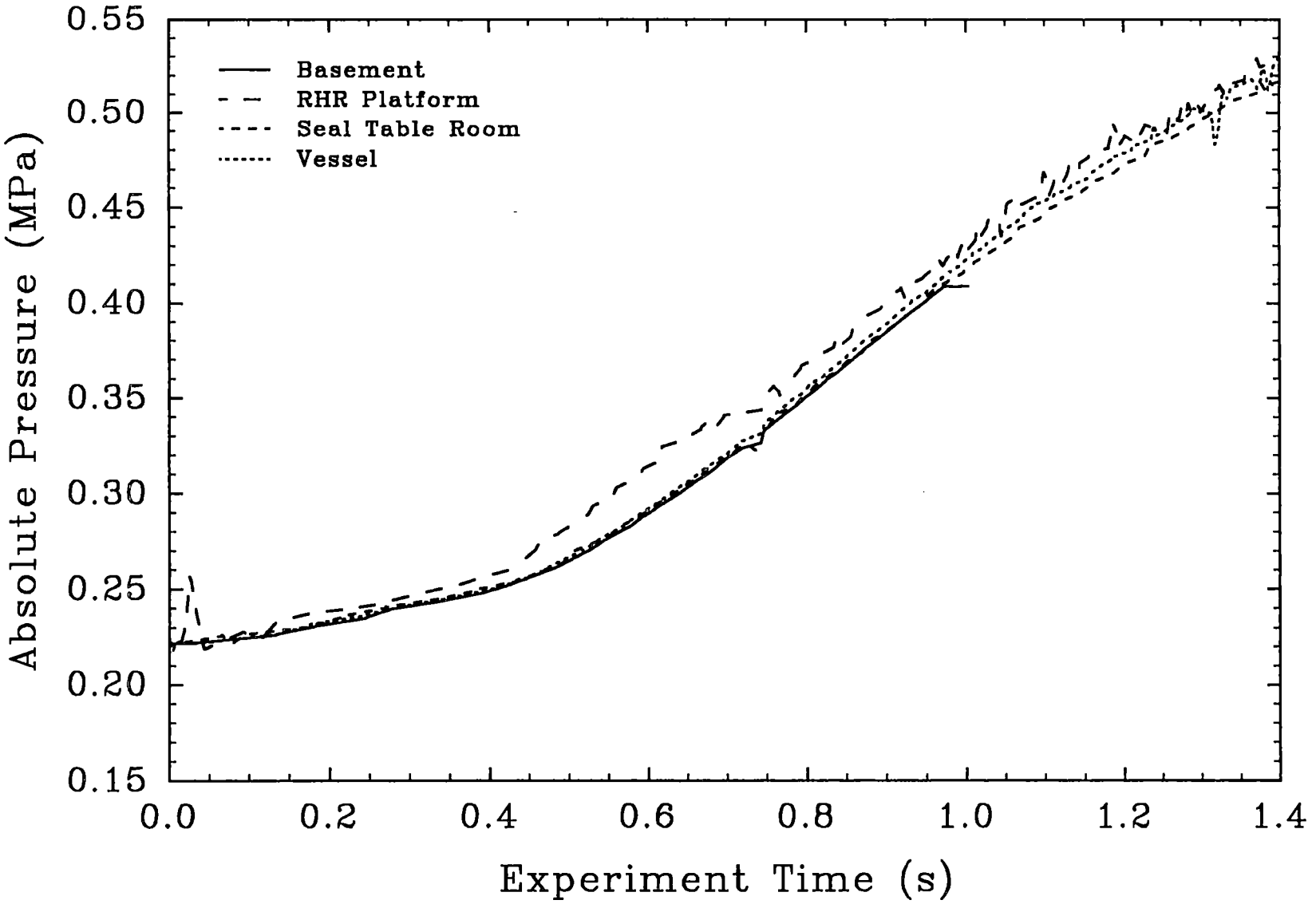

Figure 4.21 CTTF vessel, basement, RHR platform, and seal table room pressure comparisons in the IET−11 experiment.

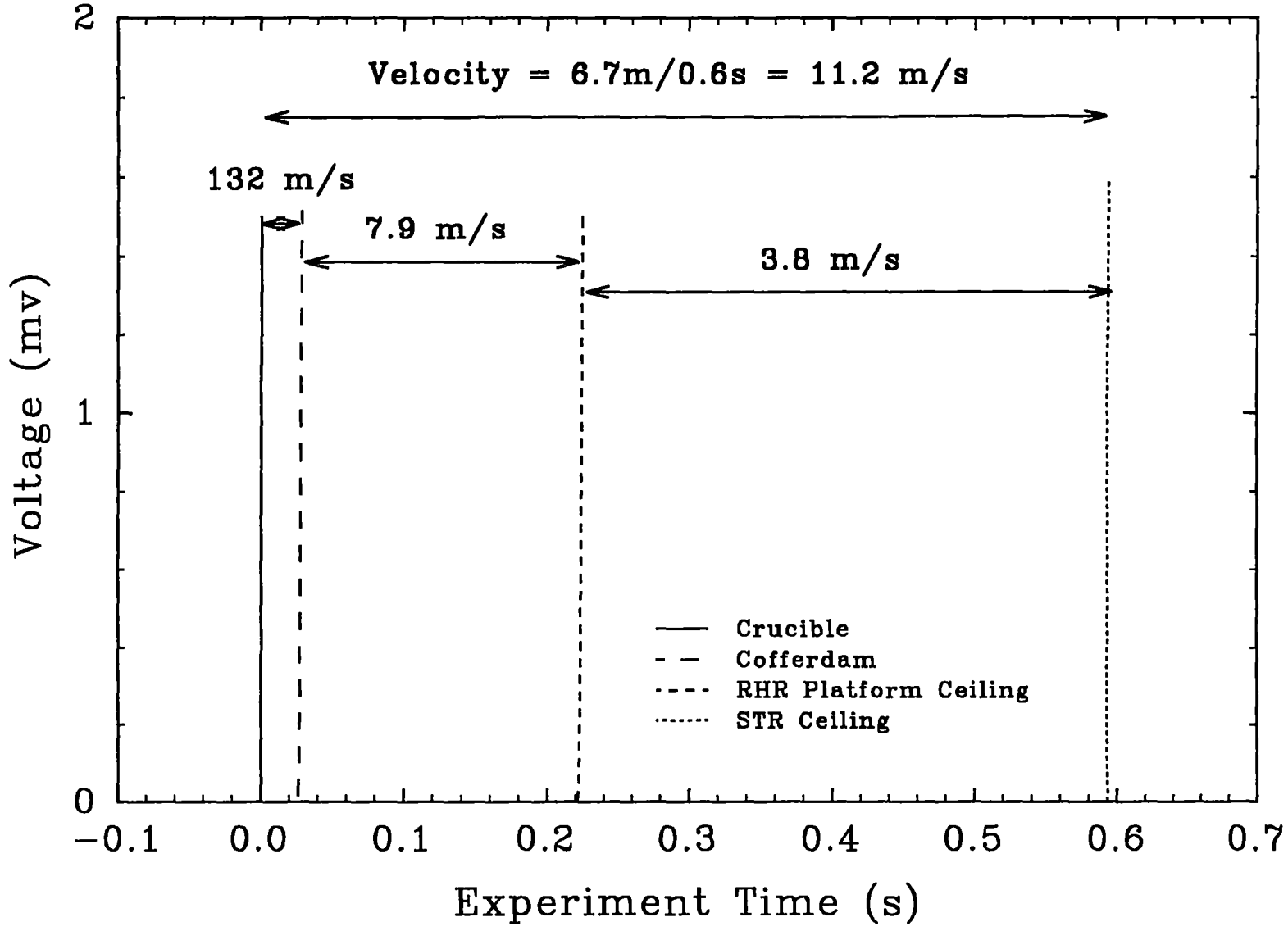

Figure 4.22 Breakwire signals versus time in the IET−10 experiment.

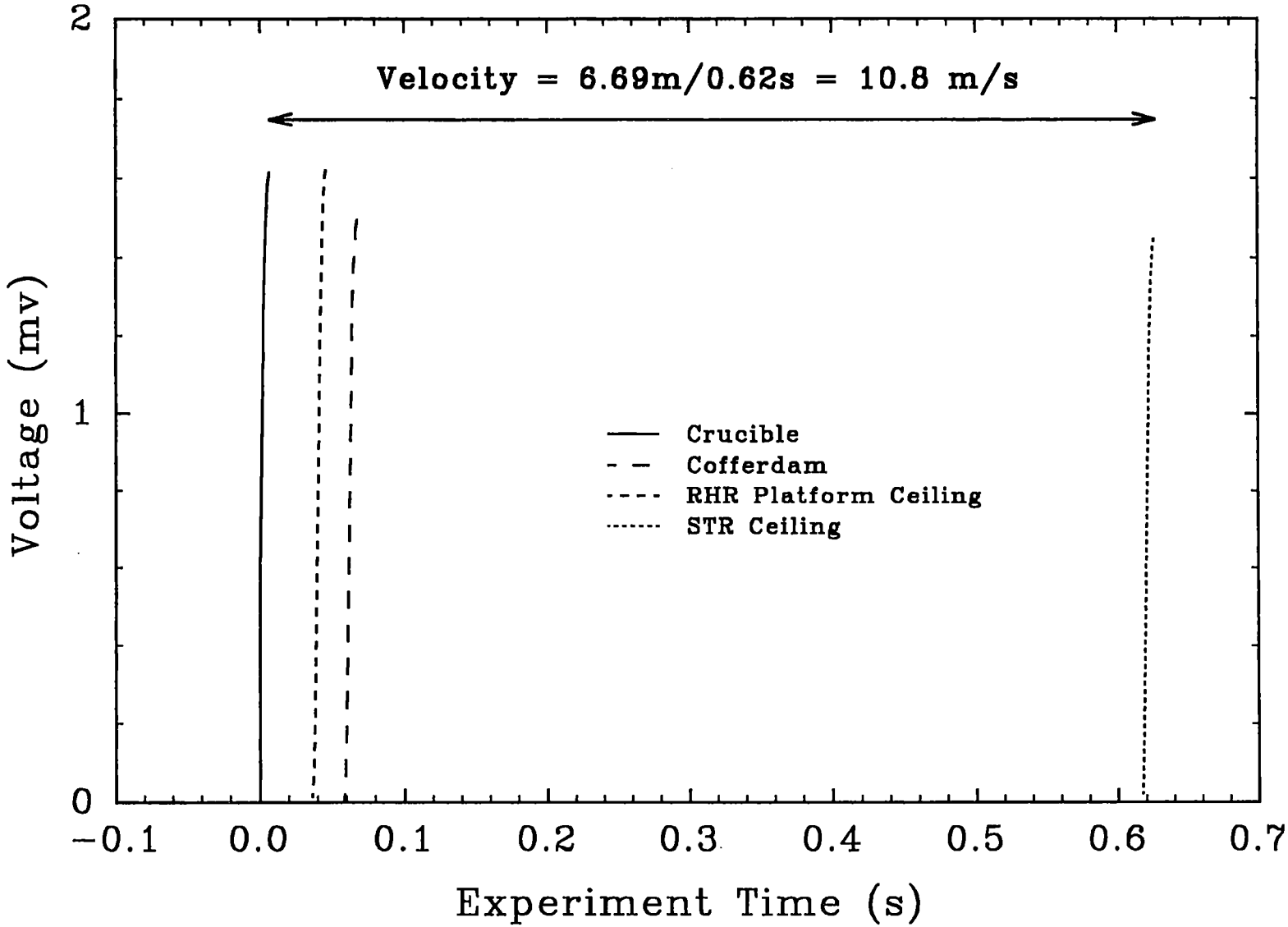

Figure 4.23 Breakwire signals versus time in the IET−11 experiment.

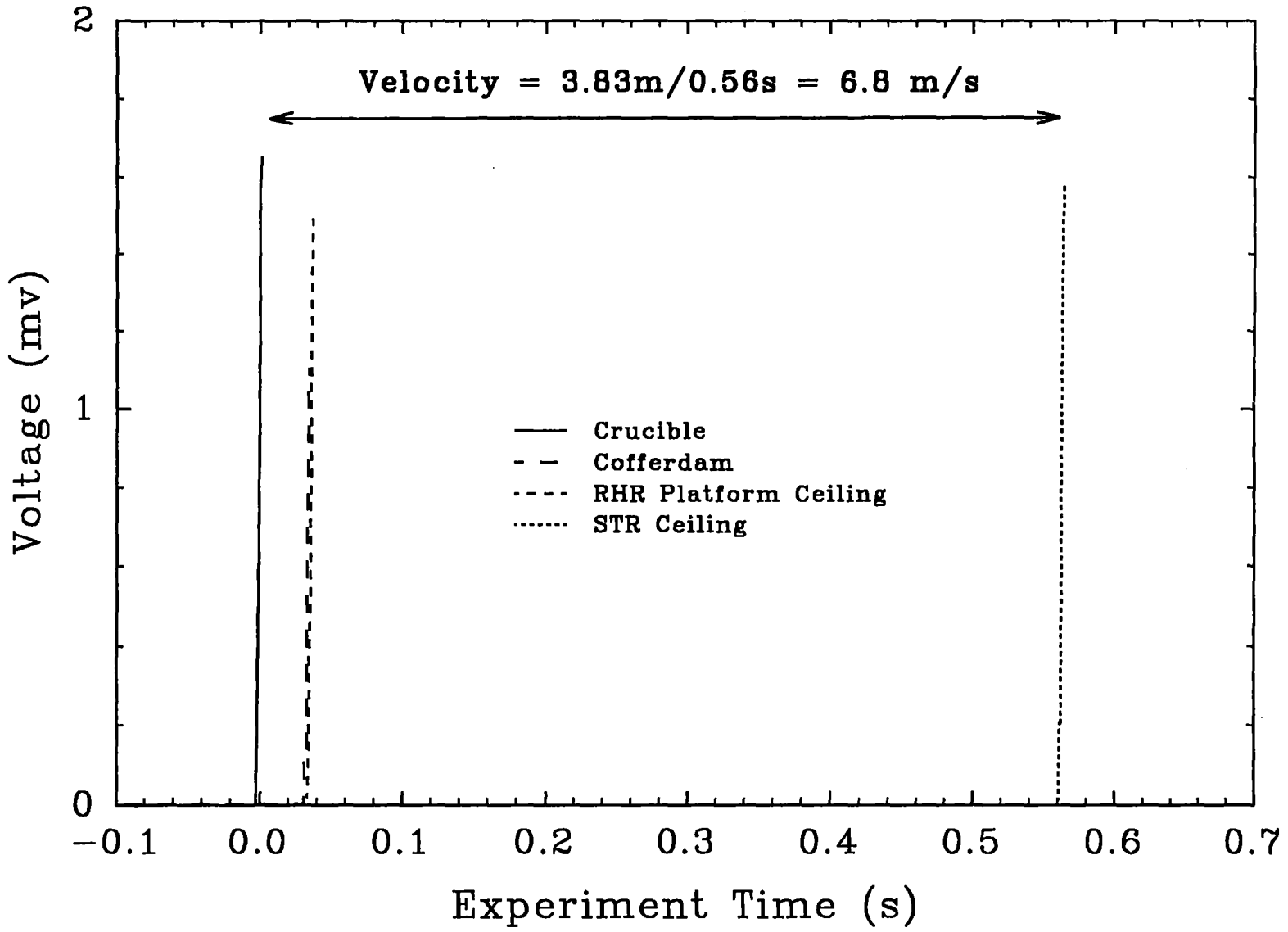

Figure 4.24 Breakwire signals versus time in the IET−12 experiment.

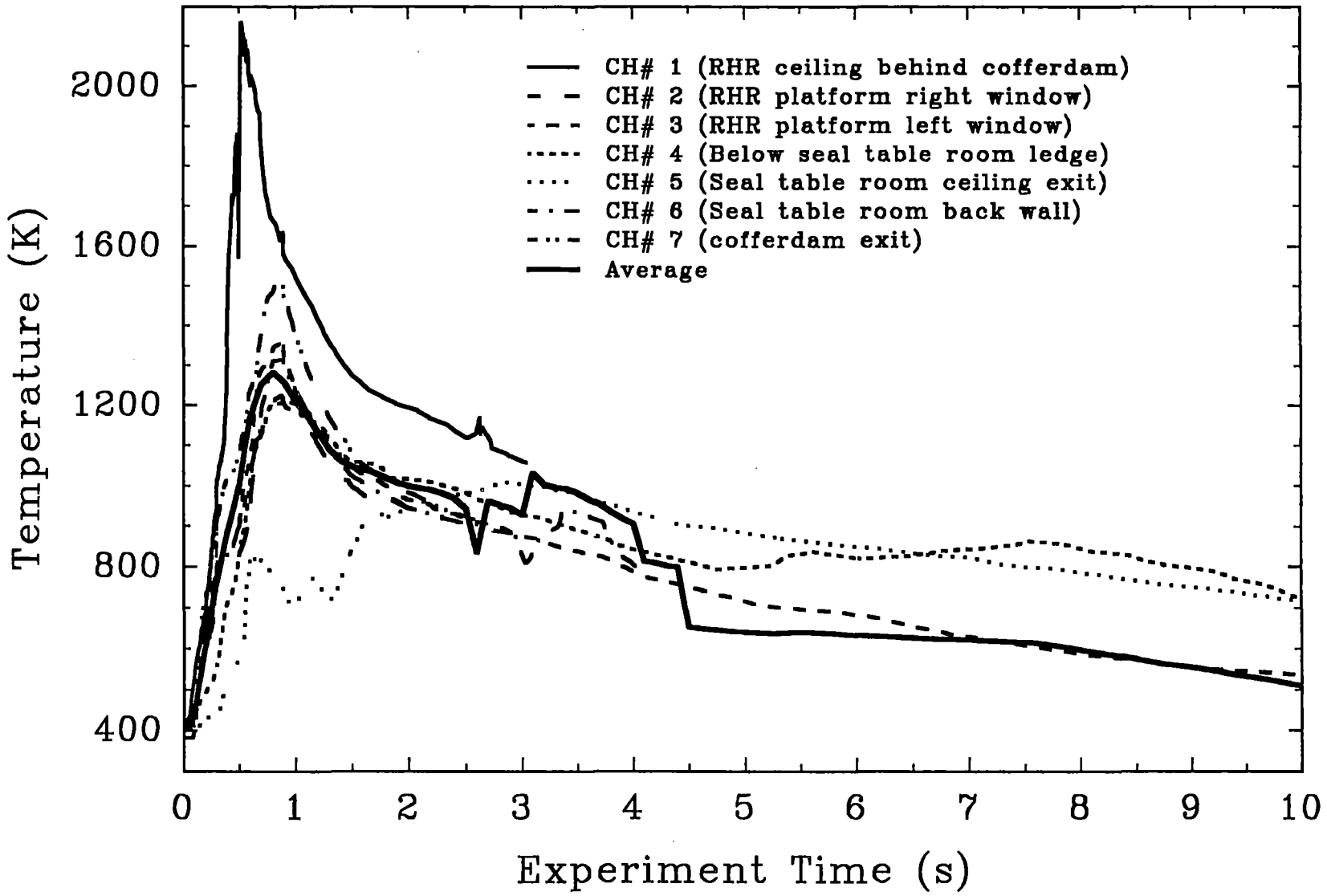

Figure 4.25 Debris/gas temperatures at the RHR platform and in the seal table room measured with type-C thermocouples in the IET-9 experiment.

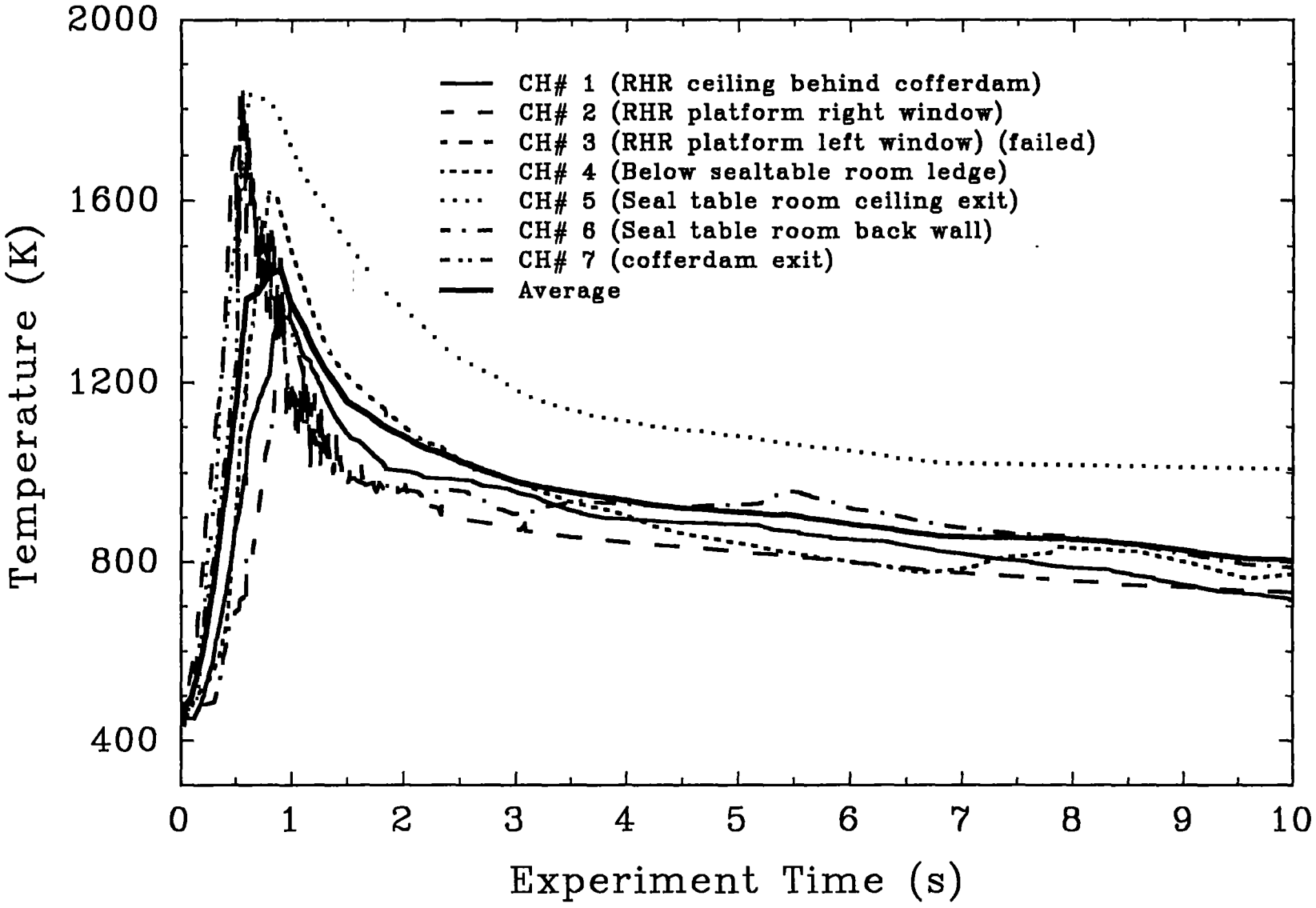

Figure 4.26 Debris/gas temperatures at the RHR platform and in the seal table room measured with type-C thermocouples in the IET-10 experiment.

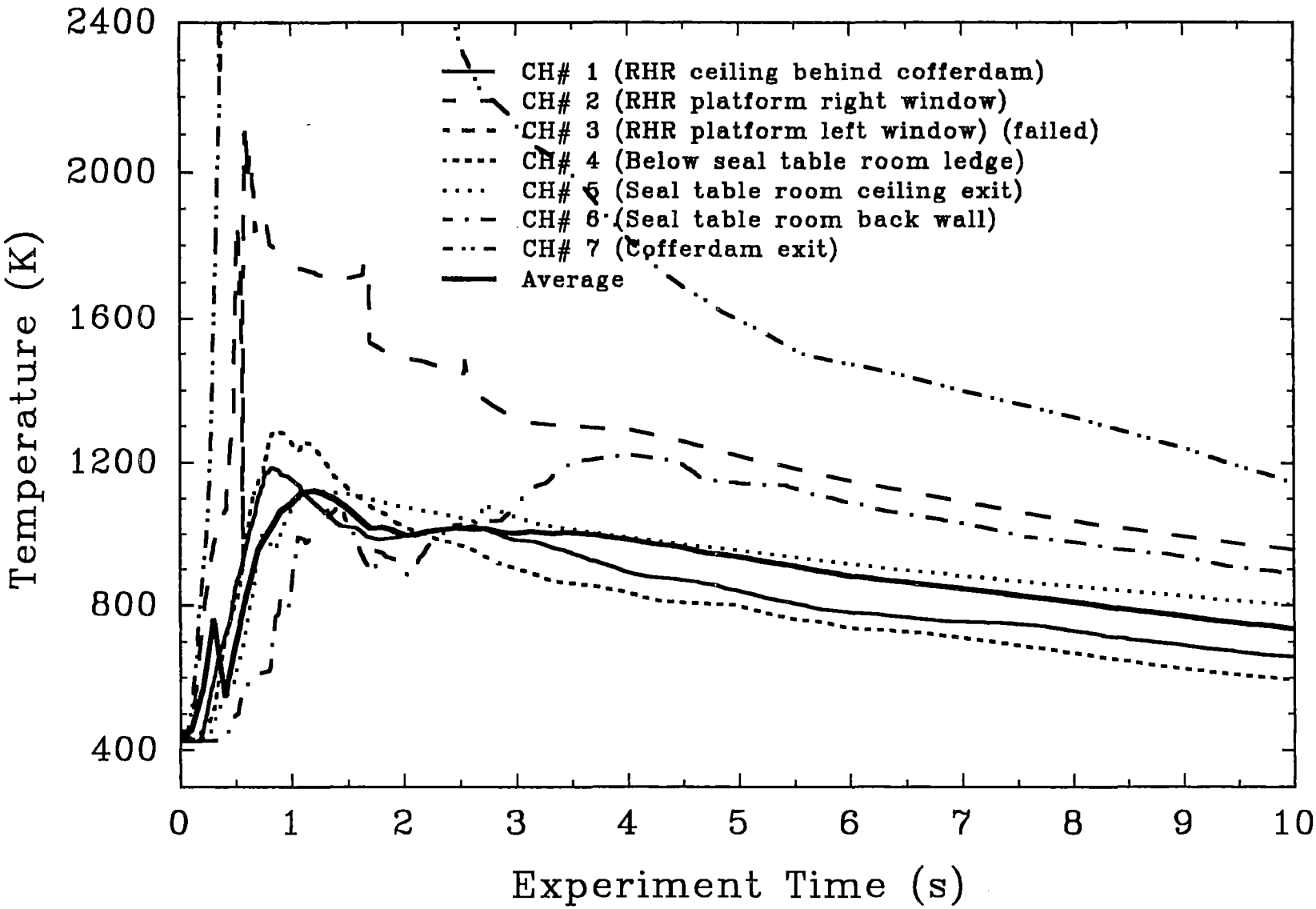

Figure 4.27 Debris/gas temperatures at the RHR platform and in the seal table room measured with type–C thermocouples in the IET–11 experiment.

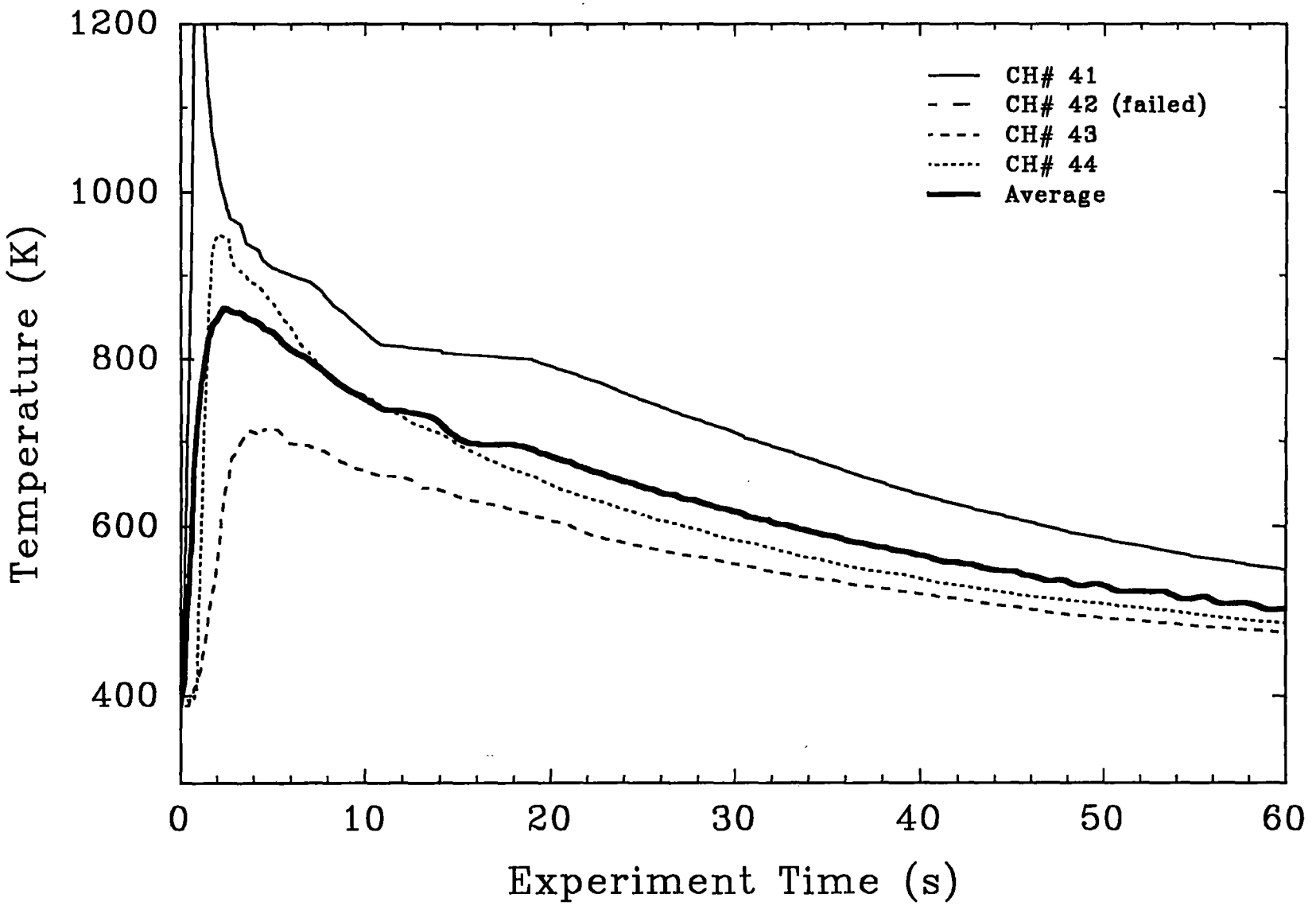

Figure 4.28 Temperature history of the basement thermocouples in the IET-9 experiment.

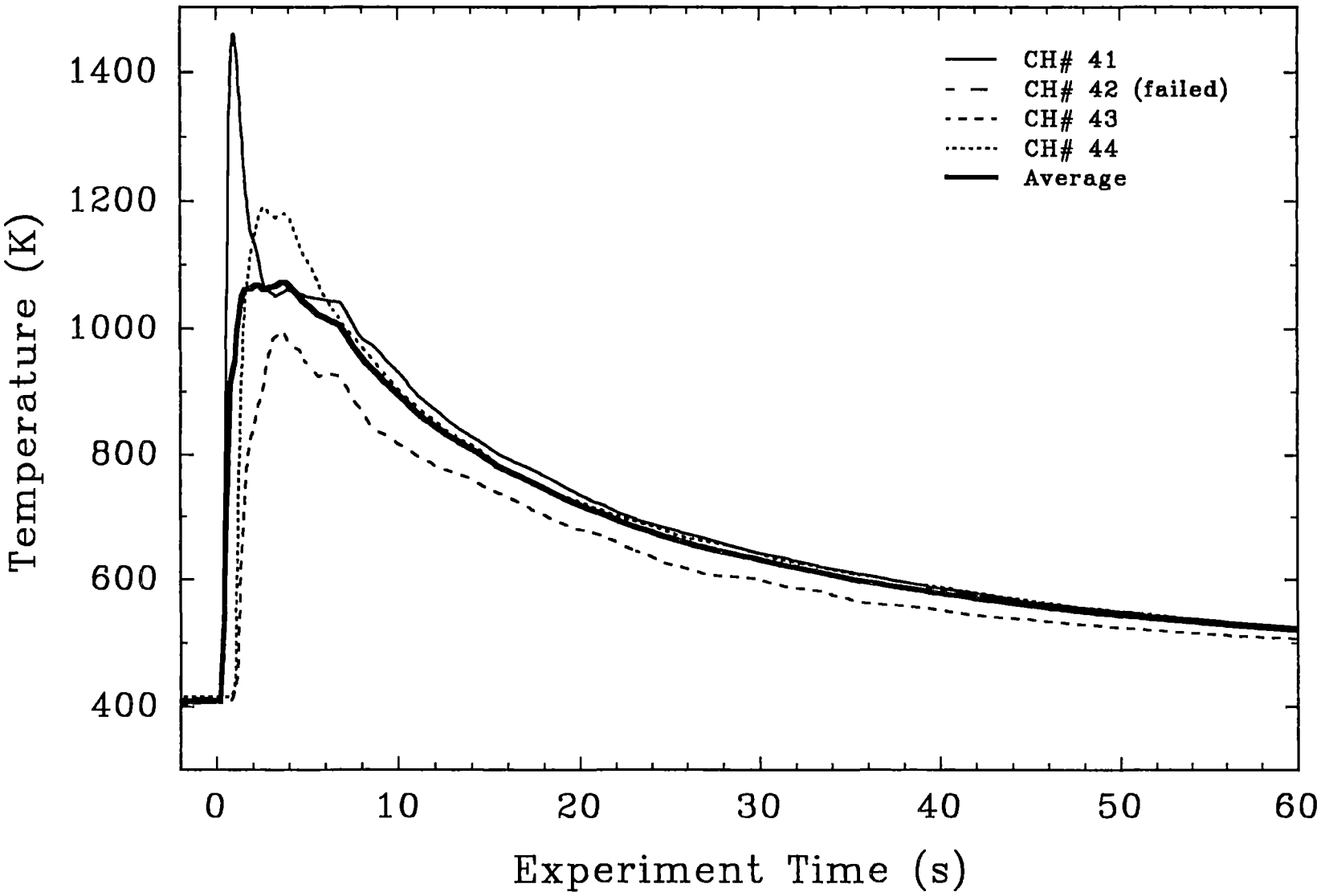

Figure 4.29 Temperature history of the basement thermocouples in the IET−10 experiment.

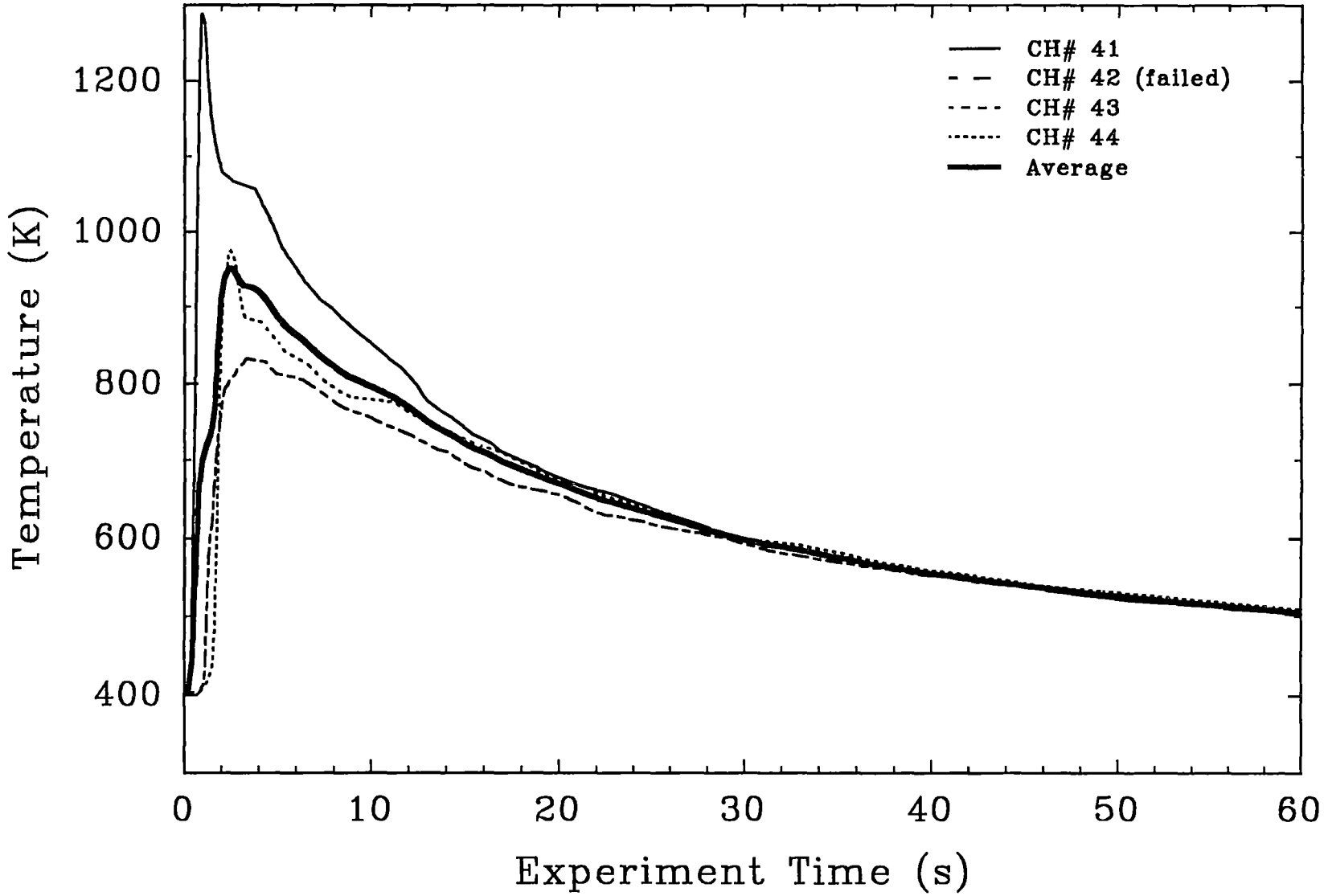

Figure 4.30 Temperature history of the basement thermocouples in the IET−11 experiment.

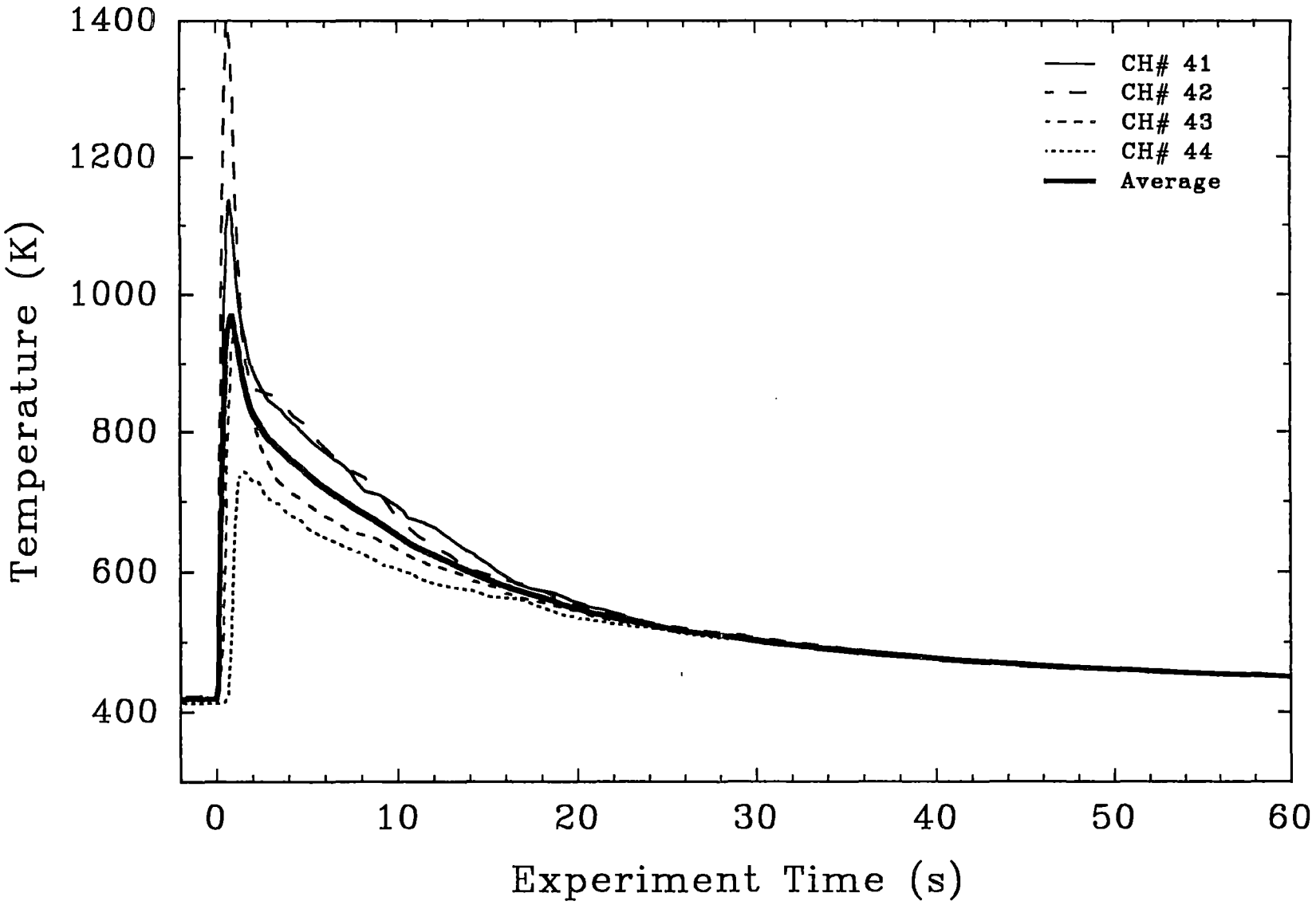

Figure 4.31 Temperature history of the basement thermocouples in the IET−12 experiment.

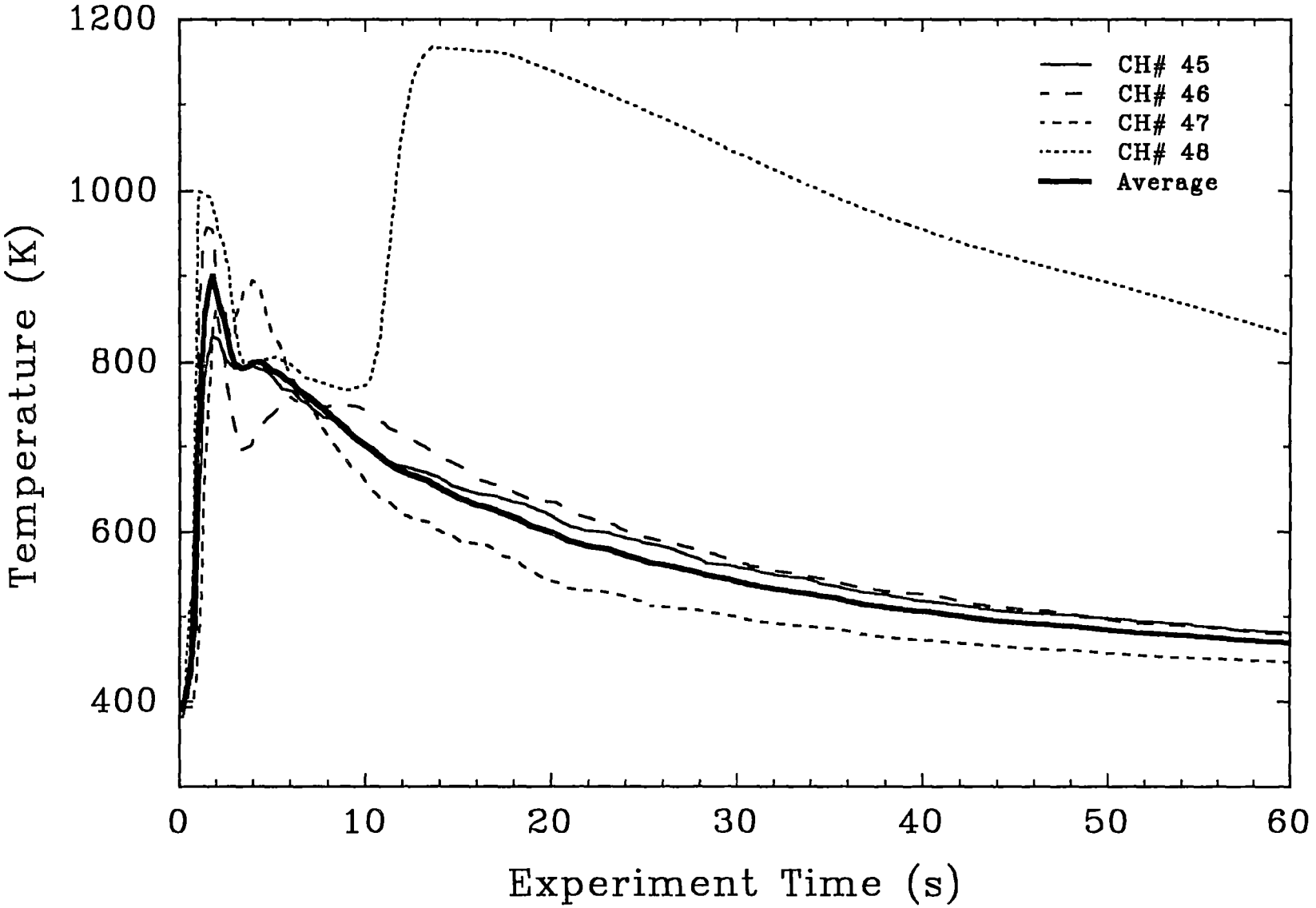

Figure 4.32 Temperature history of the thermocouples between the cranewall and the CTTF vessel in the IET−9 experiment.

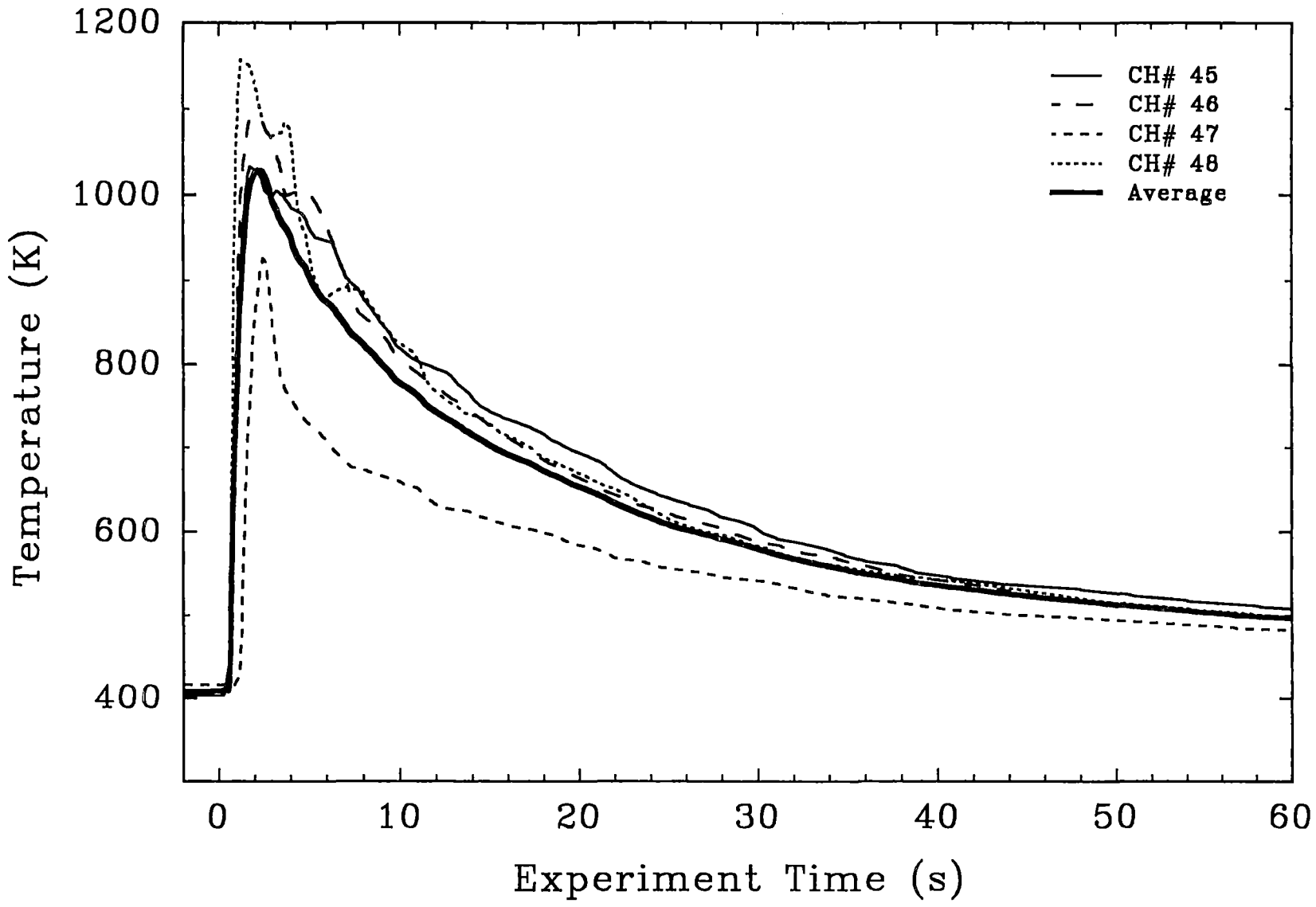

Figure 4.33 Temperature history of the thermocouples between the cranewall and the CTTF vessel in the IET−10 experiment.

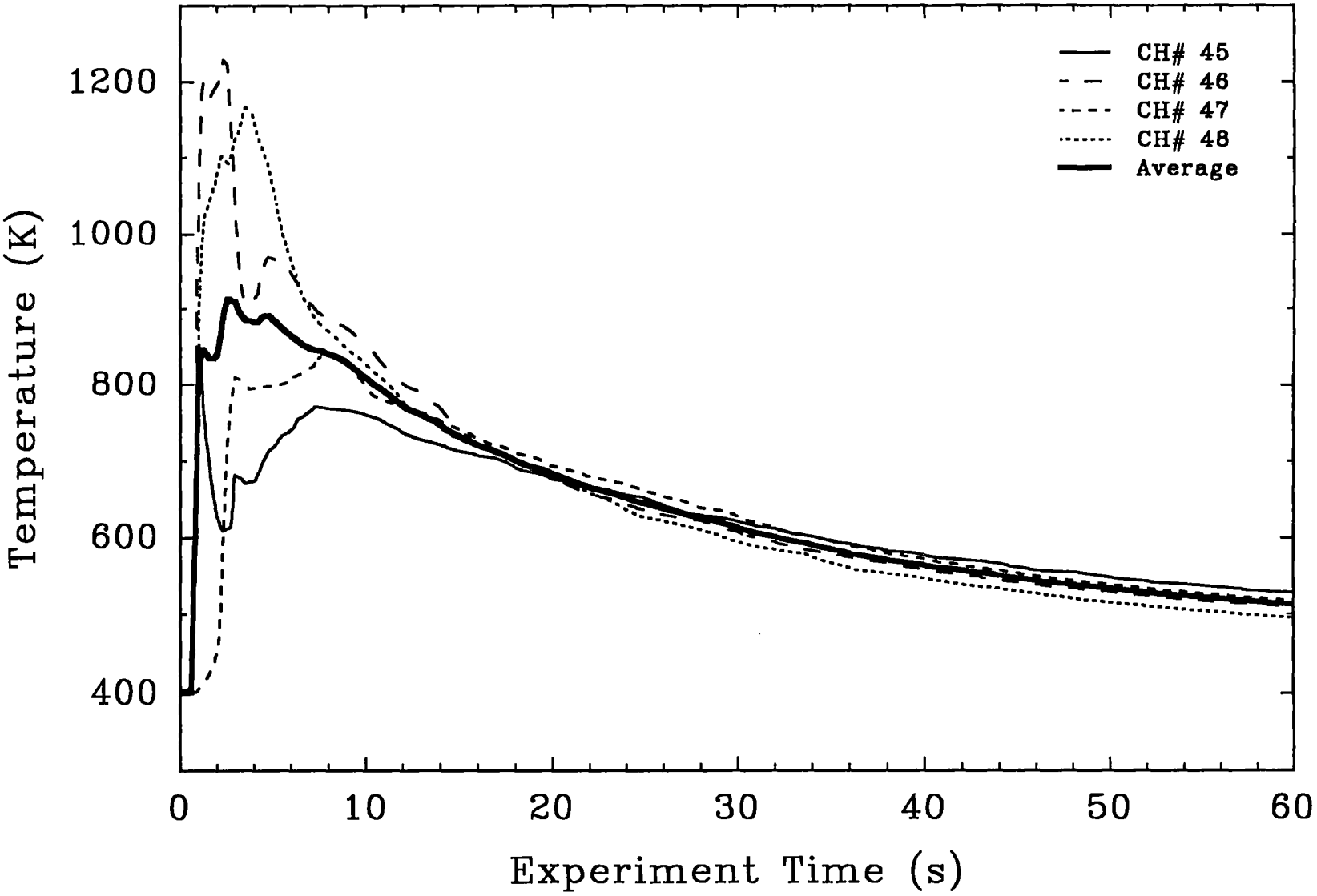

Figure 4.34 Temperature history of the thermocouples between the cranewall and the CTTF vessel in the IET−11 experiment.

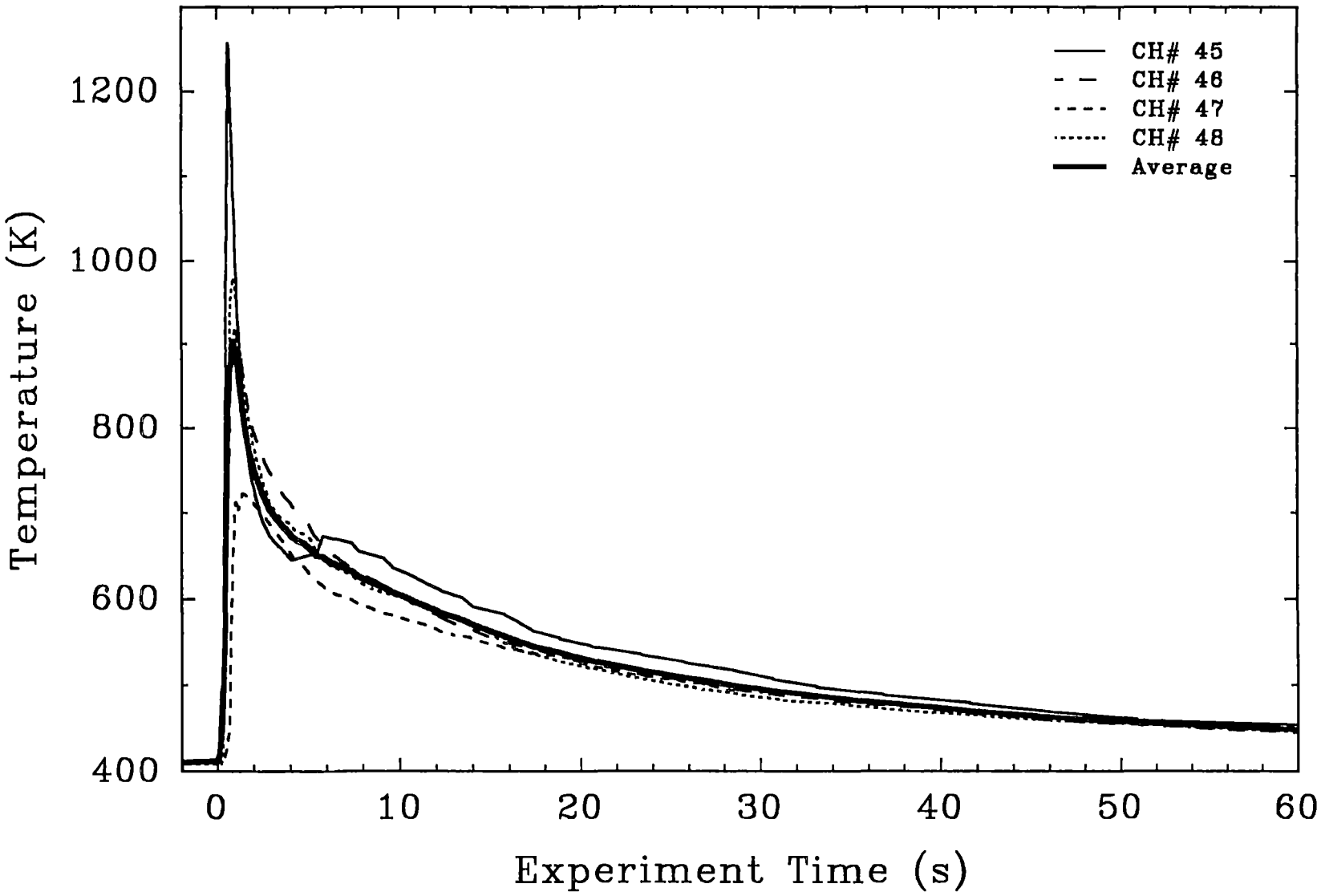

Figure 4.35 Temperature history of the thermocouples between the cranewall and the Surtsey vessel in the IET−12 experiment.

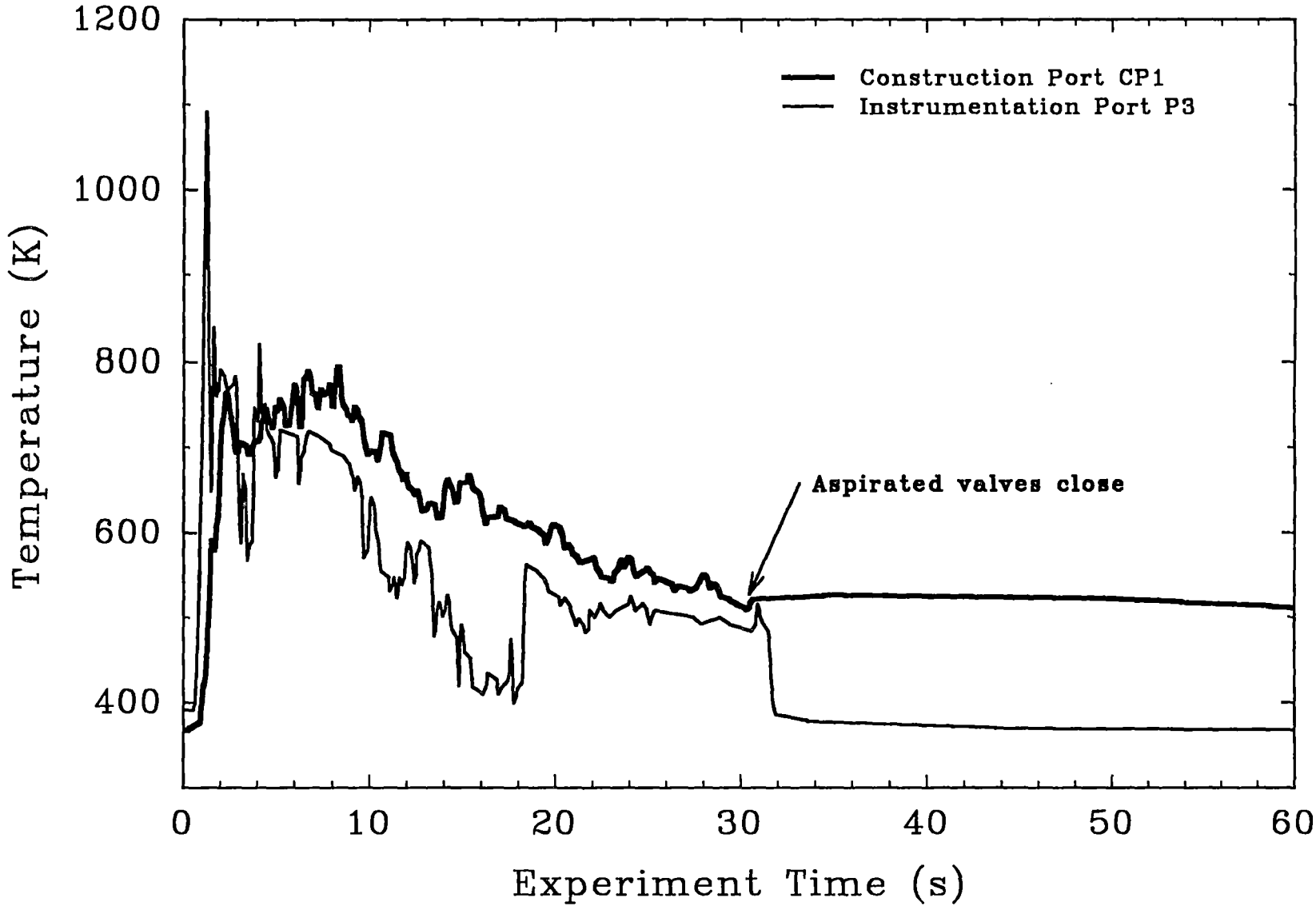

Figure 4.36 Gas temperatures measured at penetrations CP1 and P3 in the CTTF vessel with aspirated thermocouples in the IET−9 experiment.

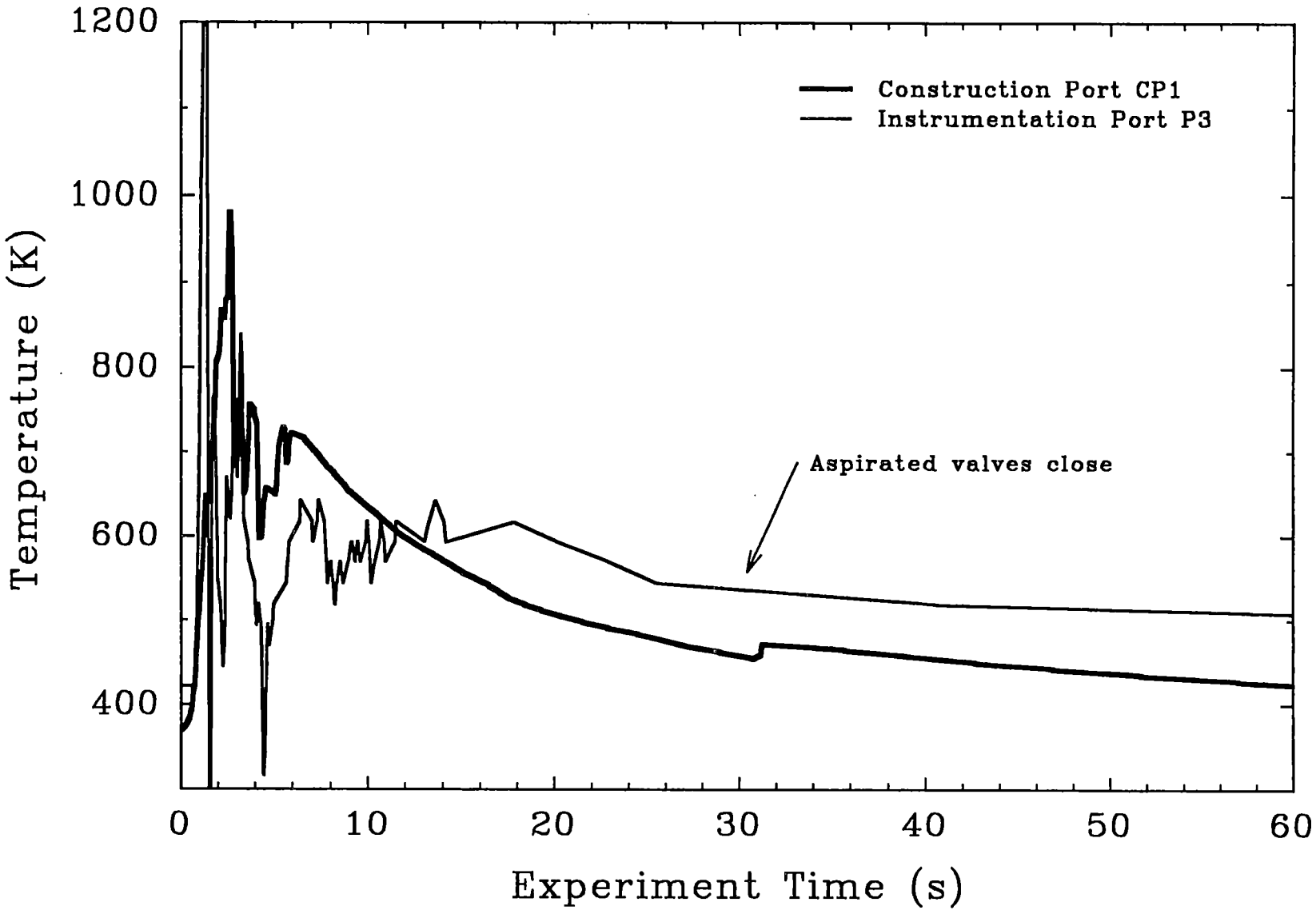

Figure 4.37 Gas temperatures measured at penetrations CP1 and P3 in the CTTF vessel with aspirated thermocouples in the IET−10 experiment.

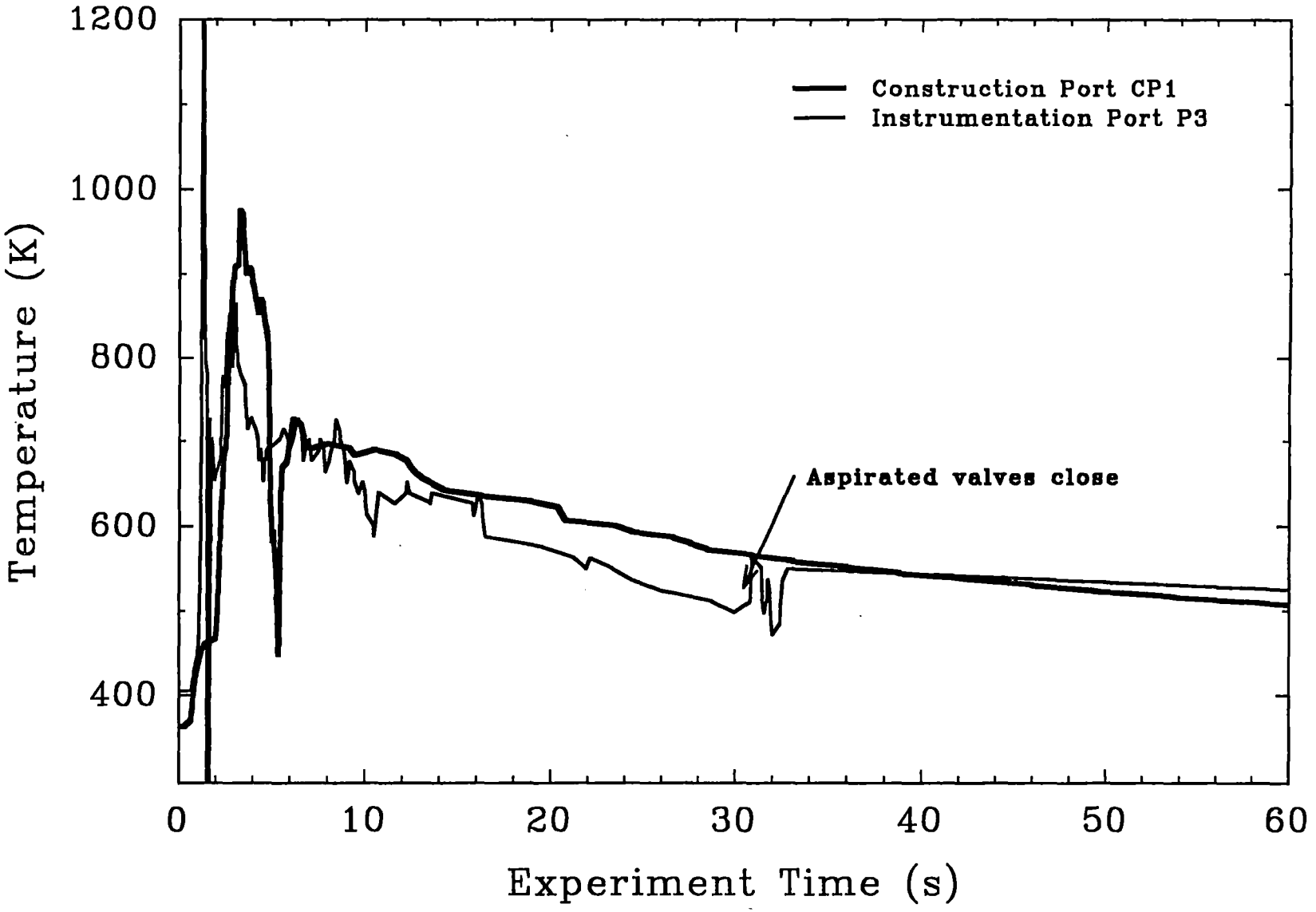

Figure 4.38 Gas temperatures measured at penetrations CP1 and P3 in the CTTF vessel with aspirated thermocouples in the IET−11 experiment.

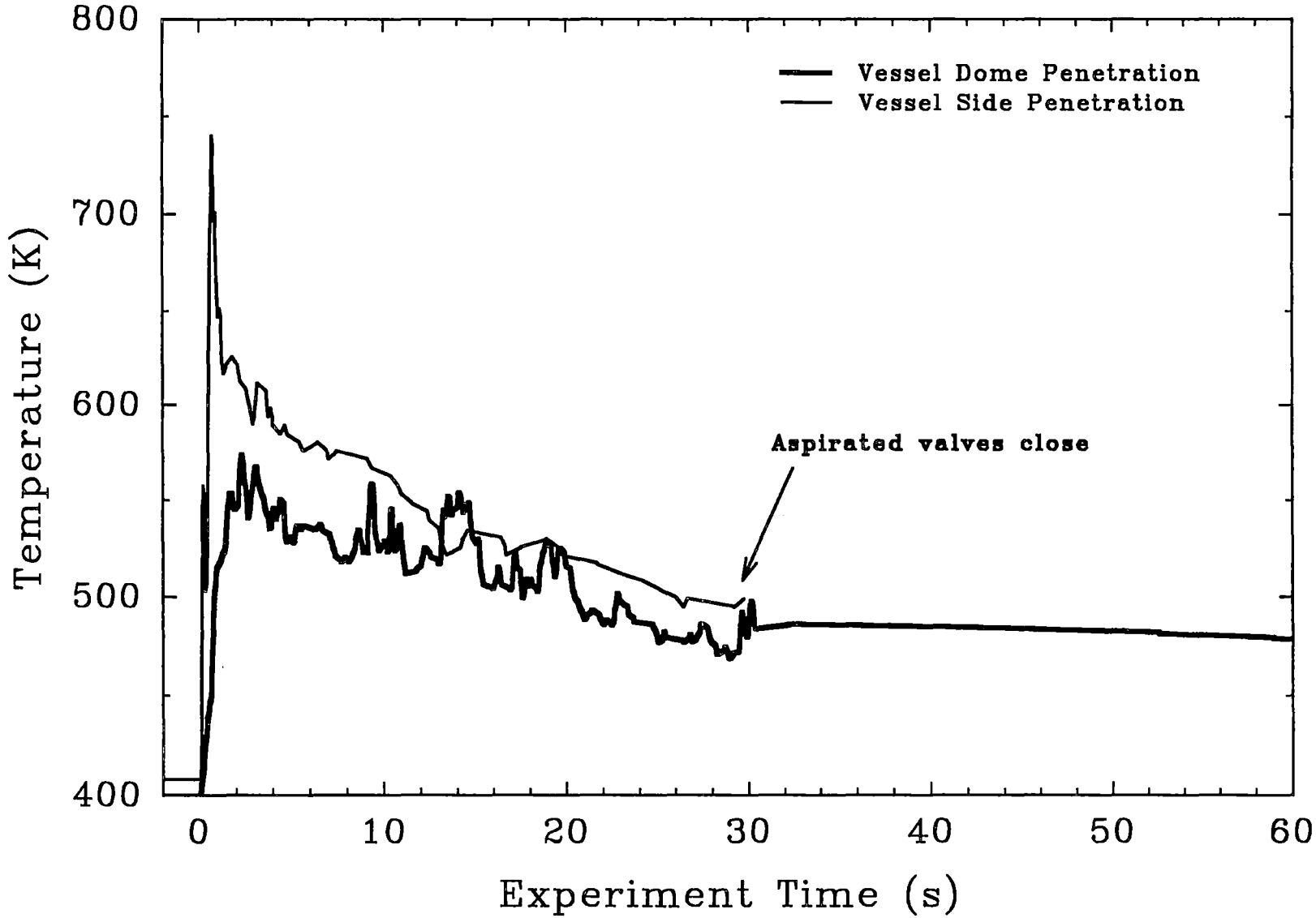

Figure 4.39 Gas temperatures measured at Surtsey vessel dome and side penetrations with aspirated thermocouples in the IET−12 experiment.

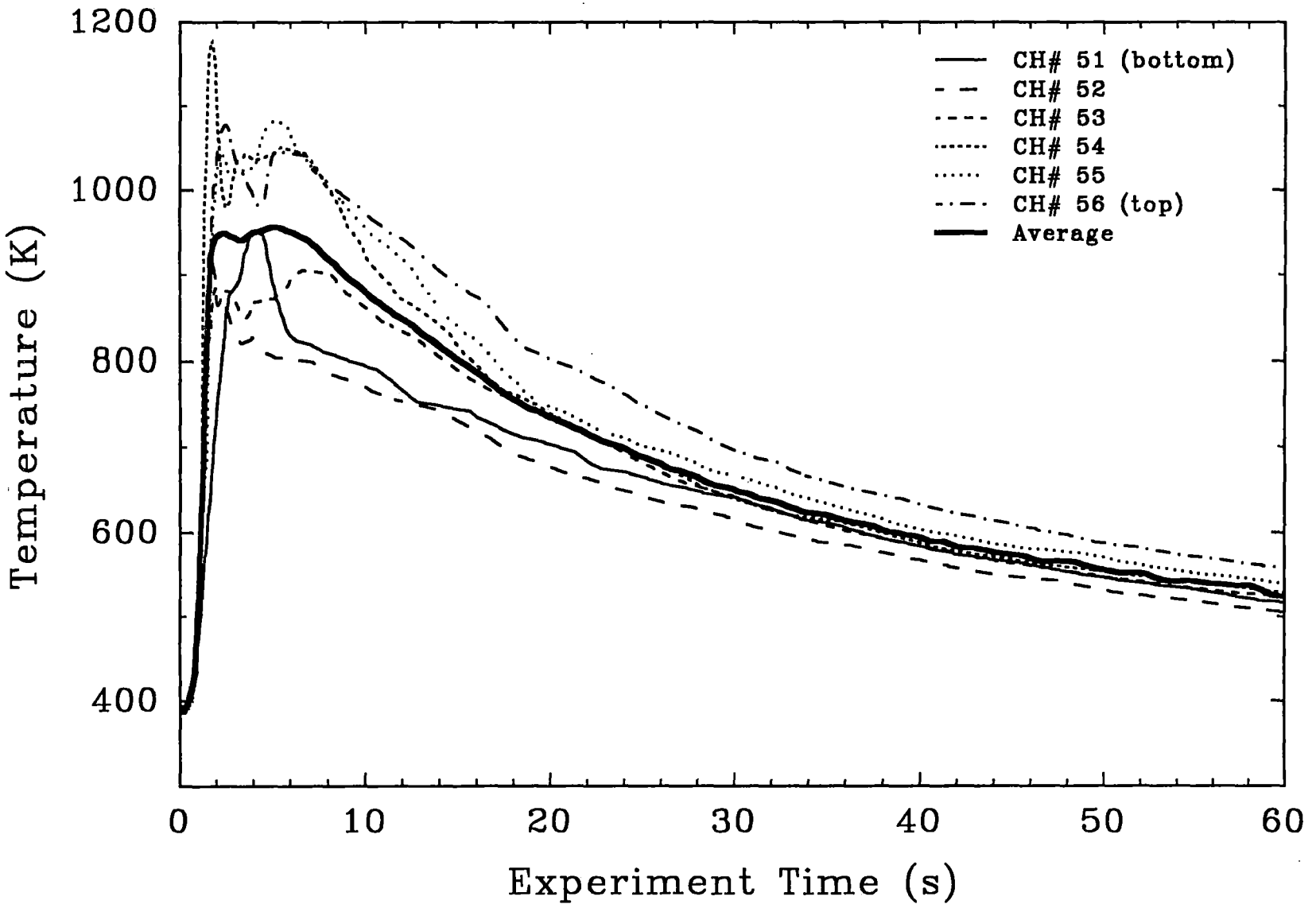

Figure 4.40 Temperature history of the A thermocouple array in the IET−9 experiment.

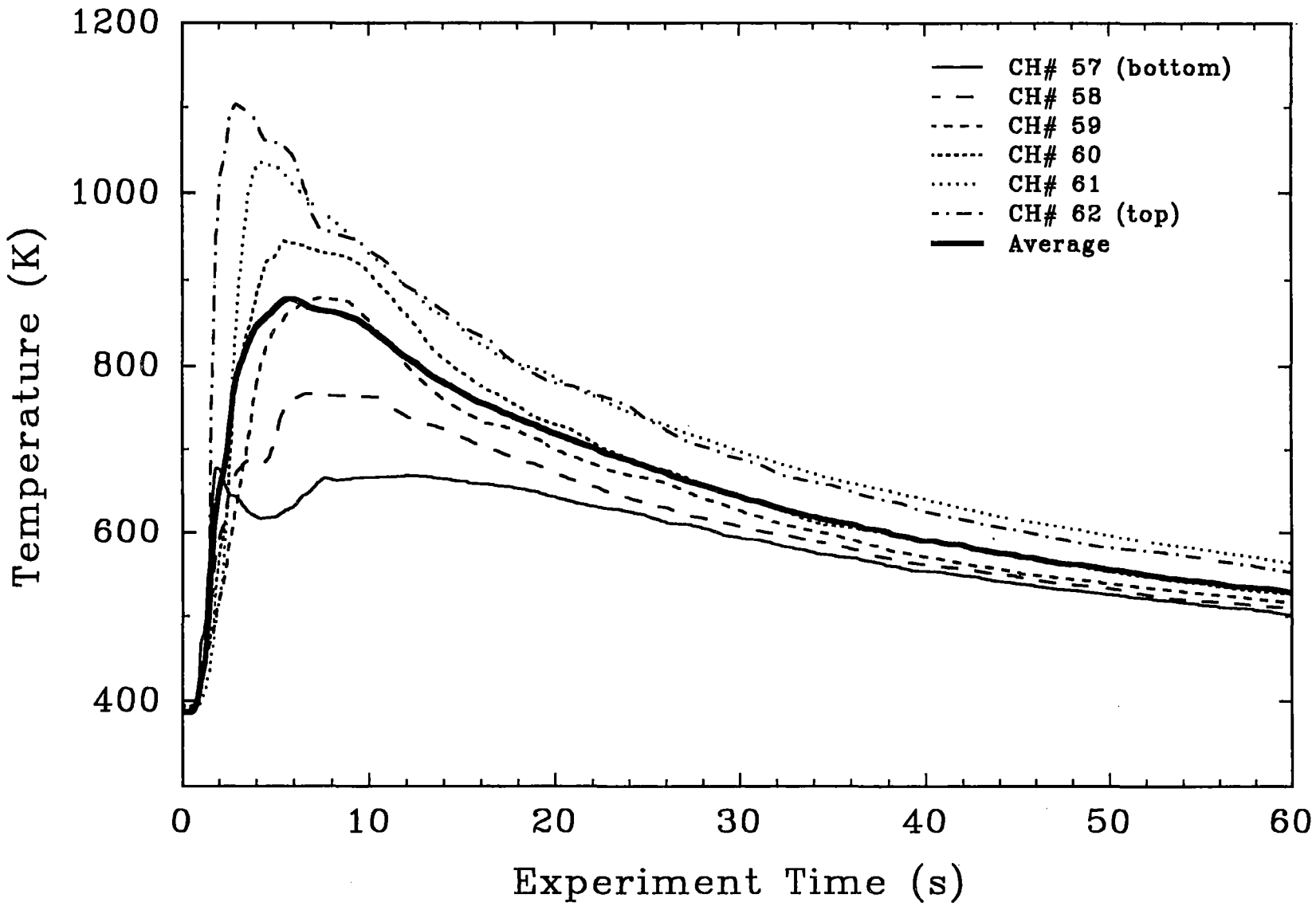

Figure 4.41 Temperature history of the B thermocouple array in the IET−9 experiment.

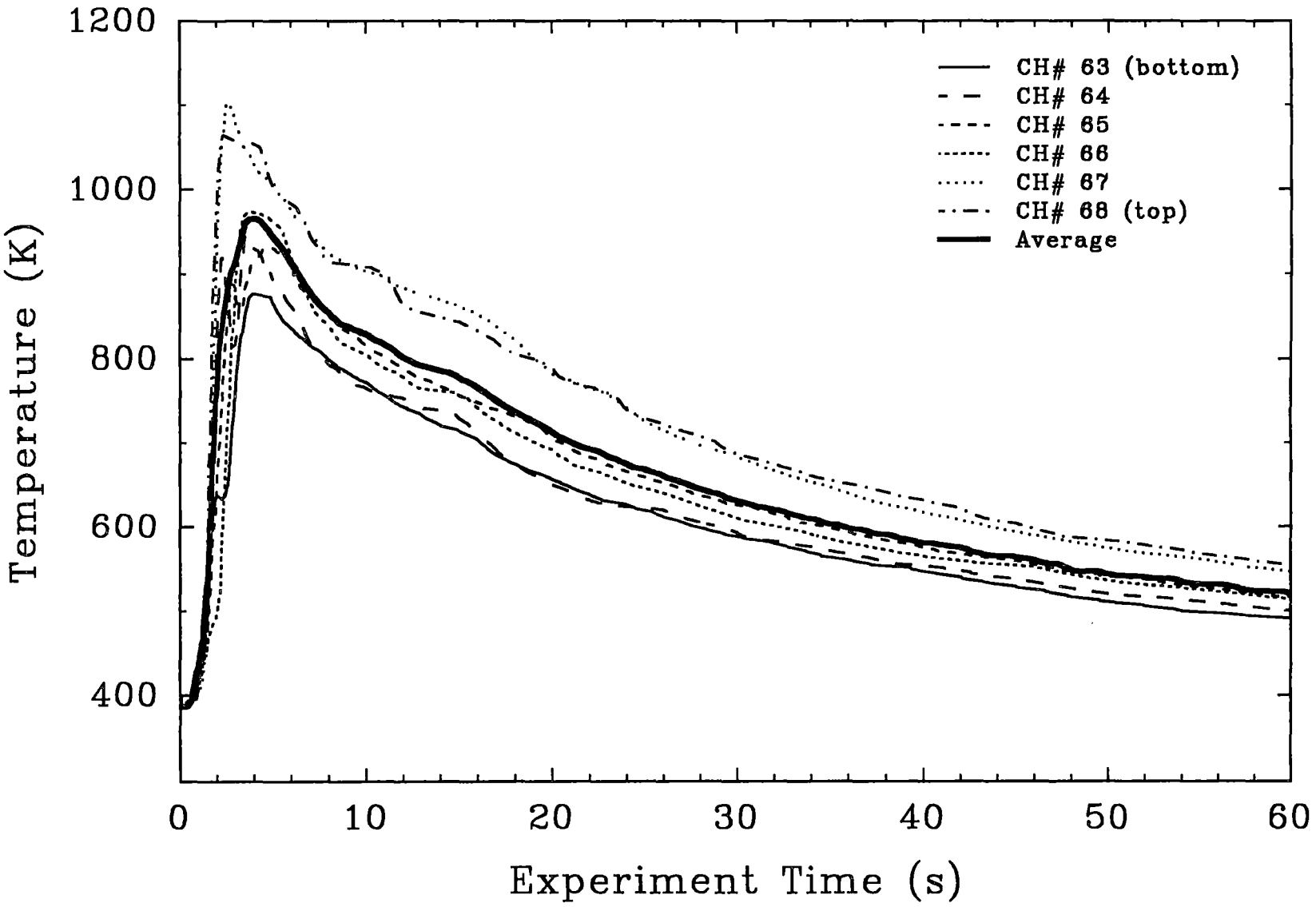

Figure 4.42 Temperature history of the C thermocouple array in the IET-9 experiment.

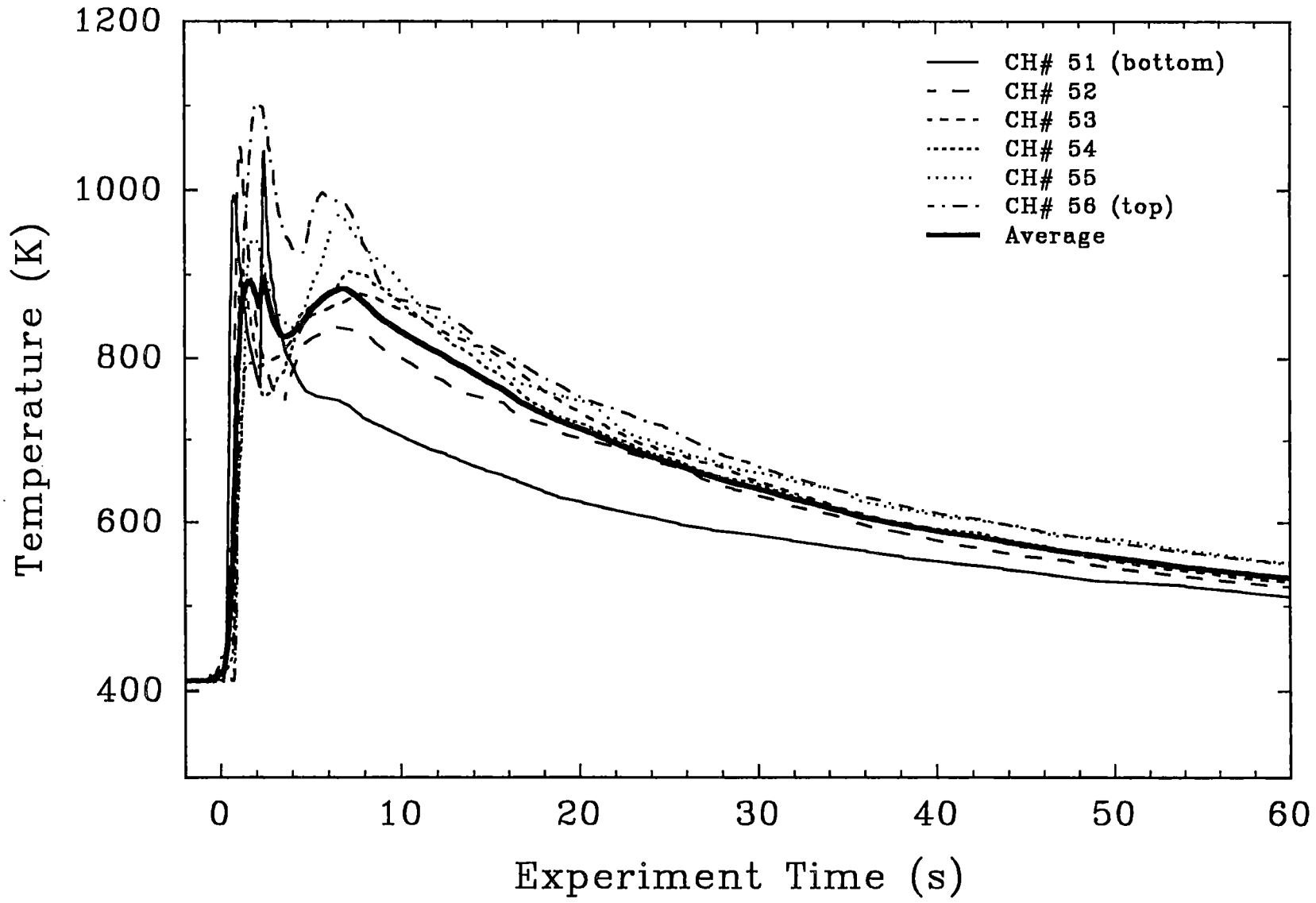

Figure 4.43 Temperature history of the A thermocouple array in the IET−10 experiment.

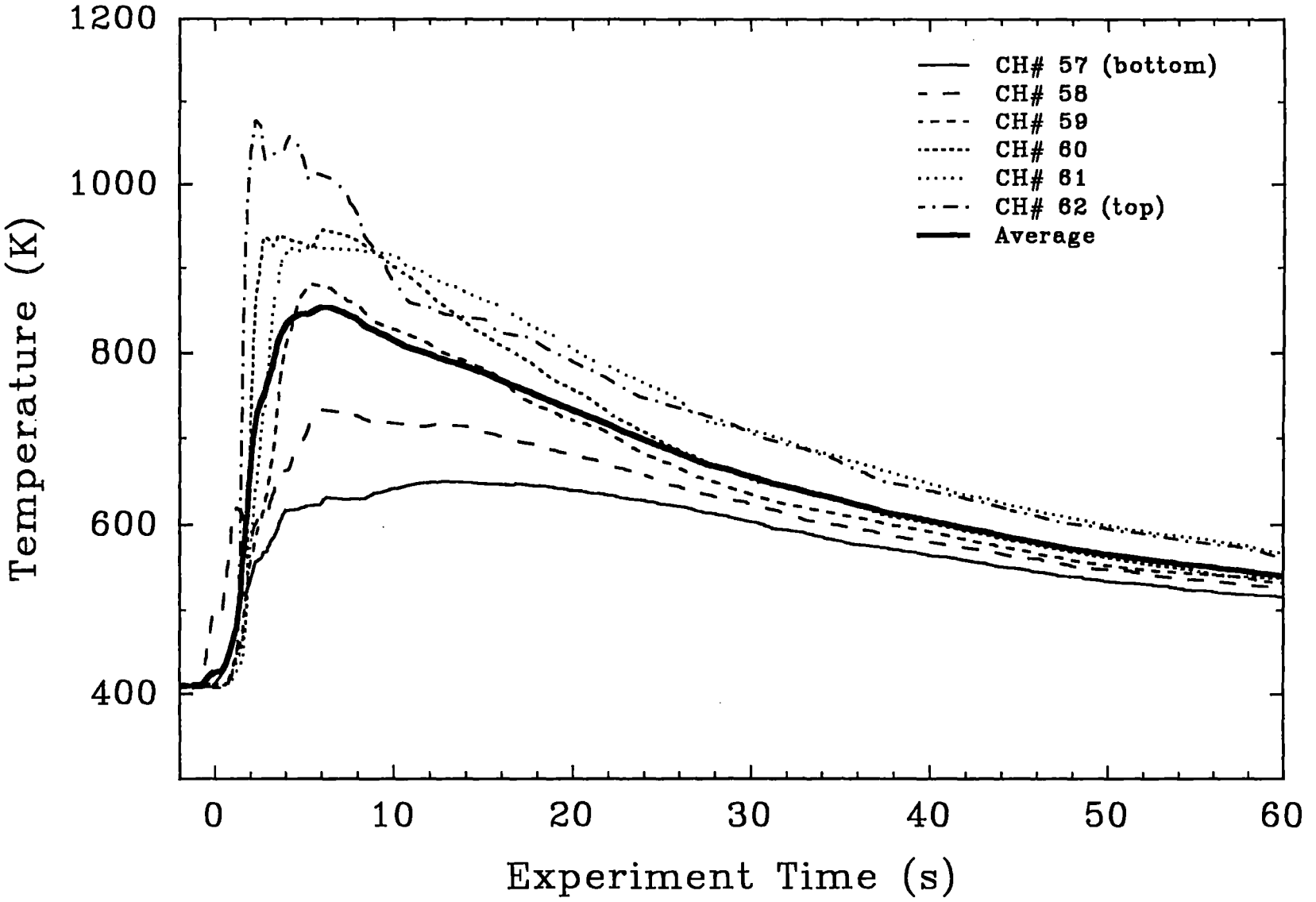

Figure 4.44 Temperature history of the B thermocouple array in the IET−10 experiment.

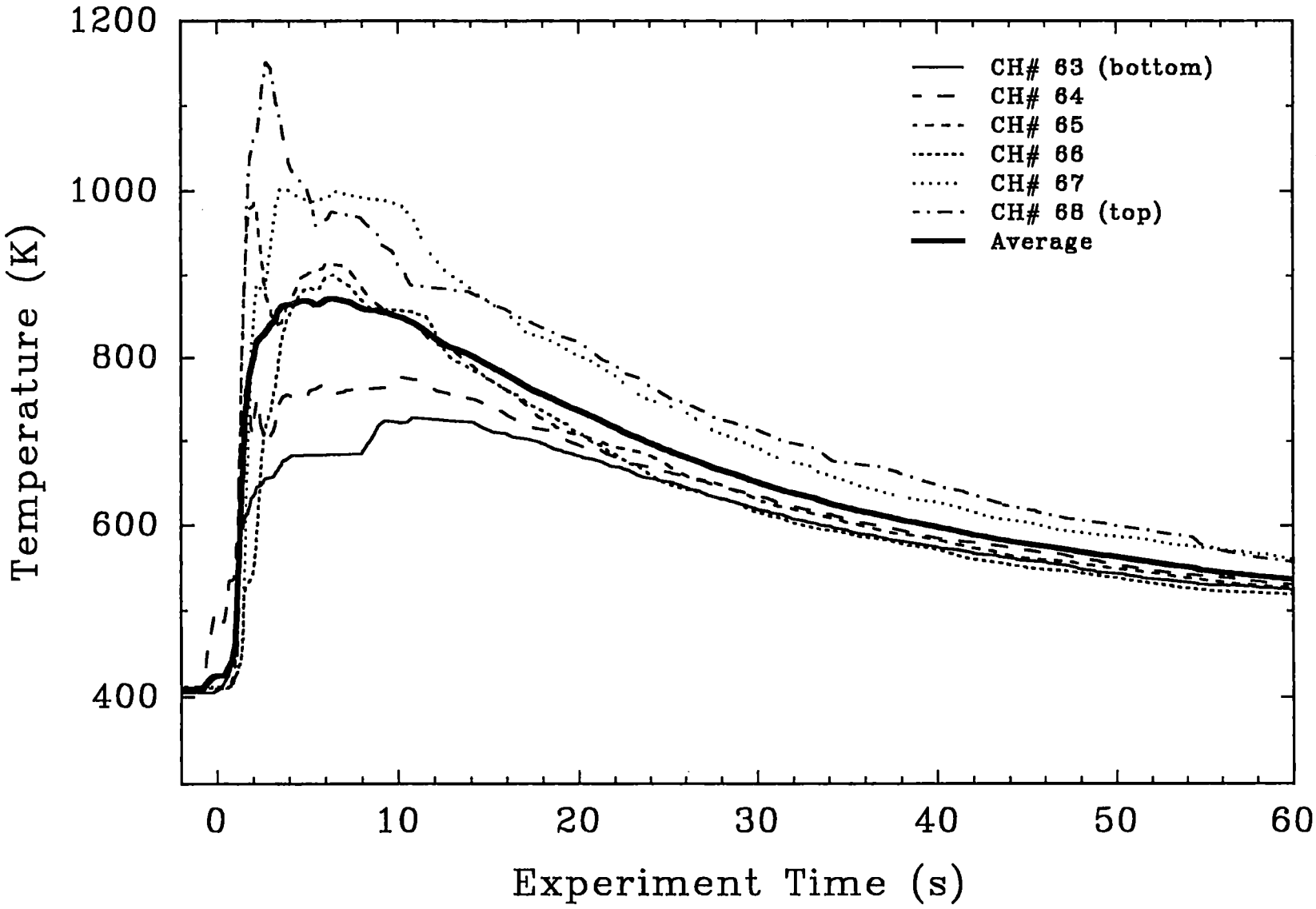

Figure 4.45 Temperature history of the C thermocouple array in the IET−10 experiment.

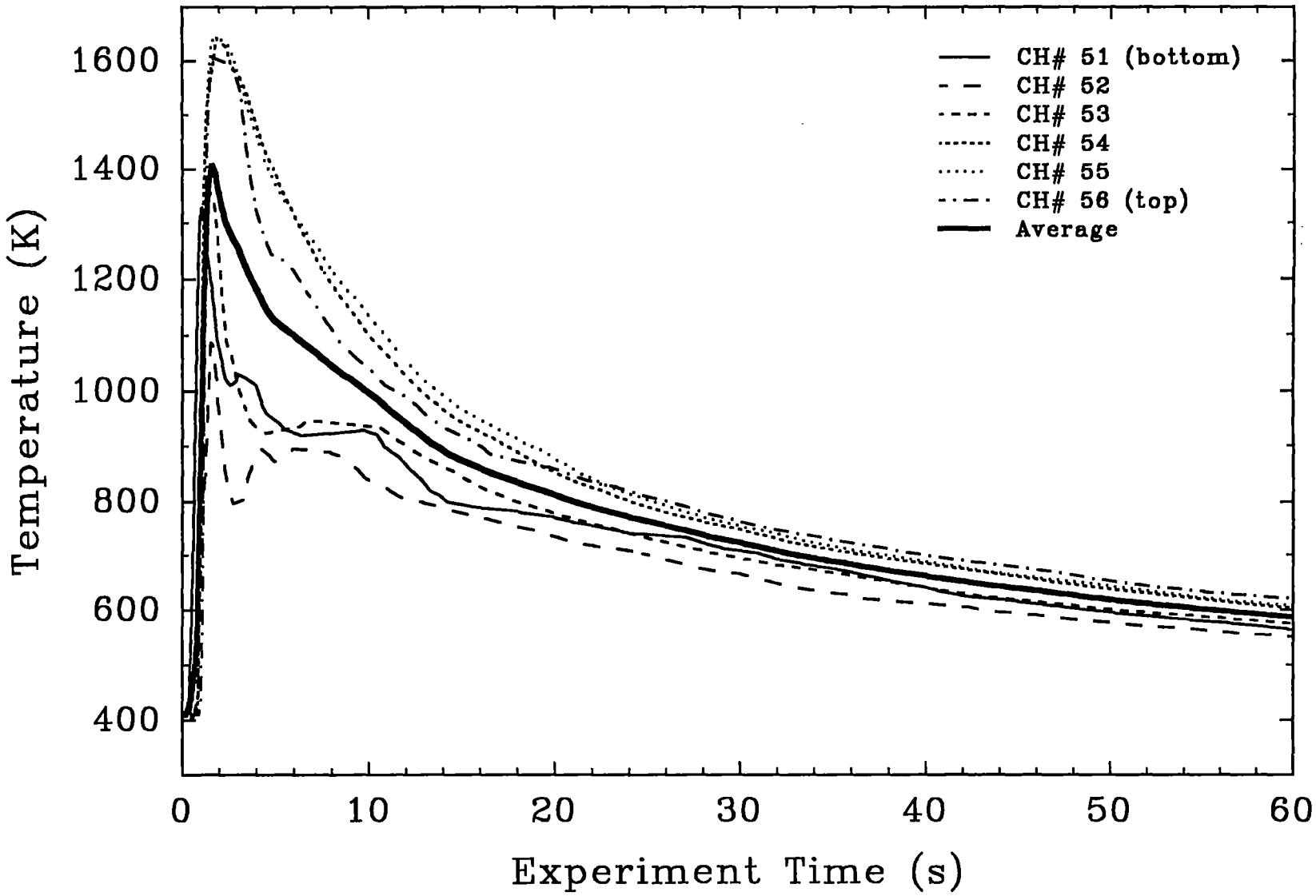

Figure 4.46 Temperature history of the A thermocouple array in the IET−11 experiment.

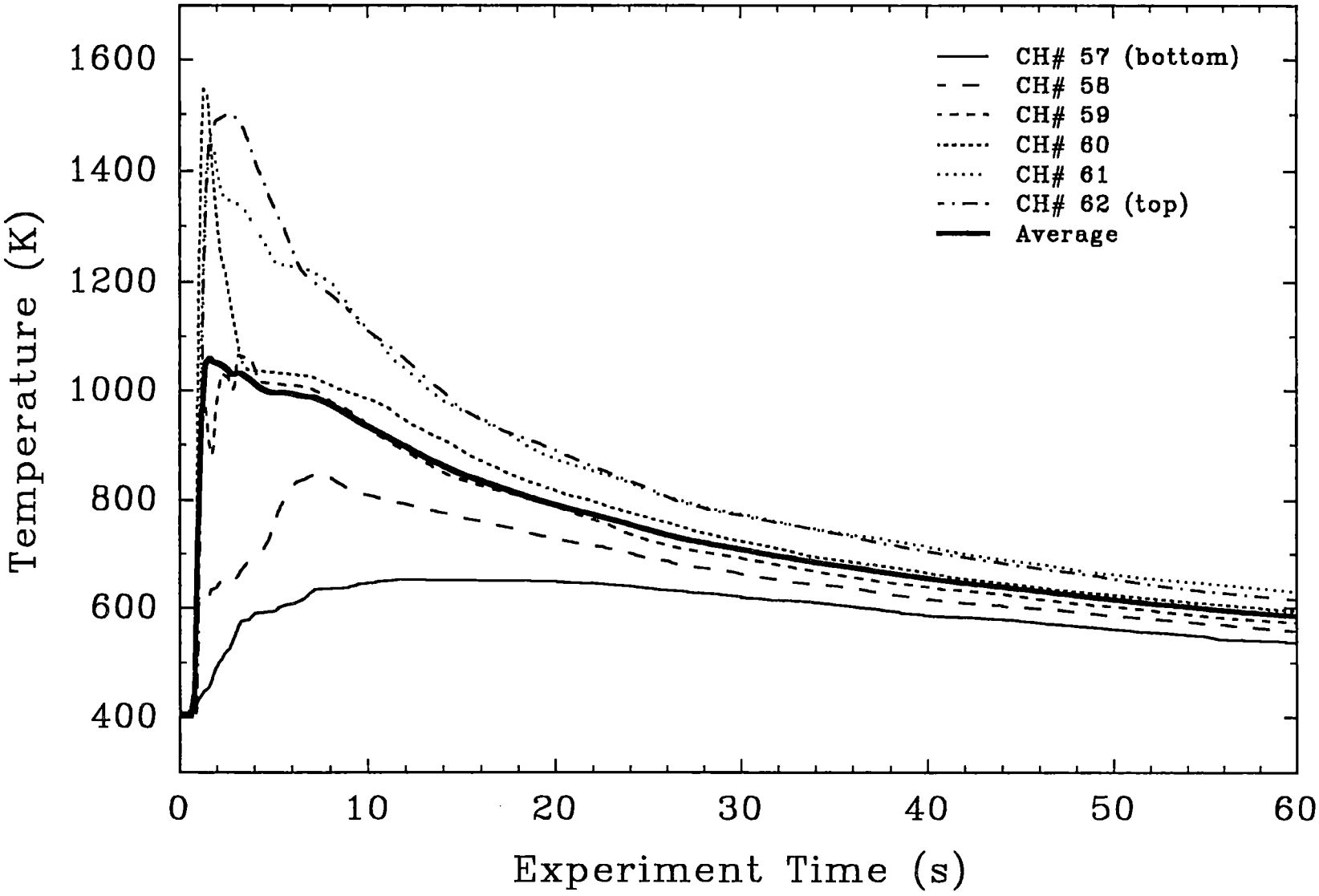

Figure 4.47 Temperature history of the B thermocouple array in the IET−11 experiment.

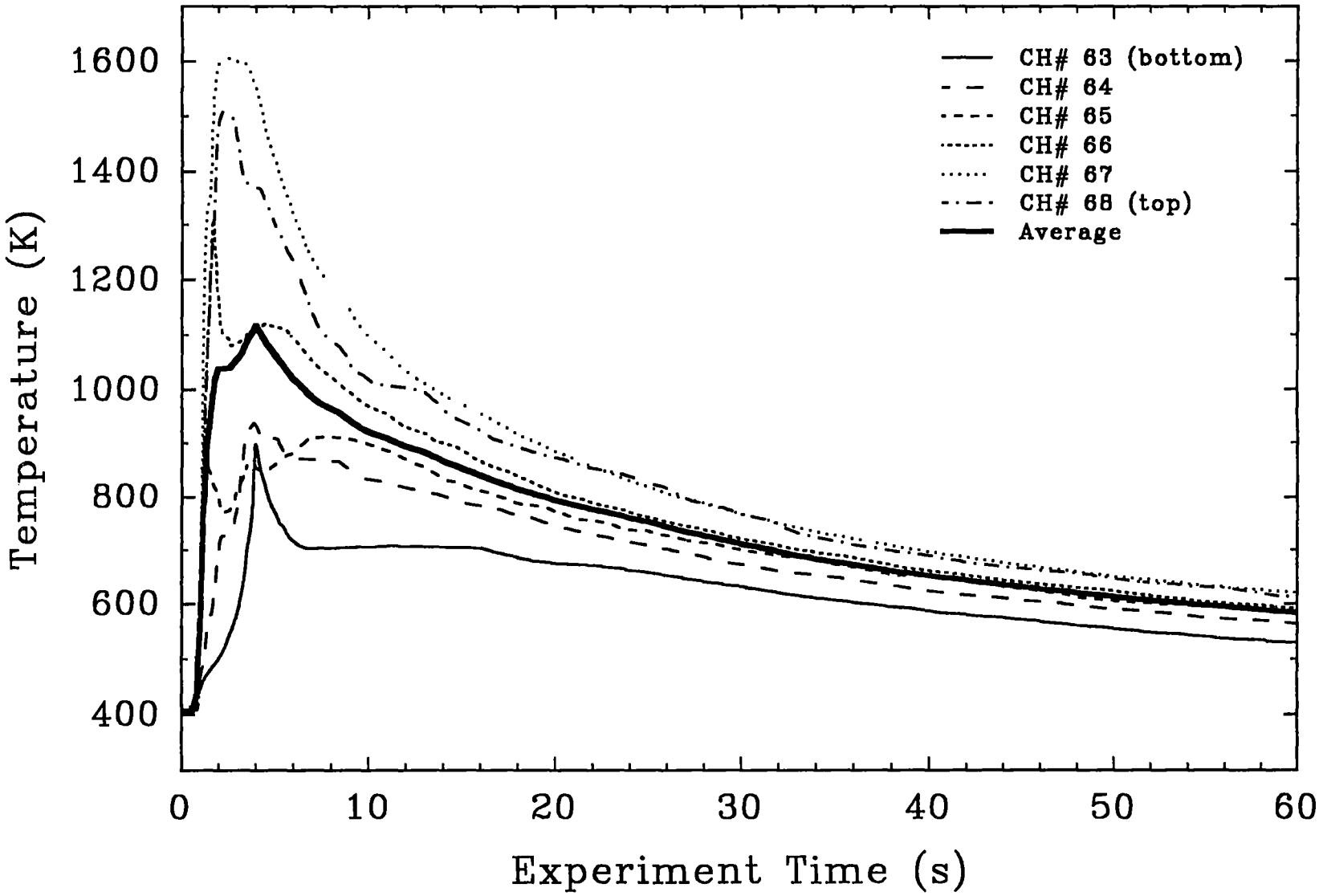

Figure 4.48 Temperature history of the C thermocouple array in the IET−11 experiment.

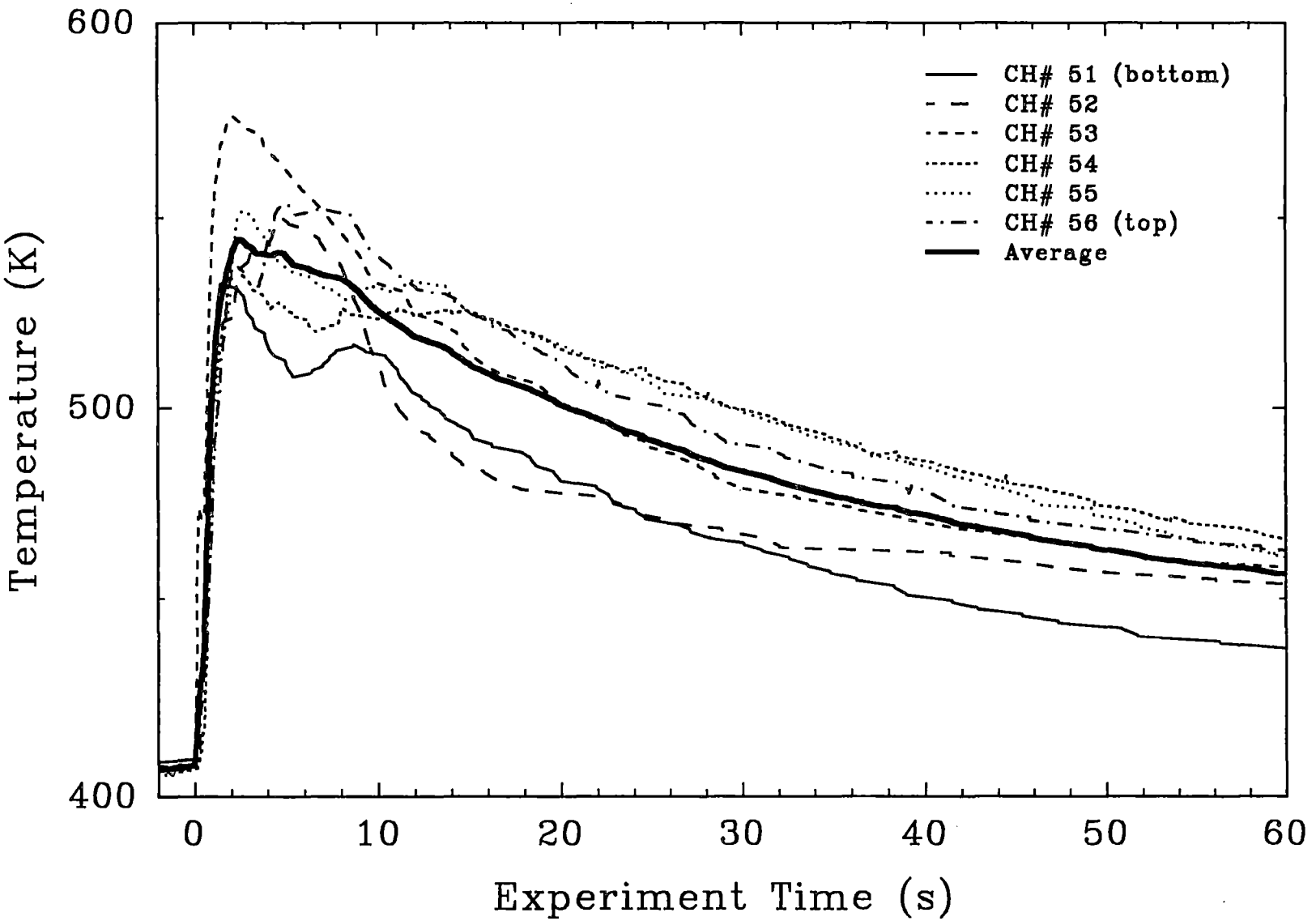

Figure 4.49 Temperature history of the A thermocouple array in the IET−12 experiment.

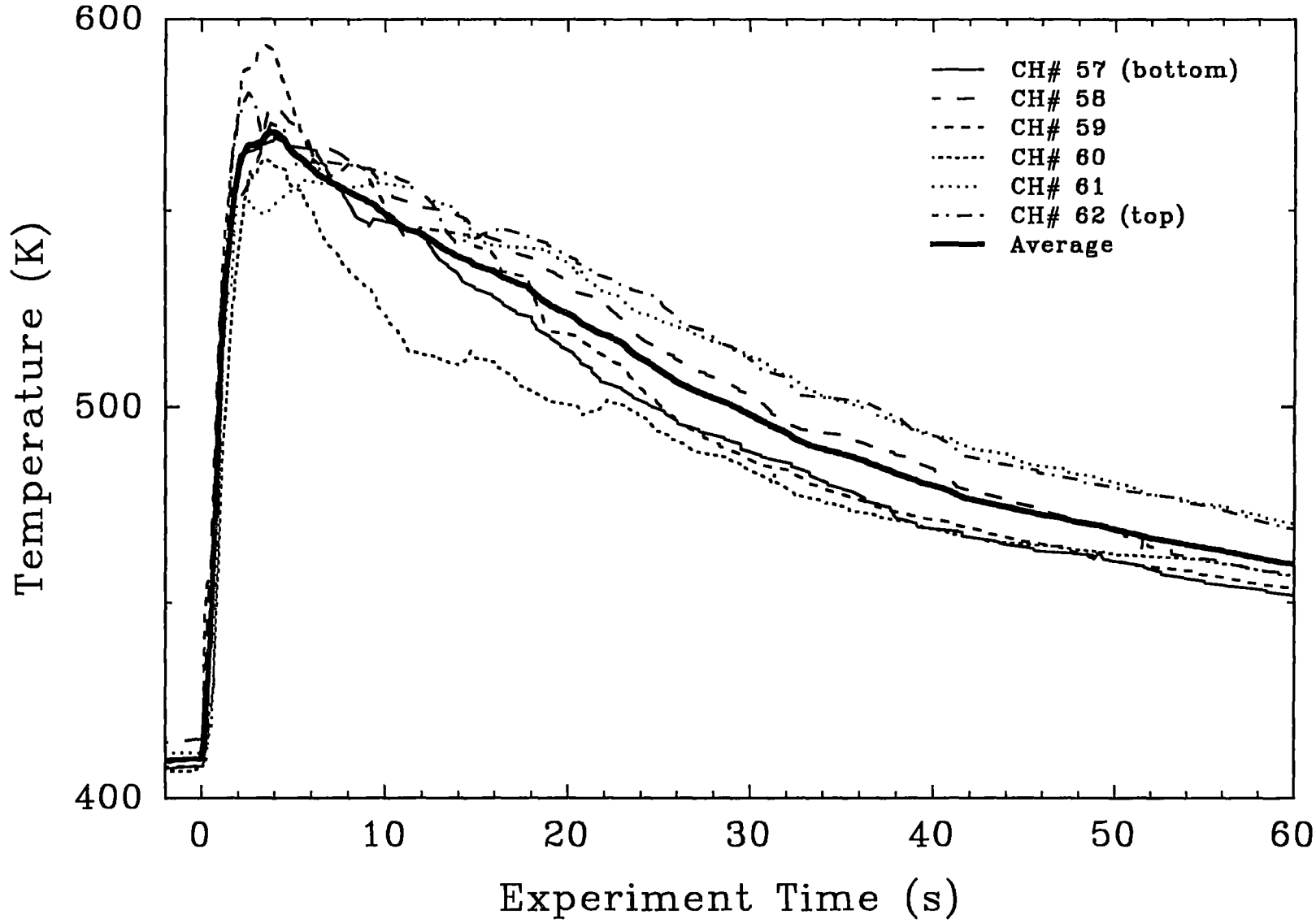

Figure 4.50 Temperature history of the B thermocouple array in the IET−12 experiment.

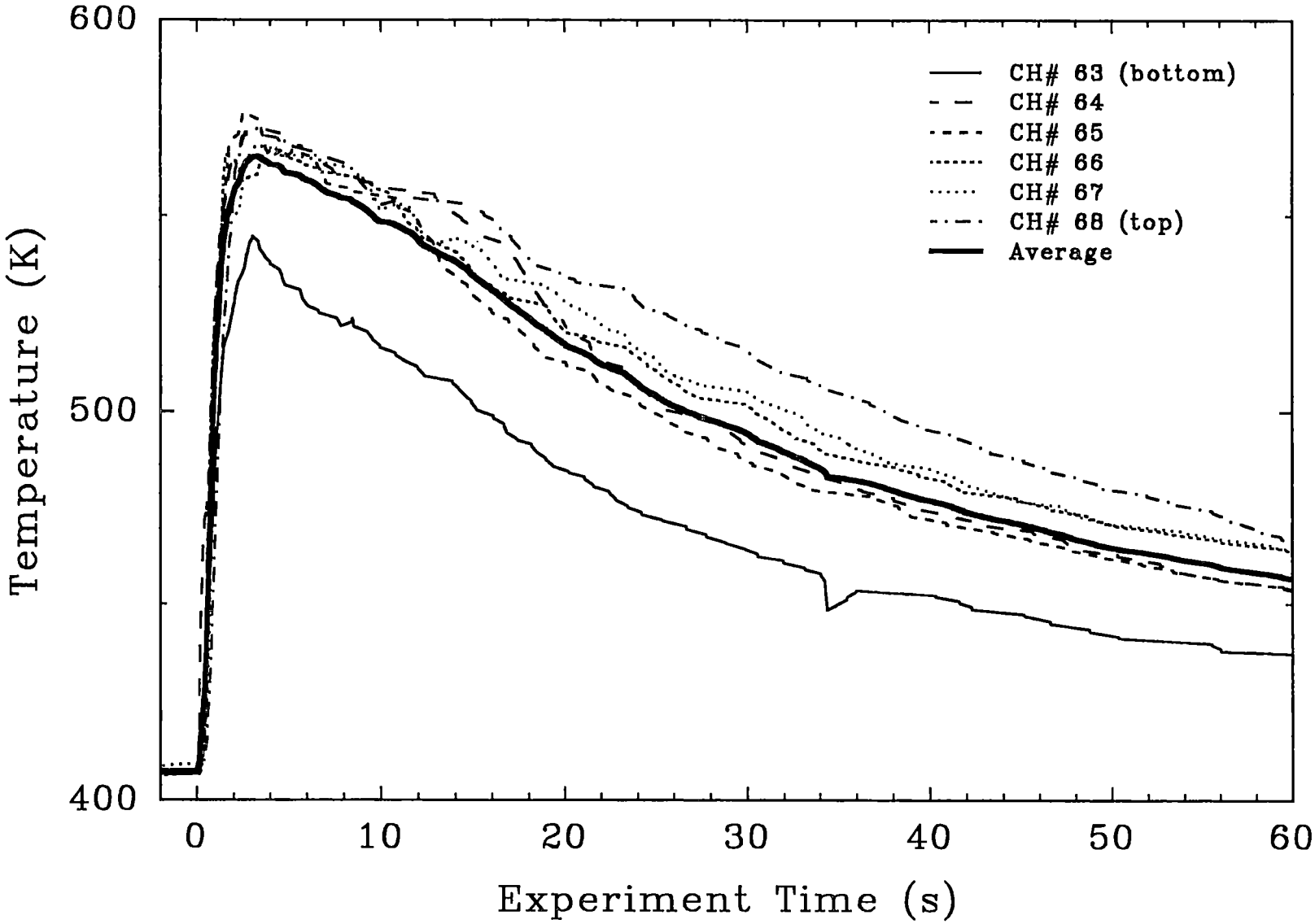

Figure 4.51 Temperature history of the C thermocouple array in the IET−12 experiment.

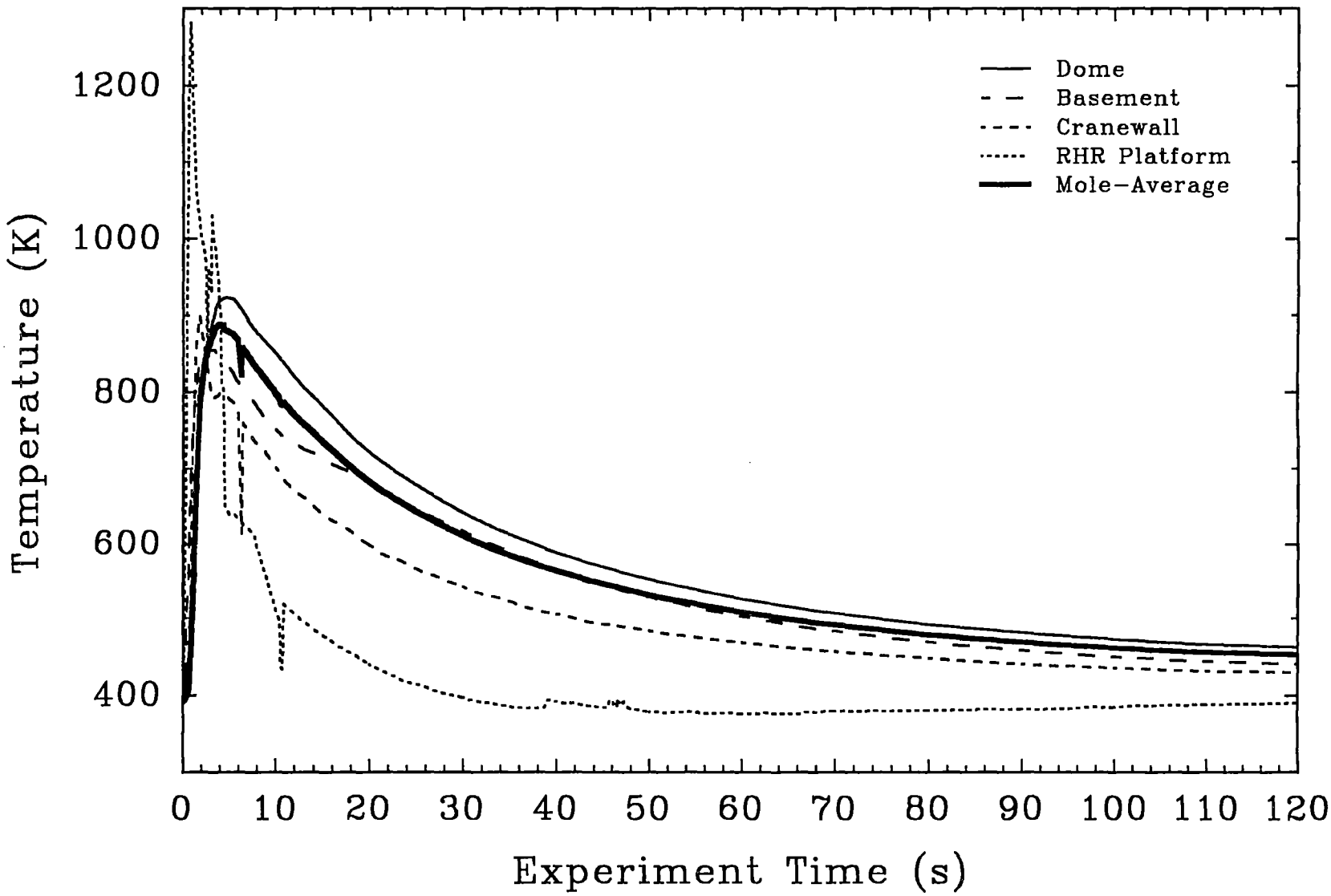

Figure 4.52 CTTF vessel dome, cranewall, basement, and RHR platform average gas temperatures compared to a mole-average gas temperature in the IET-9 experiment.

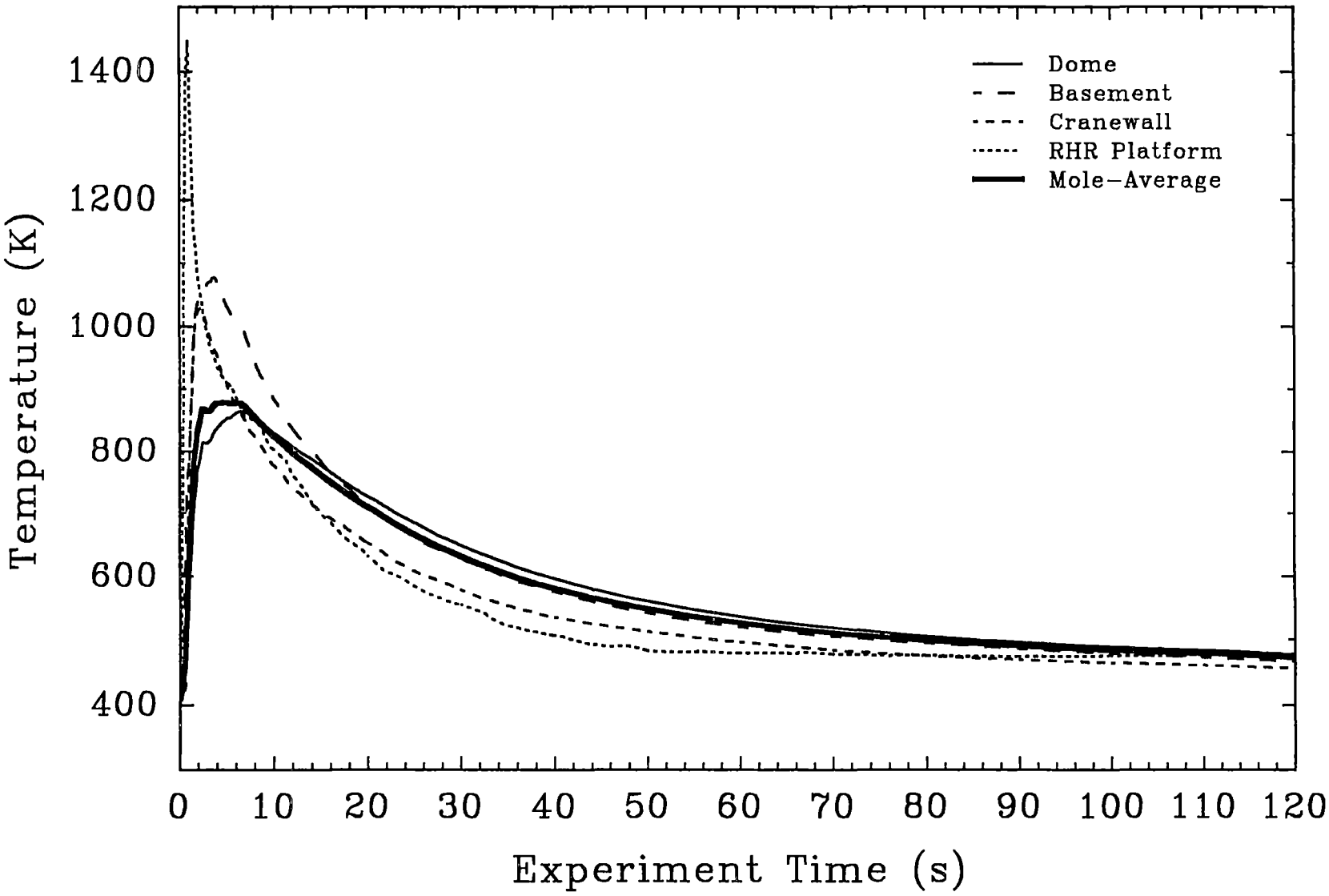

Figure 4.53 CTTF vessel dome, cranewall, basement, and RHR platform average gas temperatures compared to a mole-average gas temperature in the IET-10 experiment.

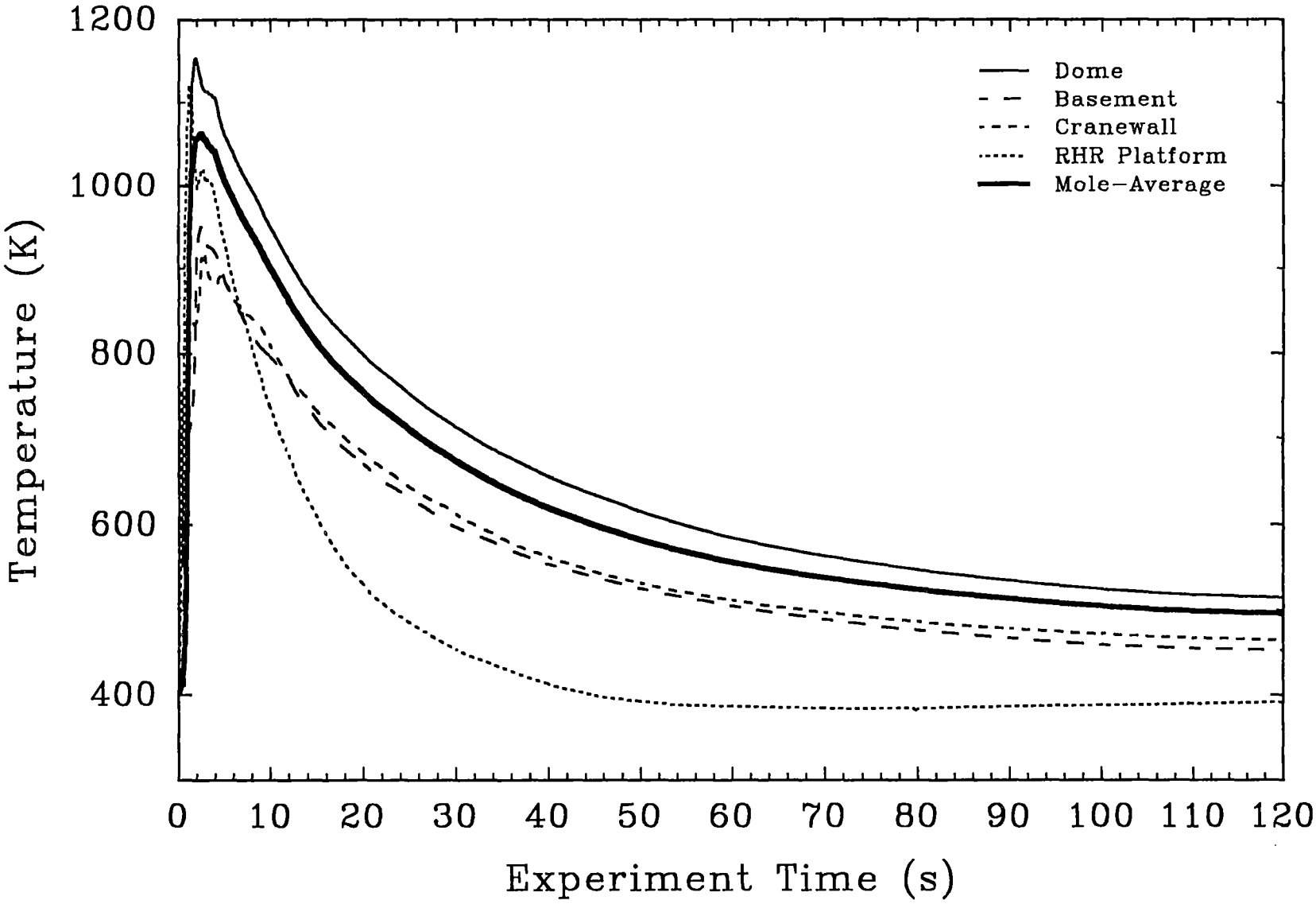

Figure 4.54 CTTF vessel dome, cranewall, basement, and RHR platform average gas temperatures compared to a mole-average gas temperature in the IET-11 experiment.

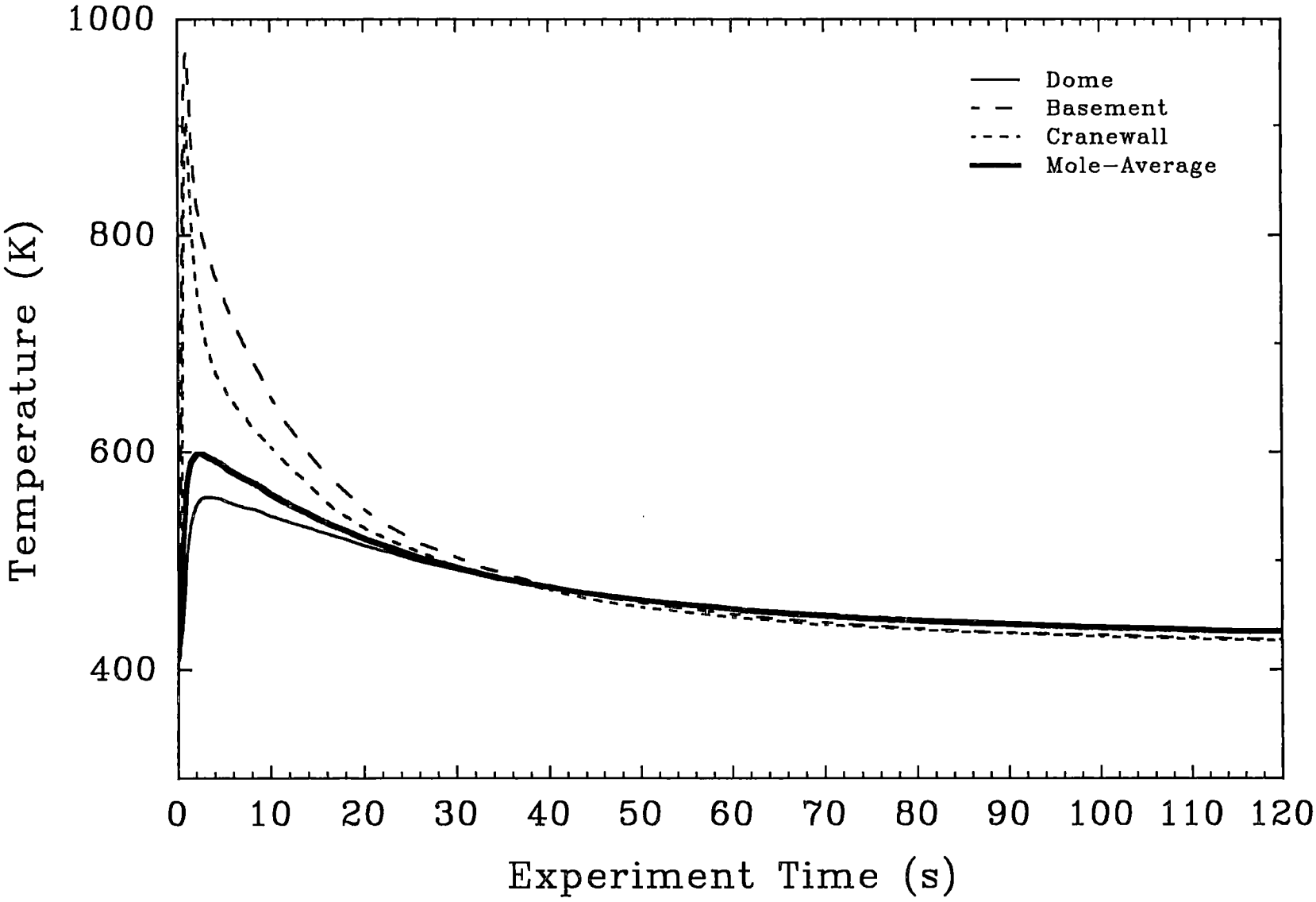

Figure 4.55 CTTF vessel dome, cranewall, and basement gas temperatures compared to a mole-average gas temperature in the IET-12 experiment.

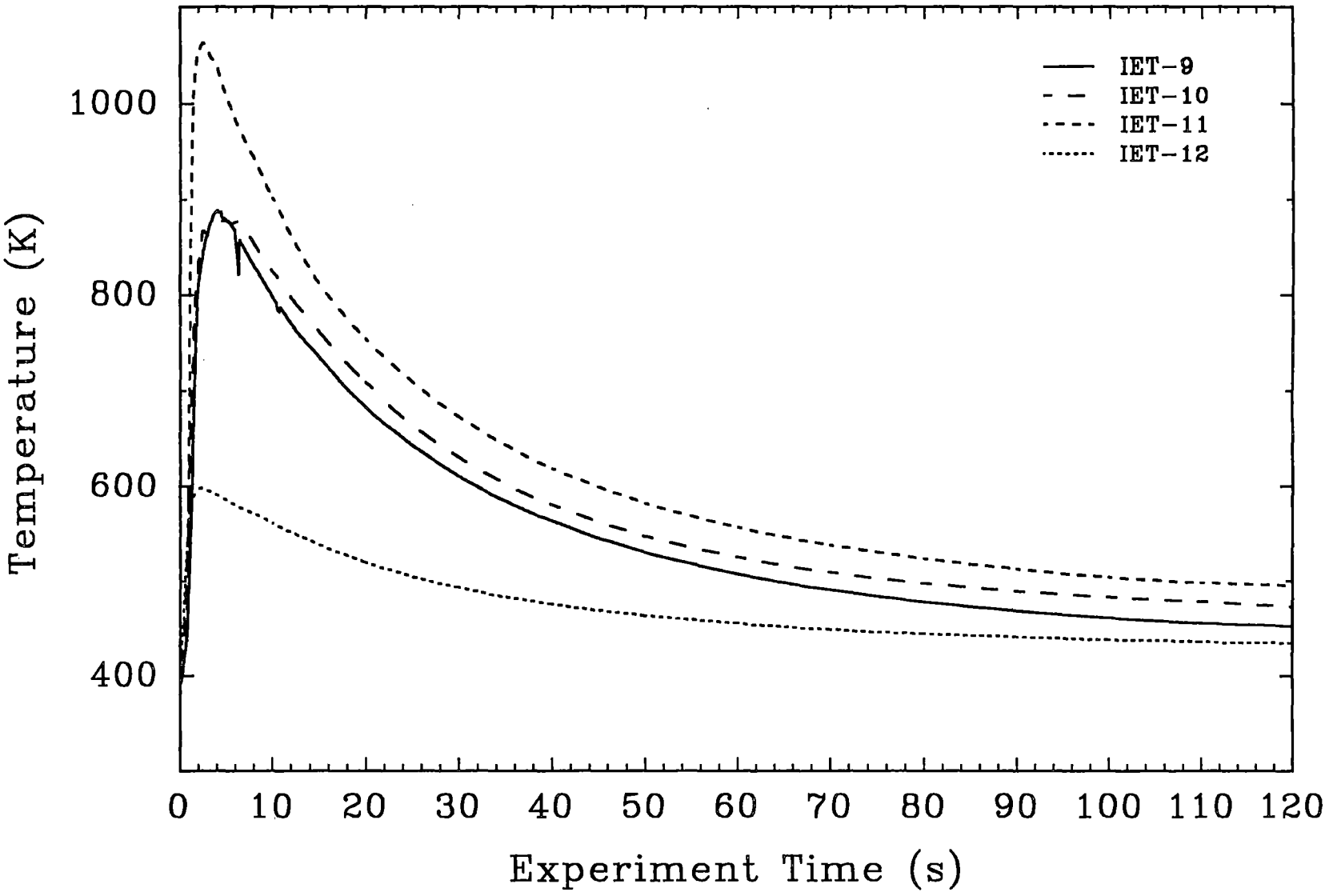

Figure 4.56 Comparison of mole-average gas temperatures in the Surry IET experiments.

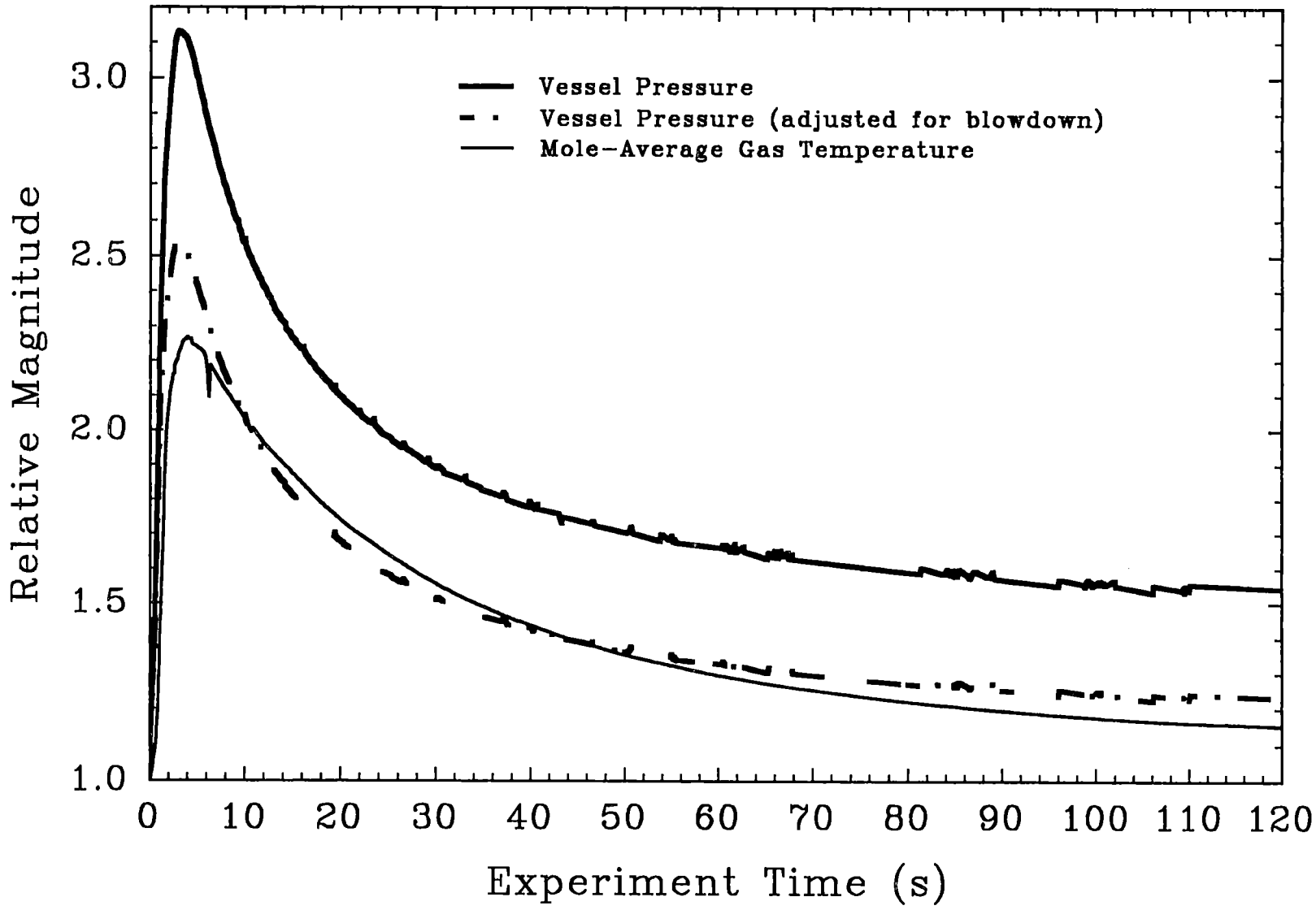

Figure 4.57 Relative magnitude of the vessel pressure compared to vessel mole-averaged gas temperature in the IET-9 experiment.

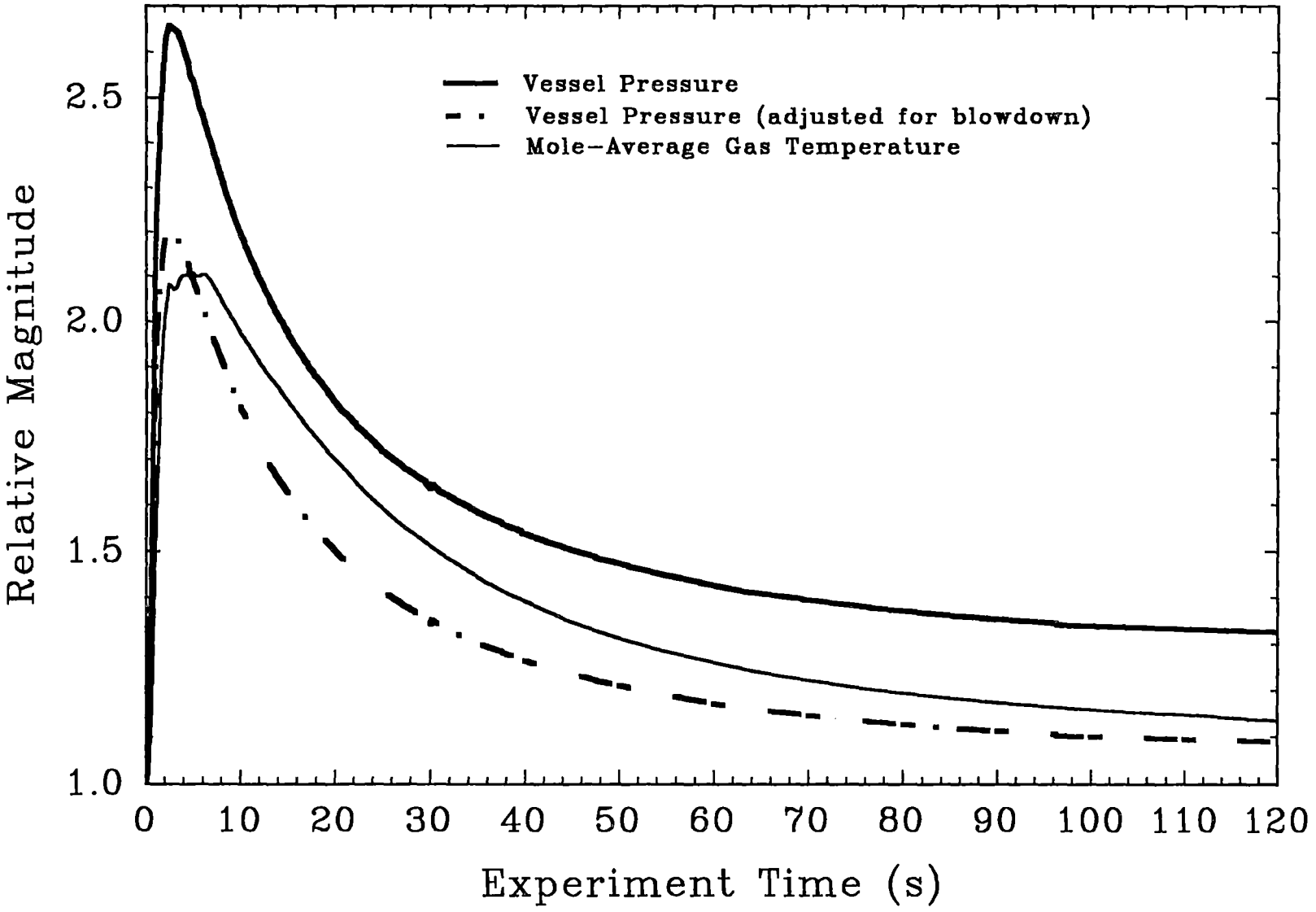

Figure 4.58 Relative magnitude of the vessel pressure compared to vessel mole-average gas temperature in the IET-10 experiment.

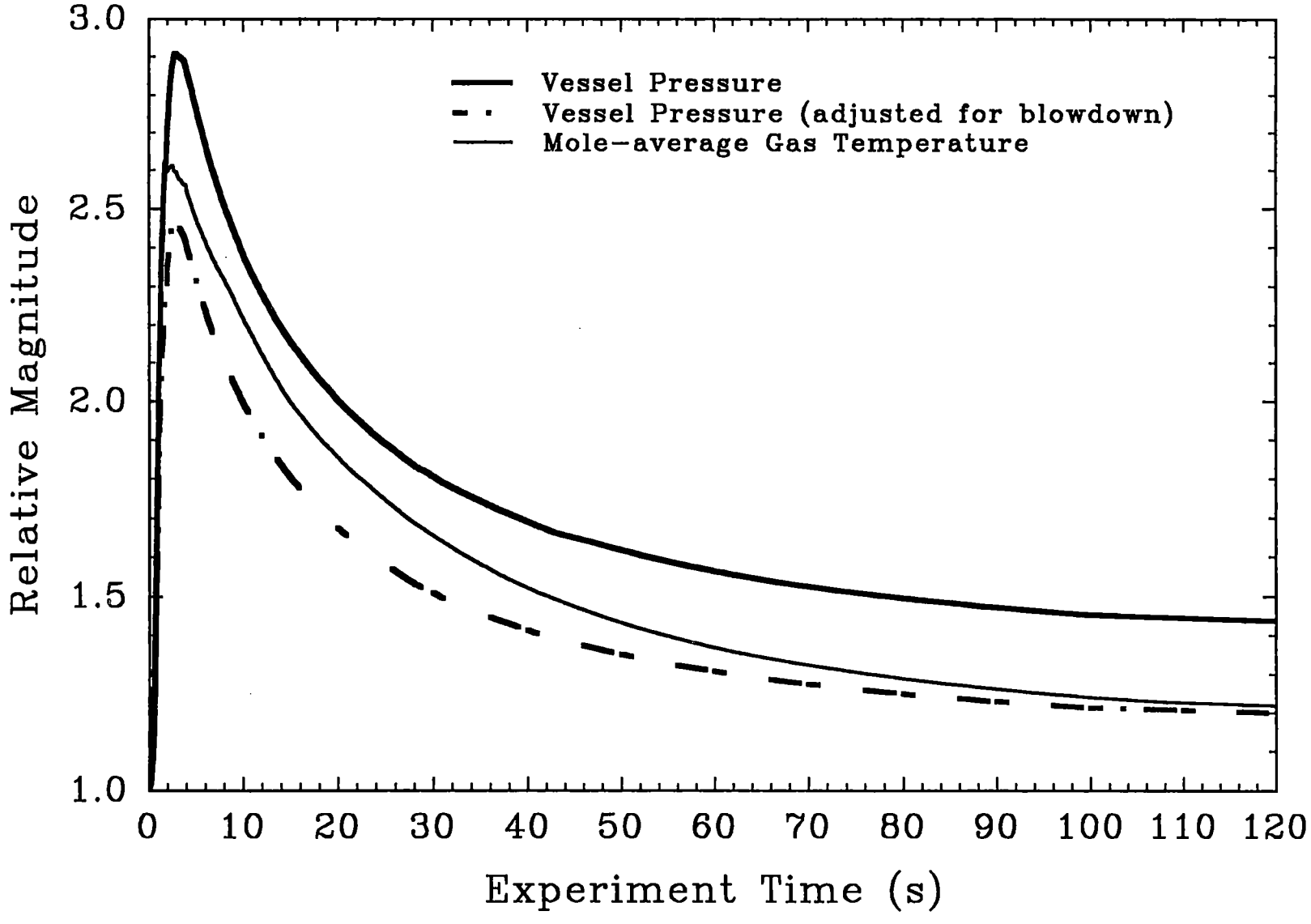

Figure 4.59 Relative magnitude of the vessel pressure compared to vessel mole-average gas temperature in the IET-11 experiment.

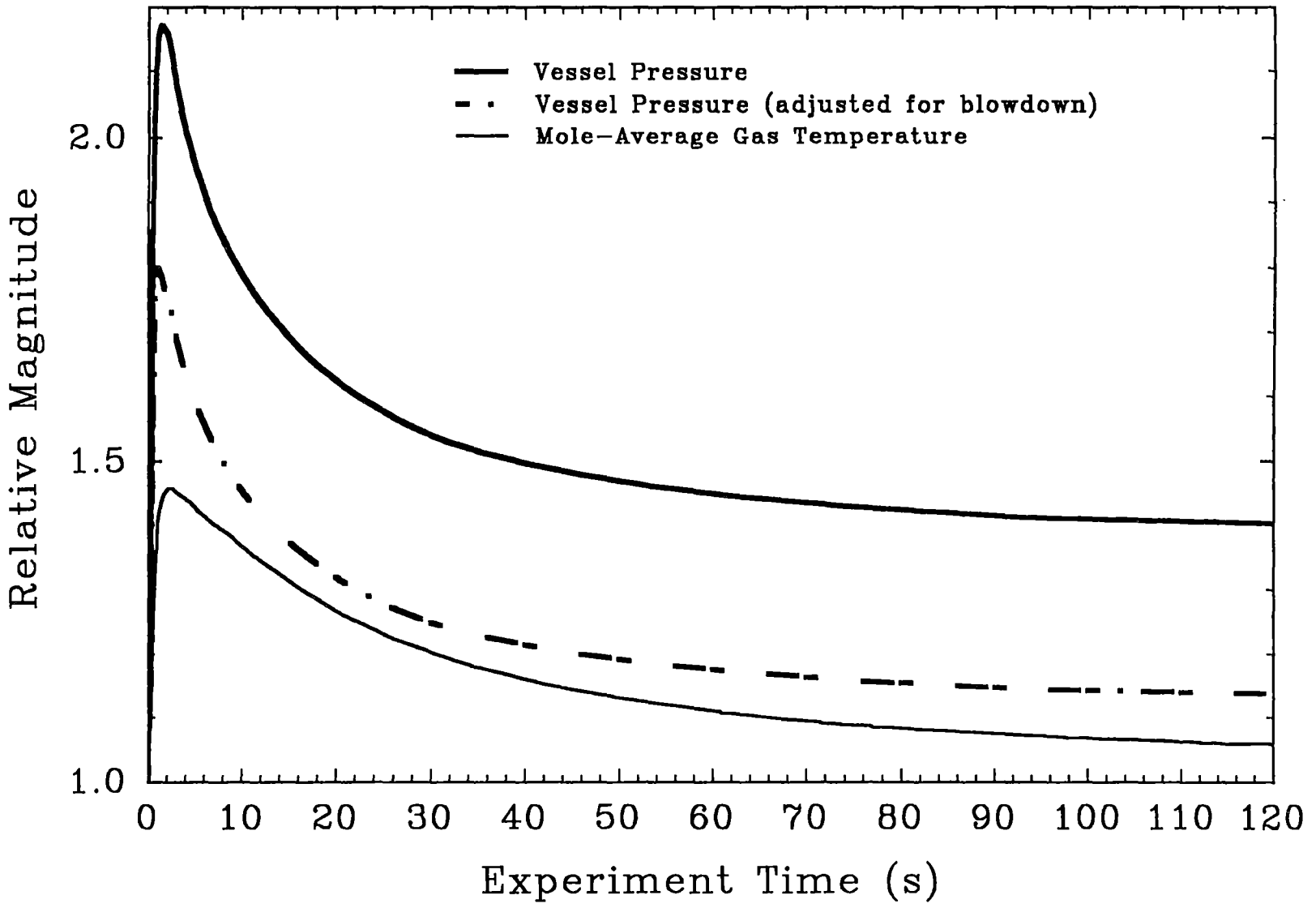

Figure 4.60 Relative magnitude of the vessel pressure compared to vessel mole-average gas temperature in the IET-12 experiment.

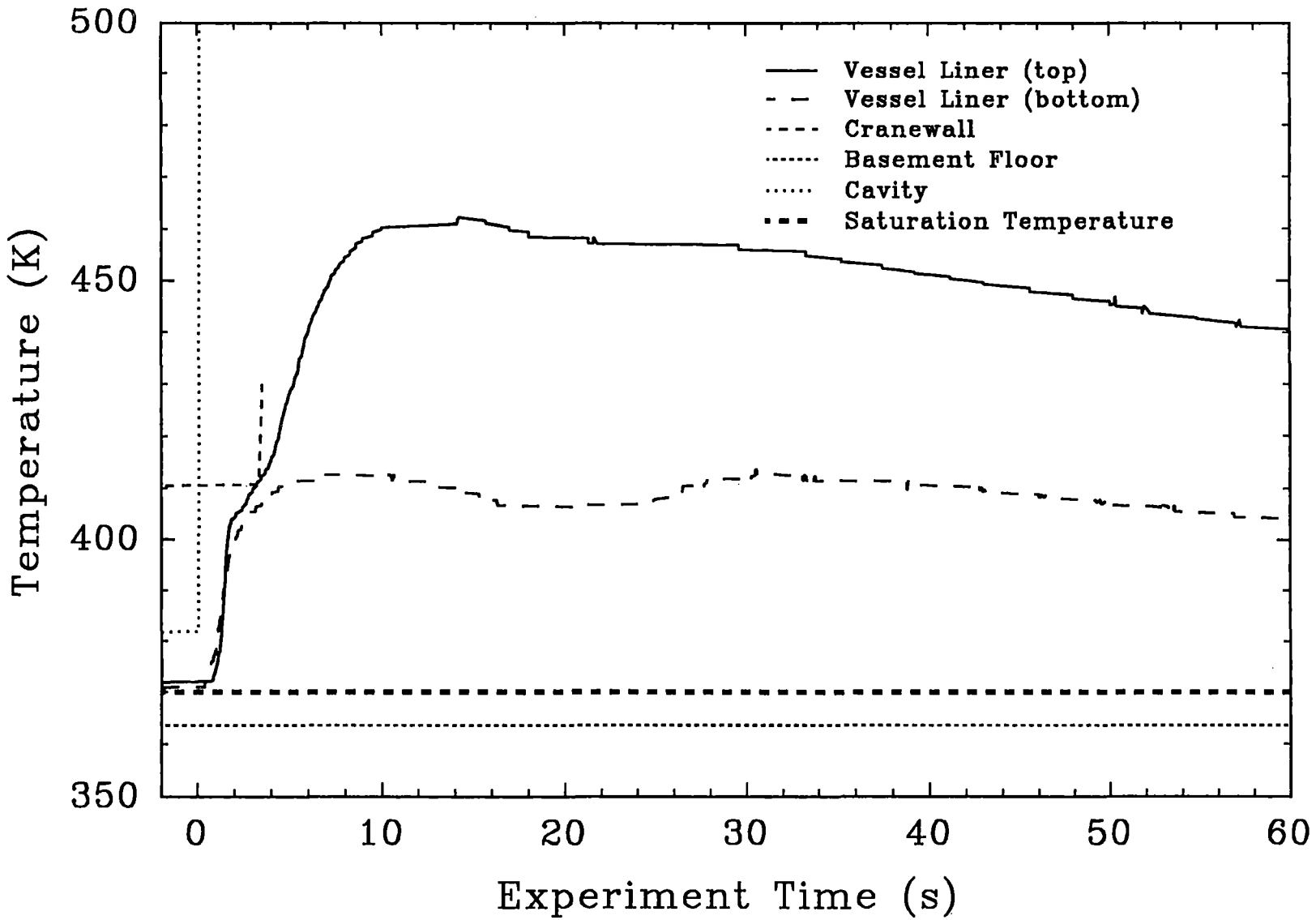

Figure 4.61 Temperature history of the CTTF vessel liner, cranewall, basement floor, and cavity compared to saturation temperature in the IET−9 experiment.

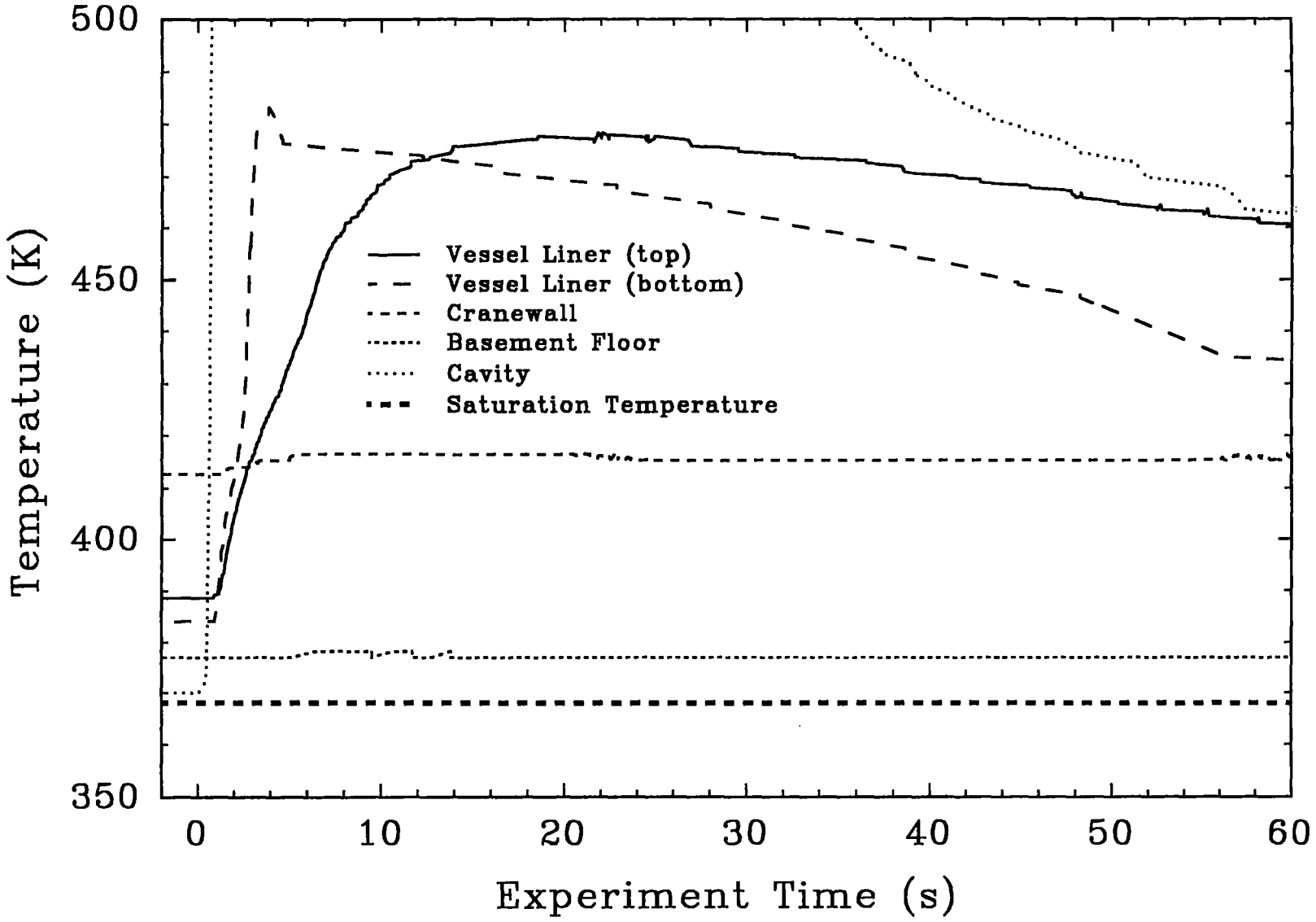

Figure 4.62 Temperature history of the CTTF vessel liner, cranewall, basement floor, and cavity compared to saturation temperature in the IET−10 experiment.

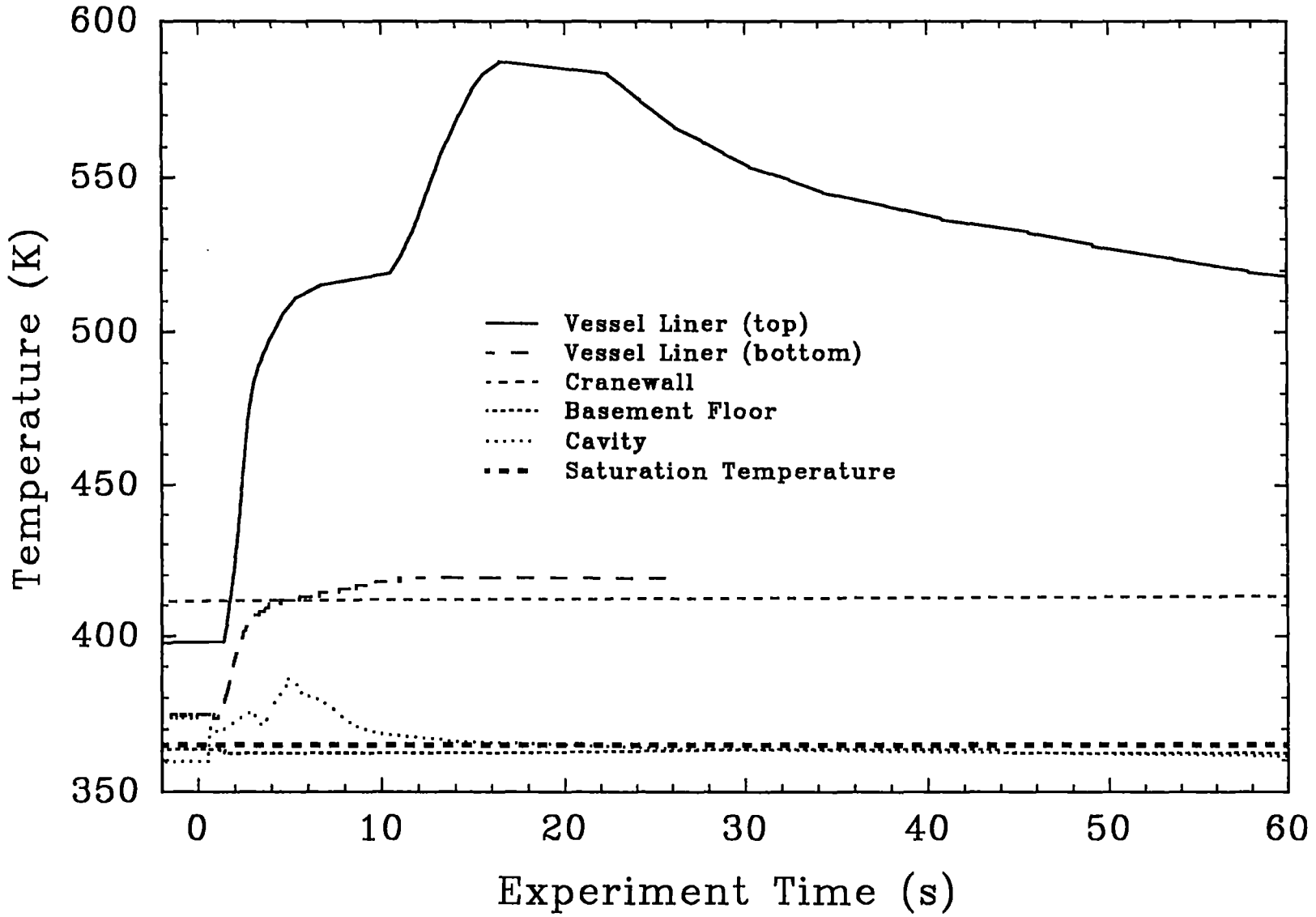

Figure 4.63 Temperature history of the CTTF vessel liner, cranewall, basement floor, and cavity compared to saturation temperature in the IET−11 experiment.

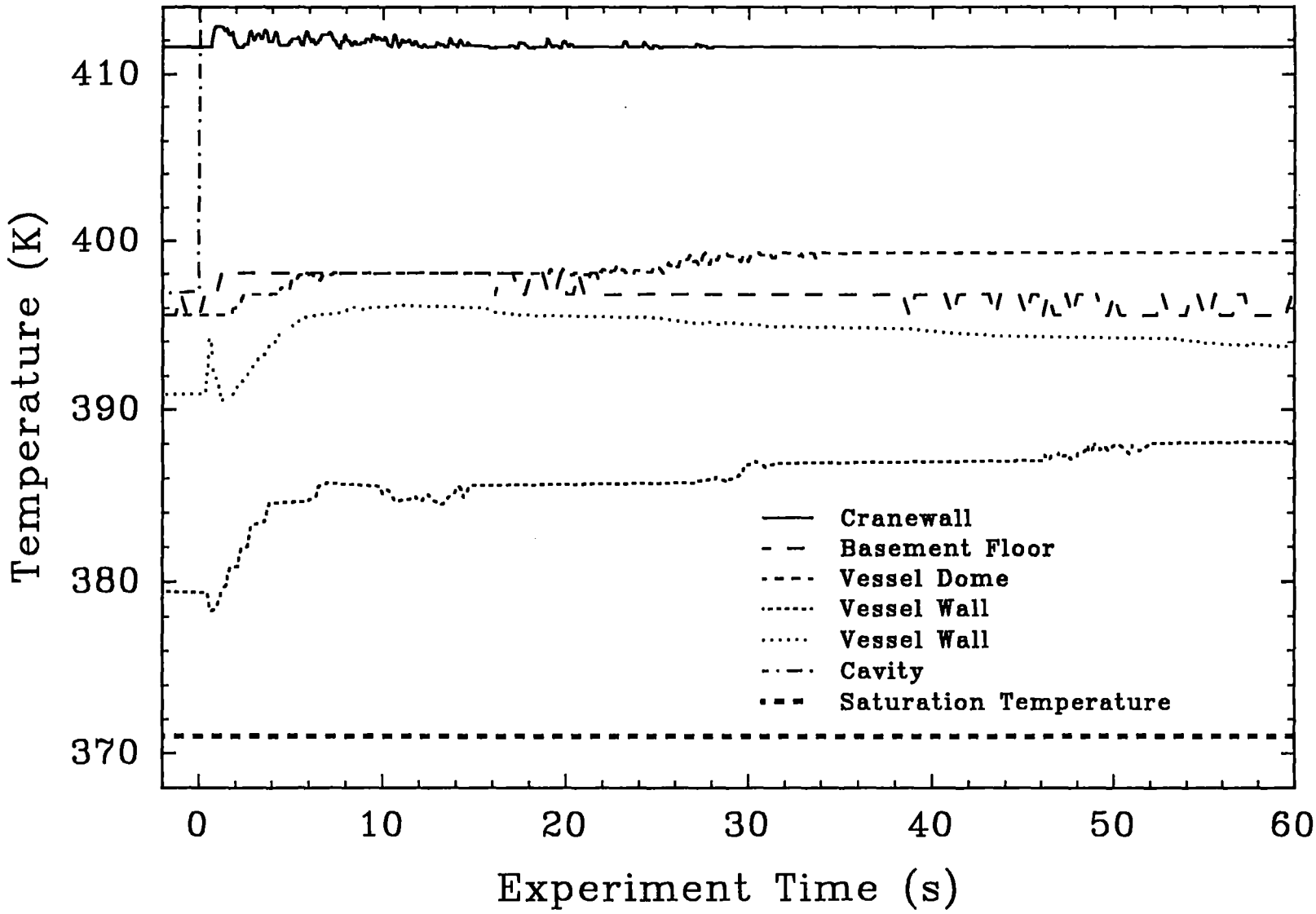

Figure 4.64 Temperature histories of the Surtsey vessel dome and walls, the cranewall, the basement floor, and the cavity compared to saturation temperature in the IET−12 experiment.

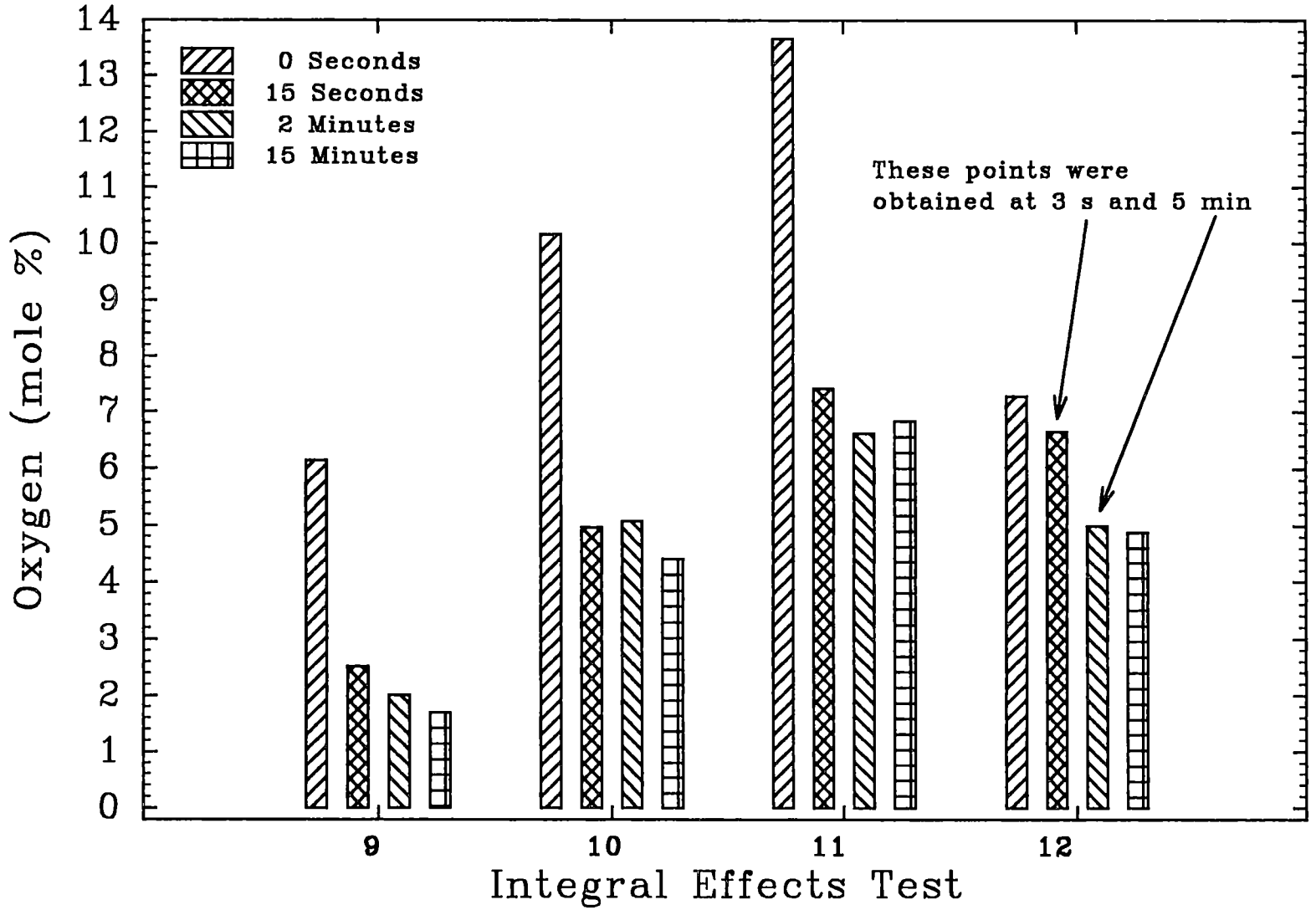

Figure 4.65 Comparison of the oxygen concentrations measured in the Surry IET experiments.

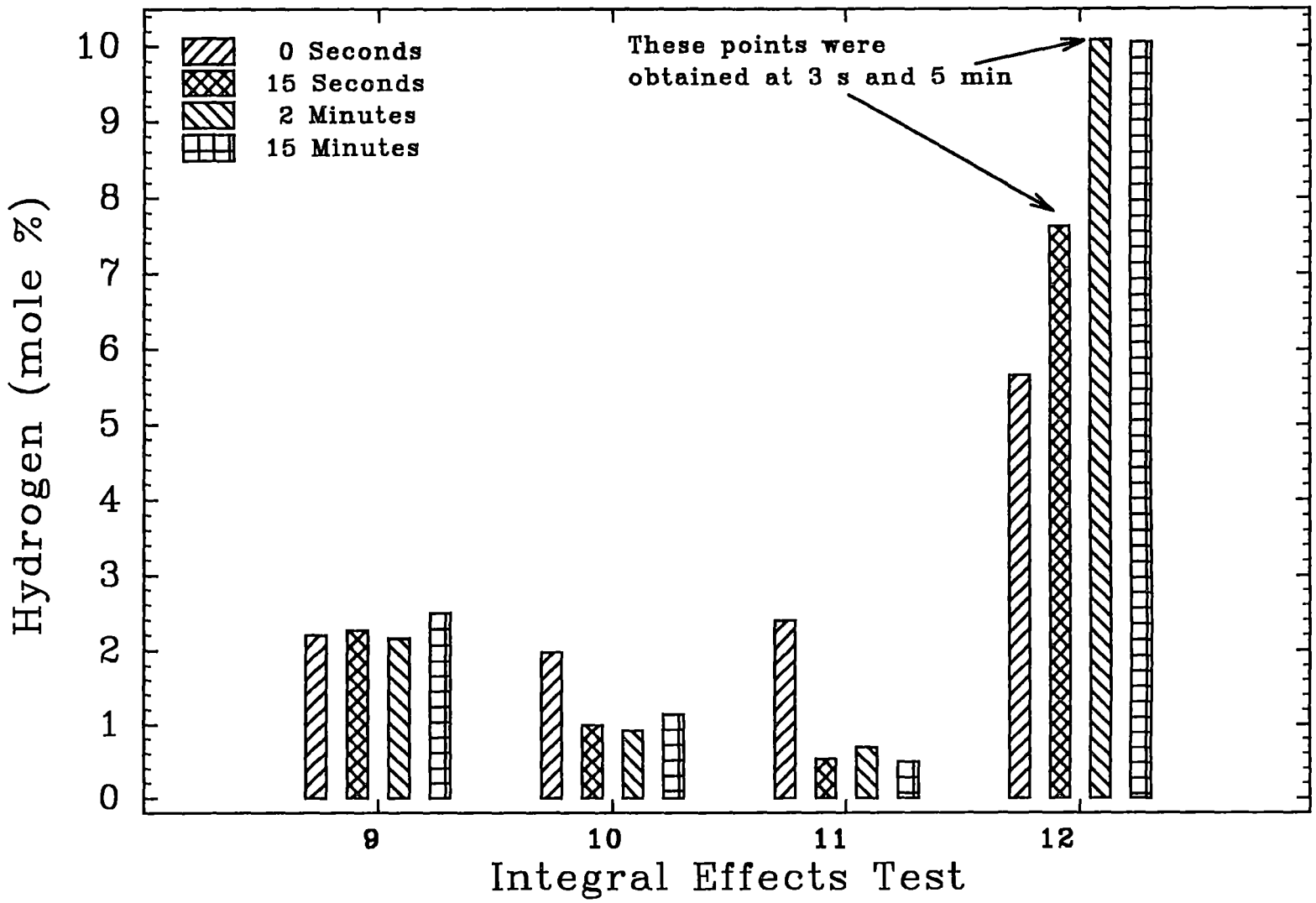

Figure 4.66 Comparison of the hydrogen concentrations measured in the Surry IET experiments.

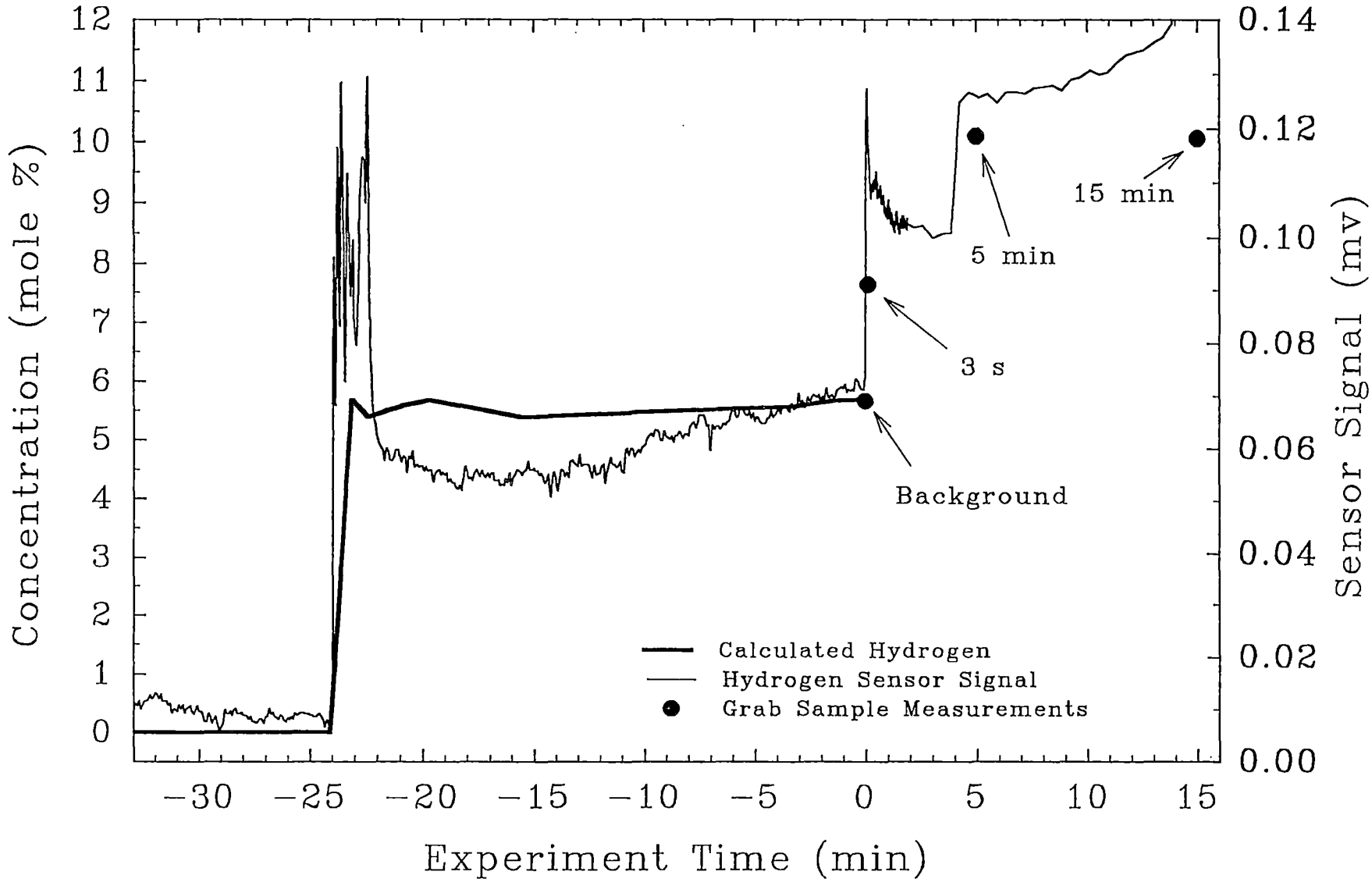

Figure 4.67 Hydrogen sensor signal compared to calculated and measured values of hydrogen in the IET−12 experiment.

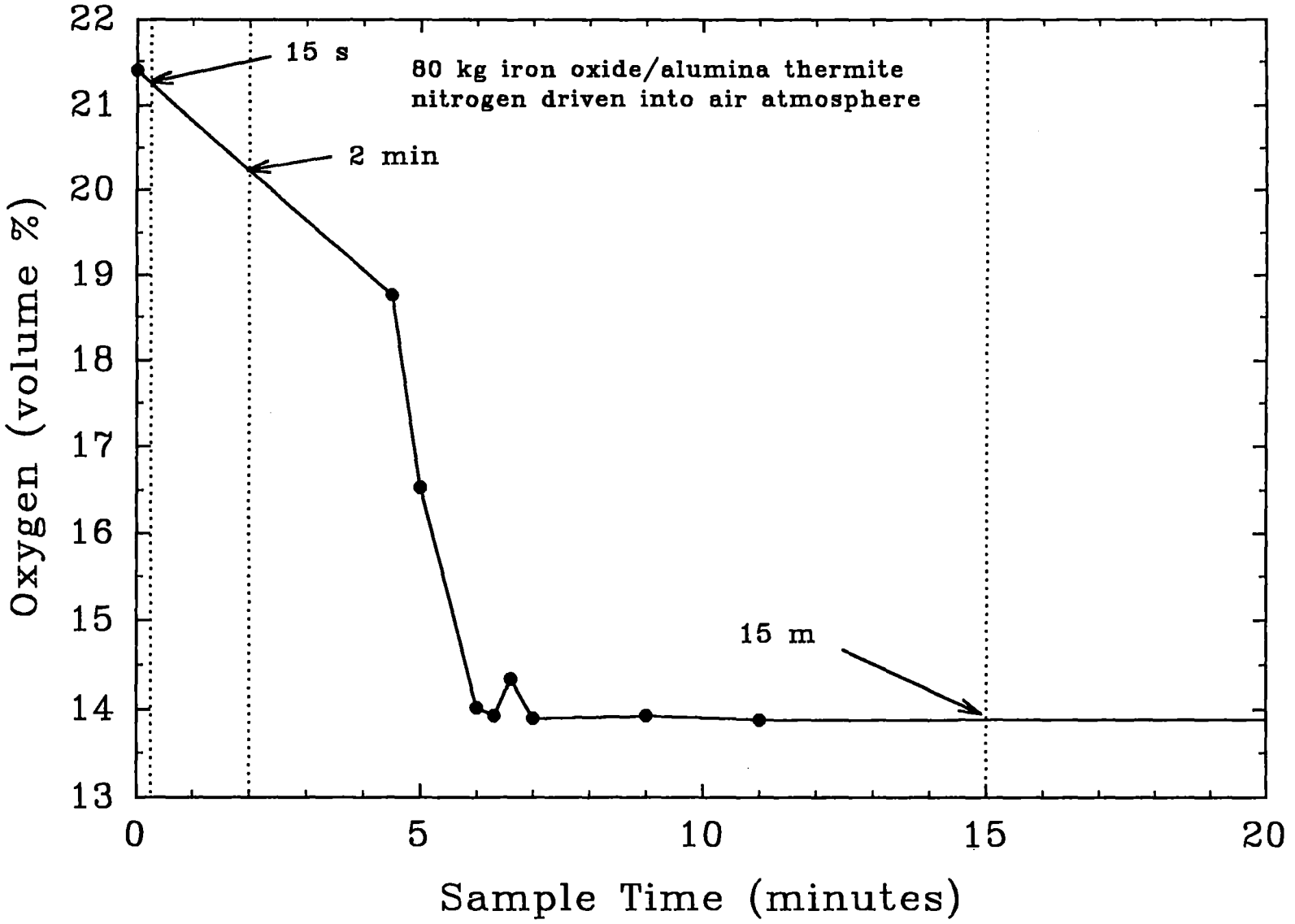

Figure 4.68 Oxygen depletion by reaction with metallic debris in DCH-3.

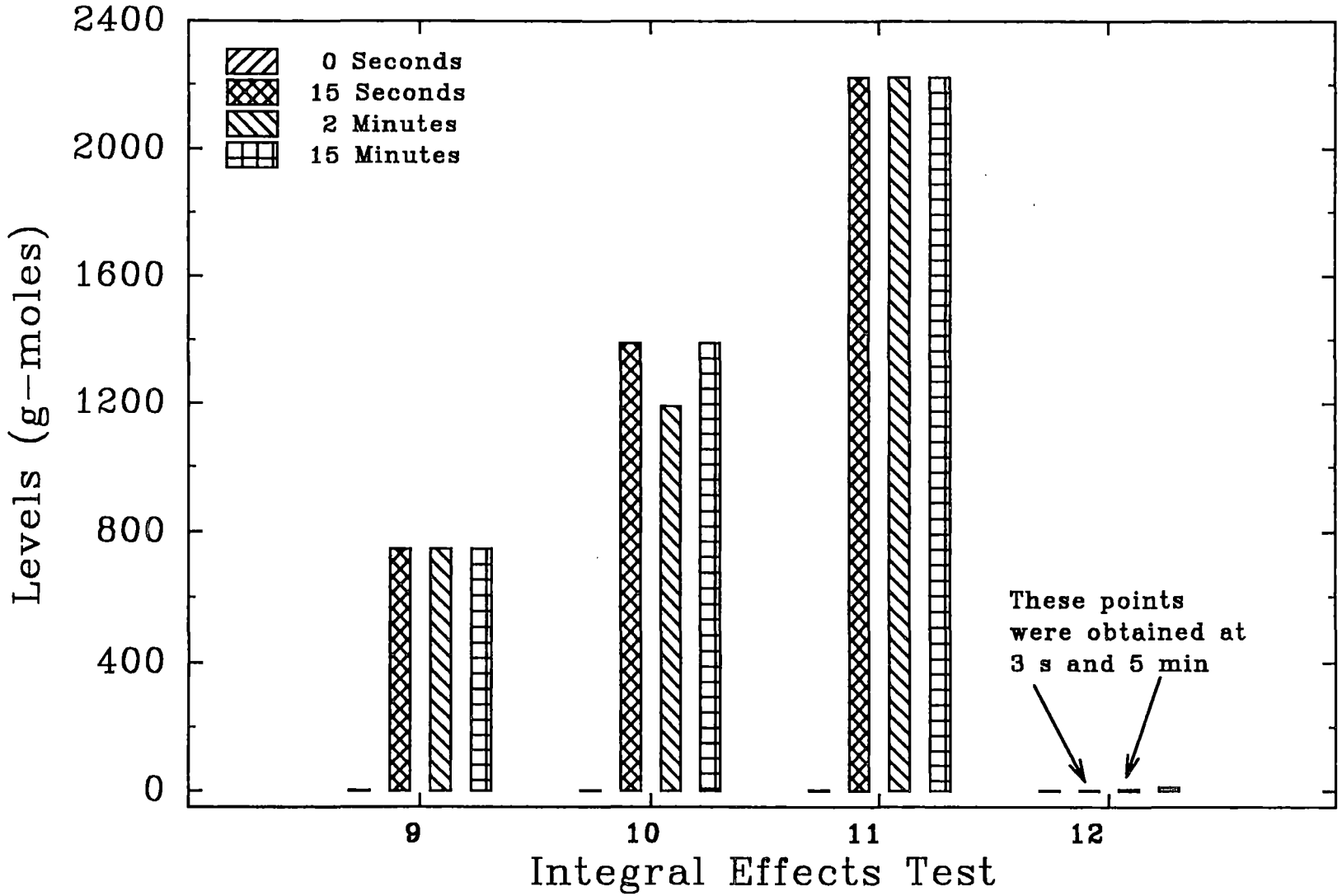

Figure 4.69 Comparison of the hydrogen combustion in the Surry IET experiments.

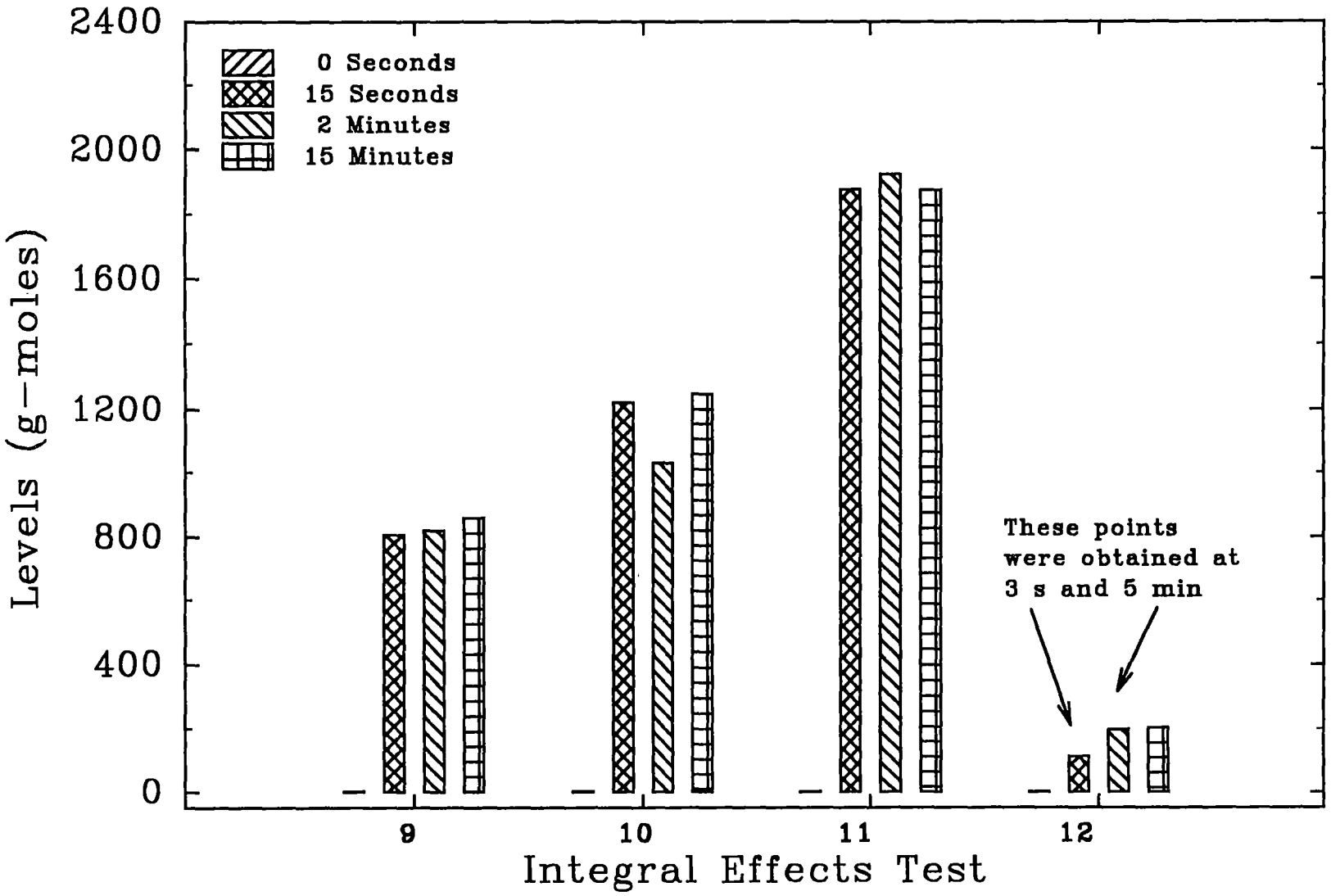

Figure 4.70 Comparison of the hydrogen production in the Surry IET experiments.

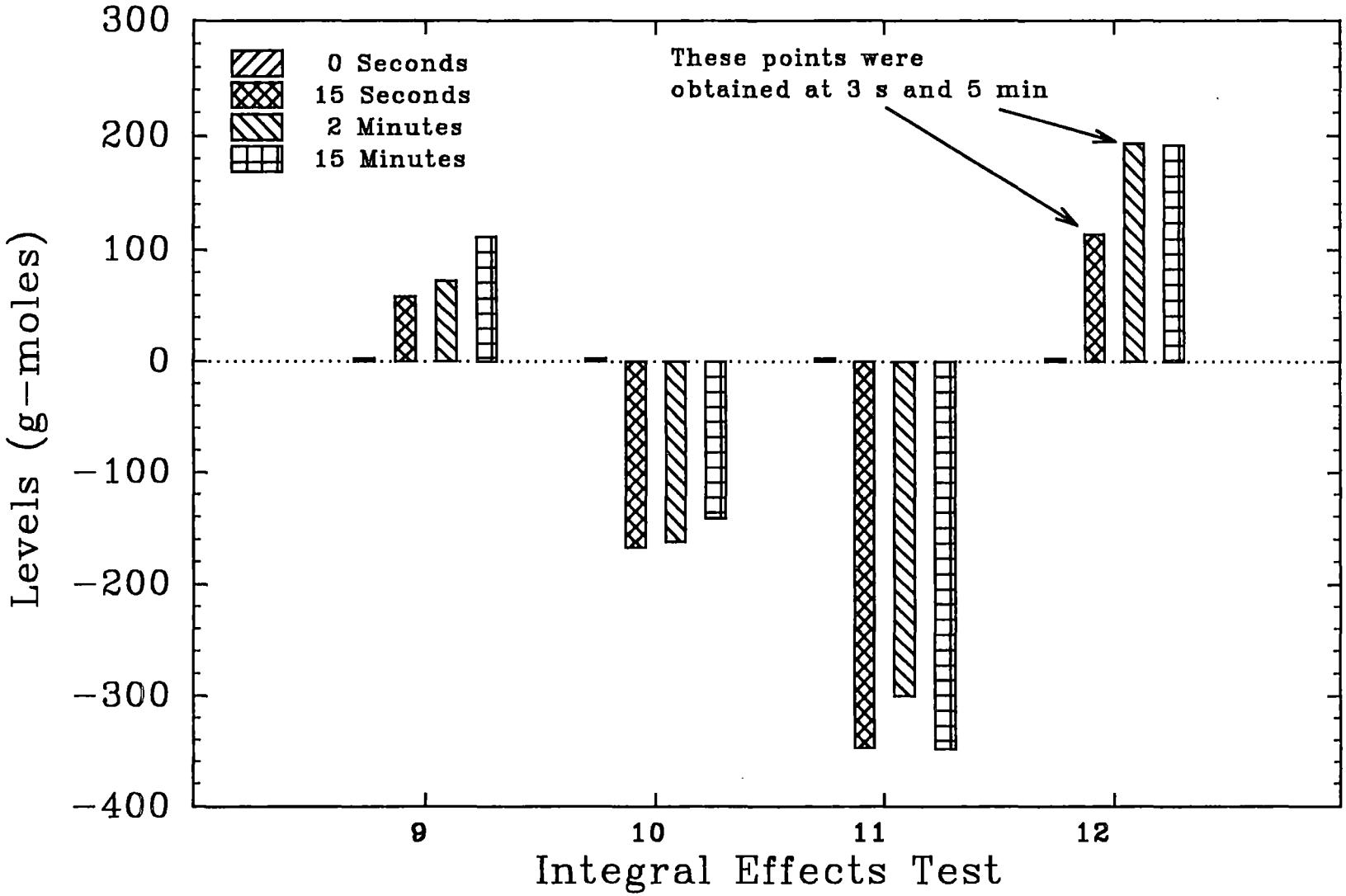

Figure 4.71 Net difference between production and combustion of hydrogen in the Surry IET experiments.

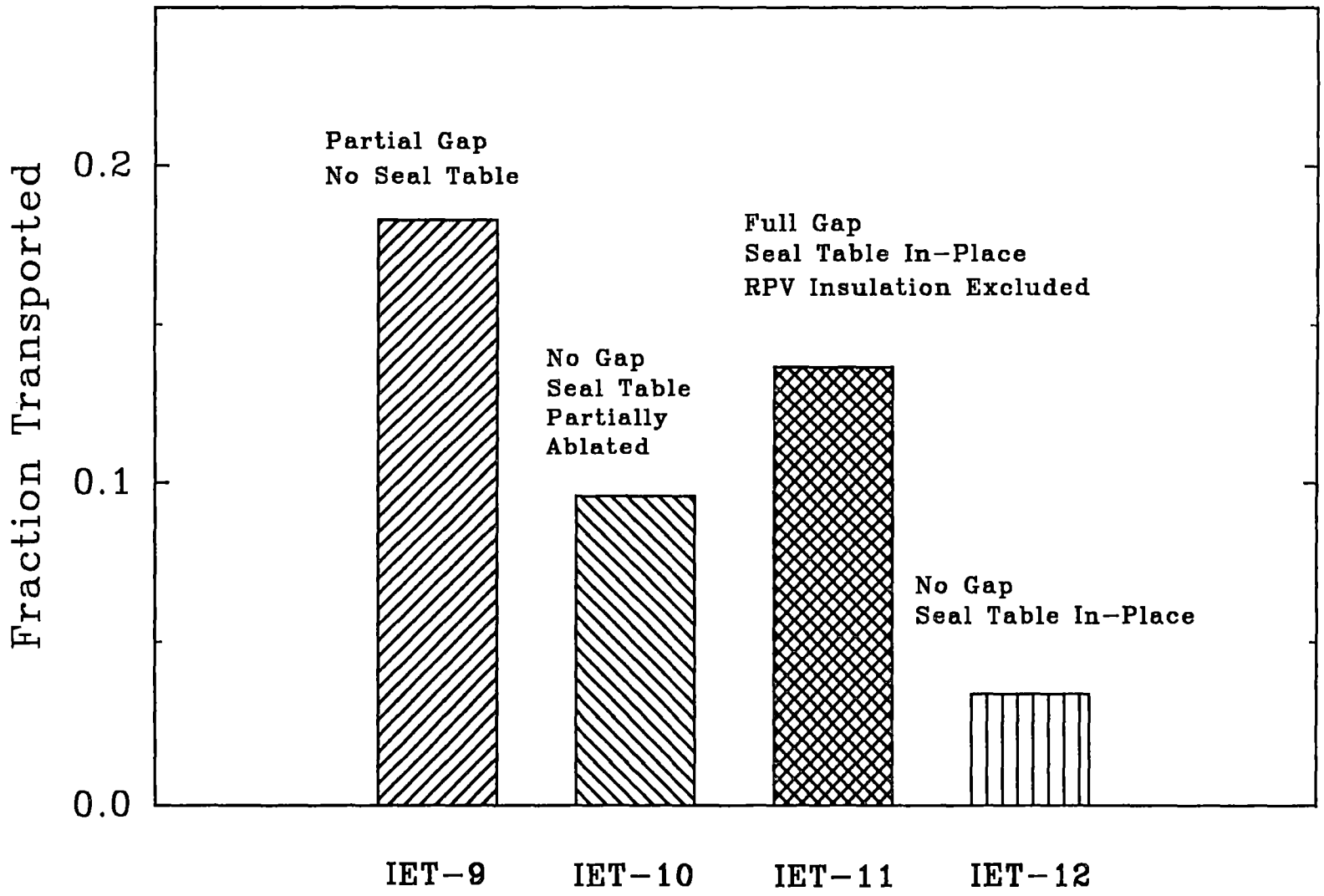

Figure 4.72 Comparison of the transport fraction for thermite to the dome in the Surry IET experiments.

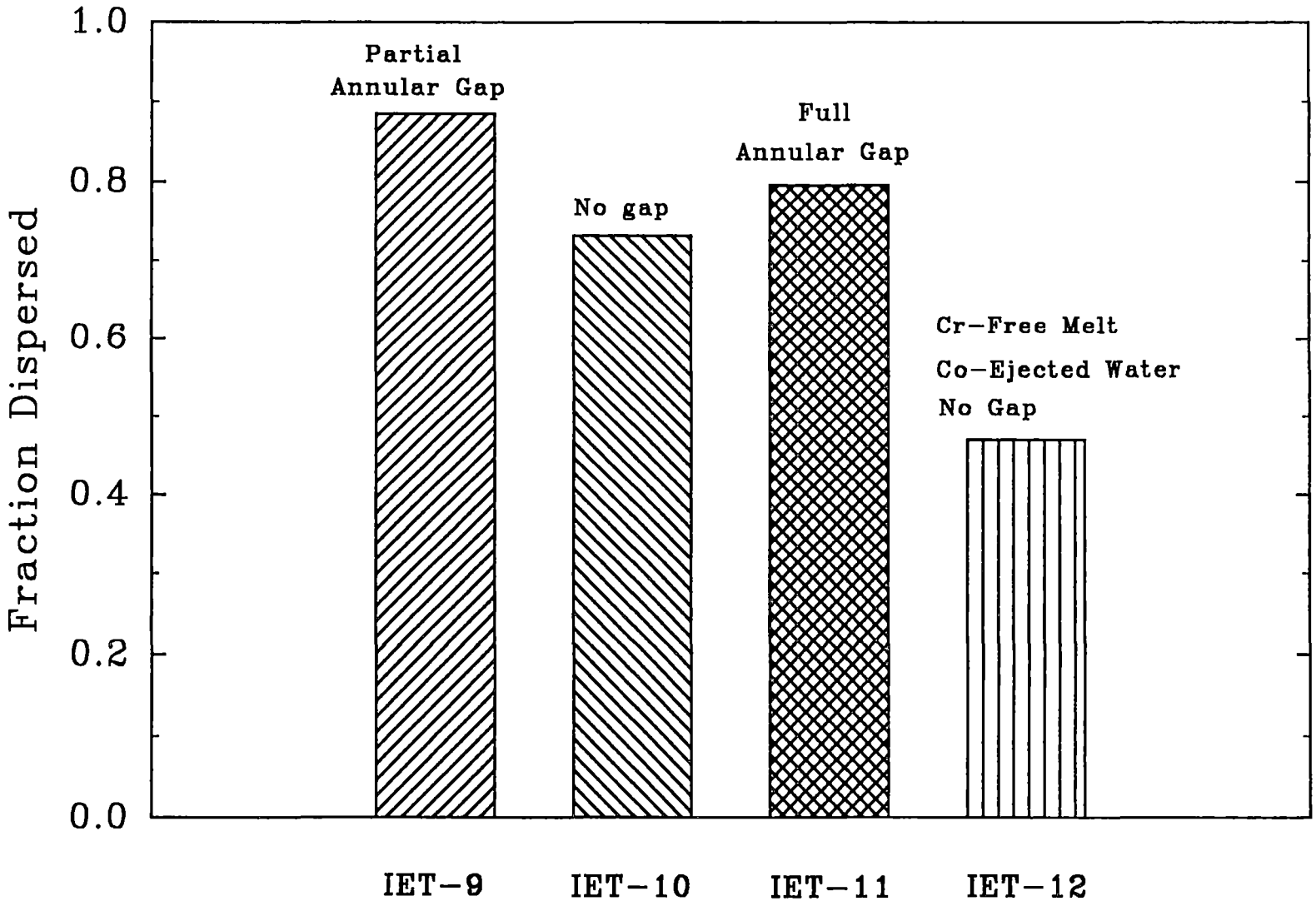

Figure 4.73 Comparison of the debris dispersal from the cavity in the Surry IET experiments.

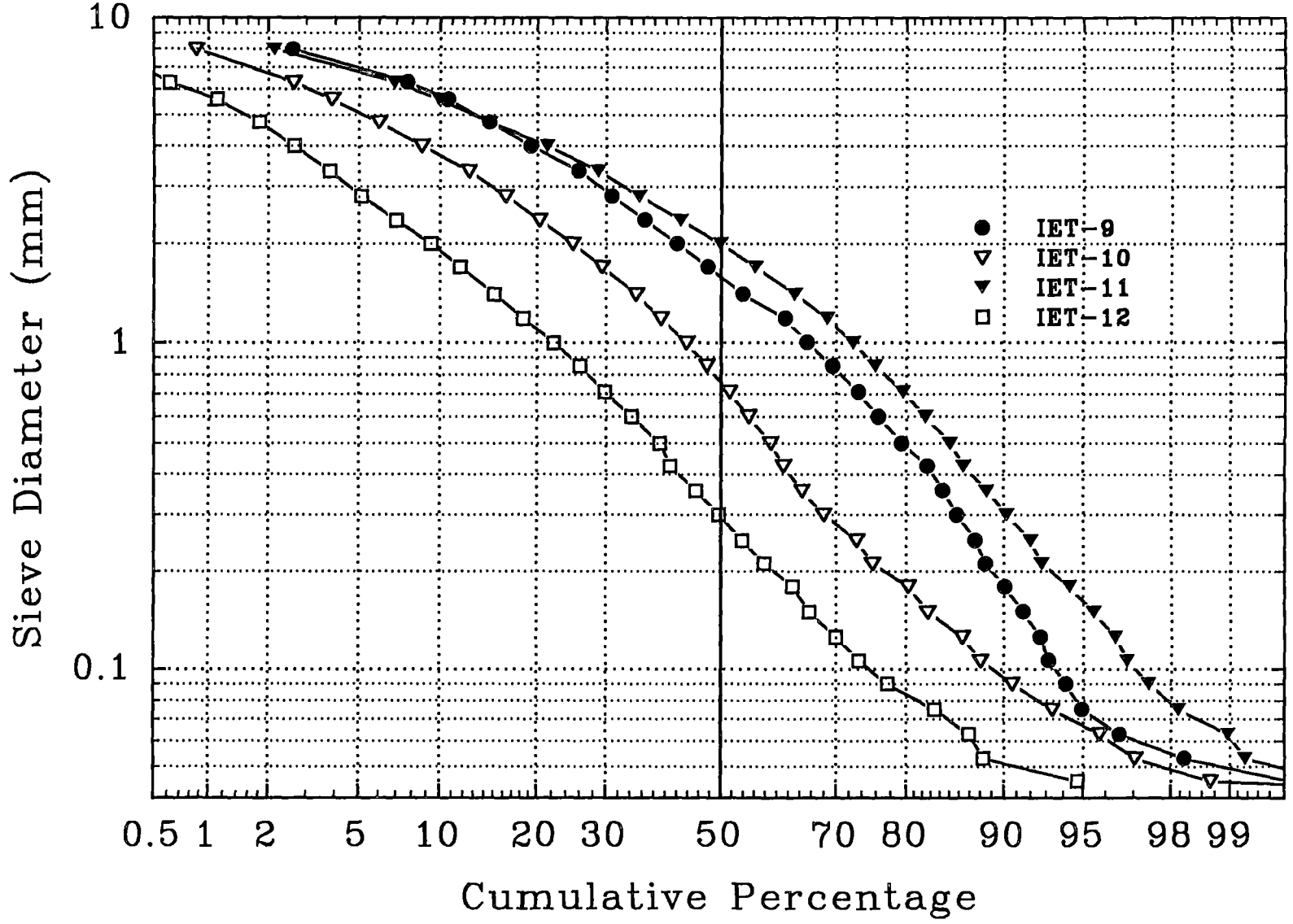

Figure 4.74 Posttest sieve analysis of debris recovered from outside of the subcompartment structures in the Surry IET experiments.

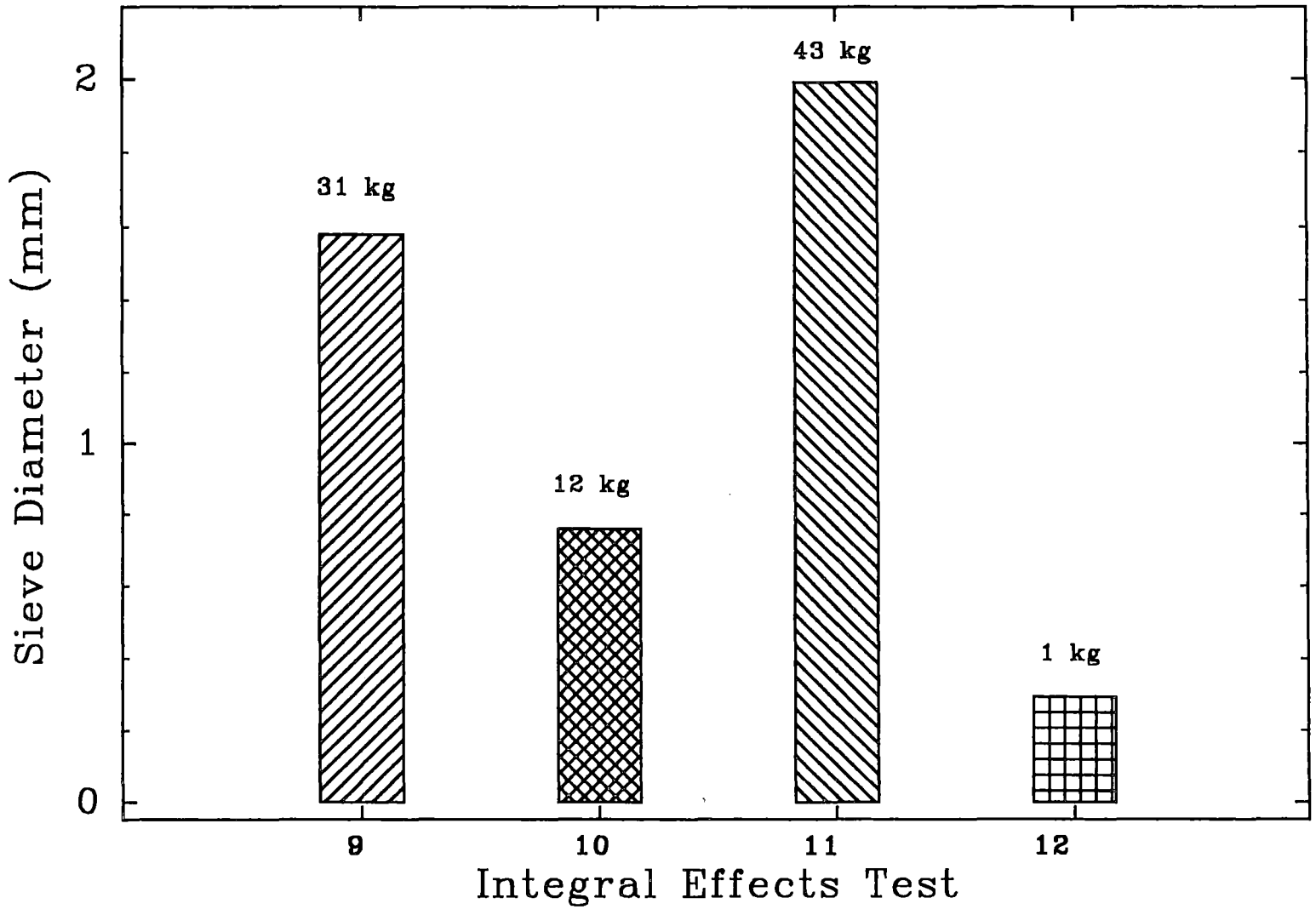

Figure 4.75 Comparison of the sieve mass median diameter for debris recovered from outside of the subcompartment structures in the Surry IET experiments.

5.0 Summary

The Surry Integral Effects Test (IET) series was conducted at the Containment Technology Test Facility and in the Surtsey vessel to investigate several unresolved DCH phenomenological issues: (1) the effect of a prototypic steam/air/H_2 atmosphere on the amount of hydrogen combustion in a HPME scenario, (2) the effect of higher driving pressures on DCH loads, (3) the effect of an annular gap between the RPV and the reactor support skirt, and (4) the effect of Surry subcompartment structures on debris distribution and containment loads. A summary of the results of the Surry IET tests is presented in Table 5.1.

High-temperature, chemically reactive melt is ejected by high-pressure steam into scaled models of the primary structures of the Surry plant. Debris was entrained by the steam blowdown into a containment model where specific phenomena, such as the effect of subcompartment structures, prototypic atmospheres, and hydrogen generation and combustion, were studied.

The experiments were conducted to investigate DCH phenomena at large-scale using a scale model of the Surry NPP. Scale models of the Surry reactor pressure vessel, RPV metal reflective insulation, reactor support skirt and missile shield, biological shield wall, cavity, instrument tunnel, residual heat removal platform and heat exchangers, seal table room and seal table, operating deck, and crane wall were constructed inside a 1:6 scale model of the Surry reactor containment building (CTTF). A 1:10 scale model was also constructed and placed inside a 1:10 scale containment (Surtsey vessel). The corium melt simulant in the 1:6 scale tests was a 158-kg charge of iron/alumina/chromium thermite. The corium melt simulant in the 1:10 scale test was a 30-kg charge of iron/alumina thermite that contained no chromium. The containment vessel was initially heated above saturation temperature, and then pressurized with a mixture of steam, air, and H_2. High-pressure, superheated steam was used to eject the charge of molten thermite into the containment vessel.

Major conclusions for the Surry IET experiments are summarized below.

1. **Pressure and temperature measurements indicated that much of the generated hydrogen burned as gas was pushed out of the subcompartment structures.**

   This was confirmed by analyses of vessel background and posttest gas samples. Experimental results suggest that the hot jets of hydrogen produced by debris oxidation in the cavity and subcompartment burned as a diffusion flame in the dome.

2. **The hydrogen combustion contributed significantly to containment pressurization.**

   In IET-9, IET-10, and IET-11, $\approx$702-747 g·moles, $\approx$1030-1389 g·moles, and $\approx$1890-2223 g·moles of hydrogen burned by 15 seconds, respectively. This resulted in peak pressures increases in the CTTF vessel of 0.283 MPa, 0.326 MPa, and 0.430 MPa for the respective experiments.

   The TCE model was used to estimate the ΔP due to hydrogen combustion alone. By "turning off" hydrogen combustion, the ΔP due to accumulator blowdown, debris/gas heat transfer, and debris oxidation could be estimated using initial conditions and posttest results. Subtracting this ΔP from the measured peak pressure increase gives the estimated peak pressure increase due to hydrogen combustion alone: 0.149 MPa in IET-9, 0.196 MPa in IET-10, and 0.273 MPa in IET-11.

3. **Hydrogen combustion, and correspondingly, peak containment pressures clearly decreased with increasing steam concentrations and decreasing oxygen concentrations.**

The background steam concentration was lowered in the three successive 1:6 scale experiments; the initial steam concentrations were 67% in IET-9, 48% in IET-10, and 32% in IET-11. Correspondingly, the initial oxygen concentrations were 6% in IET-9, 10% in IET-10, and 14% in IET-11.

4. **A significant amount of preexisting hydrogen burned in IET-11.**

The difference between production and combustion in the IET-11 test indicated that 332-347 g·moles of preexisting hydrogen (out of a total of 450 g·moles) burned by 15 s. All of the produced hydrogen burned; thus, 95% of the total available hydrogen had burned by 15 s. It appears that significant combustion of preexisting hydrogen occurred in the containment vessel, which produced very high temperatures in the upper dome ($\approx$1500-1600 K). The 32% steam concentration did not inert the atmosphere.

5. **Not all of the hydrogen burned on a DCH time scale.**

Calculations using the two-cell equilibrium model indicate that the amounts of hydrogen that burned at t = 15 s should have produced higher peak containment pressures than were measured at t = 3 s; this disparity may mean that the hydrogen recombined on a time scale too long to have an impact on peak pressures. There is also a possibility of mitigating effects (heat transfer) occurring in parallel with energy release (H_2 combustion) on comparable time scales.

6. **The open RPV annular gap can increase debris transport to the upper dome; the presence of a seal table can decrease debris transport.**

In IET-9, there was a relatively small annular gap between the RPV and the reactor support skirt (0.012 m^2) which provided $\approx$5.6% of the total flow area out of the cavity. This opening (along with the seal table opening) resulted in significant debris dispersal to the upper dome, i.e. 19% of the debris was transported to the upper dome. There was no seal table.

In IET-10, the annular gap between the RPV and the reactor support skirt remained sealed. The seal table, although somewhat ablated and moved away from the seal table room floor opening, remained partially in place and thus reduced flow out of the seal table room. Closure of these pathways significantly reduced debris dispersal to the upper dome, i.e. only 10% of the debris was transported to the upper dome.

In IET-11, the open annular gap represented a significant material transport path to the upper dome; 25% of the total recovered mass was found outside the subcompartments. Compared to IET-9 (19%) and IET-10 (10%), the IET-11 experiment had the largest material transport fraction to the dome of all the large scale IET experiments. However, after adjusting the debris recovery to account for the RPV insulation, only 14% of the molten thermite was transported to the upper dome in IET-11 (even with the open annular gap). The 14% thermite transport represents a lower bound since it assumes that all of the insulation was transported outside subcompartment structures. The seal table, though partially ablated, remained anchored to the seal table room floor and thus reduced flow out of the seal table room.

7. **RPV reflective metal insulation did not plug the annular gap.**

In IET-11, most of the RPV insulation was entrained by the gases that flowed through the annular gap.

8. **The metallic RPV insulation might be an additional source for hydrogen production.**

   More hydrogen was produced in IET-11 than in IET-10. This suggests that the stainless steel insulation can be a source of additional hydrogen. The reflective metal insulation construction approximately preserved the scale on a mass basis (the scale factor was 5.33); therefore, any hydrogen produced should be proportional to the hydrogen production in the plant. The stainless steel insulation is primarily iron and chromium. Simple analyses show that the molten iron was in chemical equilibrium with blowdown steam and probably did not enhance hydrogen production. However, chromium in the insulation could have reacted with steam to produce additional hydrogen that burned in the upper dome.

9. **Approximately 99% ± 1% of the melt in the 1:6 scale model of the RPV bottom head was expelled into the cavity by ≈12 MPa steam under the conditions used in these tests.**

10. **Approximately 81% ± 8% of the melt in the 1:6 scale reactor cavity was dispersed into the CTTF vessel.**

11. **Approximately 17% ± 4% of the melt dispersed into the 1:6 scale CTTF vessel was found outside the subcompartment structures.**

12. **Co-ejected water in the blowdown steam and/or reduced reactive metal content in the molten debris may significantly reduce DCH.**

In the IET-12 experiment, there was 47% dispersal of molten debris from the cavity, which was less than the 73-89% dispersal measured in the 1:6 scale tests (IET-9, IET-10, and IET-11). There are two potential explanations for the enhanced retention in the cavity: (1) entrained water from the steam accumulator tank that was co-ejected with the melt simulant, and (2) the absence of chromium metal in the melt simulant. Simple calculations show that it is possible for either mechanism, acting alone, to have resulted in the significantly reduced debris dispersal and containment loads measured in IET-12.

In the IET-12 experiment, water was co-ejected with the blowdown steam. The accumulator system design caused water to collect in the bottom head. Accumulator wall temperatures indicated the presence of boiling water in the bottom head and some of this water was co-ejected with the blowdown steam. We believe that co-ejected water might be a major mitigator of DCH loads in a HPME scenario.

The lack of chromium metal in the melt simulant resulted in an absence of chemical energy produced by the reaction between chromium and steam in IET-12. This may have caused increased debris retention in the cavity. The absence of chromium reaction energy needed to keep the melt hot may also have produced a cooler steam/hydrogen jet which, along with the low debris dispersal, may have contributed to the lack of hydrogen combustion.

However, in early tests [Allen et al. 1991a] in which iron/alumina thermite without chromium was entrained by nitrogen blowdown gas, the percentage of debris entrained from the cavity was high, i.e., 75 to 90%. These early tests had no chemical energy from the reaction between metal and steam, and significant debris dispersal from

the cavity was observed. This may mean that the reduced metal content in the melt was not the dominant phenomenon that caused increased cavity retention in IET-12.

Hydrogen and oxygen measurements indicated that little volumetric combustion occurred in IET-12; this was confirmed by pressure and temperature measurements. Previous experimental results suggest that the hot jets of hydrogen produced by debris oxidation in the cavity and subcompartment burned as a diffusion flame in the dome. The 58% initial steam concentration in IET-12 should not have inerted the combustion of DCH-produced hydrogen. The IET-12 experiment may have provided experimental evidence that co-ejected water or reduced reactive metals in the molten debris can significantly mitigate DCH.

Table 5.1 Results from the Surry DCH experiments

	IET-9	IET-10	IET-11	IET-12
Ablated hole diameter (cm)	7.4	9.8	7.6	5.6
Final annular gap (m^2)	0.012	0.0	0.036	0.0
Fraction of debris recovered outside structures	0.234	0.133	0.292[§]	0.046
Thermite transport fraction (to dome)	0.183	0.096	0.137*	0.034
ΔP due to the HPME (MPa)	0.283	0.326	0.430	0.198
Peak bulk gas temperature in dome (K)	922	869	1154	590
Moles of preexisting combustible gas (g • moles)	262	375	450	139
Moles of combustible gas produced at 15 s (g • moles)	806 (786)[£]	1222 (1143)	1876 (1550)	203[¶] (227)
Moles of combustible gas burned at 15 s (g • moles)	747 (710)	1389 (1260)	2223 (1882)	11[¶] (60)
Net difference between production and combustion at 15 s (g • moles)	59 (76)	-167 (-117)	-347 (-332)	192[¶] (167)
Fraction of available combustible gas that burned (N_{burn} / (N_{pre} + N_{prod}))	0.72 (0.71)	0.89 (0.83)	0.96 (0.94)	0.03 (0.16)

[§] The fraction of debris recovered outside structures was calculated using the mass recovered outside structures/the initial thermite charge (- 29 kg for the RPV insulation in IET-11).

* The thermite transport fraction was determined by reducing the amount of material recovered outside the subcompartment by the mass of the RPV insulation (29 kg), due to the RPV reflective metal insulation representing such a large contaminant.

[¶] The IET-12 values were calculated using the gas grab measurements obtained at 15 min.

[£] The hydrogen amounts shown in parenthesis were based on the nitrogen-ratio analysis method.

6.0 References

Allen, M. D., R. T. Nichols and M. Pilch, June 1990, A Demonstration Experiment of Steam-Driven High-Pressure Melt Ejection: The HIPS-10S Test, NUREG/CR-5373, SAND89-1135, Sandia National Laboratories, Albuquerque, NM.

Allen, M. D., M. Pilch, R. T. Nichols, J. E. Brockmann, D. W. Sweet and W. W. Tarbell, Aug. 1991a, Experimental Results of Direct Containment Heating by High-Pressure Melt Ejection into the Surtsey Vessel: The DCH-3 and DCH-4 Tests, SAND90-2138, Sandia National Laboratories, Albuquerque, NM.

Allen, M. D., M. Pilch, R. O. Griffith and R. T. Nichols, Mar. 1992a, Experiments to Investigate the Effect of Water in the Cavity on Direct Containment Heating (DCH) in the Surtsey Test Facility - The WC-1 and WC-2 Tests, SAND91-1173, Sandia National Laboratories, Albuquerque, NM.

Allen, M. D., M. Pilch, R. O. Griffith, D. C. Williams and R. T. Nichols, Mar. 1992b, The Third Integral Effects Test (IET-3) in the Surtsey Test Facility, SAND92-0166, Sandia National Laboratories, Albuquerque, NM.

Allen, M. D., T. K. Blanchat, M. Pilch and R. T. Nichols, Sept. 1992c, The Effects of Condensate Levels of Water on Direct Containment Heating (DCH) in Zion-Like Geometry: The Fourth Integral Effects Test (IET-4) Conducted in the Surtsey Test Facility, SAND92-1241, Sandia National Laboratories, Albuquerque, NM.

Allen, M. D., M. Pilch, R. O. Griffith, R. T. Nichols and T. K. Blanchat, July 1992d, Experiments to Investigate the Effects of 1:10 Scale Zion Structures on Direct Containment Heating (DCH) in the Surtsey Test Facility: The IET-1 and IET-1R Tests, SAND92-0255, Sandia National Laboratories, Albuquerque, NM.

Allen, M. D., T. K. Blanchat, M. Pilch and R. T. Nichols, Nov. 1992e, Experimental Results of an Integral Effects Test in a Zion-Like Geometry to Investigate the Effects of a Classically Inert Atmosphere on Direct Containment Heating: The IET-5 Experiment, SAND92-1623, Sandia National Laboratories, Albuquerque, NM.

Allen, M. D., T. K. Blanchat, M. Pilch and R. T. Nichols, Dec. 1992f, An Integral Effects Test in a Zion-Like Geometry to Investigate the Effects of Preexisting Hydrogen on Direct Containment Heating in the Surtsey test Facility: The IET-6 Experiment, SAND92-1802, Sandia National Laboratories, Albuquerque, NM.

Allen, M. D., T. K. Blanchat, M. Pilch and R. T. Nichols, Dec. 1992g, An Integral Effects Test to Investigate the Effects of Condensate Levels of Water and Preexisting Hydrogen on Direct Containment Heating in the Surtsey Test Facility: The IET-7 Experiment, SAND92-2021, Sandia National Laboratories, Albuquerque, NM.

Allen, M. D., T. K. Blanchat, M. Pilch and R. T. Nichols, Feb. 1993a, Experiments to Investigate the Effects of Fuel/Coolant Interactions on Direct Containment Heating - The IET-8A and IET-8B Experiments, SAND92-2849, Sandia National Laboratories, Albuquerque, NM.

Allen, M. D., M. Pilch,T. K. Blanchat, R. O. Griffith, and R. T. Nichols, Aug. 1993b, Experiments to Investigate Direct Containment Heating Phenomena with Scaled Models of the Zion Nuclear Power Plant in the Surtsey Test Facility, NUREG/CR-6044, SAND93-1049, Sandia National Laboratories, Albuquerque, NM.

Horschel, D. S., Jan. 1992, Experimental Results from Pressure Testing a 1:6 Scale Nuclear Power Plant Containment, NUREG/CR-5121, SAND88-0906.

Kumar, R. K., "Flammability Limits of Hydrogen-Oxygen-Diluent Mixtures," Journal of Fire Sciences, Vol. 3, July/August 1985.

Pilch, M. M., Oct. 1991, "Adiabatic Equilibrium Models for Direct Containment Heating," SAND91-2407C, presented at the 19th Water Reactor Safety Information Meeting, Washington, D.C.

Williams, D. C., September 1992, An Interpretation of the Results of Some Recent Direct Containment Heating (DCH) Experiments in the Surtsey Facility, SAND92-0442C, presented at the NURETH-5 Conference, Salt Lake City, UT.

Zuber et al. 1991, An Integrated Structure and Scaling Methodology for Severe Accident Technical Issue Resolution, NUREG/CR-5809, EGG-2659.

DISTRIBUTION

U. S. Nuclear Regulatory Commission (5)
Office of Nuclear Regulatory Research
Attn: C. Tinkler, NLN-344
R. Lee, NLN-344
A. Rubin, NLN-344
F. Eltawila, NLN-344
B. Sheron, NLS-007
Washington, D.C. 20555

U. S. Nuclear Regulatory Commission (3)
NRC/RES
Attn: E. Beckjord, NLS-007
B. Hardin, NLS-169
T. Speis, NLS-007
Washington, D.C. 20555

U. S. Department of Energy
Office of Nuclear Safety Coordination
Attn: R. W. Barber
Washington, D.C. 20545

U. S. Department of Energy (2)
Albuquerque Operations Office
Attn: C. E. Garcia, Director
For: C. B. Quinn
R. L. Holton
P. O. Box 5400
Albuquerque, NM 87185

Los Alamos National Laboratories
Attn: M. Stevenson
P.O. Box 1663
Los Alamos, NM 87545

Electric Power Research Institute
Attn: A. Michaels
3412 Hillview Avenue
Palo Alto, CA 94303

UCLA
Nuclear Energy Laboratory
Attn: I. Catton
405 Hilgaard Avenue
Los Angeles, CA 90024

Brookhaven National Laboratory (3)
Attn: R. A. Bari
T. Pratt
N. Tutu
130 BNL
Upton, NY 11973

Argonne National Laboratory (4)
Attn: J. Binder
C. Johnson
L. Baker, Jr.
B. Spencer
9700 S. Cass Avenue
Argonne, IL 60439

Fauske and Associates, Inc.
Attn: R. Henry
16W070 West 83rd Street
Burr Ridge, IL 60952

General Electric Company
Nuclear Energy
Attn: F. J. Moody
175 Curtner Avenue
San Jose, CA 95125

Battelle Columbus Laboratory (2)
Attn: R. Denning
J. Gieseke
505 King Avenue
Columbus, OH 43201

Department of Energy
Scientific and Tech. Info. Center
P. O. Box 62
Oak Ridge, TN 37831

Purdue University
School of Nuclear Engineering
Attn: M. Ishii
West Lafayette, IN 47907

University of Wisconsin
Nuclear Engineering Department
Attn: M. L. Corradini
1500 Johnson Drive
Madison, WI 53706

Richard R. Hobbins
2955 North Fish Creek Rd.
P.O. Box 971
Wilson, WY 83014

Battelle Pacific Northwest Laboratory
Attn: M. Freshley
P. O. Box 999
Richland, WA 99352

Professor Agustin Alonso
E.T.S. Ingenieros Industriales
Jost Gutierrez Abascal, 2
28006 Madrid
SPAIN

Jose Angel Martinez
Sub. Emplazamientos y Programas Coop.
CONSEJO DE SEGURIDAD
NUCLEAR
Justo Dorado 11
28040 MADRID
SPAIN

Juan Bagues
Consejo de Seguridad Nuckan
SOR Angela de la Cruz No 3
Madrid 28056
SPAIN

Gesellschaft fur Reaktorsicherheit (GRS)
Postfach 101650
Glockengrasse 2
5000 Koeln 1
GERMANY

Technische Universitat Munchen
Attn: Professor H. Karwat
8046 Garching, Forschungagelande
Munich
GERMANY

Siegfried Hagen
Kernforschungszentrum Karlsruhe
P.O. Box 3640
D-7500 Karlsruhe 1
GERMANY

Kernforschungszentrum Karlsruhe (2)
Attn: P. Hofmann
B. Kuczera
Postfach 3640
75 Karlsruhe
GERMANY

Klaus Trambauer
Gesellschaft Fuer Reaktorsicherheit
Forschungsgelande
D-8046 Garching
GERMANY

UKAEA (3)
Attn: D. Sweet
S. Kinnersly 203/A32
D. Williams 210/A32
Winfrith, Dorchester
Dorset DT2 8DH
UNITED KINGDOM

UKAEA Culham Laboratory
Attn: B. D. Turland E5.157
Abingdon
Oxfordshire OX14 3DB
UNITED KINGDOM

UKAEA
Reactor Development Division
Attn: T. Butland
Winfrith, Dorchester
Dorset DT2 8DH
UNITED KINGDOM

M. R. Hayns
AEA Reactor Services
B329
Harwell
Didcot
Oxfordshire OX11 ORA
UNITED KINGDOM

Simon J. Board
CEGB National Power
Barnett Way
Barnwood, Gloucestershire GL4 7RS
ENGLAND

Nigel E. Buttery
Central Elect. Gen. Board, Booths Hall
Chelford Road, Knutsford
Cheshire WA16 8QG
ENGLAND

Thermodynamics & Rad. Physics, TP-650 (2)
Attn: P. Fasoli-Stella
A. V. Jones
CEC Joint Research Center, Ispra
I-21020 Ispra (Varese)
ITALY

Dr. K. J. Brinkman
Reactor Centrum Nederland
1755 ZG Petten
THE NETHERLANDS

Mr. H. Bairiot, Chief
Department LWR Fuel
Belgonucleaire
Rue de Champde Mars. 25
B-1050 Brussels
BELGIUM

Japan Atomic Energy Research Institute
Severe Accident Research Laboratory
Attn: N. Yamano
Tokai-mura, Naka-gun, Ibaraki-ken
319-11
JAPAN

Japan Atomic Energy Research Institute
Dept. of Fuel Safety Research
Attn: Y. Maruyama
Tokai-Mura, Ibaraki-Ken
319-11
JAPAN

J. R. Walker
Atomic Energy Canada, Ltd.
Chalk River, Ontario
CANADA KOJ IJO

Atomic Energy Canada Ltd.
Attn: Vijay I. Nath
Sheridan Park Res. Comm.
Mississauga, Ontario
CANADA L5K 1B2

Oguz Akalin
Ontario Hydro
700 University Avenue
Toronto, Ontario
CANADA M5G 1X6

K. N. (Kannan) Tennankore
Safety Research Division
Whiteshell Nuclear Res. Establishment
Pinawa, Manitoba
CANADA ROE 1LO

L. A. Simpson
Safety Research Division
Whiteshell Nuclear Res. Establishment
Pinawa, Manitoba
CANADA ROE 1LO

M. Jankowski
IAEA
Division of Nuclear Reactor Safety
Wagranesrstrasse 5
P. O. Box 100
A/1400 Vienna
AUSTRIA

Statens Karnkraftinspektion (2)
Attn: L. Hammer
W. Frid
P. O. Box 27106
S-10252 Stockholm
SWEDEN

Studvik Energiteknik AB
Attn: K. Johansson
S-611 82 Nykoping
SWEDEN

Korea Adv Energy Research Inst
Attn: Hee-Dong Kim
P. O. Box 7
Daeduk-Danji
Taejon 305-353
KOREA

Chang K. Park
Korea Atomic Energy Research Institute
Korea Advanced Energy Research Institute
P.O. Box 7, Daeduk Danji
Taejon 305-353
KOREA

Jong In Lee
Severe Accident Assessment Department
Korea Institute of Nuclear Safety
P.O. Box 16, Daeduk-Danji
Daejeon, 305-353
KOREA

POSTECH
Department of Mechanical Engineering
Attn: Moo Hwan Kim
P. O. Box 125
Kyungbuk 790-600
KOREA

Atomic Energy Council
Attn: Yi-Bin Chen
67, Lane 144
Keedling Road, Section 4
Taipei, Taiwan 106
REPUBLIC OF CHINA

Ms. C. Lecomte
CEN FAR
60-68 Av. du G. Leclerc - B.P.6
92265 Fontenay aux Roses cedex
FRANCE

Dr. A. Meyer-Heine
CEN Cadarache
13108 Saint Paul lez Durance
FRANCE

Dr. A. Tattegrain
CEN Cadarache
13108 Saint Paul lez Durance
FRANCE

Dr. G. Hache
CEN Cadarache
13108 Saint Paul lez Durance
FRANCE

Jacques Duco
Centre d'Etudes Nucleaires (IPSN-DAS)
Commissariat a l'Energie Atomique
Boite Postale No. 6
F-92265 Fontenay-aux-Roses Cedex
FRANCE

Maurice Gomolinski
Protection and Nuclear Safety Institute
Commissariat a l'Energie Atomique
Boite Postale No. 6
F-92265 Fontenay-aux-Roses Cedex
FRANCE

Michel Livolant
Inst. de Protection et de Surete Nucl.
Commissariat a l'Energie Atomique
Boite Postale No. 6
F-92265 Fontenay-aux-Roses Cedex
FRANCE

Jorma V. Sandberg
Department of Nuclear Safety
Finnish Center Radiation & Nucl. Safety
P.O. Box 268
SF-00101 Helsinki
FINLAND

S. Chakraborty
Swiss Federal Nucl. Safety Inspectorate
CH-5303 Wurenlingen
SWITZERLAND

J. Peter Hosemann
Light Water Reactor Safety Program
Paul Scherrer Institute
CH-5232 Villigen PSI
SWITZERLAND

Vladimir Asmolov
I.V. Kurchatov Institute of Atomic Energy
Moscow 123182
Kurchatov Square
RUSSIA

Lajos Voross
Division of Nuclear & Power Engineering
Institute for Electric Power Research
POB 233
H-1368 Budapest
HUNGARY

Gianni Petrangeli
Nuclear Safety & Health Protection
Ente Nazionale Energie Altern ENEA/DISP
Via Vitaliano Brancati, 48
I-00144 Rome
ITALY

Giovanni Saponaro
Natl. Committee for R&D of Nuclear Energy
Ente Nazionale Energie Altern ENEA/DISP
Via Vitaliano Brancati, 48
I-00144 Rome
ITALY

Jun Sugimoto
Japan Atomic Energy Research Institute
Tokai-mura, Naka-gun
Ibaraki-ken, 319-11
JAPAN

Makoto Naito
Nuclear Safety Engineering Section
Toshiba Corporation
8, Shinsugita-Cho, Isogo-Ku
Yokohama 235
JAPAN

Kenji Takumi
Systems Safety Department
Nuclear Power Engineering Corporation
Fujitakanko Building
17-1, 3-Chome, Toranomon, Minato-Ku
Tokyo, 105
JAPAN

Povilas Vaisnys
Lithuanian State Nuclear Safety Inspec.
VATESI
Gediminis Prospect 36
Vilnius 2000
LITHUANIA

Jozef Misak
Nucl. Regulatory Authority, Slovak Rep.
P.O. Box 24
820 07 Bratislava 27
SLOVAK REPUBLIC

Borut Mavko
P.O. Box 100
Institut Jozef Stefan
Jamova 39
61111 Ljubljana
SLOVENIA

B. Raj Sehgal
Royal Institute of Technology
Nuclear Power Safety
S-100 44 Stockholm
SWEDEN

Peter M. Stoop
Risk and Safety Section
Netherlands Energy Research Foundation
P.O. Box 1
1755 ZG Petten
THE NETHERLANDS

Yanko Yanev
Comm. on the Use of Atomic Energy for
Peaceful Purposes - 69 Shipchenski
Prokhod Blvd., 1574, Sofia
BULGARIA

Miguel Medina Vaillard
Com. Nacional de Seguridad Nucl. Salvag
Colonia Narvarte Delegation B. Juarez
Dr. Abrragan #779
C.P. 03020
MEXICO

B. Kujal
Nuclear Research Institute plc
CS-250 68 Rez
CZECH SLOVAK FEDERAL REPUBLIC
(CSFR)

SANDIA DISTRIBUTION;
MS0338 D. W. Schaeffer (1703)
MS0736 N. R. Ortiz (6400)
MS0744 W. A. von Riesemann (6403)
MS0744 D. A. Powers (6404)
MS0748 F. T. Harper (6413)
MS0742 J. E. Kelly (6414)
MS0745 S. L. Thompson (6418)
MS0745 R. M. Summers (6418)
MS1137 M. D. Allen (5) (6422)
MS1137 T. K. Blanchat (5) (6422)
MS1137 M. Pilch (2) (6422)
MS1137 R. T. Nichols (6422)
MS1139 K. O. Reil (6423)
MS0739 K. E. Washington (6429)
MS0739 R. O. Griffith (6429)
MS0739 F. J. Davis (6429)
MS0899 Technical Library (5) (7141)
MS0619 Technical Publications (7151)
MS0100 Document Processing (7613-2)
for DOE-OSTI (10)
MS9018 Central Technical Files
(8523-2)

NRC FORM 335 (2-89) NRCM 1102, 3201, 3202

U.S. NUCLEAR REGULATORY COMMISSION

BIBLIOGRAPHIC DATA SHEET

(See instructions on the reverse)

1. REPORT NUMBER (Assigned by NRC, Add Vol., Supp., Rev., and Addendum Numbers, if any.)
NUREG/CR-6152
SAND93-2519

2. TITLE AND SUBTITLE
Experiments to Investigate Direct Containment Heating Phenomena With Scaled Models of the Surry Nuclear Power Plant

3. DATE REPORT PUBLISHED
MONTH: June
YEAR: 1994

4. FIN OR GRANT NUMBER
A1406

5. AUTHOR(S)
T.K. Blanchat, M.D. Allen, M. M. Pilch, R. T. Nichols*

6. TYPE OF REPORT
Technical

7. PERIOD COVERED *(Inclusive Dates)*

8. PERFORMING ORGANIZATION – NAME AND ADDRESS *(If NRC, provide Division, Office or Region, U.S. Nuclear Regulatory Commission, and mailing address; if contractor, provide name and mailing address.)*
Sandia National Laboratories
Albuquerque, NM 87185-1137

*Ktech Corporation
901 Pennsylvania NE
Albuquerque, NM 87110

9. SPONSORING ORGANIZATION – NAME AND ADDRESS *(If NRC, type "Same as above"; if contractor, provide NRC Division, Office or Region, U.S. Nuclear Regulatory Commission, and mailing address.)*
Division of Systems Research
Office of Nuclear Regulatory Research
U.S. Nuclear Regulatory Commission
Washington, DC 20555-0001

10. SUPPLEMENTARY NOTES

11. ABSTRACT *(200 words or less)*

The Containment Technology Test Facility (CTTF) and the Surtsey Test Facility at Sandia National Laboratories are used to perform scaled experiments that simulate High Pressure Melt Ejection accidents in a nuclear power plant (NPP). These experiments are designed to investigate the effects of direct containment heating (DCH) phenomena on the containment load. High-temperature, chemically reactive melt (thermite) is ejected by high-pressure steam into a scale model of a reactor cavity. Debris is entrained by the steam blowdown into a containment model where specific phenomena, such as the effect of subcompartment structures, prototypic air/steam/hydrogen atmospheres, and hydrogen generation and combustion, can be studied. Four Integral Effects Tests (IETs) have been performed with scale models of the Surry NPP to investigate DCH phenomena. The 1/6th scale Integral Effects Tests (IET-9, IET-10, and IET-11) were conducted in CTTF, which is a 1/6th scale model of the Surry reactor containment building (RCB). The 1/10th scale IET test (IET-12) was performed in the Surtsey vessel, which had been configured as a 1/10th scale Surry RCB. Scale models were constructed in each of the facilities of the Surry structures, including the reactor pressure vessel, reactor support skirt, control rod drive missile shield, biological shield wall, cavity, instrument tunnel, residual heat removal platform and heat exchangers, seal table room and seal table, operating deck, and crane wall. This report describes these experiments and gives the results.

12. KEY WORDS/DESCRIPTORS *(List words or phrases that will assist researchers in locating the report.)*
direct containment heating
high pressure melt ejection
Surtsey Test Facility
Containment Technology Test Facility
severe reactor accidents
two-cell equilibrium model
reactor containment building loads

13. AVAILABILITY STATEMENT
Unlimited

14. SECURITY CLASSIFICATION
(This Page)
Unclassified
(This Report)
Unclassified

15. NUMBER OF PAGES

16. PRICE

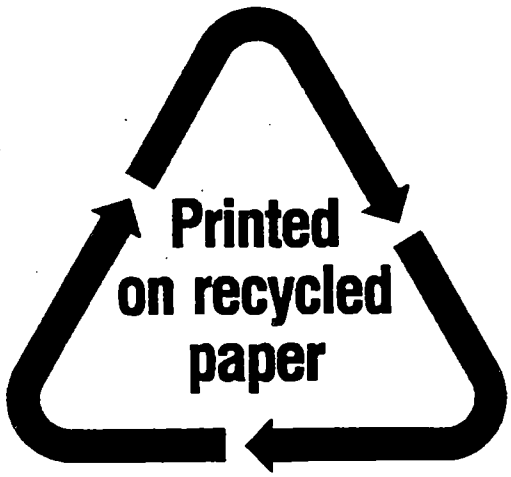

Federal Recycling Program